tRNA fragments in preeclampsia: expression, function and biomarker potential



Dr William Robert Cooke

New College

Thesis submitted for the Degree of Doctor of Philosophy

Trinity Term 2023

42 557 words

This thesis is hyperlinked throughout for the convenience of readers using an electronic format. Clicking on cross-references (including contents tables as well as figure, table and section references) will navigate to the corresponding location. Most PDF readers have keyboard shortcuts to return to the hyperlink origin after clicking the reference. Using a PDF reader's "Bookmarks" bar will display the table of contents in a side bar to facilitate easy navigation between sections.

Copyright © William Robert Cooke

All rights reserved

To our marvellous children, Robert and Lydia, who brighten my every day:

may you one day find something which excites you

as much as this has captivated me.

Contents

Abstract ..... *vii*

Acknowledgements ..... *viii*

Statement of authorship ..... *x*

List of abbreviations ..... *xi*

List of figures ..... *xiii*

List of tables ..... *xvii*

Chapter 1. General introduction *1*

1.1. Preeclampsia **2**
1.1.1. Definitions and epidemiology 2
1.1.2. Subclassification 4
1.1.3. Clinical context 4
1.1.4. Gaps in clinical knowledge 6
1.1.5. Pathophysiology 7

1.2. tRNA fragments **16**
1.2.1. Nomenclature, classification and diversity 18
1.2.2. Biogenesis 18
1.2.3. Biological activity 19
1.2.4. tRNA fragments in EVs 21

1.3. Research rationale and hypotheses **25**

1.4. Thesis aims **26**

Chapter 2. Characterisation of tRNA fragments in perfusion-derived syncytiotrophoblast extracellular vesicles in normal pregnancy and early-onset preeclampsia *27*

2.1. Introduction **28**
2.1.1. Small RNA in healthy syncytiotrophoblast extracellular vesicles 28
2.1.2. Small RNA in preeclampsia syncytiotrophoblast extracellular vesicles 29
2.1.3. Preparation of syncytiotrophoblast extracellular vesicles 30
2.1.4. Approaches to differential expression analysis of small RNA 31

2.2. Methods **33**
2.2.1. Ethical approval, sample acquisition and disease definition. 33
2.2.2. Dual-lobe placental perfusion, EV and RNA isolation, library preparation and sequencing 33
2.2.3. Bioinformatic approaches 35
2.2.4. tRNA fragment detection with quantitative PCR 38

2.3. Results **44**
2.3.1. Small RNA sequencing of normal pregnancy samples 44
2.3.2. Small RNA sequencing of early-onset preeclampsia pregnancy samples 69
2.3.3. Validation of differentially expressed tRNA fragments in preeclampsia medium-large EVs using qPCR 98

2.4. Discussion **106**

2.5. Summary Figure **112**

2.6. Appendix 1 ..... **113**

2.7. Appendix 2 ..... **117**

Chapter 3. Investigating syncytiotrophoblast tRNA fragments in the maternal circulation 126

3.1. Introduction 127
3.1.1. Rationale for 5'-tRNA fragment validation in the maternal circulation 127
3.1.2. Detecting and isolating EVs from blood 127
3.1.3. STB-EVs as a proportion of blood EVs 131
3.1.4. Approaches to enrichment of STB-EVs from blood 135
3.1.5. Approaches to testing hypotheses 135
3.1.6. Quantification and normalisation in qPCR 138

3.2. Methods 142
3.2.1. Blood collection and handling 142
3.2.2. Membrane affinity column plasma EV RNA isolation 142
3.2.3. Size exclusion column plasma EV RNA isolation 143
3.2.4. Stem-loop reverse transcription 144
3.2.5. Quantitative PCR reactions and data analysis 144
3.2.6. Particle size and concentration analysis 145
3.2.7. Whole plasma RNA isolation 145
3.2.8. Plasma STB-EV RNA isolation 145

3.3. Results 151
3.3.1. Target selection 151
3.3.2. Optimising a technique to quantify total plasma EV tRF expression 153
3.3.3. Plasma EV tRNA-fragment expression 160
3.3.4. Whole plasma tRF expression 165
3.3.5. Plasma STB-EV isolation approaches 170

3.4. Discussion 203

3.5. Summary Figure 208

Chapter 4. tRNA fragments as blood biomarkers in preeclampsia 209

4.1. Introduction 210
4.1.1. Hypothesis 4.1 210
4.1.2. Rationale to investigate biomarkers for preeclampsia 210
4.1.3. RNA biomarkers in preeclampsia 212
4.1.4. Placental perfusion as a preeclampsia biomarker-discovery system 212

4.2. Methods 214
4.2.1. Ethical approval, sample acquisition and disease definition. 214
4.2.2. General experimental principles 215
4.2.3. First attempt 215
4.2.4. Second attempt 216
4.2.5. Third attempt 216
4.2.6. Fourth attempt 216
4.2.7. Fifth attempt 216
4.2.8. Statistical methods 216

4.3. Results 218
4.3.1. miRNA validation in plasma 218
4.3.2. tRNA validation in plasma: target optimisation 222
4.3.3. tRNA validation in plasma: plasma preparation optimisation 242

4.4. Discussion 250

4.5. Summary Figure 255

4.6. Appendix 3 256

Chapter 5. Functional activity of syncytiotrophoblast tRNA-fragments in endothelial cells, macrophages and monocytes 258

5.1. Introduction 259
5.1.1. Endothelial dysfunction in preeclampsia 259
5.1.2. Sterile inflammation in preeclampsia 262
5.1.3. Summary 264

5.2. Methods 267
5.2.1. Cell culture 267
5.2.2. tRF target and negative control selection and transfection 267
5.2.3. STB-EV treatment and positive controls 270
5.2.4. Cell proliferation assay 270
5.2.5. NF-κB migration 271
5.2.6. Co-culturing HUVEC with macrophage supernatants 272
5.2.7. RNA expression 272
5.2.8. Data presentation 273

5.3. Results 274
5.3.1. Endothelial cell responses to STB-EV tRNA fragments 274
5.3.2. Macrophage responses to STB tRNA fragments 282
5.3.3. Monocyte responses to STB tRNA fragments 287
5.3.4. Endothelial cell response to macrophage activation by STB tRNA fragments 289

5.4. Discussion 291

5.5. Summary Figure 295

Chapter 6. General discussion 296

6.1. Context 297

6.2. Summary of results 297

6.3. Synthesis of results 301
6.3.1. STB-EV tRFs as placental endocrine signals 301
6.3.2. STB-EV tRFs as molecular mediators of preeclampsia 304
6.3.3. Preeclampsia STB-EV tRF dysregulation in plasma 307

6.4. Findings in context 308

6.5. Thesis limitations and future work 309

6.6. Concluding remarks 313

References 314

Abstract

Background: Preeclampsia is a placental disease, resulting in maternal hypertension and multi-organ impairment. The relationship between placental pathology and the widespread inflammation and endothelial dysfunction in preeclampsia is incompletely characterised. Mismatch between placental nutrient supply and fetal demands induces stress in the syncytiotrophoblast, the placental layer in contact with maternal blood. Such stress alters the content and release of extracellular vesicles (STB-EVs) into the maternal circulation. I have previously shown 5'-tRNA fragments (5'-tRFs) constitute the majority of small RNA in STB-EVs in healthy pregnancies. 5'-tRFs are produced in response to stress. In this thesis, I hypothesise STB-EV 5'-tRFs release might change in early-onset preeclampsia. I aim to 1) characterise STB-EV 5'-tRFs in normal pregnancy and preeclampsia; 2) investigate STB-EV tRFs in maternal blood; 3) evaluate tRFs as circulating biomarkers in preeclampsia; 4) explore functional activity of STB-EV tRFs in preeclampsia dysfunctional cells.

Methods: Placentas from eight cases and six controls were perfused, comparing small RNA sequences from STB-EVs using various bioinformatic approaches. EVs, STB-EVs and total RNA were isolated from different plasma samples and tRFs quantified using qPCR. The actions of the most abundant preeclampsia-dysregulated 5'-tRFs were investigated in monocytes, macrophages and endothelial cells.

Results: 5'-tRFs constitute the majority of small RNA in STB-EVs from both preeclampsia and normal pregnancies. >4000 small RNA fragments are differentially expressed in preeclampsia STB-EVs. Preeclampsia-dysregulated 5'-tRFs are detectable in maternal plasma, where a placentally-derived load circulates. 5'-tRFs do not currently represent blood biomarkers for preeclampsia. The most abundant preeclampsia-upregulated small RNA, 5'-tRF-Glu-CTC, induces inflammation in macrophages but has no direct effect on monocytes or endothelial cells. The conditioned media from 5'-tRF-Glu-CTC-activated macrophages reduces endothelial nitric oxide synthase expression and increases adhesion molecule expression in endothelial cells.

Conclusions: STB-EV tRFs are placental endocrine signals which contribute to the pathogenesis of preeclampsia at a molecular level.

Acknowledgements

My first acknowledgement is to my three supervisors: Professors Manu Vatish, Chris Redman and Dennis Lo. I was fortunate enough to first hear about preeclampsia from Chris as a medical student. I was captivated by his description of this confusing, heterogeneous condition about which we knew so much and yet so little. However, it was Manu who convinced me to return to Oxford some years later, with the promise of a friendly supervisor and the opportunity to pursue my passion for RNA signalling in the field of preeclampsia.

Manu and Chris, you have both supported me with wisdom, generosity and thoughtful criticism over the last six years. Manu, you have a remarkable ability to push me to greater things, always putting my personal priorities at the top of your agenda. You still share the buzz of seeing new data with me – the burden of responsibility to consider and interpret it correctly and the sheer thrill of learning new things about our world. Chris, your attention to detail and knowledge of the literature in preeclampsia are second to none. You have saved me from scientific embarrassment many times. My education under you both has been enjoyable, challenging and iterative – I have kept my promise never to do an n=1 experiment again!

We met Dennis Lo at the International Federation of Placenta Associations meeting in Tokyo in 2018, where he was as excited by the evolving tRNA fragment story as we were. Dennis, you have been very generous with your time and expertise, exemplifying the scientific method whilst showing me how to balance this against pragmatism. I am grateful too that your team have engaged so enthusiastically with this project – thanks to Prof Peiyong Jiang, Dr Ji Lu and Ms Jinyue Bae for your time and expertise.

The rest of Team Manu have been phenomenally supportive and engaged with this project. Gabriel Jones, you have offered me so much more than merely rescuing my every coding disaster; you have been a sounding board for ideas and hopefully a friend for life. Wei Zhang, you kindly taught me most of my basic laboratory skills when I arrived in the group six years ago and have always made time to apply your astute scientific reasoning to my latest question. Sofia Cerdeira, Neva Kandzija and Shuhan Jiang, you too have offered your time and skills to my education, thank you. Fenella Roseman, our research midwife, you have worked tirelessly to collect the samples and clinical data which have enabled this project to take place, always with a cheery smile. To the women

who have donated samples to this project: you have been true altruists, often sharing my enthusiasm for the research underpinning our invitation to participate.

Thanks to the Wellcome Trust who funded this research. Their fairness and support at varying times of need has been much appreciated.

Most importantly, I owe the greatest debt of gratitude to my wonderful wife, Gayle. Over the last three years you have carried, grown and nurtured our two children (our greatest accomplishment), whilst enabling me to follow my dreams in the lab. You have been patient, understanding, smart and you have perfected “The Cooke test” when I need someone to bounce an idea off. I am so grateful for the times you’ve said “go for it”, when another unmissable opportunity arises which inevitably means a sacrifice for you. I am even more grateful that you’ve made home much more fun and interesting than any of these opportunities. Science can be hard and I couldn’t have done this without your support.

Thank you all.

Statement of authorship

This thesis is entirely my own work, and describes my own research, except where clearly stated within the text. Contributions by others amount to the following (and were declared at the appointment of examiners):

1. Perfusion of placentas and sequencing of syncytiotrophoblast extracellular vesicle RNA detailed in section 2.2.2 was performed by a team of scientists within Professor Manu Vatish's group before I began my DPhil.

2. An independent analysis of perfusion sequencing data was conducted by our collaborators at the Chinese University of Hong Kong (Ms Jinyue Bai, Dr Ji Lu and Prof Peiyong Jiang), to provide external validation of my own analysis. Our collaborators' analysis is presented in Appendix 1 at the end of Chapter 2.

3. An analysis of small RNA expression in publicly available blood cell RNA sequencing data was performed by our collaborators at the Chinese University of Hong Kong (Ms Jinyue Bai, Dr Ji Lu and Prof Peiyong Jiang). This analysis is presented in Appendix 3 at the end of Chapter 4, and informs target selections made in 4.3.1, 4.3.2.2 and 4.3.2.3.

List of abbreviations

AF4	Asymmetric flow field-flow fractionation
AN	Antenatal
BMI	Body mass index
cDNA	Complementary deoxyribonucleic acid
CI	Confidence interval
Cq	Quantification cycle
DAPI	4’,6-diamidino-2-pheylindole
DBP	Diastolic blood pressure
DE	Differentially expressed
DEUS	Differential expression of unique sequences
DNA	Deoxyribonucleic acid
DOTAP	N-[1-(2,3-Dioleoyloxy)propyl]-N,N,N- trimethylammonium methylsulfate
eNOS	Endothelial nitric oxide synthase
EV	Extracellular vesicle
FAM	6-carboxyfluorescein
HUVEC	Human umbilical vein endothelial cells
ICAM-1	Intercellular adhesion molecule 1
IFNγ	Interferon gamma
IgG	Immunoglobulin G
ISEV	International society for extracellular vesicles
ISSHP	International society for the study of hypertension in pregnancy
LPS	Lipopolysaccharide
MAC	Membrane affinity columns
MIQE	Minimum information for publication of quantitative RT-PCR experiments
miRNA	Micro ribonucleic acid
MLEV	Medium-large extracellular vesicle
NF-κB	Nuclear factor k-light-chain-enhancer
NICE	National Institute for Health and Care Excellence
NO	Nitric oxide
NTA	Nanoparticle tracking analysis
nt	Nucleotides
PBMC	Peripheral blood mononuclear cells
PBS	Phosphate buffered saline
PCA	Principal component analysis
PFP	Platelet-free plasma

piRNA	Piwi-interacting RNA
PLAP	Placental alkaline phosphatase
PlGF	Placental growth factor
PMA	Phorbol 12-myristate-13-acetate
PN	Postnatal
PPP	Platelet poor plasma
qPCR	Quantitative polymerase chain reaction
RNA	Ribonucleic acid
RNAseq	RNA sequencing
RT	Reverse transcription
RT-qPCR	Reverse transcription quantitative polymerase chain reaction
SBP	Systolic blood pressure
SEC	Size-exclusion chromatography
SEM	Standard error of the mean
SEV	Small extracellular vesicle
sFlt-1	Soluble fms-like tyrosine kinase-1
sRNA	Small ribonucleic acid
sRNAseq	Small RNA sequencing
STB-EV	Syncytiotrophoblast-derived extracellular vesicle
TNFα	Tumour necrosis factor alpha
tRNA	Transfer ribonucleic acid
tRF	tRNA fragment
VCAM-1	Vascular cell adhesion molecule 1
VEGF	Vascular endothelial growth factor

List of figures

Figure 1-1 – Evolution of the two-stage model of preeclampsia, from A) Redman 1991[18] to B) Redman et al. 2020[7]. 9

Figure 1-2 – Schematic diagram showing the secondary structure of a mature tRNA molecule and known cleavage sites to generate tRNA fragments. 17

Figure 2-1 – Photograph depicting experimental setup for dual lobe placental perfusion .34

Figure 2-2 – Schematic diagram of steps involved in quantifying sRNA using stem-loop reverse transcription qPCR assays 40

Figure 2-3 – Quality control data for normal pregnancy samples. 47

Figure 2-4 – Size distribution (A-C) and mapping (D-F) of sRNA fragments in normal pregnancy samples after removal of adapters and low-quality reads. 49

Figure 2-5 – Base coverage of tRNA fragments in normal pregnancy samples, stratified by iso-acceptor. 51

Figure 2-6 – Principal Component Analysis for sRNAseq analysis of normal pregnancy MLEVs and SEVs compared to placenta, using tRAX 53

Figure 2-7 – Mapping specificity of three most abundant 5'-GlyGCC tRNA fragments using tRAX in MLEVs, SEVs and placenta. 58

Figure 2-8 – Major differences between DEUS sRNA profiling strategy and other conventional strategies. 60

Figure 2-9 – Principal Component Analysis for sRNAseq analysis of normal pregnancy MLEVs (10K) compared to placenta, using DEUS 62

Figure 2-10 – Principal Component Analysis for sRNAseq analysis of normal pregnancy SEVs (150K) compared to placenta, using DEUS 66

Figure 2-11 – Quality control data for early-onset preeclampsia pregnancy samples. 72

Figure 2-12 – Size distribution (A-C) and mapping (D-F) of sRNA fragments in early-onset preeclampsia pregnancy samples after removal of adapters and low-quality reads. 74

Figure 2-13 – Base coverage of tRNA fragments in normal pregnancy samples, stratified by iso-acceptor. 76

Figure 2-14 – Principal Component Analysis for sRNAseq analysis of early-onset preeclampsia vs normal pregnancy MLEVs, using tRAX 78

Figure 2-15 – Principal Component Analysis for sRNAseq analysis of early-onset preeclampsia vs normal pregnancy SEVs, using tRAX 82

Figure 2-16 – Principal Component Analysis for sRNAseq analysis of early-onset preeclampsia vs normal pregnancy MLEVs, using DEUS 86

Figure 2-17 – Mean normalised expression and standard deviation of 12 most abundant sRNA fragments differentially expressed in early-onset preeclampsia compared to normal pregnancy MLEVs, using DEUS. 89

Figure 2-18 – Principal Component Analysis for sRNAseq analysis of early-onset preeclampsia vs normal pregnancy SEVs, using DEUS 91

Figure 2-19 – Stem-loop assay specificity determined using synthetic oligonucleotides. .99

Figure 2-20 – Stem-loop assay linearity with dilution of RNA isolated from perfusion STB-EVs 101

Figure 2-21 – Quantification of target RNA fragments in perfusion STB-EVs 105

Figure 2-22 – Schematic figure summarising Chapter 2 key experiments and findings. .112

Figure 2-23 – Size distribution, mapping and base coverage of preeclampsia and normal sample sRNA by collaborators. 115
Figure 2-24 – Large format reproduction of quality control data for normal pregnancy samples. Panel labels consistent with Figure 2-3 for ease of reference. 118
Figure 2-25 – Large format reproduction of quality control data for normal pregnancy samples. Panel labels consistent with Figure 2-3 for ease of reference. 119
Figure 2-26 – Large format reproduction of quality control data for normal pregnancy samples. Panel labels consistent with Figure 2-3 for ease of reference. 120
Figure 2-27 – Large format reproduction of quality control data for normal pregnancy samples. Panel label consistent with Figure 2-3 for ease of reference. 121
Figure 2-28 – Large format reproduction of quality control data for early-onset preeclampsia pregnancy samples. Panel labels consistent with Figure 2-11 for ease of reference. 122
Figure 2-29 – Large format reproduction of quality control data for early-onset preeclampsia pregnancy samples. Panel labels consistent with Figure 2-11 for ease of reference. 123
Figure 2-30 – Large format reproduction of quality control data for early-onset preeclampsia pregnancy samples. Panel labels consistent with Figure 2-11 for ease of reference. 124
Figure 2-31 – Large format reproduction of quality control data for early-onset preeclampsia pregnancy samples. Panel label consistent with Figure 2-11 for ease of reference. 125
Figure 3-1 – Extracellular vesicles are a minority population amongst small particles in human plasma. 130
Figure 3-2 – Estimation of plasma EV derivations in non-pregnant donors 132
Figure 3-3 – Concentration of EVs in platelet-free plasma from non-pregnant (NonP), normal pregnancies (NormP) and pregnancies with preeclampsia (PE) using flow cytometry analysis. 134
Figure 3-4 – Schematic diagram to illustrate sample types which were selected to test the hypothesis that a placental 5'-tRF load is detectable in maternal plasma. 137
Figure 3-5 – Abundance of two placenta-specific miRNAs in AN and PN total plasma EV isolated using membrane-affinity columns (MAC, red) and size-exclusion chromatography (SEC, blue). 155
Figure 3-6 – Size and concentration of particles isolated from placental perfusate using ultracentrifugation and from plasma using MAC isolation. 157
Figure 3-7 – Comparison of target 5'-tRF detection in MAC-isolated pregnant plasma EVs using singleplex or multiplex reverse transcription reactions 159
Figure 3-8 – Expression of tRF-F, tRF-I and tRF-J in pregnant and non-pregnant venous plasma EVs, relative to the mean non-pregnant expression. 162
Figure 3-9 – Expression of tRF-F, tRF-I and tRF-J in paired samples of uterine and peripheral venous plasma EVs, relative to the mean peripheral venous abundance. 164
Figure 3-10 – Expression of tRF-F and tRF-I in pregnant and non-pregnant whole venous plasma, relative to the mean non-pregnant abundance. 167
Figure 3-11 – Expression of tRF-F and tRF-I in paired samples of uterine and peripheral whole venous plasma, relative to the mean peripheral venous expression. 169
Figure 3-12 – Approach 1 optimised plasma STB-EV isolation protocol. 171

Figure 3-13 – Expression of placenta-specific miRNAs in plasma EVs isolated by SEC, with and without PLAP/IgG1 immunoprecipitation (Approach 1). 173

Figure 3-14 – Expression of miR518b in paired samples of uterine and peripheral venous plasma EVs and serum EVs, relative to the mean peripheral venous expression. 175

Figure 3-15 – Expression of placenta-specific miRNAs in serum EVs isolated by ExoEasy, with and without PLAP/IgG1 immunoprecipitation (Approach 2). 177

Figure 3-16 – Western blot showing recovery of 5 ug biotinylated PLAP antibody (bP) using 50 uL streptavidin coated beads (n=3) compared to non-biotinylated antibody (nP). 181

Figure 3-17 – Bead recovery after handling equal quantities in four different tube types (4 to 7), compared to control unhandled beads (8). 183

Figure 3-18 – Expression of tRF-F in PLAP bead-bound MLEVs, empty bead-bound MLEVs and unprocessed MLEVs. 185

Figure 3-19 – Comparing different NDOG2 (PLAP antibody) biotinylation concentrations to beads with PBS and a commercially biotinylated antibody. 187

Figure 3-20 – Representative images from NTA of untreated beads (A) and macroscopically clumped beads (B) after addition of 20X biotinylated NDOG2 antibody 188

Figure 3-21 – Expression of tRF-F in perfusion MLEVs isolated using NDOG2 antibody with different biotinylation levels, relative to 2X biotinylation. 192

Figure 3-22 – Approach 3 optimised plasma STB-EV isolation protocol. 194

Figure 3-23 – Expression of miR518b and tRF-F in PLAP-EV RNA isolated from pregnant plasma alongside positive and negative controls (Approach 3). 196

Figure 3-24 – Expression of tRF-F in RNA isolated from pregnant plasma with empty beads and non-pregnant plasma with PLAP-beads, to see whether pre-depletion with empty beads reduces the background signal. 198

Figure 3-25 – Approach 4 optimised plasma STB-EV isolation protocol. 200

Figure 3-26 –Expression of miR518b and tRF-F in PLAP-EV RNA isolated from pregnant plasma alongside positive and negative controls (Approach 4). 202

Figure 3-27 – Schematic figure summarising Chapter 3 key experiments and findings. .208

Figure 4-1 – Relative expression of six RNA fragments mapping to four target miRNAs in preeclampsia and normal pregnancies from different samples and studies. 221

Figure 4-2 – Expression of targets F, I and J in EVs from women with early-onset preeclampsia and normal pregnancies (First attempt). 225

Figure 4-3 – Expression of targets J, M, P, Q and N in paired uterine and peripheral venous plasma from healthy term pregnancies (Second attempt). 231

Figure 4-4 – Expression of targets J, Q, M and control miRNA N in EVs from women with early-onset preeclampsia and normal pregnancies (Second attempt). 234

Figure 4-5 – Expression of targets F, S, W, D and control miRNA N in EVs from women with early-onset preeclampsia and normal pregnancies (Third attempt). 241

Figure 4-6 – Expression of targets F, S, W and J in whole plasma from women with early-onset preeclampsia and gestation-matched controls (Fourth attempt). 244

Figure 4-7 – Expression of targets F, S and W relative to J in whole plasma from women with early-onset preeclampsia and gestation-matched controls (Fourth attempt). 246

Figure 4-8 – Expression of targets F, S and W in STB-EV enriched from peripheral plasma from women with early-onset preeclampsia and gestation-matched controls (Fifth attempt).....249
Figure 4-9 – Schematic diagram illustrating hypotheses which may explain why differences in STB-EV tRF expression between preeclampsia and normal pregnancies, identified using placental perfusion, may not reflect plasma tRF expression. 252
Figure 4-10 – Schematic figure summarising Chapter 4 key experiments and findings..255
Figure 5-1 – Schematic figure showing known functions of STB-EVs relating to endothelial activation and sterile inflammation in the context of preeclampsia. 266
Figure 5-2 – Optimisation of CyQUANT® proliferation assay in HUVEC 275
Figure 5-3 – HUVEC proliferation quantified by CyQUANT® assay 278
Figure 5-4 – HUVEC functions following treatment with EV tRFs packaged with DOTAP 281
Figure 5-5 – NF-κB migration in macrophages.....284
Figure 5-6 – Cytokine mRNA expression in differentiated THP-1 cells (macrophages)..286
Figure 5-7 – Cytokine mRNA expression in undifferentiated THP-1 cells (monocytes) ..288
Figure 5-8 – Macrophage activation by STB-EV tRFs can induce endothelial cell activation.....290
Figure 5-9 – Schematic figure summarising Chapter 5 key experiments and findings....295
Figure 6-1 – Schematic figure summarising key results from this thesis. 298
Figure 6-2 – Schematic figure highlighting the novelty of tRFs as endocrine signals. 303
Figure 6-3 – Schematic figure highlighting the novelty of tRFs as molecular mediators of preeclampsia pathophysiology. 306

List of tables

Table 1-1 – ISSHP classification for hypertensive disorders of pregnancy[1] 3

Table 1-2 – Thresholds for diagnosis of preeclampsia, as defined by ISSHP[1] 3

Table 1-3 – Studies quantifying STB-EVs in preeclampsia plasma compared to normal pregnancy plasma, stratified by gestational age of disease onset 14

Table 1-4 – Seminal studies describing different mechanisms of tRF action 20

Table 1-5 – Studies evaluating specific biofluid EV tRFs as non-invasive biomarkers for disease 23

Table 2-1 – Target tRF sequences 43

Table 2-2 – Demographic data for women donating placentas from normal pregnancies. 45

Table 2-3 – Top twelve tRNA fragments differentially expressed in normal pregnancy MLEVs compared to placenta using tRAX. 55

Table 2-4 – Twelve most abundant tRNA fragments differentially expressed in SEVs compared to placenta in normal pregnancy samples, using tRAX. 57

Table 2-5 – Twelve most abundant sRNA fragments differentially expressed (DE) in MLEVs compared to placenta in normal pregnancy samples, using DEUS. 64

Table 2-6 – Twelve most abundant sRNA fragments differentially expressed (DE) in SEVs compared to placenta in normal pregnancy samples, using DEUS. 68

Table 2-7 – Demographic data for women donating placentas from pregnancies with early-onset preeclampsia, compared to normal pregnancies 70

Table 2-8 – Twelve most abundant tRNA fragments differentially expressed in early-onset preeclampsia compared to normal pregnancy MLEVs, using tRAX. 80

Table 2-9 – Twelve most abundant tRNA fragments differentially expressed in early-onset preeclampsia compared to normal pregnancy SEVs, using tRAX. 84

Table 2-10 – Twelve most abundant sRNA fragments differentially expressed (DE) in early-onset preeclampsia compared to normal pregnancy MLEVs, using DEUS. 88

Table 2-11 – Twelve most abundant sRNA fragments differentially expressed (DE) in early-onset preeclampsia compared to normal pregnancy SEVs, using DEUS. 93

Table 2-12 – Differentially expressed sRNA fragments discovered between early-onset preeclampsia and normal samples, comparing three approaches to analysis 95

Table 2-13 – The three most abundant fragments from DEUS, compared to collaborators' analysis. 97

Table 2-14 – Stability values for reference genes in preeclampsia and normal STB-EV samples 103

Table 2-15 – Twelve most abundant sRNA fragments differentially expressed (DE) in early-onset preeclampsia compared to normal pregnancy MLEVs, following bespoke analysis by collaborators 116

Table 3-1 – Table summarising studies which investigate blood-borne miRNAs as biomarkers for prediction or diagnosis of preeclampsia. 140

Table 3-2 – Table showing tRNA target sequences selected for investigation in plasma. 152

Table 3-3 – Table showing absorbance at 500 nm of HABA/avidin solution (standard), compared to biotinylated antibody every minute for 8 minutes after reaction started 179

Table 3-4 – Table showing observations and software-generated particle concentrations following NTA analysis of different bead samples. 190
Table 4-1 – miRNAs differentially expressed in preeclampsia STB-EVs compared to normal pregnancies. 219
Table 4-2 – Summary of published studies quantifying expression of miRNA targets from Table 4-1 in blood. EDTA (ethylenediaminetetraacetic acid), PE (preeclampsia). 219
Table 4-3 – Demographic data for women donating blood; first attempt. 223
Table 4-4 – 28 fragments identified by second target selection attempt.....228
Table 4-5 – Expression of targets selected for second attempt biomarker evaluation in normal and preeclampsia perfusion STB-EVs as well as blood cell datasets. 229
Table 4-6 – Demographic data for women donating blood; second attempt. 233
Table 4-7 – 27 fragments identified by third target selection attempt 237
Table 4-8 – Expression of targets selected for third attempt biomarker evaluation in normal pregnancy and preeclampsia perfusion STB-EVs as well as blood cell datasets. 238
Table 4-9 – Demographic data for women donating blood; third attempt. 240
Table 4-10 – Demographic data for women donating blood; fourth attempt.....243
Table 4-11 – Demographic data for women donating blood; fifth attempt. 248
Table 4-12 – Sequence read archive identifiers for blood cell datasets.....257
Table 5-1 – Oligonucleotide sequences used in this chapter.....269
Table 5-2 – Information regarding positive controls 269

Chapter 1. General introduction

1.1. Preeclampsia

1.1.1. Definitions and epidemiology

Hypertension in pregnancy is defined by the International Society for the Study of Hypertension in Pregnancy (ISSHP) as a confirmed systolic blood pressure ≥140 and/or diastolic blood pressure ≥90 mmHg[1]. The ISSHP classification for hypertensive disorders of pregnancy is shown in Table 1-1.

Preeclampsia is a progressive hypertensive disorder of pregnancy, involving multiple organs. It is defined by the new onset of hypertension after 20 weeks of gestation associated with either proteinuria, maternal organ dysfunction (hepatic, renal, neurological, haematological) or uteroplacental dysfunction (abnormal umbilical artery doppler, fetal growth restriction, stillbirth)[1]. Thresholds for diagnosis defined by ISSHP are summarised in Table 1-2. Preeclampsia is estimated to affect 4.6% of pregnancies worldwide, disproportionately affecting lower income countries[2]. It causes significant mortality, accounting for 14% maternal deaths globally[3]. For each maternal death, it is estimated that 50-100 women suffer significant morbidity[4]. Preeclampsia also represents a significant disease burden for the fetus. Globally, preeclampsia is estimated to account for 500 000 perinatal deaths every year[5]. Even in higher income countries, the burden from perinatal morbidity is significant; preeclampsia accounted for 18% iatrogenic preterm births in England in 2015-17[6].

Hypertension known before pregnancy or present in the first 20 weeks	Hypertension arising de novo at or after 20 weeks
Chronic hypertension - Essential - Secondary	Preeclampsia - De novo - Superimposed on chronic hypertension
White-coat hypertension	Gestational hypertension
Masked hypertension	Transient gestational hypertension

Table 1-1 – ISSHP classification for hypertensive disorders of pregnancy[1]

Feature	Measurement	Threshold
Hypertension	Blood pressure	Systolic ≥140 and/or diastolic ≥90 mmHg, confirmed by repeating over a few hours
Proteinuria	Urine protein-creatinine ratio (PCR)	≥30 mg/mmol
	Urinalysis (if PCR not available)	≥1+
Maternal organ dysfunction	Creatinine	≥90 µmol/L
	ALT/AST	≥40 IU/L
	Neurological complications	Eclampsia, altered mental status, blindness, stroke, clonus, severe headaches, persistent visual scotomata
	Haematological complications	Platelet count <150,000/µL, disseminated intravascular coagulopathy, haemolysis
Utero-placental dysfunction	Ultrasound parameters	Fetal growth restriction, abnormal umbilical artery Doppler wave form analysis
	Fetal demise	Stillbirth

Table 1-2 – Thresholds for diagnosis of preeclampsia, as defined by ISSHP[1]

1.1.2. Subclassification

Preeclampsia is considered a syndrome; a collection of clinical features, rather than a single disease with a common pathophysiology[7]. The first significant attempt at subclassification of preeclampsia in 2003 defined early-onset (<34 weeks of gestation) and late-onset (≥34 weeks of gestation) disease[8]. The authors argued that gestational age at onset represented the most important variable to predict maternal and perinatal morbidity and mortality. They summarised evidence that pathophysiology and epidemiology differ between the two subtypes. This included observations of different neutrophil function, cytokine levels, recurrence in subsequent pregnancies and long-term risk of cardiovascular disease. This subclassification has persisted, with studies of pathophysiology commonly focussing on early-onset disease as the more homogenous phenotype.

Recently, there has been some consensus that these two subtypes drastically underestimate the heterogeneity of preeclampsia[9]. A significant barrier to progress in understanding pathophysiology is the assumption that the same molecular pathways underlie the varied clinical presentations. Different grouping strategies have been proposed including specific organ involvement, long-term outcomes, immunological phenotypes, and plasma protein expression. However, whilst the problem has been identified, there is a paucity of studies employing any of these strategies.

1.1.3. Clinical context

Attempts to mitigate the consequences of preeclampsia in clinical practice are made from the first trimester of pregnancy through the postnatal period and beyond. The clinical approach in the UK, outlined in the National Institute for Health and Care Excellence (NICE) guideline “Hypertension in Pregnancy” can be summarised in seven stages[10].

1. *Prevention*

   Risk of developing preeclampsia is assessed when a mother first registers her pregnancy. A number of demographic features and past medical history are used to determine women at higher risk. These women are offered prophylaxis with aspirin at 75-150 mg daily from 12 weeks of gestation until delivery. Data from the largest meta-analysis (including over 40 000 women) suggests this intervention reduces the risk of proteinuric pre-eclampsia by 18%[11].

2. *Screening*

   Pregnant women are warned about the signs and symptoms of preeclampsia and advised to seek medical attention should these develop. Additionally, blood pressure is measured and urine analysed for protein at each antenatal visit to screen for preeclampsia[12].

3. *Diagnosis*

   Clinical diagnostic criteria for preeclampsia are clearly defined and summarised above. In addition, placental growth factor (PlGF)-based tests are recommended to help rule in or rule out preeclampsia when it is suspected between 20 and 37 weeks of gestation[13]. A variety of tests are approved, with different proprietary technologies and associated thresholds and efficacies. Overall, these tests offer an excellent negative predictive value (around 98-100%); however their positive predictive value is poorer (around 40%)[14,15]. In practice this means they are useful to rule out the condition and avoid inappropriate patient reassurance; but can still result in over-diagnosis.

4. *Supportive care*

   Once diagnosed with preeclampsia, pregnant women are closely monitored to minimise morbidity. Blood pressure is controlled to avoid cerebral haemorrhage. Liver,

renal and haematological tests are performed regularly to identify complications early. Fetal wellbeing and growth are assessed to prevent stillbirth.

5. *Delivery*

   Delivery remains the only cure for preeclampsia. Birth is timed to balance the risks of preterm morbidity for the neonate against maternal and fetal morbidity from continuing the pregnancy. Prognostic tools such as the fullPIERS model can be used to guide decisions about location of care and thresholds for intervention[5].

6. *Postnatal care*

   Complications of preeclampsia are actively sought and monitored after the baby is delivered, with supportive care such as renal replacement therapy and blood products being administered until the woman has recovered. Antihypertensive medications are titrated to avoid both cerebral haemorrhage from hypertension and collapse from hypotension.

7. *Post-pregnancy care*

   Lifetime cardiovascular disease risk is increased following a pregnancy with preeclampsia, with cardiovascular mortality being doubled[16]. Clinicians educate affected women about this risk, helping them to reduce their modifiable cardiovascular risk factors such as smoking, weight and persistent hypertension. Inter-pregnancy counselling can also take place to educate women about the risk of preeclampsia in any future pregnancies.

1.1.4. Gaps in clinical knowledge

There are significant shortcomings in the care that can be offered at every stage of preeclampsia management. Two broad concepts encompass the knowledge deficit: a lack of suitable preeclampsia *biomarkers* and *treatments*.

Improved predictive biomarkers could allow better targeting of aspirin therapy. The current model used to target aspirin in clinical practice identifies only 35% of women who will go on to require delivery for preeclampsia[17]. With better biomarkers, some of the remaining 65% could be identified and receive aspirin, which may prevent further cases of preeclampsia. Preeclampsia screening at later gestations may be more efficacious if better disease biomarkers were identified. Whilst angiogenic assays represent a paradigm shift in preeclampsia diagnosis, novel biomarkers might allow the positive predictive value to be enhanced. This could avoid over-diagnosis and associated morbidity. A lack of prognostic biomarkers represents the greatest challenge in preeclampsia management. The condition is considered unpredictable; NICE guidelines recommend against repeat testing of PlGF[13]. Over-intervention by obstetricians (with resulting preterm morbidity) might be reduced if objective markers could be used to time delivery.

Preeclampsia is a progressive syndrome, which worsens until delivery. No treatment has been found which modifies the natural history of preeclampsia. Any such treatment might extend pregnancy duration and prevent maternal and fetal morbidity. The greatest barrier to developing novel treatments is our poor understanding of preeclampsia pathophysiology. An understanding of the molecular pathways which underlie preeclampsia might facilitate the design of therapeutics to modify the process.

1.1.5. Pathophysiology

The two-stage model of preeclampsia was first described in 1991[18]. Thirty years later, it is still widely considered the most effective paradigm to frame the underlying mechanisms[4,19].

The first stage of preeclampsia was originally described as abnormal placental development, termed malplacentation[18]. Classically (in early-onset disease) this was considered to be a consequence of impaired remodelling of the spiral arteries during

placental development. Oxygenated blood reaches the developing placenta by passing through spiral arteries which penetrate the layers of the myometrium. In healthy pregnancy, extravillous trophoblast cells migrate from the placenta into the spiral arteries, triggering remodelling of these vessels[20]. Wider spiral arteries result in low resistance and low velocity blood-flow to the placenta facilitating materno-fetal nutrient exchange. In many cases of preterm preeclampsia, the spiral arteries fail to remodel, resulting in tortuous vessels with turbulent, high velocity blood-flow to the placenta[21]. This causes placental ischaemia-reperfusion injury, damage to placental villi and thus impaired nutrient exchange; the placenta and fetus become growth restricted. These histological observations are supported by the correlation between failed spiral artery remodelling and the clinical severity of the condition[22].

The second stage of preeclampsia represents the maternal syndrome. By definition, this develops after 20 weeks of gestation; placental development is considered to be complete by 18 weeks[7]. Clinical features are unified by sterile inflammation and widespread endothelial dysfunction[23,24]. Gap formation between endothelial cells globally causes proteinuria alongside peripheral, pulmonary and cerebral oedema. Hepatic inflammation can cause liver capsule rupture and impaired synthetic function. Endothelial activation can trigger the consumption of clotting factors and platelets. Impaired release of nitric oxide from the dysfunctional endothelium reduces the vasodilatory signal to adjacent vascular smooth muscle cells, contributing to hypertension. This original description of the two-stage model is summarised in Figure 1-1A.

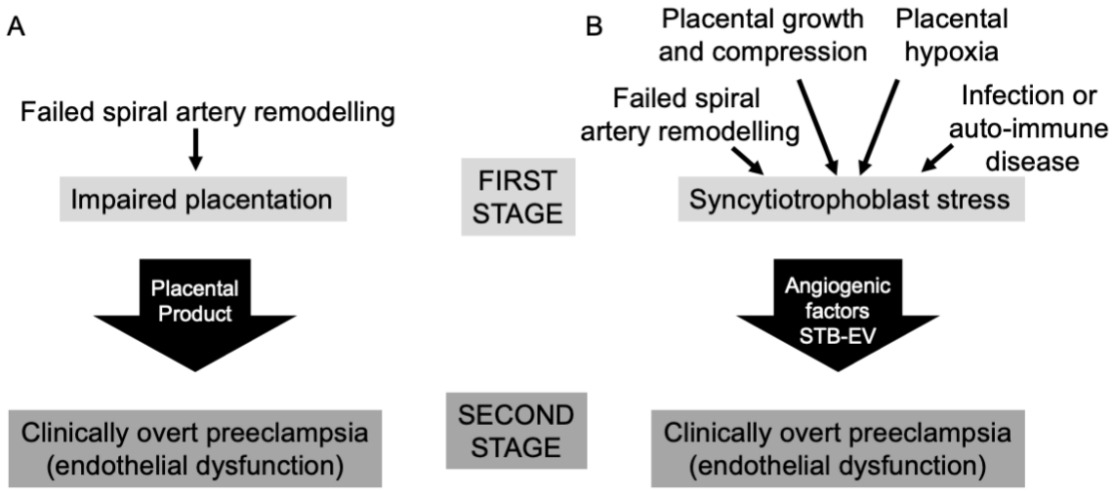


Figure 1-1 – Evolution of the two-stage model of preeclampsia, from A) Redman 1991[18] to B) Redman et al. 2020[7].

1.1.5.1. Syncytiotrophoblast

Contrary to the classical description, preeclampsia is not always associated with growth restriction. Indeed, the majority of preeclampsia develops after 34 weeks of gestation and without fetal growth restriction[25]. The two-stage model has evolved to consider a greater variety of placental pathologies which can encompass the first stage. Stress at the syncytiotrophoblast has replaced malplacentation as the convergence point between different aetiologies (Figure 1-1B)[7].

The syncytiotrophoblast is a true multinucleated syncytium which forms the barrier between maternal and fetal circulations in the human placenta[20]. This single, terminally differentiated cell is formed and enlarged by fusion of underlying cytotrophoblast cells. It has a surface area of 12-14 square metres at term and has a variety of functions. As well as actively facilitating exchange of nutrients and waste products between mother and fetus, it is an endocrine gland producing steroid and peptide hormones and functions as a barrier against infection and immunological rejection of the fetus.

In classical early-onset disease, failed spiral artery remodelling results in placental malperfusion and hypoxic stress in the syncytiotrophoblast. In late-onset disease, Redman and Staff have proposed that the placenta grows at a rate outstripping uterine capacity (termed the “pot-bound” placenta)”[26]. This causes placental compression, villous overcrowding, placental hypoxia and consequently syncytiotrophoblast stress. This stress manifests as oxidative stress (accumulation of free radicals), organellar stress (mitochondrial swelling and impairment, endoplasmic reticulum), nuclear stress (DNA damage as a consequence of free radical damage), complement deposition, inflammation, and autophagy.

Syncytiotrophoblast stress can also be caused by factors beyond the most common (malplacentation and placental compression), reflecting other aetiologies of preeclampsia.

For example, multiple pregnancy, macrosomia and molar pregnancy all increase placental mass and consequently fetoplacental demands[19]. Placental malarial infection is associated with preeclampsia and syncytial knots, a manifestation of syncytiotrophoblast stress[27]. Both parvovirus infection and auto-immune diseases such as antiphospholipid syndrome result in systemic inflammation, with factors directly reaching the syncytiotrophoblast and triggering inflammatory stress[28,29].

1.1.5.2. Syncytiotrophoblast stress signals

The link between the stressed syncytiotrophoblast and the dysfunctional maternal endothelium remains an important focus of research. Syncytiotrophoblast-derived factors, released into the maternal circulation, are considered the most likely candidates.

The discovery of unbalanced angiogenic factors in preeclampsia serum in 2003 represented a significant advance[30]. The healthy endothelium is maintained by vascular endothelial growth factor (VEGF) binding to fms-like tyrosine kinase 1 (Flt-1). In pregnancy, this signal is potentiated by placental growth factor (PlGF), a VEGF homolog released by the placenta. VEGF promotes angiogenesis and induces production of vasodilators including nitric oxide by endothelial cells[31]. VEGF inhibitors cause hypertension and proteinuria in clinical trials outside pregnancy[32].

In early-onset preeclampsia, placental and serum PlGF levels are reduced[30,33]. Conversely, abundance of placental and serum soluble Flt-1 (sFlt-1), a decoy receptor which binds to VEGF/PlGF, increases. This results in reduced endothelial Flt-1 activation by VEGF/PlGF, postulated to be a cause of endothelial dysfunction. In animal models, administering sFlt-1 induces a preeclampsia phenotype, which can be rescued by PlGF[30]. sFlt-1 and PlGF, particularly in ratio, have proved valuable serum biomarkers of early-onset preeclampsia, and have transformed diagnosis in clinical practice[14].

Whilst a major driver of preeclampsia, it appears angiogenic proteins alone do not explain feto-maternal signalling in preeclampsia. Dextran-sulfate plasma apheresis to remove sFlt-1 from women with preeclampsia has had mixed results[34,35]. Additionally, the sFlt-1/PlGF ratio is poor at distinguishing late-onset preeclampsia from normal pregnancy[36]. Pro-inflammatory cytokines and extracellular vesicles released from the syncytiotrophoblast are also proposed to play a role[4,7,19].

1.1.5.3. Syncytiotrophoblast extracellular vesicles (STB-EVs) in preeclampsia

Extracellular vesicles (EVs) are defined as "particles naturally released from the cell that are delimited by a lipid bilayer and cannot replicate, i.e. do not contain a functional nucleus"[37]. Historically, EVs were classified by biogenesis: smaller exosomes being created intracellularly from endosomes and trafficked to the cell surface, with larger microvesicles or ectosomes budding from the plasma membrane. Proving biogenesis is extraordinarily difficult, so the International Society for Extracellular Vesicles (ISEV) now recommends classification by physical characteristics such as size to describe small EVs (SEVs, <200 nm diameter) and medium-large EVs (MLEVs, >200 nm diameter)[37].

Microvillous membrane fragments from the syncytiotrophoblast were first generated in 1974 as an experimental model to understand the immunological properties of the tissue[38]. Placental tissues were agitated in saline to fragment the villi, then small particles isolated by high-speed ultracentrifugation, a technique still employed in studies over 40 years later[39]. In 1998, the previously studied syncytiotrophoblast fragments were discovered to be naturally circulating in the plasma of pregnant women[40]. In this landmark study, EVs were isolated from plasma using high-speed ultracentrifugation. The subpopulation of syncytiotrophoblast-derived extracellular vesicles (STB-EVs) were quantified using antibodies to placentally-expressed epitopes. The authors reported STB-EVs to be more abundant in uterine than peripheral venous plasma, confirming their placental origin *in-vivo*.

Knight *et al.* also demonstrated increased plasma abundance of STB-EVs in women with early-onset preeclampsia[40]. This finding has been replicated by several studies in early-onset and mixed gestation disease (Table 1-3). However, the finding is more controversial in late-onset disease, where several studies do not reach significance and one shows reduced plasma STB-EVs in preeclampsia.

STB-EVs are strong candidates as feto-maternal signals in preeclampsia. In addition to differential release, there is evidence for differential expression of a variety of putative signalling molecules carried by STB-EVs in early-onset disease. I reviewed these studies in detail in a publication at the beginning of my DPhil[41].

STB-EVs are known to carry proteins, lipids, RNA and DNA. At least 16 proteins have been shown in different studies to be differentially expressed in preeclampsia STB-EVs[41]. Some of these proteins can be directly linked to disease pathophysiology. For example, neprilysin is more abundant on preeclampsia STB-EVs[42]. Neprilysin degrades vasodilatory peptides. Increased circulating levels of neprilysin in preeclampsia could easily be linked to hypertension[43]. Tissue factor activity is upregulated on preeclampsia STB-EVs, increasing thrombin production[44]. This could contribute to the disordered coagulation seen in the condition. Endothelial nitric oxide synthase (eNOS) is less abundant on preeclampsia STB-EVs[45]. eNOS produces the vasodilator nitric oxide (NO); downregulation in preeclampsia STB-EVs could contribute to maternal hypertension.

Disease Onset	STB-EV abundance in preeclampsia, compared to normal (significance)	STB-EV size	STB-EV isolation	Detection assay	Mean preeclampsia gestation (weeks)	Mean normal gestation (weeks)	Sample size (PE/N)	Ref
Early	Higher (p=0.005)	Mixed	150,000 *g* for 45 minutes	PLAP ELISA using NDOG2 antibody	30.9	32.7	15/35	226
	Higher (p<0.05)	Small	110,000 *g* for 2 hours, then sucrose gradient	PLAP ELISA using Elabscience kit	30.5	30.8	15/15	227
	Higher (non-significant)	Medium-large	18,890 *g* for 30 minutes	Flow using ED822 antibody	28, 32	28, 32	11/8	228
Mixed	Higher (p=0.01)	Mixed	150,000 *g* for 45 minutes	PLAP ELISA using H317 and NDOG2	33.3	33.1	20/20	40
	Higher (p<0.01)	Mixed	150,000 *g* for 45 minutes	PLAP ELISA using NDOG2 antibody	33.5	33.4	13/14	120
	Higher (p<0.001)	Medium-large	None – direct plasma interrogation	Flow using PLAP and annexin-V antibodies	33.1	32.7	54/33	229
	Higher (non-significant)	Medium-large	14,000 *g* for 90 minutes	Flow using NDOG2 antibody	33.5	33.9	28/30	230
Late	Higher (p<0.005)	Medium-large	10,000 *g* for 30 minutes	PLAP ELISA using Elabscience kit	35.8	36.2	7/15	231
	Lower (p<0.05)	Small	110,000 *g* for 2 hours, then sucrose gradient	PLAP ELISA using Elabscience kit	36.7	38	15/15	227
	Higher (non-significant)	Mixed	150,000 *g* for 45 minutes	PLAP ELISA using NDOG2 antibody	35.5	32.7	10/35	226
	Higher (non-significant)	Medium-large	18,890 *g* for 30 minutes	Flow using STB antibody (ED822)	36	36	11/8	228
Unclear	Higher (p<0.0005) but repeated measures from same participant	Small	100,000 *g* for 2 hours, then iodixanol gradient	PLAP ELISA using Elabscience kit	Unable to determine – samples ranging from 11 to 34 weeks of gestation		13/32	47

Table 1-3 – Studies quantifying STB-EVs in preeclampsia plasma compared to normal pregnancy plasma, stratified by gestational age of disease onset

Studies demonstrate differential expression of a large number of microRNAs (miRNAs) in preeclampsia serum and specifically within STB-EVs[46–48]. There is evidence this dysregulation may play a role in pathogenesis. miR-517a transfer to endothelial cells from STB-EVs correlated with altered expression of genes including *FLT1*[49]. miR-155 is over-expressed in preeclampsia STB-EVs, suppressing eNOS expression in recipient endothelial cells[50]. A contemporary DPhil thesis identified differential mRNA expression in preeclampsia STB-EVs[51].

I recently discovered that 30-32 nucleotide 5'-transfer RNA fragments (5'-tRFs) represent the majority of small RNA (sRNA) in healthy STB-EVs[52]. This finding is supported by the report of tRFs in larger trophoblast-derived particles deported from placental tissues grown in culture[46]. Expression of transfer RNA (tRNA) fragments in preeclampsia STB-EVs is yet to be explored.

In summary, STB-EVs are complex placental particles with good evidence for differential release and composition in preeclampsia. They have actions, in cell culture experiments, which correlate with clinical features of the disease. In this heterogeneous condition, STB-EVs represent a potential feto-maternal signal with the complexity to produce different preeclampsia phenotypes in response to different syncytiotrophoblast stresses. This makes them an appealing candidate, alongside angiogenic proteins, for the link between placental disease (stage one) and maternal syndrome (stage two) in preeclampsia (Figure 1-1B). tRFs, as the predominant sRNA signal in STB-EVs, are yet to be explored as syncytiotrophoblast stress signals in preeclampsia.

1.2. tRNA fragments

In 1958 Francis Crick proposed the “Central Dogma of Molecular Biology”: that sequential information is transferred, residue-by-residue, between the polymers DNA, RNA and protein[53]. Translation describes the production of proteins at the ribosome, using information transferred from messenger RNA (mRNA). The canonical function of transfer RNA (tRNA) molecules is to carry amino acids to the ribosome[54]. tRNAs bind an amino acid specific to their 3-nucleotide anticodon, enabling accurate transfer of information. tRNAs demonstrate highly conserved morphology (Figure 1-2). They are typically around 76 nucleotides in length and are arranged in a four-leaf clover secondary structure, with three loops: the D-loop (dihydrouridine), anticodon loop and T-loop (thymidine). Their tertiary confirmation is an L-shape, with amino acid and T-loop on one arm and anticodon and D-loop on the other.

tRNA fragments (tRFs) were first reported in the urine of cancer patients in 1977[55]. They have become an intense focus for research following more recent reports of their regulatory activity. In early 2009, two groups in China and the USA reported cleavage of tRNA in response to cellular stress induced translational repression[56,57]. Since then tRF publications have increased exponentially, with data demonstrating conservation between species and implicating tRFs in the pathogenesis of diverse diseases[58].

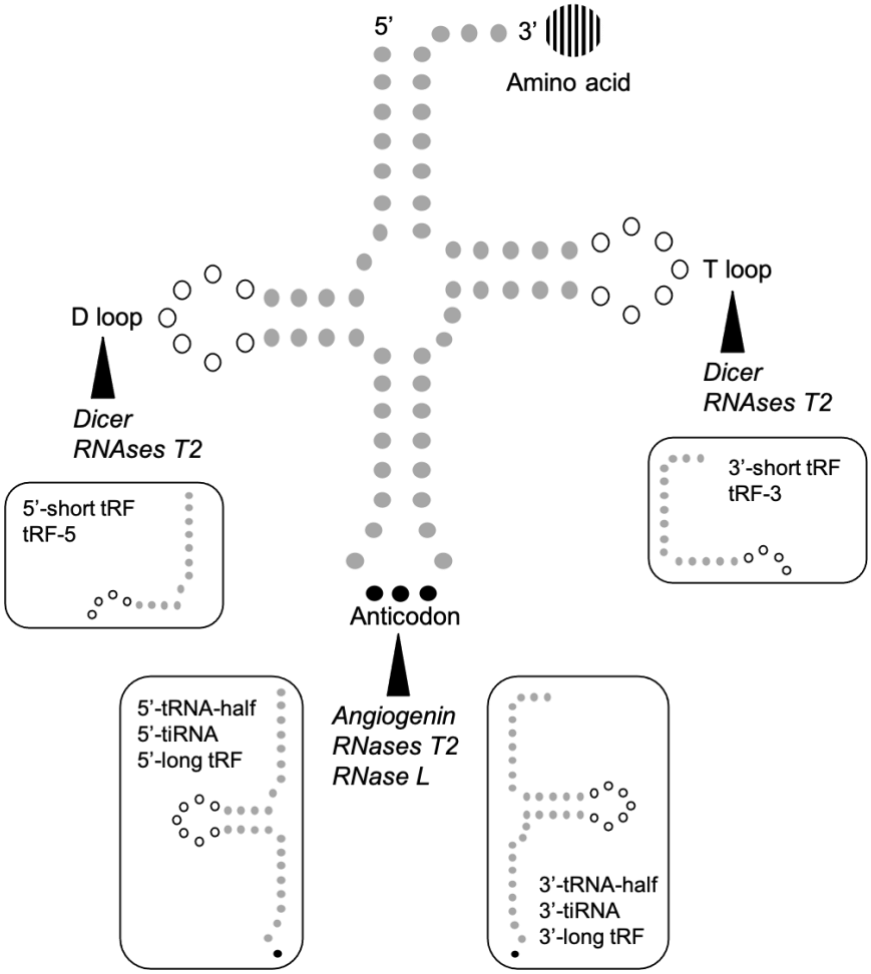


Figure 1-2 – Schematic diagram showing the secondary structure of a mature tRNA molecule and known cleavage sites to generate tRNA fragments.

1.2.1. Nomenclature, classification and diversity

As an emerging field, tRF biology falls victim to inconsistent nomenclature. tRFs are variably referred to as tRNA halves, tRNA-derived stress-induced RNA (tiRNA), tRNA-derived small RNA (tsRNA), tRNA-derived RNA (tDR or tdRNA) and, given sequence homology with piwi-interacting RNA (piRNA), tRNA-derived piRNA (td-piR)[59,60]. In this thesis the term tRF will be used to refer to any fragment of a mature tRNA, regardless of length.

tRFs are usually classified by their length and sequence alignment. For example, a 5'-tRF would align to the first or 5'- end of a whole tRNA. This leads to classification systems with equally variable nomenclature, summarised in the boxes within Figure 1-2. tRFs which align to the middle of a tRNA, excluding either end are referred to internal or i-tRFs[61].

There is significant redundancy in tRNA genetics. 20 amino acids are encoded by 64 anticodons. In humans, at least 429 genes encode the tRNA which contain these anticodons[62]. With multiple ribonucleases able to cleave tRNA in different locations, an even greater variety of tRFs are produced. No standardised system exists to refer to one specific tRF. Whereas miRNAs are now labelled by a universal miR-Base scheme, tRNA fragment labels are driven by the mapping database used, creating significant ambiguity[62–64]. Ultimately only the nucleotide sequence itself provides a complete description[59].

1.2.2. Biogenesis

Full-length tRNA are transcribed by RNA polymerase III to produce pre-tRNA, which have a 5'-leader and a 3-trailer[65]. During maturation, these sequences are cleaved by RNAse P and RNAse Z respectively. Seven percent of human tRNA genes contain introns; these

are spliced by the tRNA splicing endonuclease complex. Mature tRNA are modified after transcription; this facilitates folding but also modulates codon-anticodon interactions[65]. tRFs are produced by various enzymes which cleave mature tRNA, creating fragments of different lengths (Figure 1-2). Cellular stress drives tRF production; this includes hypoxia, oxidative stress, nutritional deprivation, arsenite, heat shock, hypothermia and irradiation[56,57,66]. Angiogenin, the most studied tRNA ribonuclease, cleaves at the anticodon loop in response to various stressors including hypoxia, irradiation heat shock, hypothermia and starvation[57]. Other enzymes including Dicer and RNases T2 can create shorter and longer fragments.

1.2.3. Biological activity

There is evidence that tRFs can regulate cellular function through a variety of mechanisms. These include influencing transcription, translation and epigenetic inheritance. Table 1-4 summarises seminal studies which advance novel mechanisms of tRF action. The specificity of these actions and the pleiotropism of tRFs have not been explored.

Action	Proposed mechanisms	Model cell line used	First report	Ref
Regulate transcription	Inhibit RNA polymerase II by preventing DNA template binding	Yeast	2014	[232]
Bind Argonaute proteins and regulate mRNA (miRNA-like)	Repress mRNA transcripts in a sequence-specific manner	Human B cells, HEK293 (kidney) cells, mice, *Drosophila*, *C. Elegans*, fungi, bacteria	2013	[233–235]
Regulate mRNA	Bind to 3'-UTRs in mRNA	Drosophila, A549 (human alveolar epithelial) cells	2015	[236,237]
	Displace target 3'-UTRs from YBX1 protein, silencing mRNA	MDA-MB-231 (breast cancer) cells	2015	[238]
Regulate translation	Bind to translation-initiation complex, displacing eiF4G	U20S (epithelial) cells	2011	[239]
	Bind to Argonaute proteins and inhibit translational machinery	Drosophila	2018	[235]
	Displaces mRNA from initiation complex at ribosome	Archaea	2017	[240]
Regulate ribosome synthesis	Part of pre-rRNA splicing complex	Tetrahymena	2012	[241]
	Bind ribosomal mRNAs to enhance their translation	HeLa (cervical), HCT-116 (colon), HEK293T (kidney) cells	2017	[242]
Regulate epigenetic inheritance	Facilitate DNA target methylation, inhibiting transcription	Human monocytes	2016	[60]
	Regulate histone production	Mouse embryonic stem cells	2020	[243]
	Unclear – changes F_1 offspring metabolism independent of DNA methylation	Mouse sperm	2016	[244]
Promote stress granule assembly	Bind YB-1 protein	U20S (epithelial) and MCF-7 (breast) cells	2010	[239,245,246]
Protect cells from apoptosis	Bind cytochrome *c* protein, inhibiting apoptosome formation in response to hyperosmotic stress	Mouse embryonic fibroblasts	2014	[247]
Trigger pro-inflammatory response	Bind to Toll-like receptor 7	Human monocyte-derived macrophages	2020	[76]

Table 1-4 – Seminal studies describing different mechanisms of tRF action

1.2.4. tRNA fragments in EVs

tRFs have been discovered within cells, bound to ribonucleoprotein complexes or packaged into EVs. Li *et al.* discovered that intra- and extra-cellular tRF profiles in response to cellular stressors were distinct[66]. Extracellular tRFs, isolated from EVs in this study, were predominantly 5'-tRFs.

1.2.4.1. tRNA fragments in EVs as biomarkers

A detailed systematic review has outlined numerous studies investigating the clinical significance of EV tRFs in different diseases[67]. Many of the referenced papers report the presence of tRFs in biofluid EVs from specific disease-states, but do not investigate further. Other studies investigate cell culture supernatants, or whole plasma/serum RNA[68–70]. Table 1-5 summarises and critiques relevant studies evaluating specific candidate tRFs isolated from biofluid EVs as non-invasive clinical biomarkers for different diseases.

EV isolation technique represents a strong source of variation between these studies. There is good evidence that EV tRF profiles change depending on the isolation approach used[71,72]. Three studies stand out for their strong methodologies, offering greater confidence in their findings. Meng *et al.* isolated plasma EVs from 23 paediatric patients with atopic dermatitis and 23 healthy controls[73]. They confirmed EV isolation by transmission electron microscopy. Samples were divided into separate discovery and validation cohorts, identifying 135 differentially expressed EV tRFs with RNA sequencing and validating two with quantitative polymerase chain reaction (qPCR). This allowed the authors to produce meaningful receiver-operative characteristic curves, finding an area under the curve (AUC) for one of their targets of 0.9. Lu and colleagues applied a similar methodology, comparing 10 colorectal cancer plasma EV RNA sequencing profiles to 10 controls to discover 25 differentially regulated tRFs[74]. These findings were validated using qPCR in a larger sample (n=39), producing AUC >0.80 for three targets. Wang *et al.* used

even larger sample sizes and more cohorts to investigate tRF plasma biomarkers in breast cancer patients[75]. tRF targets were identified from whole plasma screening of 8 cancer and 4 control patients. Thirty tRF targets were filtered to six by validation in a larger cohort of 144 cancer and 112 control samples using qPCR. These findings were verified externally in a cohort of 48 samples from a different hospital. Finally, differential plasma EV expression of two tRFs was validated in 24 cancer and 16 normal samples. The reproducibility of these tRFs across multiple samples, populations and sample types offers strong confidence in their validity.

Overall, Table 1-5 illustrates a range of diseases and biofluids where tRFs have shown promise as EV biomarkers. These studies provide a rationale for considering tRFs within circulating EVs as putative biomarkers in preeclampsia.

Disease	Biofluid	EV isolation technique	Sample size (disease/ control)	Number of DE tRF	tRF subtype	Critique	Ref
Breast cancer	Plasma	Exo-Quick™ (System Biosciences, USA)	24/16 (validation of discoveries from 316 whole plasma samples)	2	5'-halves	-	[248]
Cervical cancer	Plasma	Exo2D™(Exosome Plus, Korea)	30/12	474	Not specified	None validated – low sensitivity	[249]
Colon cancer	Plasma	Ribo™ Exosome Isolation Reagent (Ribobio, China)	10/10 discovery, 20/19 validation	25, 2 validated in external samples	Not specified	-	[74]
Hypopharyngeal carcinoma	Plasma	Ultracentrifugation	5/5	55, 3 validated with qPCR	Two 5'-halves, one 3'-tRF	Small sample size, internal validation only	[250]
			30 (disease only, comparing clinical features)	1 correlated with tumour stage and differentiation	5'-half	No validation	
Liver cancer	Plasma	Total exosome isolation kit (Invitrogen, USA)	5/5	46, 4 validated with qPCR	Three 5'-halves, one 3'-tRF	Disease poorly defined, no data regarding possible confounders, internal validation only	[251]
Pancreatic cancer	Serum	Exo-Quick™ Ultra (System Biosciences, USA)	2/2	5	Not specified	Very small sample size, no external validation	[252]
Atopic dermatitis	Plasma	Exo-Quick™ (System Biosciences, USA)	3/3 discovery, 20/20 validation	135 discovered, 2 validated in second cohort	5'-half and i-tRF	Small discovery cohort	[73]
Chronic kidney disease	Urine	Ultracentrifugation	15/10	2	5'-halves	No validation, EV not characterised	[253]
Chronic obstructive pulmonary disorder	Plasma	Plasma exosome purification kit (Norgen Biotek, Canada)	8/6	5	Not specified	Small sample size, no external validation	[254]
Osteonecrosis of femoral head	Plasma	Exo-Quick™ (System Biosciences, USA)	3/3	223, 3 validated with qPCR	Not specified	Internal validation only	[255]
Osteoporosis	Plasma	Exo-Quick™ (System Biosciences, USA)	40/40	29 discovered, 3 validated with qPCR	3'-tRF	Internal validation only (same cohort)	[256]
Successful sperm extraction	Plasma	Umibio exosome isolation kit (Umibio, China)	18/12	24, 2 validated by qPCR	Not specified	No external validation	[257]

Table 1-5 – Studies evaluating specific biofluid EV tRFs as non-invasive biomarkers for disease

1.2.4.2. tRNA fragments in EVs as signalling molecules

In addition to biomarker potential, data suggest differential EV tRF expression may contribute to disease pathophysiology.

tRFs 3022b and 3030b are upregulated in colorectal cancer plasma EVs. Inside colorectal cancer cells they associate with macrophage migration inhibitory factor and galectin 1, in turn modulating cancer cell apoptosis and macrophage polarisation[74]. This suggests EV tRFs might represent a cancer promoting signal within the tumour microenvironment, as well as spilling into the circulation.

Human macrophages release 5'-tRNA^{HisGUG} half packaged in EVs when infected with tuberculosis[76]. These EV tRFs are delivered to endosomes in neighbouring macrophages, triggering a pro-inflammatory response which is dependent on Toll-like receptor 7. Similarly, T cell activation induces release of specific 5'-tRFs (Leu-TAA and Leu-TAG) in EVs[77]. Antisense oligos against these tRFs enhanced T-cell activation, implicating EV 5'-tRFs as autocrine negative feedback signals.

These three studies, suggesting EV tRFs contribute to cancer and immune responses at a molecular level, justify the investigation of STB-EV tRFs as possible signalling molecules in preeclampsia.

1.3. Research rationale and hypotheses

Preeclampsia remains a leading cause of maternal and perinatal morbidity and mortality. Improvement to clinical care in preeclampsia is hampered by a paucity of accurate biomarkers and a limited understanding of disease pathophysiology. In the latest models, syncytiotrophoblast stress is considered a common step between subtypes of preeclampsia. STB-EVs, as complex bioactive particles, represent a strong candidate for the link between placental disease and maternal symptoms in preeclampsia.

The majority of sRNA in healthy STB-EVs are tRFs. tRFs are released in extracellular vesicles in response to stress. tRFs appear to be disease biomarkers in various contexts. tRFs can regulate cellular function by influencing transcription, translation and epigenetic inheritance. EV tRFs are known to contribute to disease pathophysiology.

I hypothesise that syncytiotrophoblast stress in preeclampsia may lead to differential expression of tRFs in STB-EVs. If exported into the maternal circulation, I suggest STB-EV tRFs may represent a useful non-invasive biomarker of preeclampsia. I speculate that differential expression of STB-EV tRFs may play a role in preeclampsia pathogenesis, influencing distant cellular function and representing a novel mechanism of feto-maternal signalling. I propose to limit this investigation to early-onset preeclampsia as the most homogenous (and severe) subtype currently recognised.

1.4. Thesis aims

1. Characterise tRFs in perfusion-derived STB-EVs in normal pregnancy and early-onset preeclampsia
2. Investigate syncytiotrophoblast tRFs in the maternal circulation
3. Evaluate tRFs as blood biomarkers in preeclampsia
4. Explore functional activity of STB-EV tRFs in preeclampsia dysfunctional cells, namely endothelial cells, macrophages and monocytes

Chapter 2. Characterisation of tRNA fragments in perfusion-derived syncytiotrophoblast extracellular vesicles in normal pregnancy and early-onset preeclampsia

2.1. Introduction

2.1.1. Small RNA in healthy syncytiotrophoblast extracellular vesicles

In 2019, we were the first to report that 5'-tRNA fragments (5'-tRFs) are the predominant small RNA (sRNA) in syncytiotrophoblast-derived extracellular vesicles (STB-EVs) in healthy pregnancy[52]. We perfused six healthy, term placentas, separating STB-EVs from maternal perfusate by ultracentrifugation. Our data demonstrated that tRNA species represent >95% STB-EV sRNA. We found most reads aligned to only the first or 5'-half of tRNA molecules. This finding was corroborated using reverse transcription quantitative polymerase chain reaction (RT-qPCR). We found one of the most abundant STB-EV 5'-tRFs inhibited protein synthesis in fibroblasts. We speculated that STB-EV 5'-tRFs may play a role in feto-maternal signalling, in both health and disease.

At the time this research was conducted, a number of bioinformatic challenges limited our ability to explore STB-EV tRF biology further. Databases for tRF annotation such as MINTmap and GtRNAdb were only just emerging[62,64]. sRNA sequencing workflows had not been adapted to the specific challenges that tRFs present. Our analysis identified a list of tRNA anticodons, fragments of which were upregulated in STB-EVs, compared to their tissue of origin (placenta). However, we could not easily identify specific 5'-tRF sequences, making it difficult to validate these fragments or use them in functional studies.

There is significant redundancy in tRNA genetics. The canonical function of tRNA is to decode messenger RNA at the ribosome during the translation reaction, matching each of the 20 amino acids to their respective tri-nucleotide codon. However, with four potential nucleotides able to occupy each of the three spaces in a codon, this results in 4^3 (64) different codons. Thus, multiple "synonymous" codons encode for the same amino acid. Their corresponding tRNAs, which carry the same amino acid but with different codons, are named tRNA isotypes or iso-acceptors. The redundancy continues further, as the

human genome contains at least 429 different tRNA genes[62]. This results in iso-decoders: tRNA molecules with different sequences which encode the same anticodon. Thus, the list of tRNA anticodons we generated in our published analysis could represent a number of underlying tRNA sequences. This made the design of both specific qPCR assays to corroborate our discovery, and synthetic oligonucleotides to investigate STB-EV tRF functions, impossible.

Coverage plots for all tRNAs in our published analysis demonstrated most reads were 5'-tRFs cleaved around 32 nucleotides. However, the start and end nucleotide for each tRF within the tRNA molecule was also lost as a consequence of fragment annotation. Even if we could confine our work to unique STB-EV tRNA molecules without iso-decoders, the fragment within that unique sequence remained unclear.

Consequently, the first aim of this chapter was to fully characterise the tRNA fragments which are expressed within STB-EVs in normal pregnancy, utilising the latest advances in tRF sequencing analysis. This is reflected in Hypothesis 2.1.

2.1.1.1. Hypothesis 2.1

Specific 5'-tRFs are packaged into STB-EVs in healthy pregnancies at term.

2.1.2. Small RNA in preeclampsia syncytiotrophoblast extracellular vesicles

Trophoblast cells in culture release tRFs packaged in EVs in response to stress[66]. Preeclampsia is characterised by stress in the syncytiotrophoblast (see 1.1.5)[7]. This led to Hypothesis 2.2.

2.1.2.1. Hypothesis 2.2

STB-EV tRF expression changes in early-onset preeclampsia.

2.1.3. Preparation of syncytiotrophoblast extracellular vesicles

In theory, the most physiological approach to study STB-EV sRNA would be isolation from maternal blood. No compelling technique has yet been reported to separate STB-EVs from the other more abundant contaminating particles in plasma[78]. Chapter 3 summarises publications in this field and describes optimisation of a technique for this purpose in more detail. In the absence of satisfactory blood-derived preparations, three approaches to prepare STB-EVs are described in the literature.

The first technique was reported in 1974 and modified to its present form in 1993[38,79]. Villous tissues from the placenta are isolated, minced and mechanically stimulated with a magnetic stirrer in sodium chloride solution for 30 minutes. The solution is centrifuged at slower speeds to remove cellular debris, and using an ultracentrifuge at higher speeds to separate EVs, referred to as mechanically-derived STB-EVs. This approach results in significant contamination of STB-EVs with other placental cell membranes and intracellular organelles[80].

The second approach is to grow placental explants. Placental villous tissues are dissected, washed and cultured in inserts within culture plates[81]. STB-EVs are isolated by centrifugation from the culture medium. Whilst apparently more physiological, continuing to culture the syncytiotrophoblast for some days after delivery has significant shortcomings as a model. One paper studied term placental explants for 11 days in culture, using electron microscopy alongside a number of functional assays[82]. The authors demonstrated that the existing syncytiotrophoblast degenerates by apoptosis over the first few hours; a new syncytiotrophoblast layer forms approximately two days after explant preparation.

The third approach is to separately perfuse the maternal and fetal circulations of a recently delivered placenta with oxygenated medium for three hours[83]. STB-EVs are isolated by centrifugation of the perfusion medium[84].

A comparison of these three approaches discredited mechanical STB-EVs as biologically different particles, which were not physiological in view of their apoptotic effect on endothelial cells[85]. The validity of explants is questionable if the terminally differentiated syncytiotrophoblast apoptoses and regenerates in culture. Placental perfusion has led to the discovery of several disease-dysregulated STB-EV proteins, which have been successfully validated in maternal plasma[42,45,86]. Thus, I chose to pursue placental perfusion as a model to study STB-EV sRNA, considering it to be the closest *ex-vivo* mimic to the living placenta.

2.1.4. Approaches to differential expression analysis of small RNA

Once STB-EV RNA is isolated and sequenced, samples from different sources can be compared to determine differential expression of specific RNA fragments. sRNA sequencing and differential expression analysis, specifically seeking tRFs, presents a number of challenges.

Some tRF reads can be lost at the stage of adapter ligation. Angiogenin, one of the ribonucleases which generates tRFs, leaves a 2',3'-cyclic phosphate (cP) at the 3' end of the tRF[87]. Conventional RNA sequencing adapters ligate only to 3'-hydroxyl groups, meaning cP-tRNAs are not captured[88].

tRNAs are also heavily modified after transcription. Despite successful adapter ligation, these modified nucleotides (e.g. 1-methyladenosine) can cause reverse transcriptase to prematurely terminate the complementary DNA (cDNA) molecule, hiding these fragments from the sequencing dataset[89].

Analysis of tRF sequencing data poses unique bioinformatic challenges. tRNA database selection is important. Given the complexity of tRNA sequences in the human genome, a large database is required to minimise unmapped reads. Additionally, tRNA fragments can be generated by either cleaving mature tRNA molecules or pre-tRNA molecules. It is important to select a database which includes fragments of both origins. Finally, if tRFs are mapped only against full-length tRNA molecules, two halves of a fragmented tRNA can create two counts for one molecule, biasing results.

Large proportions of individual tRNA molecules are highly conserved, with some only differing by a few nucleotides[89]. This is especially true of iso-decoders. Consequently, tRF reads often map to multiple tRFs and it is impossible to uniquely identify their originating full-length locus. Many RNA sequencing (RNAseq) annotation tools only include uniquely mapped reads when quantifying (e.g. FeatureCounts), which can lead to massive data loss in tRF analysis[90]. However, careful strategies are required to avoid counting reads against each of their potential annotations, falsely increasing read counts.

tRFs are short reads; this results in more frequent unmapped reads. Strict annotation rules (such as not allowing mismatches) are often implemented to avoid inappropriately over-mapping short reads to multiple loci within the genome. This conservative approach can instead result in under-mapping; unmapped reads are usually disregarded in differential expression analyses.

In this chapter I have applied two sRNA sequencing analysis tools to the sequencing data obtained by placental perfusion. To increase confidence in the results, I optimised qPCR assays to validate a selection of identified targets as well as comparing my findings to an independent analysis of the same dataset conducted by collaborators (Appendix 1).

2.2. Methods

2.2.1. Ethical approval, sample acquisition and disease definition.

This project was approved by the Central Oxfordshire Research Ethics Committee (07/H0607/74 and 07/H0606/148). Participants for placental donation were identified from inpatient wards and elective caesarean section operating lists and provided informed, written consent. All placentas were obtained at the time of caesarean section and perfused within 10 minutes of delivery. Preeclampsia was defined using the International Society for the Study of Hypertension in Pregnancy (ISSHP) classification; diagnostic thresholds are shown in Table 1-2[1]. Full demographic data including relevant confounders were recorded and are presented.

2.2.2. Dual-lobe placental perfusion, EV and RNA isolation, library preparation and sequencing

Placental perfusion and sequencing were carried out by a team of scientists in our group, before I began my DPhil. Their methods are described in detail in previous publications, but are recapitulated here in brief[84,91]. An individual placental lobule was identified and the fetal circulation cannulated and perfused at 5 ml/min (see Figure 2-1). The maternal surface of the placenta was perfused from a separate circulation at 20 ml/min. M-199 tissue culture medium was used with L-glutamine, 0.8% Dextran 20, 0.5% BSA, 5000 U/L heparin, 2.75 g/L sodium bicarbonate, pH 7.4. Medium and placenta were kept at 37°C and medium oxygenated with 95% oxygen and 5% carbon dioxide. The lobule was perfused for 20 minutes discarding the outflow, before the circuit was closed for 3 hours. Placental biopsies were taken from the maternal surface of the placenta, aiming to incorporate majority syncytiotrophoblast (i.e. the cell of STB-EV origin).



Figure 2-1 – Photograph depicting experimental setup for dual lobe placental perfusion

Cellular debris was removed from the maternal perfusate by centrifuging twice at 1500 *g* for 10 minutes at 4°C. The supernatant was centrifuged at 10 000 *g* for 30 minutes at 4°C to isolate medium-large EVs (MLEVs). MLEVs are an EV subtype defined by ISEV as >200 nm diameter[37]. The pellet was washed with phosphate-buffered saline (PBS), then centrifuged under the same conditions again to minimise soluble protein isolation.

The 10 000 *g* supernatant was filtered through a 0.22 µm filter then centrifuged at 150 000 *g* for 2 hours at 4°C to isolate small EVs (SEVs). SEVs are defined by the International Society for Extracellular Vesicles (ISEV) as <200 nm diameter[37]. This pellet was also washed again in PBS. All pellets were stored at -80°C before further analysis. EV fractions were characterised by electron microscopy, Nanoparticle Tracking Analysis, bicinchoninic protein assay and Western blotting as previously published[42,52].

RNA was isolated using Total RNA Purification Plus Kit (Norgen Biotek Corporation, Canada) following manufacturer's instructions. RNA size and integrity were confirmed using Nanodrop™ ND-1000 (ThermoFisher, UK) and Agilent 2100 Bioanalyzer Pico kits (Agilent, Germany). 250 ng of total RNA was used for sRNA library preparation, using the NEBNext Multiplex Small RNA library preparation kit (New England Biolabs, USA) following manufacturer's instructions. This process ligates Illumina adapters (Illumina, USA) to the 3' and 5' ends of RNA fragments, reverse transcribes these fragments to cDNA and amplifies them by polymerase chain reaction. Libraries were size selected for fragments <50 nucleotides (nt). Library size and concentration were confirmed using High Sensitivity D1000 ScreenTape (Agilent, Germany). Single-end sequencing was undertaken using a HiSeq 2500 instrument (Illumina, USA) in rapid mode.

2.2.3. Bioinformatic approaches

For single-end sequencing, each sample generated a *.fastq* file containing all of the reads from the sample. Each read consisted of four lines: 1) a sequence identifier with

information about the run; 2) the sequence itself with base calls A, C, T, G and N for unknown or uncalled; 3) the base call quality score (also known as Phred-score), Q, which is empirically determined from observed parameters during sequencing; 4) a separator from the preceding read (+)[92]. The industry standard is to exclude Q scores <30, corresponding to 1 in 1000 calls being in error[93]. I assessed the quality of the raw reads by using FastQC to extract quality data and descriptive metrics from the *.fastq* files[94]. Outputs were aggregated using MultiQC, a tool designed to summarise the output from multiple bioinformatic analyses[95].

Illumina adapters were trimmed and low-quality reads removed using Trimmomatic V0.32 in single end mode[96]. The ILLUMINACLIP function was used to compare short sections of each Illumina adapter (known as a seed, ≤16 bp) in each possible position within reads. If ≤2 mismatches were identified, the alignment between read and adapter was scored. Alignment score was calculated by adding 0.6 for each matching base and subtracting one tenth of the base matching quality score for each mismatch. This approach reduced the impact of a mismatch which is called with low certainty by the sequencer. A perfect match of a 12 base sequence would score 7.2 and a perfect match of a 25 base sequence would score 15. I chose to trim adapters reaching the lowest recommended alignment score threshold of 7, aiming to minimise data loss. The SLIDINGWINDOW function was used to trim low quality reads. This function started at the 5' end of each read and was set to terminate any reads where the average quality score (Q) over four bases fell below 28. Again, these settings were chosen to minimise data loss whilst keeping within accepted standards. Trim efficacy was confirmed by repeating FastQC analysis. Fragment size profiles were obtained from FastQC analysis of trimmed reads.

In view of the reported discovery that the majority of sRNA are 5'-tRFs[52], the tRNA Analysis of eXpression (tRAX) software package was initially used to annotate and count fragments, as well as interrogate base coverage[89]. tRAX was unable to use previously

trimmed RNAseq files, so raw data were used and the tRAX package removed adapters using Cutadapt[97]. tRAX aligned reads to a reference database built from GtRNAdb2.0 and the hg38 reference genome from UCSC Genome Browser using Bowtie2[62,98,99]. Read coverage statistics produced by this analysis included A) normalised read counts of sRNA types per sample, used to generate mapping figures and B) read coverage summary of tRNA isotypes per sample.

tRAX was used to perform differential expression analyses of annotated sRNA reads between groups of samples. tRAX employs DESeq2, one of the most widely used RNAseq differential expression packages[100]. DESeq2 estimates the dispersion of annotated fragment expression levels from replicate samples in each group. Dispersion reflects the relationship between mean and variance. In RNAseq data the variance is often greater than the mean, referred to as over-dispersed. Consequently, dispersion estimates are shrunk towards mean values, allowing for accurate identification of differentially expressed genes despite small sample sizes. Dispersion estimates are then fitted to a negative binomial distribution model for each fragment. Hypothesis tests are performed to determine whether each model coefficient differs significantly from zero. The Wald test is used for these tests, with a Benjamini and Hochberg correction for multiple testing. Only fragments with normalised counts for both groups >0 and $p<0.05$ were considered.

A second package written to analyse differential expression of unique sequences (DEUS) was also used[101]. DEUS enables differential expression analysis of fragments with reference to their sequences, rather than their annotations. Source sequencing files (*.fastq*) were trimmed with Trimmomatic as described above. DEUS functions were used to perform the following steps:

1) Create a count table for all unique sequences;

2) Assign a unique identifier to each unique sequence;

3) Run a DESeq2 differential expression analysis to compare groups of samples, adjusting for multiple hypothesis testing by Independent Hypothesis Weighting;
4) Annotate fragments against a MINTmap FASTA file[64];
5) Compute mean and standard deviation of normalised counts for each group;
6) Merge the results.

During optimisation of the analysis, annotation with MINTmap and GtRNAdb2.0 were compared as the two leading tRNA fragment databases, which have different naming conventions. MINTmap resulted in fewer unmapped sequences than GtRNAdb2.0, so was chosen as the best available mapping solution.

2.2.4. tRNA fragment detection with quantitative PCR

2.2.4.1. RNA isolation

RNA was isolated from 180 µg perfusion STB-EVs using Trizol LS (ThermoFisher, UK). Samples were diluted to 250 µL in PBS and lysed in 750 µL Trizol LS by vortex and 5 minute incubation. 2.5 µL bacteriophage carrier RNA (#10165948001, Roche, Basel, Switzerland) was added to improve yield. 200 µL chloroform was added and samples were vortexed then centrifuged at 12 000 *g* at 4°C in phasemaker tubes (ThermoFisher, UK) for phase separation. The aqueous phase was removed and 1 µL RNAse-free glycogen added as a carrier (#10901393001, Roche, Switzerland). RNA was precipitated by adding 500 µL isopropanol, vortexing and incubating for 10 minutes. Aqueous supernatant was removed by centrifugation at 12 000 *g* for 10 minutes at 4°C and the RNA was washed twice in 1 mL 75% ethanol, pelleting between by centrifugation at 7500 *g* for 5 minutes at 4°C. RNA pellets were air dried at room temperature for 15 minutes, then resuspended in 20 µL RNAse-free water. RNA quantity and quality was assessed by Nanodrop™ spectrophotometry (ThermoFisher, UK) and Agilent RNA 6000 Pico analysis using BioAnalyzer (Agilent, Germany). All RNA samples were diluted to 9.3 ng/µL using BioAnalyzer concentrations. RNA was aliquoted and frozen at -80°C.

2.2.4.2. RNA quantification

tRNA fragments from our analysis (30-35 nt) are difficult to detect using reverse transcription quantitative polymerase chain reaction (RT-qPCR) as they do not have sufficient length for amplification by conventional primers (20 nt each for forward and reverse primers). Additionally, tRFs can differ from each other by just one nucleotide requiring a high degree of assay specificity. Similar problems exist when detecting miRNAs (20-22 nt); stem-loop assays were developed to overcome this[102].

Stem-loop reverse transcription primers bind to target RNA with high specificity despite a short complementary sequence (Step 1, Figure 2-2)[103]. This is attributed to the spatial constraints related to the 3D structure of the primers. Base-stacking within the stem is thought to enhance the thermal stability of the primer-target complex. Reverse transcriptase then creates a longer first strand cDNA, which can be amplified in a PCR reaction using conventional forward and reverse primers (Step 3, Figure 2-2). The PCR product can be quantified by probes complementary to a region in the target sequence first strand cDNA, which fluoresce when hydrolysed by the advancing DNA polymerase (Step 5, Figure 2-2). Empirical work has demonstrated stem-loop primers can differentiate miRNA targets which differ by a single nucleotide with a high degree of specificity[103].

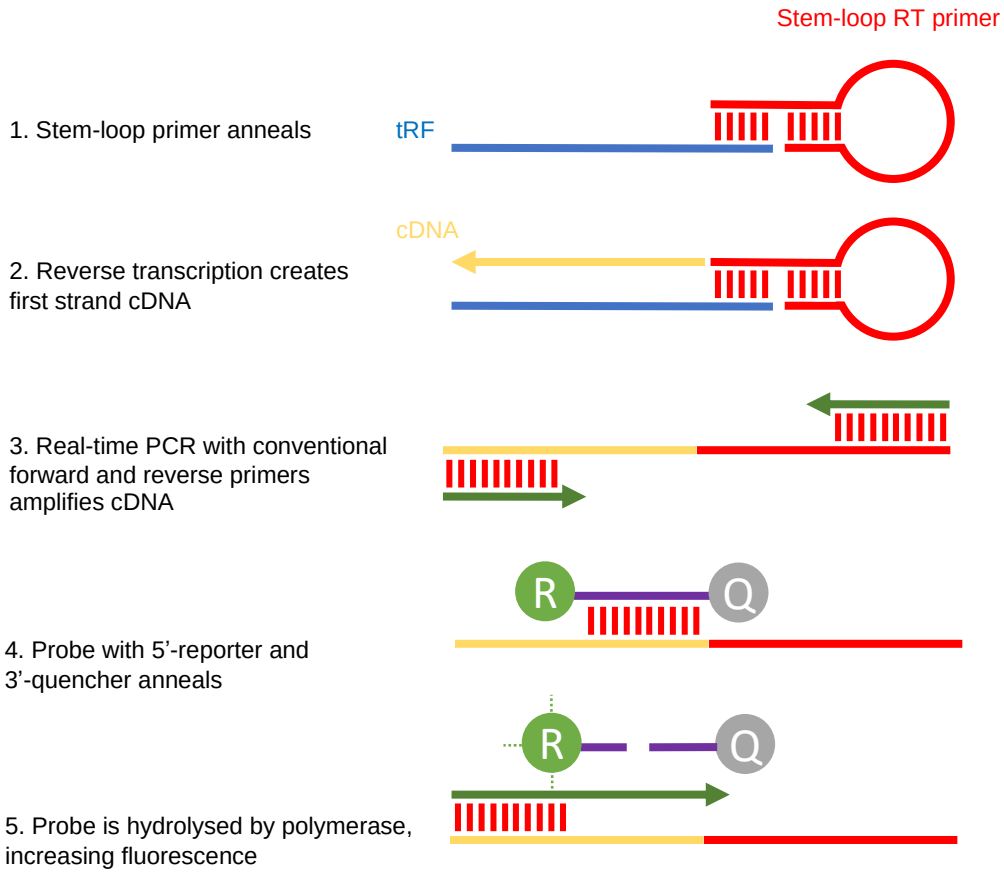


Figure 2-2 – Schematic diagram of steps involved in quantifying sRNA using stem-loop reverse transcription qPCR assays

I purchased stem-loop assays against specific target RNA sequences identified from the DEUS analysis of preeclampsia MLEVs as Custom TaqMan™ Small RNA Assays (#4398987, Applied Biosystems, USA). The target sequences/assay numbers are shown in Table 2-1; the specific primer sequences are proprietary.

tRF reverse transcription (RT) reactions were carried out using TaqMan® MicroRNA Reverse Transcription Kit (#4366596, Applied Biosystems, USA), according to manufacturer's instructions. For each target, STB-EV RNA was diluted 1 in 100 and 5 µL was loaded into 200 µL tubes. 7 µL reverse transcription master mix was added to each tube alongside 3 µL specific tRF stem-loop primer. The 15 µL reactions were incubated in a QIAamplifier 96 thermal cycler (Qiagen, Germany) at 16°C for 30 minutes, 42°C for 30 minutes, 85°C for 5 minutes and then cooled to 4°C.

Reference gene reverse transcription reactions were carried out in parallel. For each target, 5 µL undiluted STB-EV RNA was loaded into a universal reverse transcription reaction with 15 µL RT master mix using the High Capacity cDNA Reverse Transcription Kit (Applied Biosystems, USA). 20 µL reactions were incubated in a QIAamplifier 96 thermal cycler at 25°C for 10 minutes, 37°C for 2 hours, 85°C for 5 minutes and then cooled to 4°C. cDNA was then diluted by adding 5 µL nuclease-free water to each tube.

Target mRNA and tRF expression were quantified on two qPCR instruments: QuantStudio™ 3 or QuantStudio™ 7, depending on availability (Applied Biosystems, USA). Results from both were confirmed to be comparable (Figure 2-20), and data were only ever compared within a single qPCR plate to avoid confounding from inter-plate or inter-instrument variation. Fast Advanced Master Mix (#4444557, Applied Biosystems, USA) and fast thermal cycling conditions were used (20 seconds 95°C, 40 cycles of 1 second 95°C and 20 seconds 60°C with data collected for 6-carboxyfluorescein [FAM] green during the 60°C phase). Reference genes were quantified using TaqMan™ Assays

Hs00188166_m1 (*TBP*), Hs01122445_g1 (*YWHAZ*) and Hs00188166_m1 (*SDHA*). tRFs were quantified using hydrolysis probes corresponding to custom stem-loop primers (Table 2-1). Quantification cycles (Cq) were determined automatically by instrument-associated software using standard settings. qPCR efficiency for each reaction was extrapolated using linear regression during the log-linear amplification phase[104,105]. Mean qPCR efficiency for each assay was calculated. Relative expression was determined by following the Pfaffl approach, using *TBP* as a reference gene in light of optimisation data (Table 2-14)[106]. The reaction efficiency was raised to the power of the negative Cq value. Target values were normalised against the reference gene for the corresponding sample and then returned to one by dividing by the mean value for the control condition (in this case normal STB-EVs).

Two-tailed unpaired Mann-Whitney tests were performed on normalised relative expression data in view of the small sample size. Statistical analyses and figures were generated using Prism9 (GraphPad, USA).

Thesis identifier	DEUS identifier (rank)	Collaborator identifier (rank)	Length	Assay #	Target Sequence
F	seq_12 (1)	Glu-CTC-1-1 (5)	33	CT2W736	TCCCTGGTGGTCTAGTGGTTAGGATTCGGCGCT
G	seq_46 (3)	Glu-CTC-1-1 (14)	33	CT322N3	TCCCTGGTGGTCTAGTGGTTAGGATTCGGCGCC
H	seq_177 (19)	Glu-TTC-2-1 (55)	33	CT47V9Z	TCCCACATGGTCTAGCGGTTAGGATTCCTGGTT
J	seq_29 (8)	CysGCA-4-1 (38)	31	CT9HJEV	GGGGGTATAGCTCAGTGGTAGAGCATTTGAC
S	seq_184 (28)	Gly-GCC-2-1 (74)	33	CTXGREZ	GCATTTGTGGTTCAGTGGTAGAATTCTCGCCTG
T	seq_166 (29)	His-GTG-1-1 (91)	34	CTYMJYX	GCCGTGATCGTATAGTGGTTAGTACTCTGCGTTG
W	seq_1055 (97)	Unmatch (95)	32	CTRWE4F	CCCCTGTGGTCTAGTGGTTAGGATTCGGCGCC

Table 2-1 – Target tRF sequences

Includes thesis, DEUS and collaborator identifiers and abundance ranks, manufacturer assay number and target sequence

2.3. Results

2.3.1. Small RNA sequencing of normal pregnancy samples

2.3.1.1. Demographics

Normal pregnancy placentas were obtained from women with otherwise low-risk pregnancies undergoing elective caesarean section for an indication unrelated to preeclampsia, e.g. breech presentation. These placentas were delivered at a median gestational age of 39.2 weeks with median blood pressure 132/74 (Table 2-2). All were from primiparous women and the median birthweight (3775 g) was normal.

	Normal (n=6)
Median maternal age (IQR) – years	34.5 (30.5-38.75)
Median pre-pregnancy BMI (IQR)	27 (20.8-33.8)
First pregnancy – no. (%)	0 (0)
Diabetes – no. (%)	0 (0)
Essential hypertension – no. (%)	0 (0)
Current smoker – no. (%)	0 (0)
Male fetus – no. (%)	4 (67)
Median birthweight (IQR) – g	3775 (3419-4090)
Median gestational age at delivery (IQR) – weeks	39.2 (38.8-40)
Median highest recorded SBP (IQR) – mmHg	132 (113-135)
Median highest recorded DBP (IQR) – mmHg	74 (64-75)

Table 2-2 – Demographic data for women donating placentas from normal pregnancies. Continuous variables are described using median and interquartile range (IQR). Categorical variables are described using number (no.) and percentage (%). Other abbreviations used: body mass index (BMI), systolic blood pressure (SBP) and diastolic blood pressure (DBP).

2.3.1.2. Quality assessment

Raw sequencing data demonstrated that all samples contained sequences of a single length (51 bp), consistent with the single-end sequencer read length. Read depth ranged from 7.6E6 to 13.0E6 reads per sample (Figure 2-3A). Mean quality scores were >30 with very low per-base N (uncalled) content (Figure 2-3C, E). Adapters were present (Figure 2-3G). After removal of adapters and low-quality reads, FastQC confirmed no samples were found with any adapter contamination >0.1%. Whilst read depth and quality scores were unchanged (Figure 2-3B, D), all N reads were removed (Figure 2-3).

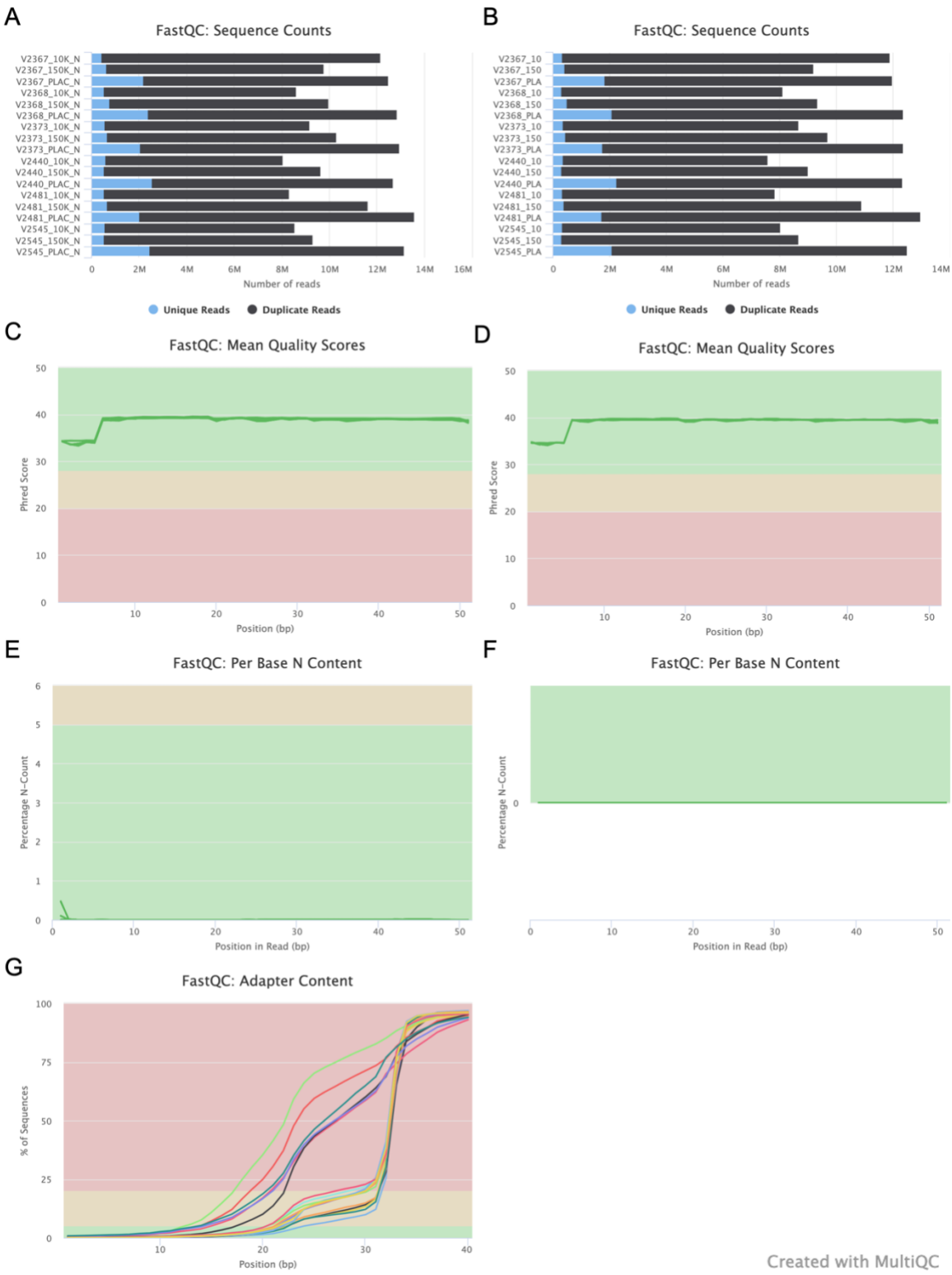


Figure 2-3 – Quality control data for normal pregnancy samples.

A, C, E, G represent summary data from raw reads

B, D, F represent summary data after removal of adapters and low-quality reads

Panels displayed together for comparison; reproduced as larger figures in Appendix 2.

2.3.1.3. Size distribution, mapping and base coverage

After removal of adapters and low-quality reads, a previously reported striking finding was replicated: the majority of reads in MLEVs and SEVs were 30-35 nt in length (Figure 2-4A, B)[52]. This was in contrast to placental samples, where a peak at 22 nt was the most abundant (Figure 2-4C).

Fragments were mapped to hg38 and GtRNAdb2.0 using tRAX software, demonstrating median 2.9% unmapped fragments (range 1.2 – 5.1%). The majority of fragments in SEVs (minimum 86.7%) and MLEVs (minimum 82.3%) mapped to tRNA species (Figure 2-4D, E). This was in contrast to placental tissue where maximum 19.3% reads mapped to tRNA species (Figure 2-4F).

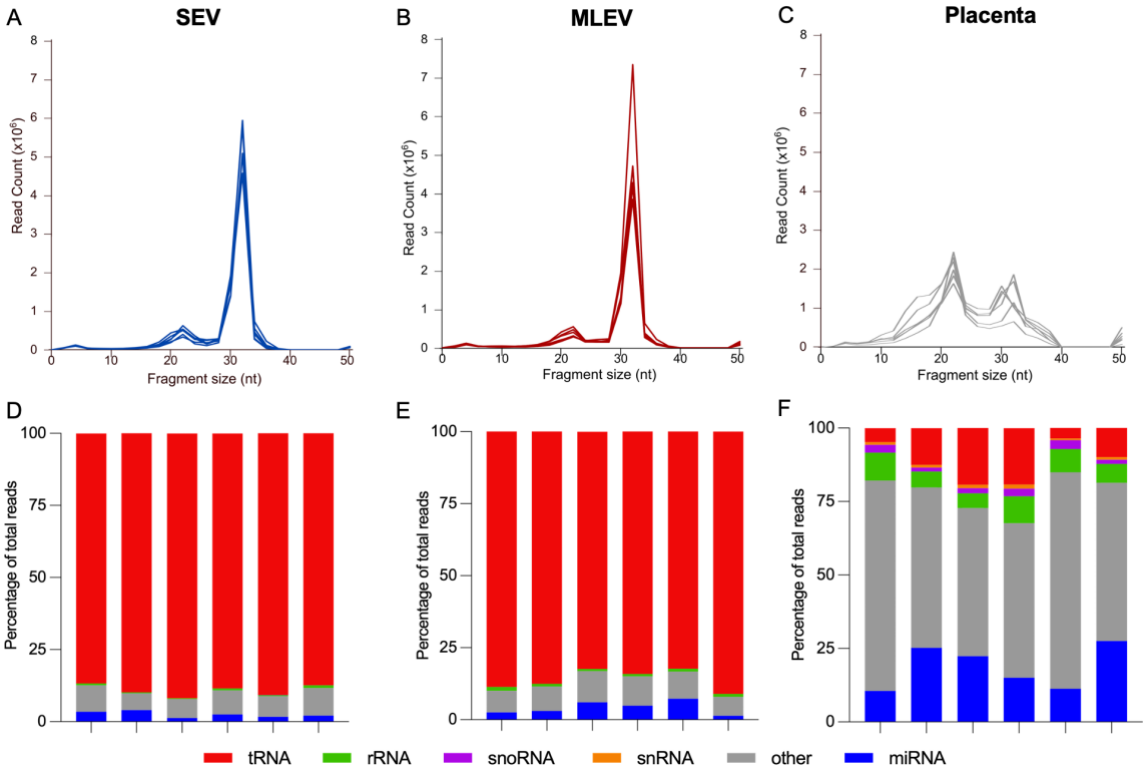


Figure 2-4 – Size distribution (A-C) and mapping (D-F) of sRNA fragments in normal pregnancy samples after removal of adapters and low-quality reads.

Y axis in A-C displays absolute read count; mapping data in D-F expressed as a percentage of mapped fragments.

When tRNA read counts are displayed by nucleotide position, it is apparent that the majority of tRNA species in SEVs and MLEVs are represented by only the first or 5' half of a tRNA fragment (5'-tRF) (Figure 2-5).

Together these data provide evidence to support the previously reported conclusion that the majority of sRNA in normal pregnancy STB-EVs are 5'-tRFs[52].

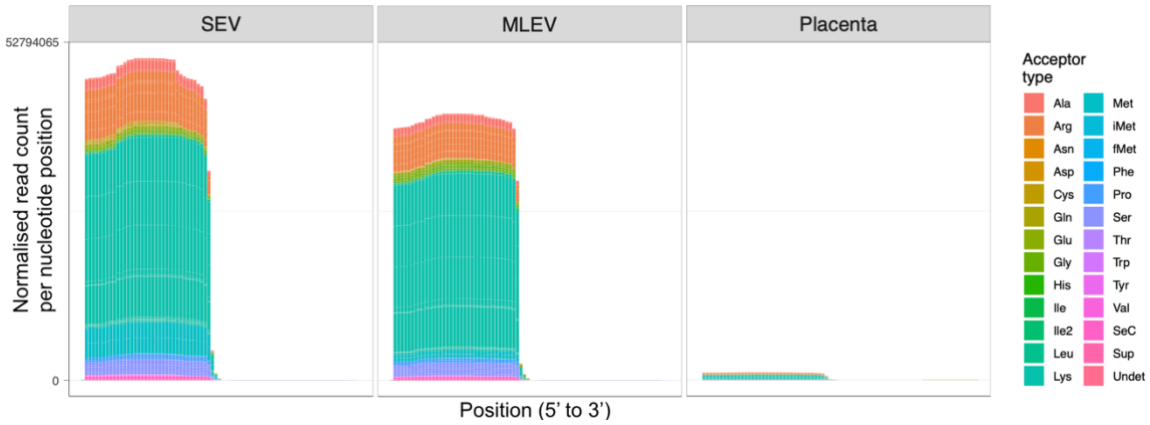


Figure 2-5 – Base coverage of tRNA fragments in normal pregnancy samples, stratified by iso-acceptor.

Y axis displays normalised read count per nucleotide position. X axis displays nucleotide positions for each tRNA fragment from 5' to 3'. Colours represent tRNA iso-acceptor type.

2.3.1.4. Differential expression analysis using tRAX

Previous analysis of tRNA fragments in STB-EVs had compared EV fractions to placental tissue, reporting the most abundant differentially expressed tRNA fragments by codon and amino acid[52]. The specific fragments involved, and their sequences, had not been reported, making validation with qPCR and downstream functional work impossible. I aimed to identify the most abundant tRFs packaged into STB-EVs, by performing a differential expression analysis of MLEVs compared to placenta and SEVs compared to placenta.

Differential expression analysis relies on the assumption that the experimental condition (i.e. SEVs vs MLEVs vs placenta) represents a major source of variation in RNA expression. To assess this, I reduced the dimensionality of the RNAseq data by plotting principal components against each other to assess whether samples cluster by condition. Whilst it is still possible to compare samples which do not cluster by condition using DESeq2, this would provide an early indication that condition did not explain the majority of variance seen in RNA expression.

When comparing sample types (MLEVs, SEVs and placenta), the strong clustering seen in Principal Component Analysis (PCA) clearly demonstrates that the first two principal components appropriately separate the different conditions (Figure 2-6). This provides confidence that sRNA differs by sample type, offering validation of subsequent differential expression analyses.

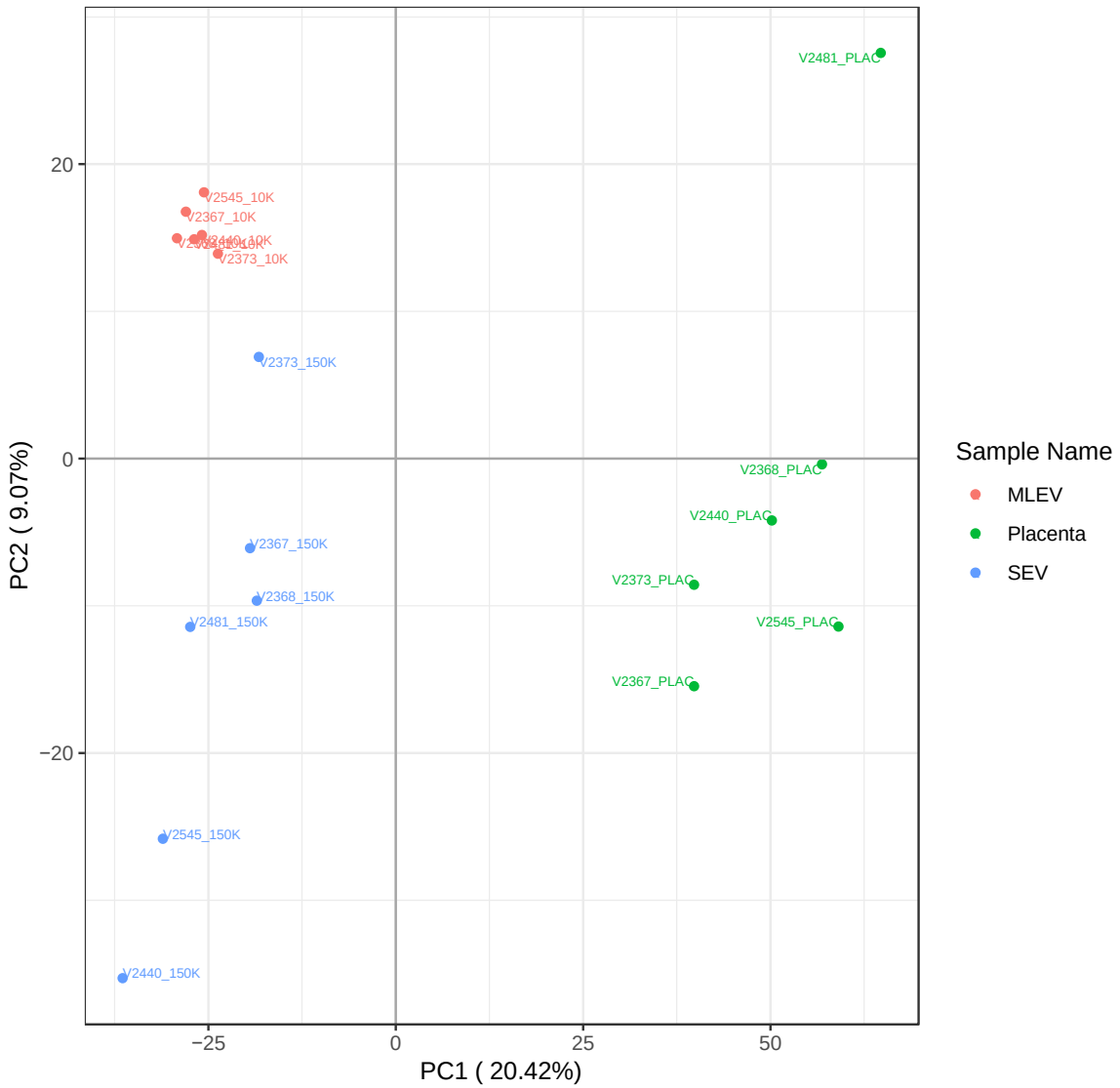


Figure 2-6 – Principal Component Analysis for sRNAseq analysis of normal pregnancy MLEVs and SEVs compared to placenta, using tRAX

Differential expression analysis is often presented using volcano plots, showing p-values against log2fold change. Whilst this helps to identify highly differentially expressed RNA fragments, it overlooks the biological significance of their relative abundance. I considered the most abundant differentially expressed RNA fragments to be of primary importance in these analyses. To facilitate appreciation of all three parameters I have chosen to present tables showing log2fold change, p-values and normalised abundance for each sample type.

2.3.1.4.1. Medium-large EVs vs placenta using tRAX

tRAX analysis identified 2482 RNA fragments differentially expressed between MLEVs and placenta in normal pregnancies. The twelve most abundant fragments in MLEVs are shown in Table 2-3. These twelve fragments map to variants of three 5'-tRNA-fragment anticodons: 5'-tRF-Gly-GCC, 5'-tRF-Val-CAC, and 5'-tRF-Glu-CTC. All twelve fragments are highly significantly upregulated in MLEVs compared to placenta.

Rank	tRNA fragment annotation	log2fold change	p-value	Normalised Count Placenta	Normalised Count MLEV
1	tRNA-Gly-GCC-5_fiveprime	5.37	5.58E-26	85526	5647683
2	tRNA-Gly-GCC-2_fiveprime	5.37	5.48E-26	85542	5647507
3	tRNA-Gly-GCC-3_fiveprime	5.37	5.48E-26	85542	5647506
4	tRNA-Gly-CCC-1_fiveprime	5.42	1.15E-25	77736	5302553
5	tRNA-Val-CAC-1_fiveprime	4.42	8.80E-17	30099	908071
6	tRNA-Val-CAC-4_fiveprime	4.42	8.80E-17	30099	908071
7	tRNA-Val-CAC-5_fiveprime	4.42	8.80E-17	30099	908071
8	tRNA-Val-AAC-1_fiveprime	4.45	9.54E-17	28849	886191
9	tRNA-Val-AAC-3_fiveprime	4.45	9.55E-17	28849	886188
10	tRNA-Val-AAC-4_fiveprime	4.45	9.55E-17	28849	886188
11	tRNA-Gly-GCC-1_fiveprime	5.33	6.99E-27	12483	788731
12	tRNA-Glu-CTC-2_fiveprime	3.30	2.29E-15	52446	530905

Table 2-3 – Top twelve tRNA fragments differentially expressed in normal pregnancy MLEVs compared to placenta using tRAX.

Ranked by abundance in MLEVs, annotations coloured by iso-acceptor.

2.3.1.4.2. Small EVs vs placenta using tRAX

tRAX analysis identified 2379 RNA fragments differentially expressed between SEVs and placenta in normal pregnancies. The twelve most abundant fragments in SEVs are shown in Table 2-4. These twelve fragments map to variants of the same three 5'-tRNA-fragment iso-decoders as the MLEV analysis: 5'-tRF-Gly-GCC, 5'-tRF-Val-CAC, and 5'-tRF-Glu-CTC. All twelve fragments are highly significantly upregulated in SEVs compared to placenta.

There are three key limitations of the tRAX analysis. Firstly, the annotation process relies on the prior discovery of relevant tRNA fragment targets: only a limited number of sRNA annotations are possible (4986). Whilst the majority of reads have mapped to these fragments in my analyses (described in 2.3.1.3), some unmapped data are lost, meaning potentially important molecules not previously described cannot be discovered. Secondly, information is lost during fragment annotation. Whilst the fragment sequence can be looked up using the annotation provided, the first and last nucleotides as well as the length of the fragment remain unknown. Thus, the exact sequence of the differentially expressed fragment is lost, making it impossible to either design qPCR assays to validate findings, or test their putative functions using RNA oligonucleotides. Thirdly, the software's approach to multi-mapping reads can be misleading. For example, the three most abundant tRNA fragments upregulated in MLEVs and SEVs compared to placenta are described as Gly-GCC-5-fiveprime, Gly-GCC-2-fiveprime and Gly-GCC-3-fiveprime (Table 2-3 and Table 2-4). Normalised read counts are very similar between these fragments. When the mapping specificity of these fragments is investigated, it becomes apparent that none of the reads are transcript-specific, meaning most of the same reads are counted as belonging to all three of the annotated fragments. This is illustrated by Figure 2-7, where reads for the same iso-acceptor are coloured green, whereas reads specific to the transcript are coloured purple. In order to mitigate some of the issues raised by this analytical approach, I elected to use the DEUS workflow.

Rank	tRNA fragment	log2fold change	p-value	Normalised Count SEV	Normalised Count Placenta
1	tRNA-Gly-GCC-5_fiveprime	5.44	1.35E-26	6341256	85526
2	tRNA-Gly-GCC-2_fiveprime	5.43	1.33E-26	6341151	85542
3	tRNA-Gly-GCC-3_fiveprime	5.43	1.33E-26	6341151	85542
4	tRNA-Gly-CCC-1_fiveprime	5.42	1.22E-25	5590466	77736
5	tRNA-Glu-CTC-2_fiveprime	5.33	1.45E-37	2272863	52446
6	tRNA-Glu-CTC-1_fiveprime	5.33	1.45E-37	2272863	52446
7	tRNA-Val-CAC-1_fiveprime	4.88	4.16E-20	1023326	30099
8	tRNA-Val-CAC-4_fiveprime	4.88	4.16E-20	1023326	30099
9	tRNA-Val-CAC-5_fiveprime	4.88	4.16E-20	1023326	30099
10	tRNA-Val-AAC-1_fiveprime	4.90	5.51E-20	978214	28849
11	tRNA-Val-AAC-3_fiveprime	4.90	5.52E-20	978211	28849
12	tRNA-Val-AAC-4_fiveprime	4.90	5.52E-20	978211	28849

Table 2-4 – Twelve most abundant tRNA fragments differentially expressed in SEVs compared to placenta in normal pregnancy samples, using tRAX.

Ranked by abundance in SEVs, annotations coloured by iso-acceptor.

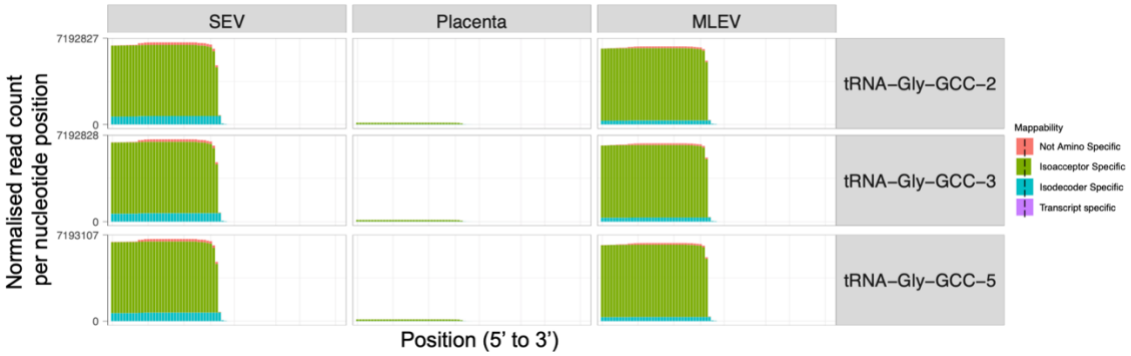


Figure 2-7 – Mapping specificity of three most abundant 5'-GlyGCC tRNA fragments using tRAX in MLEVs, SEVs and placenta.

2.3.1.5. Differential expression analysis using DEUS

The DEUS workflow circumvents the three limitations described in 2.3.1.4.2 by changing the order of steps in RNAseq analysis (Figure 2-8). All unique reads are assigned an identifier and the differential expression analysis is carried out using these identifiers as annotations, meaning the raw sequence of each read is retained. Annotations are applied subsequently, so that unmapped sequences are retained, multi-mapping sequences can be labelled as such and all relevant annotations and the precise sequence of each fragment in the analysis is retained. Whilst this approach is more computationally intense it removes any *a priori* assumptions about the fragments contained within the dataset.

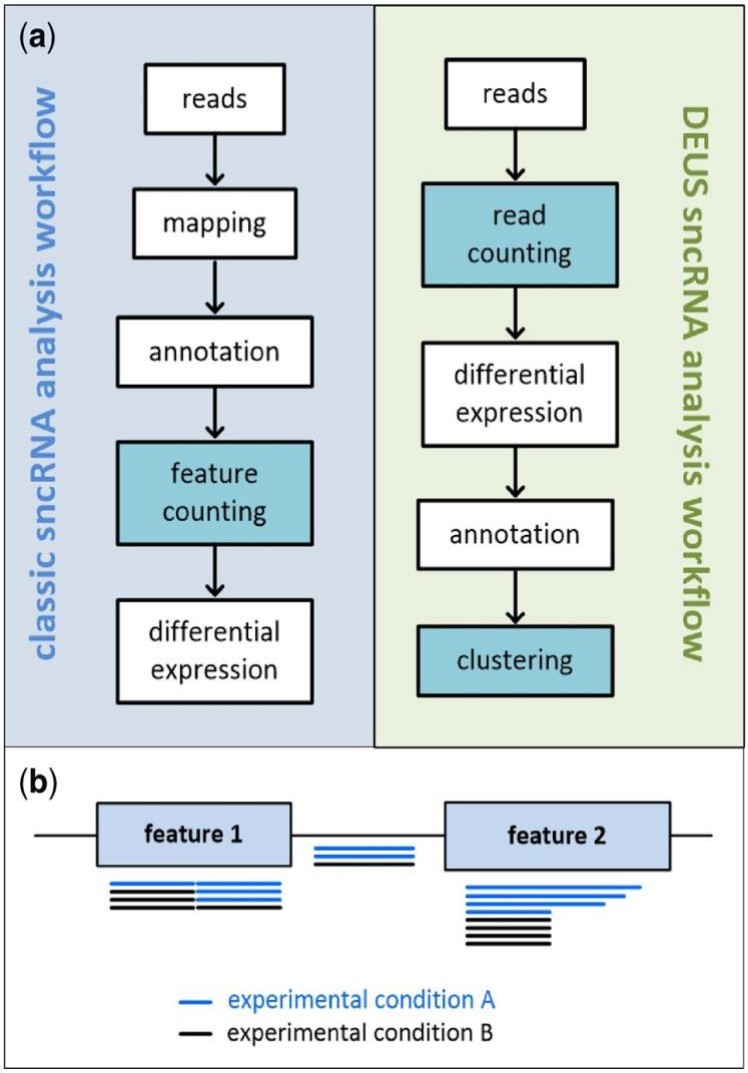


Figure 2-8 – Major differences between DEUS sRNA profiling strategy and other conventional strategies.

A. Diagram representing workflow of conventional sRNA workflows compared to DEUS

B. Diagram representing scenarios resulting in data loss with conventional workflows, namely that they overlook non-annotated reads (shown between two features) and overlook the alignment of reads, distorting sequence length, variations in nucleotide sequence and even allowing one RNA fragment split in two to be counted as two whole fragments.

Figure reproduced without changes from Jeske et al.[101]*, under creative commons licence CC BY 4.0, available at https://creativecommons.org/licenses/by/4.0/; sncRNA is a synonym for sRNA.*

2.3.1.5.1. Medium-large EVs vs placenta using DEUS

DEUS analysis identified 9 739 287 unique fragments, when comparing MLEVs to placenta in normal pregnancy samples. After filtering fragments with an average raw count >1 and performing DESeq2 analysis, 49 960 fragments were found to be significantly differentially expressed in MLEVs compared to placenta. PCA plot demonstrated good group clustering, with one potential outlier (Figure 2-9).

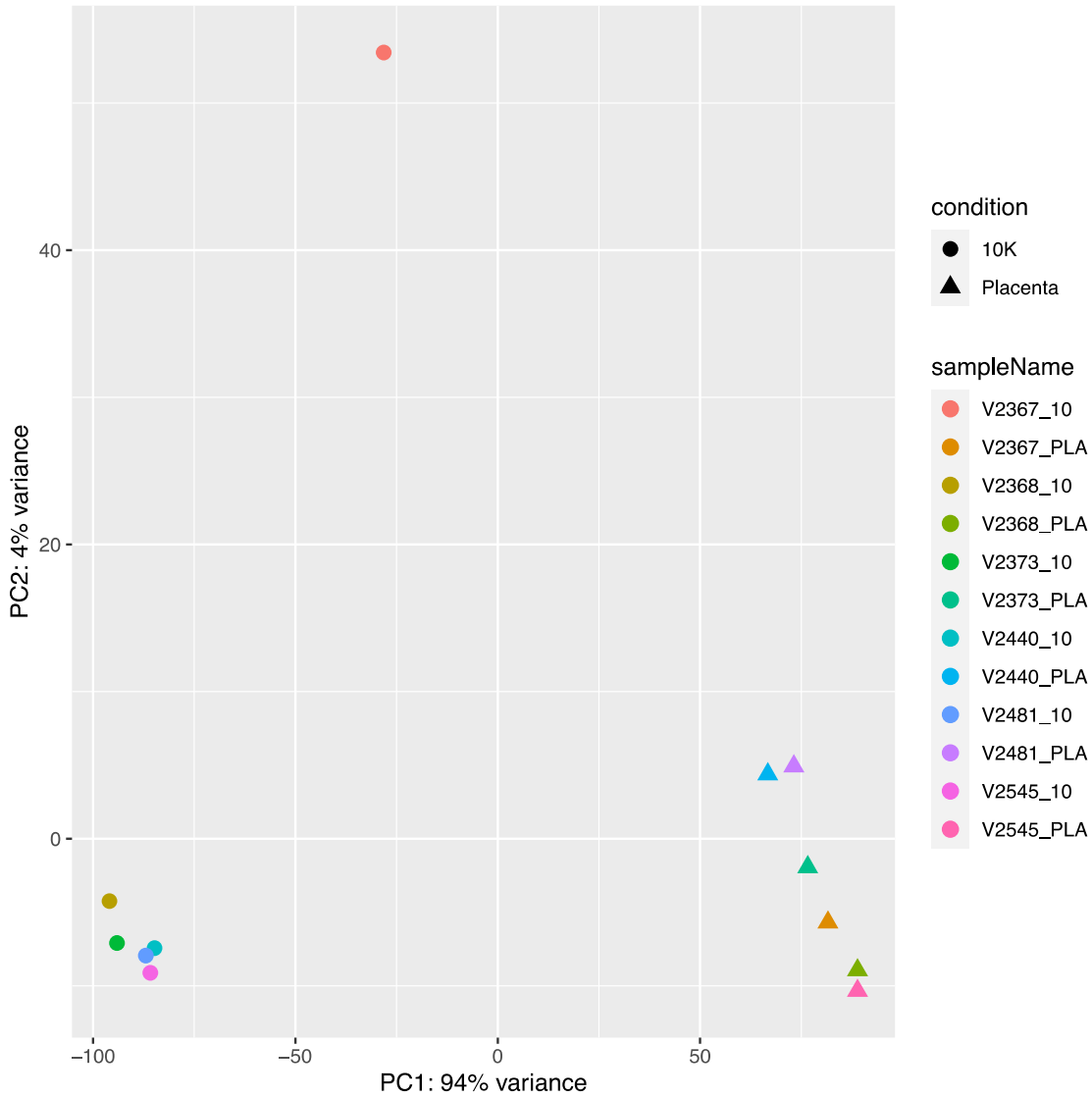


Figure 2-9 – Principal Component Analysis for sRNAseq analysis of normal pregnancy MLEVs (10K) compared to placenta, using DEUS

The analysis was repeated with this sample excluded, identifying 50 401 differentially expressed fragments. The 12 most abundant differentially expressed fragments were identical in both analyses and are shown in Table 2-5. Using the sum of MLEV normalised counts as a denominator, these 12 fragments account for 49.1% of the differentially expressed counts.

Comparing to the MINTmap tRNA database, eight of the twelve most abundant differentially expressed fragments map to four different 5'-tRNA fragments (Gly-GCC, Val-AAC, Glu-CTC and Cys-GCA). The remaining four had no directly matched reference sequences and are referred to as "unmapped". Review of fragment sequences demonstrated substantial similarities; indeed all four showed only one or two nucleotide insertions or deletions differentiating them from the four known 5'-tRFs (differences highlighted in Table 2-5). A complex profile of differential expression in normal MLEVs compared to placenta was thus dominated by minor variants of a handful of abundant 5'-tRNA fragments.

The targets identified are the same as the tRAX analysis (Table 2-4), despite different trimming and mapping protocols. However, the DEUS approach has included highly abundant unmapped fragments, was not vulnerable to multi-mapping inaccuracies and provided the RNA sequence for the differentially expressed fragments.

Rank	Sequence	Length	tRNA fragment	Mapping with ≤2 indels	log2fold change	p-value	Normalised Count Placenta	Normalised Count MLEV	% MLEV DE sRNA	Cumulative % MLEV DE sRNA
1	GCATTGGTGGTTCAGT GGTAGAATTCTCGCCT	32	Gly-GCC	Gly-GCC	-6.09	2.72E-24	50951	3702444	22.5	22.5
2	GCATTGGTGGTTCAGT GGTAGAATTCTCGCC_C	32	Unmapped	Gly-GCC	-6.21	1.66E-25	11965	945344	5.7	28.3
3	GCATTGGTGGTTCAGT GGTAGAATTCTCGCC	31	Gly-GCC	Gly-GCC	-5.01	6.65E-16	24501	835827	5.1	33.3
4	GCATGGGTGGTTCAGT GGTAGAATTCTCGCCT	32	Gly-GCC	Gly-GCC	-6.16	1.38E-34	6276	471446	2.9	36.2
5	GCATTG_TGGTTCAGT GGTAGAATTCTCGCCT	31	Unmapped	Gly-GCC	-5.89	4.09E-26	5541	347781	2.1	38.3
6	GTTTCCGTAGTGTAGT GGTTATCACGTTCGCCT	33	Val-AAC	Val-AAC	-5.22	4.00E-25	8672	335054	2.0	40.4
7	GTTTCCGTAGTGTAGT GGTTATCACGTTCGCC	32	Val-AAC	Val-AAC	-4.35	1.18E-12	13846	296242	1.8	42.2
8	GCATTGGTGGTTCAGT GGTAGAATTCTCGCCTG	33	Gly-GCC	Gly-GCC	-4.77	1.11E-14	9727	279245	1.7	43.9
9	GCATTGGTGGTTCAGT GGTAGAATTCT_CGC_T	31	Unmapped	Gly-GCC	-4.59	1.39E-14	9619	243152	1.5	45.3
10	GCATTGGTGGTTCAGT GGTAGAATTCT_CGCCA	32	Unmapped	Gly-GCC	-5.41	1.51E-22	5442	242380	1.5	46.8
11	TCCCTGGTGGTCTAGT GGTTAGGATTCGGCGCT	33	Glu-CTC	Glu-CTC	-3.60	4.63E-11	16559	207225	1.3	48.1
12	GGGGGTATAGCTCAGG GGTAGAGCATTTGACT	32	Cys-GCA	Cys-GCA	-6.72	1.43E-27	1548	176239	1.1	49.1

Table 2-5 – Twelve most abundant sRNA fragments differentially expressed (DE) in MLEVs compared to placenta in normal pregnancy samples, using DEUS. Ranked by abundance in MLEVs. Column titled tRNA fragment represents mapping to MINTmap database. Annotations coloured by iso-acceptor.

2.3.1.5.2. Small EVs vs placenta using DEUS

DEUS analysis identified 10 171 552 unique fragments, when comparing SEVs to placenta in normal pregnancy samples. After filtering fragments with an average raw count >1 and performing DESeq2 analysis, 51 177 fragments were found to be significantly differentially expressed in SEVs compared to placenta. PCA plot demonstrated good group differentiation, with no single clear outlier warranting exclusion (Figure 2-10).

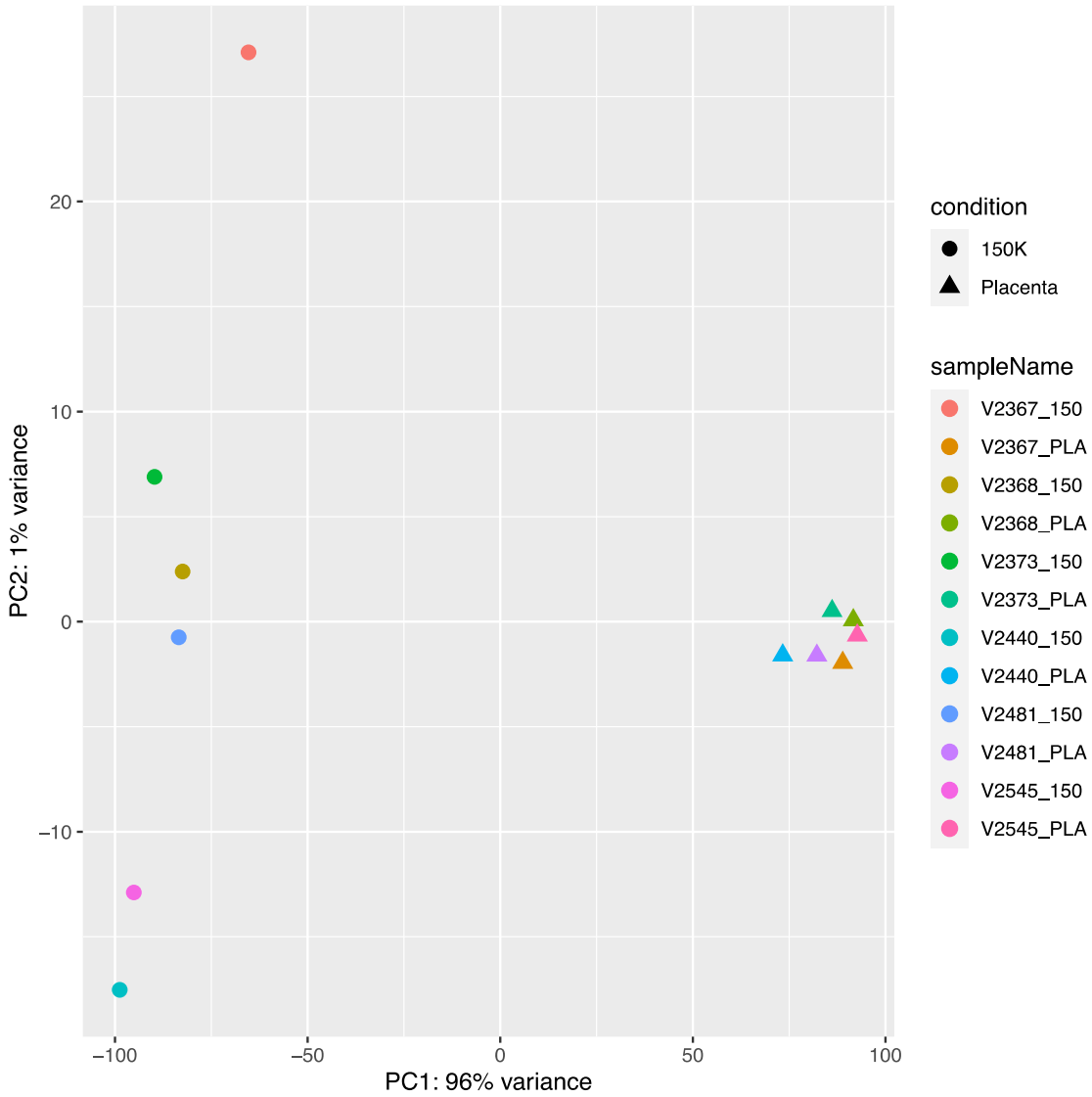


Figure 2-10 – Principal Component Analysis for sRNAseq analysis of normal pregnancy SEVs (150K) compared to placenta, using DEUS

The twelve most abundant differentially expressed fragments were identical in both analyses and are shown in Table 2-6. Using the sum of SEV normalised counts as a denominator, these twelve fragments account for 48.6% of the differentially expressed counts.

Comparing to the MINTmap tRNA database, eight of the twelve most abundant differentially expressed SEV fragments map to 3 different 5'-tRNA fragments (Gly-GCC, Glu-CTC, Val-AAC). These are the same fragments which were abundantly upregulated in normal MLEVs compared to placenta. The remaining four fragments had no directly matched reference sequences and are referred to as "unmapped". Review of fragment sequences showed similarities; indeed all four showed only one nucleotide insertion or deletion differentiating them from the three known 5'-tRFs (differences highlighted in Table 2-6). A complex profile of differential expression in normal SEVs compared to placenta was thus dominated by minor variants of handful of abundant 5'-tRNA fragments. Again, this analysis identified the same targets as the tRAX analysis, but included unmapped abundant sequences, was not biased by multi-mapping and provided target fragment sequences.

Rank	Sequence	Length	tRNA fragment	Mapping with ≤2 indels	log2fold change	p-value	Normalised Count Placenta	Normalised Count SEV	% SEV DE sRNA	Cumulative % SEV DE sRNA
1	GCATTGGTGGTTCAGT GGTAGAATTCTCGCCT	32	Gly-GCC	Gly-GCC	-6.20	3.48E-25	45594	3579812	18.0	18.0
2	GCATTGGTGGTTCAGT GGTAGAATTCTCGCC	31	Gly-GCC	Gly-GCC	-5.66	4.19E-18	22931	1246491	6.3	24.3
3	TCCCTGGTGGTCTAGT GGTTAGGATTCGGCGCT	33	Glu-CTC	Glu-CTC	-6.13	8.15E-26	14730	1097701	5.5	29.8
4	GCATTGGTGGTTCAGT GGTAGAATTCTCGCCTG	33	Gly-GCC	Gly-GCC	-6.08	2.50E-24	8691	627272	3.2	33.0
5	GCATTGGTGGTTCAGT GGTAGAATTCTCGCCC	32	Unmapped	Gly-GCC	-5.70	4.33E-22	10760	591677	3.0	36.0
6	TCCCTG TGGTCTAGT GGTTAGGATTCGGCGCT	32	Unmapped	Glu-CTC	-6.04	3.04E-25	6894	483198	2.4	38.4
7	GTTTCCGTAGTGTAGT GGTTATCACGTTCGCC	32	Val-AAC	Val-AAC	-5.00	1.36E-14	12844	436138	2.2	40.6
8	GTTTCCGTAGTGTAGT GGTTATCACGTTCGCCT	33	Val-AAC	Val-AAC	-5.58	1.02E-25	7955	397643	2.0	42.6
9	GCATTGGTGGTTCAGT GGTAGAATTCTCGC	30	Gly-GCC	Gly-GCC	-5.50	2.28E-16	7421	362634	1.8	44.4
10	GCATGGGTGGTTCAGT GGTAGAATTCTCGCCT	32	Gly-GCC	Gly-GCC	-5.69	4.13E-31	5727	306828	1.5	46.0
11	GCATTGGTGGTTCAGT GGTAGAATTCTCGCT	31	Unmapped	Gly-GCC	-4.90	3.81E-14	9086	287615	1.4	47.4
12	GCATTG TGGTTCAGT GGTAGAATTCTCGCCT	31	Unmapped	Gly-GCC	-5.42	1.50E-22	5024	225622	1.1	48.6

Table 2-6 – Twelve most abundant sRNA fragments differentially expressed (DE) in SEVs compared to placenta in normal pregnancy samples, using DEUS.

Ranked by abundance in SEVs. Column titled tRNA fragment represents mapping to MINTmap database. Annotations coloured by iso-acceptor.

2.3.2. Small RNA sequencing of early-onset preeclampsia pregnancy samples

2.3.2.1. Demographics

Early-onset preeclampsia placentas were obtained from preterm pregnancies undergoing caesarean section. Preeclampsia was defined using ISSHP criteria[1]. These placentas were delivered at a median gestational age of 31.4 weeks, which represents an important but uncontrollable confounder when comparing to the normal pregnancy placentas (Table 2-7). This is an issue encountered by all working on early-onset preeclampsia: it is not possible (and indeed would be unethical to attempt) to acquire healthy gestation-matched control placentas. Other variables differing between the two groups represent correlates of preeclampsia and gestational age: birthweight was lower (median 1398 g in preeclampsia compared to 3775 g in normal) and median blood pressure was higher (164/108 in preeclampsia compared to 132/74 in normal). Additional potentially confounding variables were reported but not found to differ substantially between groups.

	Normal (n=6)	Preeclampsia (n=8)
Median maternal age (IQR) – years	34.5 (30.5-38.75)	32 (30.3-37.5)
Median pre-pregnancy BMI (IQR)	27 (20.8-33.8)	28.3 (23.8-38)
First pregnancy – no. (%)	0 (0)	4 (50)
Diabetes – no. (%)	0 (0)	0 (0)
Essential hypertension – no. (%)	0 (0)	2 (25)
Current smoker – no. (%)	0 (0)	0 (0)
Male fetus – no. (%)	4 (67)	4 (50)
Median birthweight (IQR) – g	3775 (3419-4090)	1398 (1110-2270)
Median gestational age at delivery (IQR) – weeks	39.2 (38.8-40)	31.4 (30-35.3)
Median highest recorded SBP (IQR) – mmHg	132 (113-135)	164 (140-178)
Median highest recorded DBP (IQR) – mmHg	74 (64-75)	108 (94-112)

Table 2-7 – Demographic data for women donating placentas from pregnancies with early-onset preeclampsia, compared to normal pregnancies.
Continuous variables are described using median and interquartile range (IQR).
Categorical variables are described using number (no.) and percentage (%).
Other abbreviations used: body mass index (BMI), systolic blood pressure (SBP) and diastolic blood pressure (DBP).

2.3.2.2. Quality assessment

Early-onset preeclampsia raw sequencing data demonstrated that all samples had sequences of a single length (51 bp), consistent with the single-end sequencer read length. Read depth varied from 7.6E6 to 14.9E6 reads per sample (Figure 2-11A). Mean quality scores were >30 with very low per-base N (uncalled) content (Figure 2-11C, E). Adapters were present (Figure 2-11G). After removal of adapters and low-quality reads, FastQC confirmed no samples were found with any adapter contamination >0.1%. Whilst read depth and quality scores were unchanged (Figure 2-11B, D), all N reads were removed (Figure 2-11F).

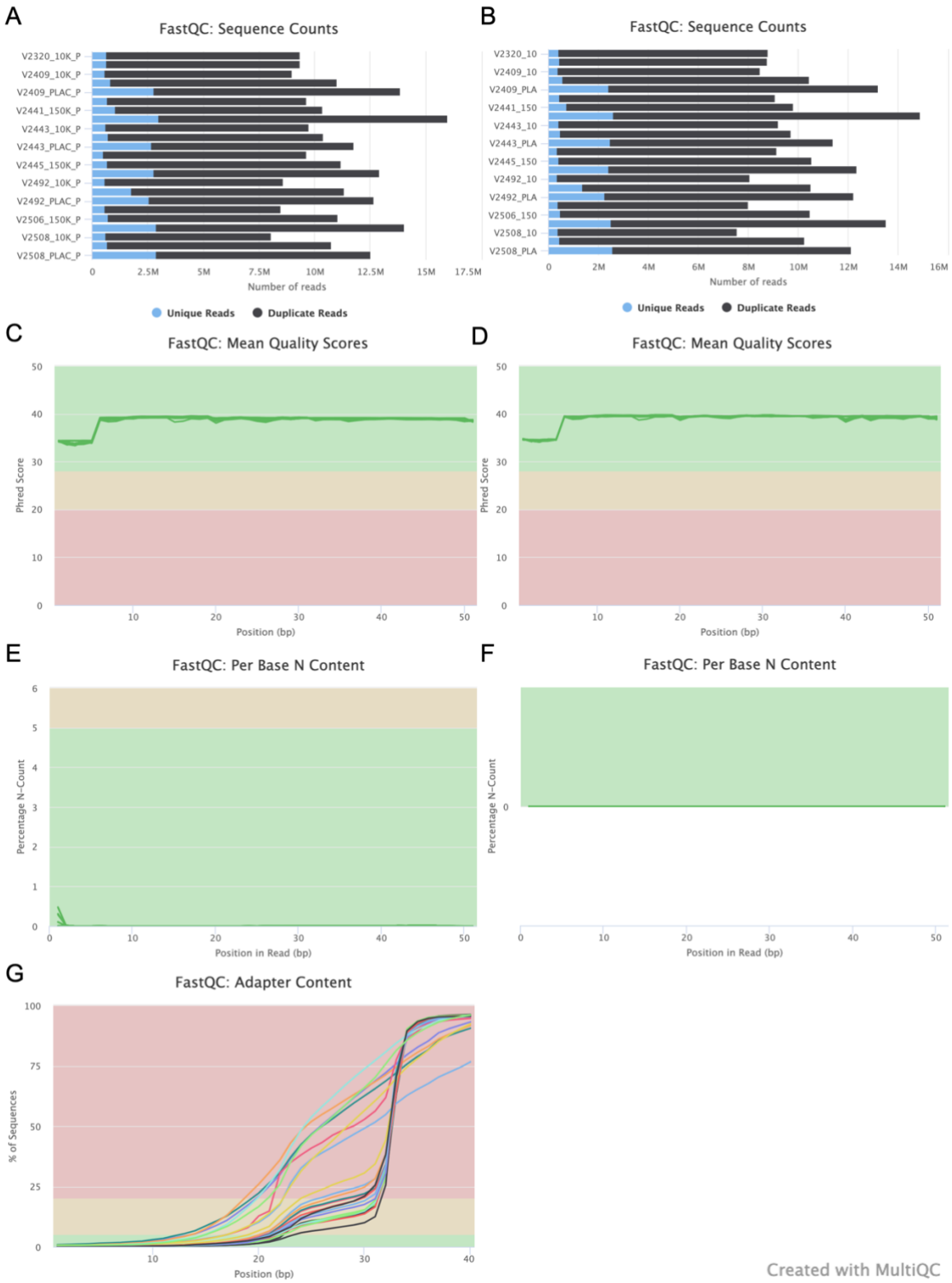


Figure 2-11 – Quality control data for early-onset preeclampsia pregnancy samples.

A, C, E, G represent summary data from raw reads

B, D, F represent summary data after removal of adapters and low-quality reads

Panels displayed together for comparison; reproduced as larger figures in Appendix 2.

2.3.2.3. Size distribution, mapping and base coverage

After removal of adapters and low-quality reads, the majority of reads in MLEVs and SEVs were 30-35 nt in length (Figure 2-12A, B), consistent with the finding in normal pregnancy (Figure 2-4A, B). Similarly, this represented a substantial difference from placental samples, where a peak at 22 nt was the most abundant (Figure 2-12C).

Mapping using tRAX software identified median 3.2% unmapped fragments (range 2.3 – 7.0%). The majority of fragments in SEVs (minimum 80.9%, with the exception of a single outlier of 46.5%) and MLEVs (minimum 79.6%) mapped to tRNA species (Figure 2-12D, E). This contrasts to placental tissue where maximum 9.1% reads mapped to tRNA species (Figure 2-12F). The single outlier identified in SEV samples (Figure 2-12D) was excluded from subsequent analyses. Similar to normal pregnancy (Figure 2-4), these data suggest the majority of sRNA in early-onset preeclampsia STB-EVs are tRNA species.

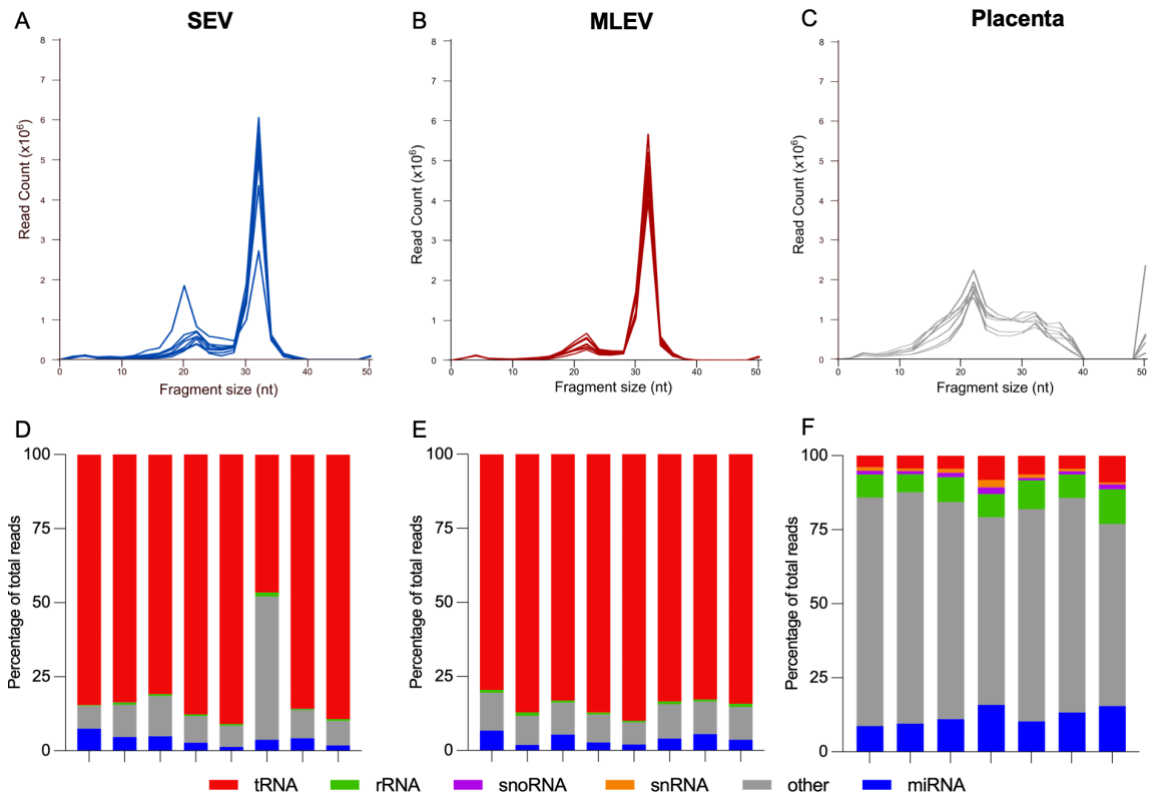


Figure 2-12 – Size distribution (A-C) and mapping (D-F) of sRNA fragments in early-onset preeclampsia pregnancy samples after removal of adapters and low-quality reads.

Y axis in A-C displays absolute read count; mapping data in D-F expressed as a percentage of mapped fragments.

When tRNA read counts are displayed by nucleotide position, it is apparent that the majority of tRNA species in preeclampsia SEVs and MLEVs are 5’-tRFs (Figure 2-13).

Together these data support a novel conclusion that the majority of sRNA in preeclampsia STB-EVs are 5’-tRFs. This appears very similar to data from normal pregnancy STB-EVs.

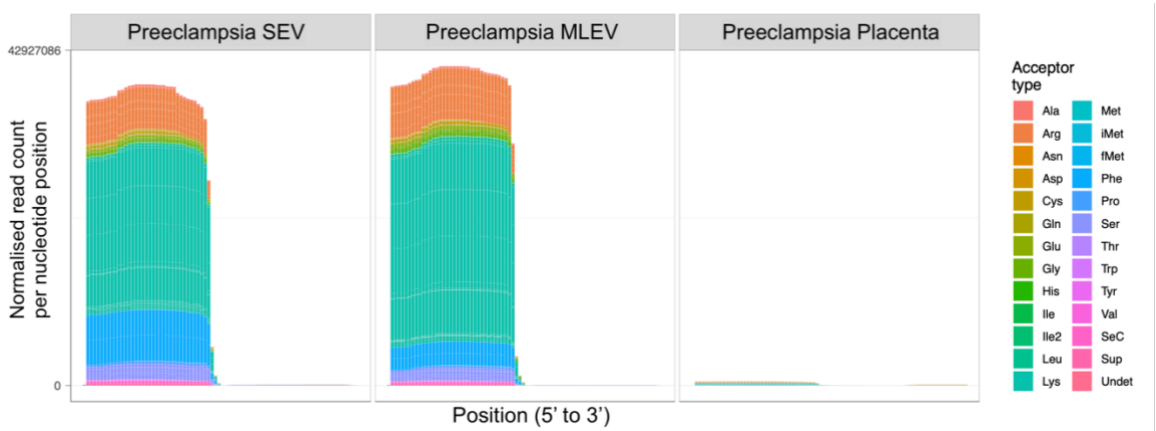


Figure 2-13 – Base coverage of tRNA fragments in normal pregnancy samples, stratified by iso-acceptor.

Y axis displays normalised read count per nucleotide position. X axis displays nucleotide positions for each tRNA fragment from 5' to 3'. Colours represent tRNA iso-acceptor type.

2.3.2.4. Differential expression: early-onset preeclampsia vs normal pregnancy samples using tRAX

2.3.2.4.1. Medium-large EVs using tRAX

tRAX analysis identified 535 differentially expressed fragments ($p<0.05$) mapping to GtRNAdb2.0 when comparing early-onset preeclampsia and normal pregnancy MLEVs. PCA demonstrated good separation of the two sample groups (Figure 2-14).

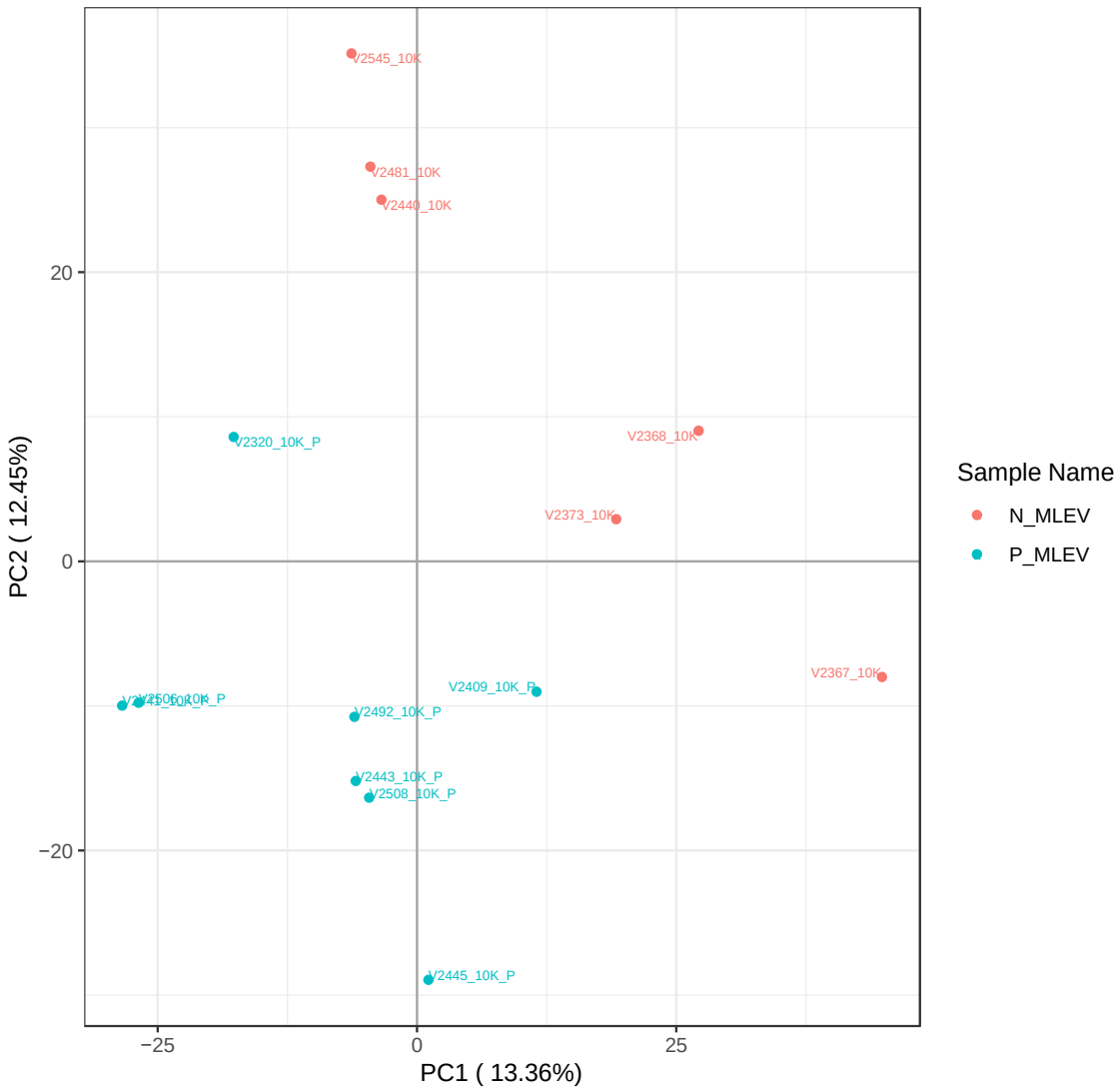


Figure 2-14 – Principal Component Analysis for sRNAseq analysis of early-onset preeclampsia vs normal pregnancy MLEVs, using tRAX

The twelve most abundant tRNA fragments differentially expressed in early-onset preeclampsia MLEVs compared to normal pregnancy MLEVs are shown in Table 2-8. Differences between groups are much smaller than comparing STB-EVs to placenta, demonstrated by log2fold change values ranging from -0.78 to 0.93. Four iso-detectors (5'-tRF-Gly-GCC, 5'-tRF-Gly-CCC, 5'-tRF-Glu-CTC and 5'-tRF-CysGCA) were the most abundant differentially expressed fragments. All were downregulated in preeclampsia MLEVs except 5'-tRF-GluCTC.

Rank	tRNA fragment annotation	log2fold change	p-value	Normalised Count PE MLEV	Normalised Count Normal MLEV
1	tRNA-Gly-GCC-5_fiveprime	-0.50	4.22E-02	2778688	4404924
2	tRNA-Gly-GCC-2_fiveprime	-0.50	4.22E-02	2778519	4404790
3	tRNA-Gly-GCC-3_fiveprime	-0.50	4.22E-02	2778519	4404789
4	tRNA-Gly-CCC-1_fiveprime	-0.55	2.73E-02	2552030	4135262
5	tRNA-Glu-CTC-2_fiveprime	0.93	1.62E-06	828114	400771
6	tRNA-Glu-CTC-1_fiveprime	0.93	1.62E-06	828114	400771
7	tRNA-Gly-GCC-1_fiveprime	-0.65	1.02E-02	368411	614327
8	Y_RNA	0.47	2.12E-02	195617	155357
9	tRNA-Cys-GCA-4_fiveprime	-0.62	1.14E-02	139632	214856
10	tRNA-Cys-GCA-2_fiveprime	-0.62	1.14E-02	139632	214855
11	tRNA-Cys-GCA-13_fiveprime	-0.78	3.16E-03	109586	149565
12	tRNA-Cys-GCA-9_fiveprime	-0.78	3.16E-03	109585	149564

Table 2-8 – Twelve most abundant tRNA fragments differentially expressed in early-onset preeclampsia compared to normal pregnancy MLEVs, using tRAX.

Ranked by abundance in preeclampsia MLEVs, annotations coloured by iso-acceptor.

2.3.2.4.2. Small EVs using tRAX

tRAX analysis identified 343 differentially expressed fragments ($p<0.05$) mapping to GtRNAdb2.0 when comparing early-onset preeclampsia and normal pregnancy SEVs. PCA demonstrated significant overlap between the two sample groups (Figure 2-15). This suggests that disease state is not likely to explain the majority of the variation between samples.

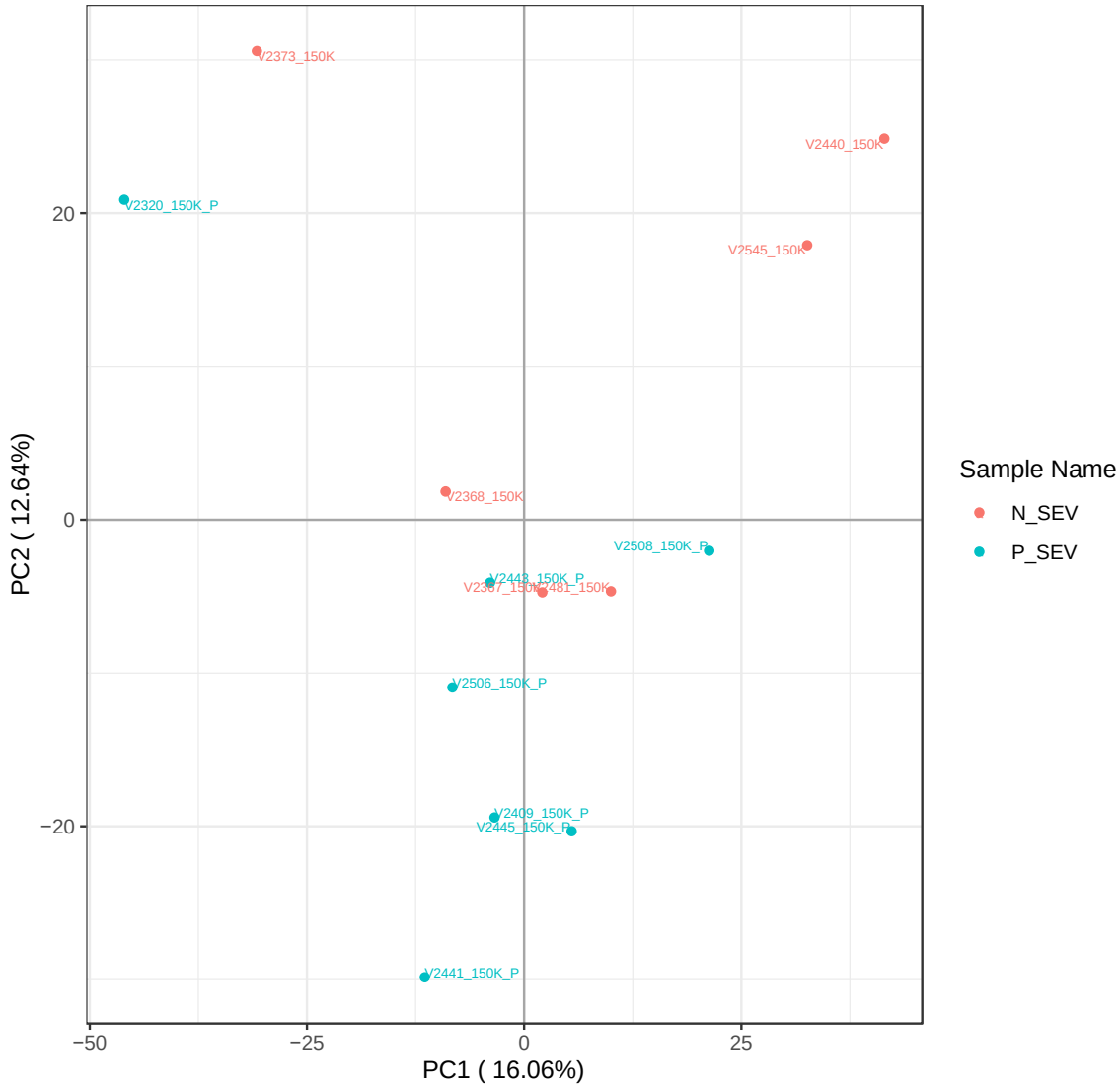


Figure 2-15 – Principal Component Analysis for sRNAseq analysis of early-onset preeclampsia vs normal pregnancy SEVs, using tRAX

The twelve most abundant tRNA fragments differentially expressed in early-onset preeclampsia SEVs compared to normal pregnancy SEVs are shown in Table 2-9. All fragments are downregulated in preeclampsia SEVs. There is some overlap with the targets identified in preeclampsia MLEVs by tRAX. Indeed 5'-GlyGCC-2, -3 and -5 are the most abundant fragments upregulated in normal MLEVs and SEVs compared to placenta, as well as the most abundant differentially expressed in preeclampsia MLEVs and SEVs compared to normal. It may be that the sheer abundance of this molecule allows it to achieve significant differences between disease states. The clinical significance of a molecule downregulated in preeclampsia STB-EVs by 0.7 fold (log2fc -0.5) is questionable. Increased STB-EV release in early-onset preeclampsia may confound this result entirely[40].

As with the normal pregnancy STB-EVs vs placenta comparisons, the key shortcomings of tRAX analysis remained: unmapped fragments are lost, the sequence of identified fragments is unknown and multi-mapping can result in misleading over-counting of reads.

Rank	tRNA fragment annotation	log2fold change	p-value	Normalised Count PE SEV	Normalised Count Normal SEV
1	tRNA-Gly-GCC-5_fiveprime	-0.64	2.46E-02	3395869	4854407
2	tRNA-Gly-GCC-2_fiveprime	-0.64	2.46E-02	3395826	4854119
3	tRNA-Gly-GCC-3_fiveprime	-0.64	2.46E-02	3395826	4854120
4	tRNA-Gly-CCC-1_fiveprime	-0.70	1.75E-02	2974485	4342359
5	tRNA-Val-CAC-1_fiveprime	-0.81	2.08E-02	608804	740885
6	tRNA-Val-CAC-4_fiveprime	-0.81	2.08E-02	608804	740885
7	tRNA-Val-CAC-5_fiveprime	-0.81	2.08E-02	608804	740885
8	tRNA-Val-AAC-1_fiveprime	-0.82	1.98E-02	587280	710517
9	tRNA-Val-AAC-3_fiveprime	-0.82	1.98E-02	587278	710516
10	tRNA-Val-AAC-4_fiveprime	-0.82	1.98E-02	587278	710517
11	tRNA-Gly-GCC-1_fiveprime	-0.74	2.78E-03	297490	537788
12	tRNA-Cys-GCA-4_fiveprime	-0.52	4.85E-02	231992	308784

Table 2-9 – Twelve most abundant tRNA fragments differentially expressed in early-onset preeclampsia compared to normal pregnancy SEVs, using tRAX. Ranked by abundance in preeclampsia SEVs, annotations coloured by iso-acceptor.

2.3.2.5. Differential expression: early-onset preeclampsia vs normal pregnancy samples using DEUS

2.3.2.5.1. Medium-large EVs using DEUS

DEUS analysis identified 2 521 420 unique fragments, when comparing preeclampsia MLEVs to normal MLEVs. After filtering fragments with an average raw count >1 and performing DESeq2 analysis, 4530 fragments were found to be significantly differentially expressed in preeclampsia MLEVs compared to normal MLEVs. PCA plot demonstrated poor group clustering, with no obvious outliers to exclude (Figure 2-16). This would suggest that disease state does not explain all of the variance between samples.

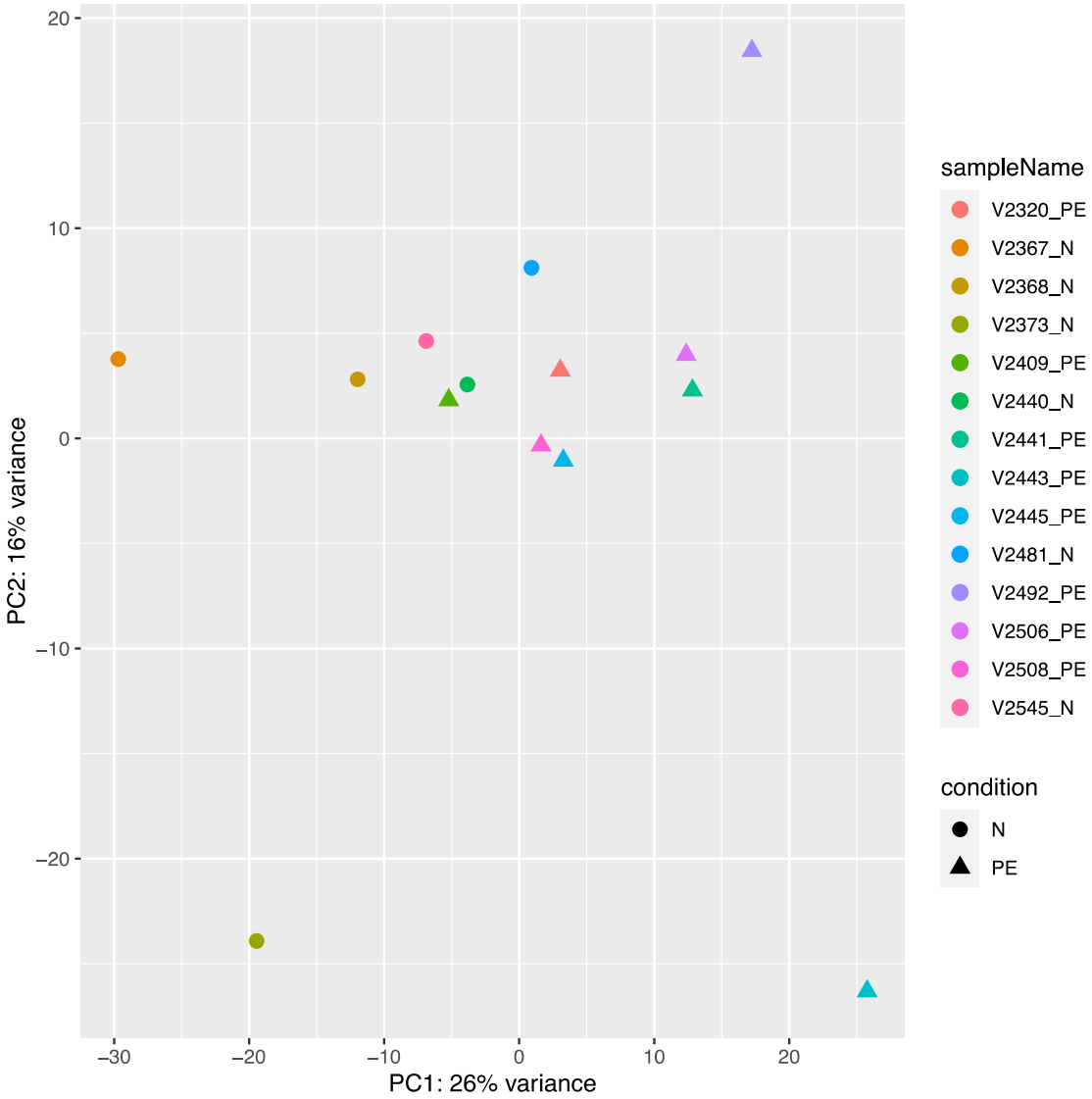


Figure 2-16 – Principal Component Analysis for sRNAseq analysis of early-onset preeclampsia vs normal pregnancy MLEVs, using DEUS

The twelve most abundant tRNA fragments differentially expressed in early-onset preeclampsia MLEVs compared to normal pregnancy MLEVs using DEUS are shown in Table 2-10. Normalised counts by condition are also shown in Figure 2-17. Five of these mapped to 5'-tRF-Glu-CTC, five were unmapped, the remaining two mapped to 5'-tRFs Val-AAC and Cys-GCA. DEUS software allows for mismatched nucleotides but not insertions or deletions. Review of the unmapped sequences showed they all differed from known 5'-tRFs by one or two insertions or deletions. 5'-tRF-Glu-CTC accounted for nine out of twelve of the fragment annotations; all variations of this tRF were more abundant in preeclampsia than normal MLEVs. Together these data suggest 5'-tRF-Glu-CTC as a potentially differentially expressed tRF target in preeclampsia MLEVs, warranting further investigation.

Rank	Sequence	Length	tRNA fragment	Mapping with ≤2 indels	log2fold change	p-value	Normalised Count N MLEV	Normalised Count PE MLEV	% PE MLEV DE sRNA	Cumulative % PE MLEV DE sRNA
1	TCCCTGGTGGTCTAGTG GTTAGGATTCGGCGCT	33	Glu-CTC	Glu-CTC	1.38	5.13E-06	97247	264726	21.8	21.8
2	TCCCTG_TGGTCTAGTGG TTAGGATTCGGCGCT	32	Unmapped	Glu-CTC	1.34	7.06E-06	41522	109139	9.0	30.8
3	TCCCTGGTGGTCTAGTG GTTAGGATTCGGCGCC	33	Unmapped	Glu-CTC	1.17	3.26E-06	25627	59147	4.9	35.6
4	TCCCTGGTGGTCTAGTG GTTAGGATTCGGCGCTCT	35	Glu-CTC	Glu-CTC	0.82	3.33E-02	22828	41777	3.4	39.1
5	TCCCTGGTGGTCTAGTG GTTAGGATTCGGCGC	32	Glu-CTC	Glu-CTC	1.24	2.81E-05	12180	29780	2.5	41.5
6	TCCCTG_TGGTCTAGTGG TTAGGATTCGGCGCC	32	Unmapped	Glu-CTC	1.13	9.96E-06	11189	25097	2.1	43.6
7	TCCCTGGTGGTCTAGTG GTTAGGATTCGGCGCTC	34	Glu-CTC	Glu-CTC	0.98	4.04E-04	8282	16766	1.4	45.0
8	GGGGGTATAGCTCAGTG GTAGAGCATTTGAC	31	Cys-GCA	Cys-GCA	-1.09	1.16E-04	35609	16258	1.3	46.3
9	TCCCTGGTGGTCTAGTG GTTAGGATTCGGCG	31	Glu-CTC	Glu-CTC	1.95	5.17E-08	3555	15041	1.2	47.6
10	GTTTCCGTAGTGTAGTGG TTATCACGTTCGC	31	Val-AAC	Val-AAC	-0.73	3.65E-02	23408	13817	1.1	48.7
11	GCATTGGTGGTTCAGTG GTAGAATTCTCGCCTT	33	Unmapped	Gly-GCC	0.96	4.52E-02	6385	13286	1.1	49.8
12	TCCCTG_TGGTCTAGTGG TTAGGATTCGGCGC	31	Unmapped	Glu-CTC	1.21	4.46E-05	5471	13140	1.1	50.9

Table 2-10 – Twelve most abundant sRNA fragments differentially expressed (DE) in early-onset preeclampsia compared to normal pregnancy MLEVs, using DEUS. Ranked by abundance in preeclampsia MLEVs, annotations coloured by iso-acceptor.

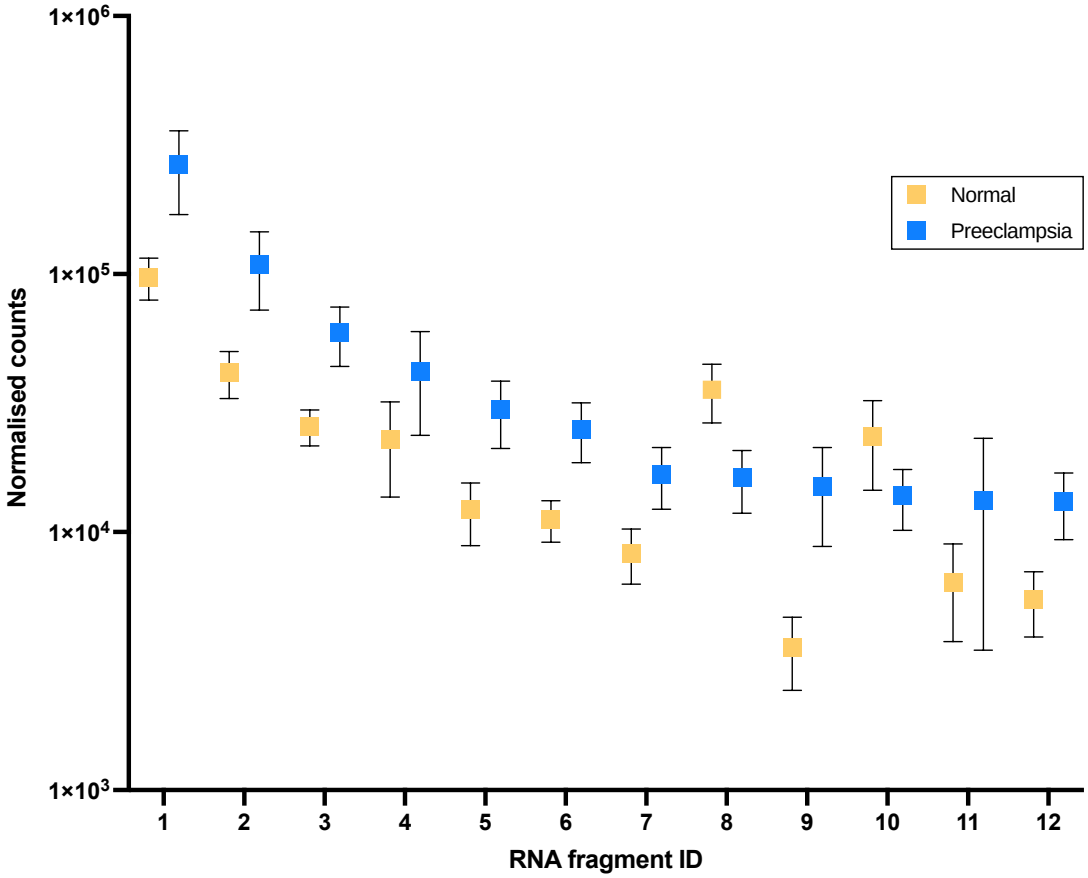


Figure 2-17 – Mean normalised expression and standard deviation of 12 most abundant sRNA fragments differentially expressed in early-onset preeclampsia compared to normal pregnancy MLEVs, using DEUS.

Ranked by abundance in preeclampsia MLEVs.

2.3.2.5.2. Small EVs using DEUS

DEUS analysis identified 3 551 072 unique fragments, when comparing preeclampsia SEVs to normal SEVs. After filtering fragments with an average raw count >1 and performing DESeq2 analysis, 225 fragments were found to be significantly differentially expressed in preeclampsia SEVs compared to normal SEVs.

PCA analysis demonstrated significant overlap between the two sample groups (Figure 2-18), mirroring the result seen with tRAX (Figure 2-15). Once again, this observation suggests disease state may not explain the majority of the sRNA variation between samples.

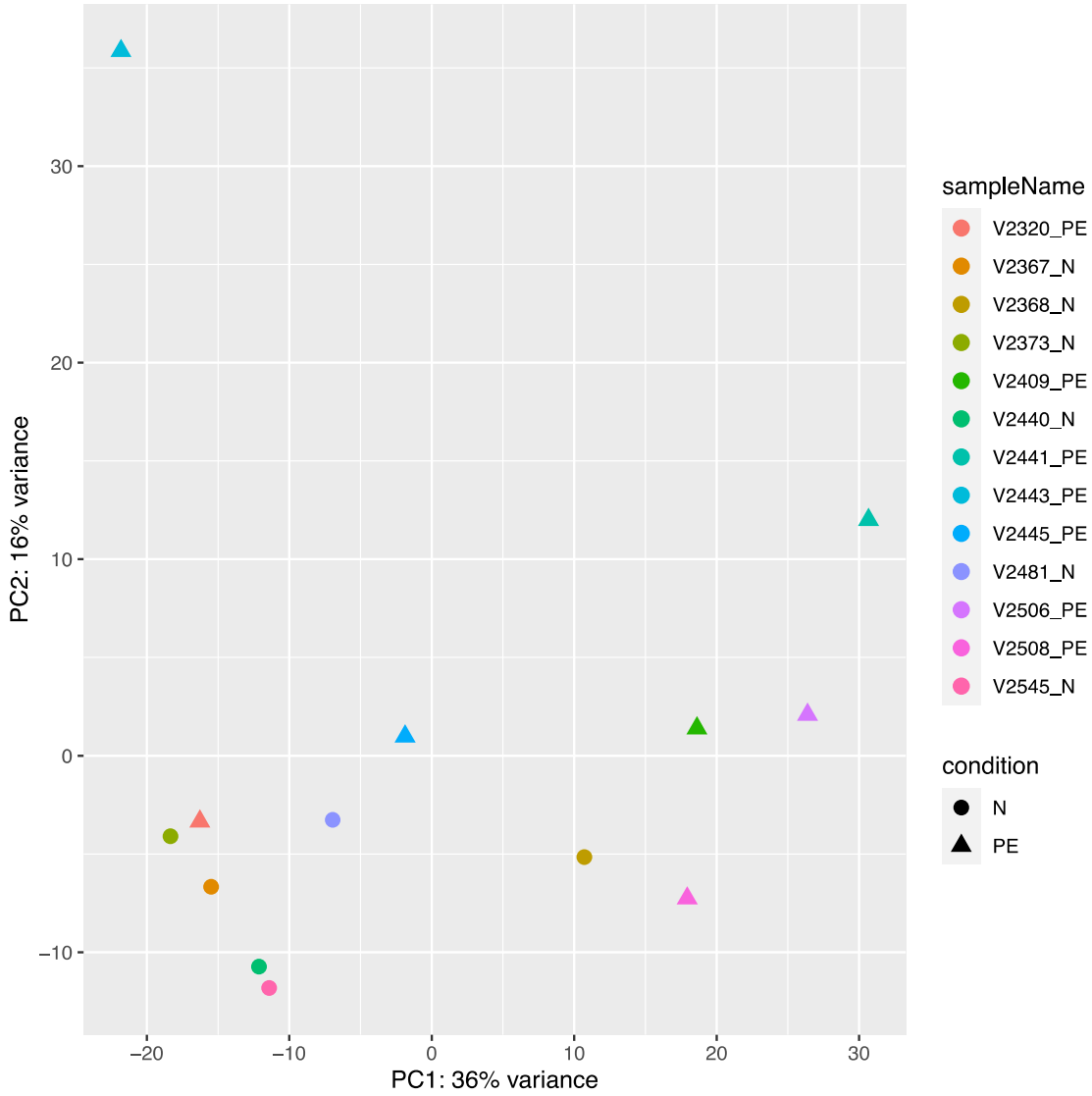


Figure 2-18 – Principal Component Analysis for sRNAseq analysis of early-onset preeclampsia vs normal pregnancy SEVs, using DEUS

The twelve most abundant tRNA fragments differentially expressed in early-onset preeclampsia SEVs compared to normal pregnancy SEVs are shown in Table 2-11.

The normalised abundance of these differentially expressed reads is an order of magnitude lower than expression in MLEVs (Table 2-10). Using the sum of preeclampsia SEV normalised counts as a denominator, these 12 fragments account for 64.1% of the differentially expressed counts. The targets identified as differentially expressed in preeclampsia SEVs by DEUS are quite different from MLEVs: six of the twelve are less than 30 nt in length suggesting they do not represent 5'-tRFs.

Rank	Sequence	Length	tRNA fragment	log2fold change	p-value	Normalised Count N SEV	Normalised Count PE SEV	% PE SEV DE sRNA	Cumulative % PE SEV DE sRNA
1	GGGGGTATAGCTCAGGG GTAGAGCATTTGAC	31	Cys-GCA	-0.96	4.33E-02	19044	9495	27.6	27.6
2	GGGGATGTAGCTCAGTG G	18	Ala-TGC	1.79	2.13E-02	610	2521	7.3	35.0
3	AAAGTGCTTCCCTTTGG ACTGT	22	Unmapped	1.59	3.53E-02	587	2020	5.9	40.9
4	GGGGGTGTAGCTCAGTG GTAGAGCGCGTGCTTGG	34	Unmapped	1.15	2.74E-04	879	1980	5.8	46.6
5	GGGGGTGTAGCTCAGTG GTAGAGCATTTGACC	32	Unmapped	-1.16	1.18E-02	3361	1456	4.2	50.9
6	GGGGGTGTAGCTCAGTG GTAGAGCATTTGAC	31	Cys-GCA	-1.35	1.19E-02	3045	1122	3.3	54.1
7	GGCCGTGATCGTATCGT GGTTAGTACTCTGCGTT	34	Unmapped	1.36	7.31E-03	311	846	2.5	56.6
8	GCATGGGTGGTTCAGTG GTAGAATTCT	27	Gly-GCC	-1.22	1.65E-02	1628	671	2.0	58.6
9	TCCATGGTGGTCTAGTG GTTAGGATTCGGCGC	32	Unmapped	2.04	2.48E-02	99	559	1.6	60.2
10	AAAGTGCTTCCCTTTGG ACTG	21	Unmapped	1.65	2.13E-02	130	469	1.4	61.5
11	GACGAGGTGGCCGAG	15	Ser-GCT	1.89	4.06E-02	93	464	1.4	62.9
12	CGGCGACTCTGGACGC GAGCC	21	Unmapped	1.62	4.29E-02	113	409	1.2	64.1

Table 2-11 – Twelve most abundant sRNA fragments differentially expressed (DE) in early-onset preeclampsia compared to normal pregnancy SEVs, using DEUS. Ranked by abundance in preeclampsia SEVs, annotations coloured by iso-acceptor.

2.3.2.6. Comparison between tRAX, DEUS and collaborator approaches

All three approaches to comparing sRNA expression in preeclampsia and normal STB-EVs identified fewer differentially expressed targets in SEVs than MLEVs (Table 2-12). This is consistent with the likely different biogenesis of EVs depending on size. Medium-large EVs in this study are defined as those which pellet from placental perfusate at 10 000 *g;* previous work has demonstrated their size, appearance and protein expression are consistent with microvesicles[84]. Microvesicles are formed by direct budding from the cell surface, meaning they offer a representation of cellular stress[107]. Small EVs, pelleting at 150 000 *g* have been phenotyped as exosomes[84]. Exosomes are generated constitutively through a 4-stage process beginning with invagination of the cell membrane to form endosomes, accumulation of intraluminal vesicles by inward budding of endosomal membrane (during which proteins, lipids and nucleic acids are loaded), endosomal transportation to the cell surface and fusion with the cell membrane to release the vesicles as exosomes[107]. Thus, it is biologically reasonable that MLEVs from the acutely stressed syncytiotrophoblast in preeclampsia will differ more from normal pregnancy than SEVs.

The differing rate of discovery of differentially expressed targets by the three approaches likely represents different filtering processes. The tRAX analysis excluded mapped fragments if mean normalised read counts were 0 in either group. Our collaborators, using a bespoke approach, excluded targets where no MLEV samples had an expression level less than 100 reads per million (RPM). The DEUS analysis filtered discoveries before normalisation, excluding targets with a raw count less than 1, consequently made the most discoveries.

	tRAX	DEUS	Collaborators
MLEVs	535	4530	983
SEVs	343	225	None

Table 2-12 – Differentially expressed sRNA fragments discovered between early-onset preeclampsia and normal samples, comparing three approaches to analysis

There was strong corroboration of differentially expressed targets in MLEVs between the different analyses. 636 out of 983 fragments identified by our collaborators' approach were also identified by the DEUS analysis. Global comparison with tRAX is not possible because sequences are not retained after mapping and annotations differ. The 12 most abundant differentially expressed targets showed substantial overlap between all three approaches after mapping (Table 2-8, Table 2-10, Table 2-15). Reads mapping to 5'-Glu-CTC were the most abundant upregulated fragments in preeclampsia in all three analyses. Specifically, the three most abundant differentially expressed targets in the DEUS analysis represented the fifth, third and 14th most abundant in our collaborators' analysis (Table 2-13). From a bioinformatic perspective, these represent good targets for validation with qPCR and in plasma samples.

There is less confidence regarding differentially expressed sRNA in preeclampsia SEVs. Our collaborators found no differentially expressed targets. PCA plots from both tRAX (Figure 2-15) and DEUS analyses (Figure 2-18) did not show samples clustering by condition. The number of differentially expressed targets was an order of magnitude lower in SEVs than MLEVs using DEUS. Half of the most abundant differentially expressed fragments in the DEUS SEV preeclampsia analysis (Table 2-11) were not 30-35 nt tRNA species, so did not represent the majority of sRNA within the vesicles as shown in Figure 2-4 and Figure 2-12. Only two of the 12 most abundant fragments identified by DEUS and tRAX were common to both analyses. Thus, validation of discovered targets was only pursued for MLEVs and not for SEVs.

		DEUS					Collaborators			
	Mapping	Rank	Mean PE	Mean N	Log2fc	p-value	Rank	Mean PE	Mean N	Log2fc	p-value
TCCCTGGTGGTCTAGTGGT TAGGATTCGGCGCT	Glu-CTC	1	264726	97247	1.38	5.13E-06	5	52051	18405	1.4998	0.0054
TCCCTGTGGTCTAGTGGTT AGGATTCGGCGCT	Glu-CTC	2	109139	41522	1.34	7.06E-06	3	91226	42503	1.1019	0.0058
TCCCTGGTGGTCTAGTGGT TAGGATTCGGCGCC	Glu-CTC	3	59147	25627	1.17	3.26E-06	14	11566	4849	1.2541	0.0054

Table 2-13 – The three most abundant fragments from DEUS, compared to collaborators' analysis.

2.3.3. Validation of differentially expressed tRNA fragments in preeclampsia medium-large EVs using qPCR

2.3.3.1. Detection assay specificity and linearity

In order to validate bioinformatic discoveries, it is necessary to detect tRFs using an alternative technique to RNA sequencing. Conventional qPCR assays are not capable of detecting tRFs, as forward and reverse primers are longer than their target. Two competing technologies exist for miRNA detection: stem-loop reverse transcription primers and polyadenylation of targets with oligo dT reverse transcription primers[102]. There are numerous publications where stem-loop assays have been co-opted for tRF detection[77,108,109], whilst no studies have used polyadenylation assays. A direct comparison of the two techniques in miRNAs concluded that stem-loop assays offered less variable measurements[110]. Thus, I elected to optimise stem-loop assays; their biochemistry is explained in Methods, section 2.2.4.2 and Figure 2-2.

Seven targets were chosen from the MLEV preeclampsia DEUS analysis, aiming to include a spectrum of RNA fragments discovered: five different iso-acceptor tRNAs, one unmatched, one fragment differing from another target by only a single nucleotide. These targets were labelled F, G, H, J, S, T and W for convenient identification in this thesis and their full identities are described in Table 2-1. Four of these were selected to confirm assay specificity. Stem-loop assays and synthetic oligonucleotides corresponding to these fragments were purchased (Table 2-1). Three 1.5 pM RNA oligonucleotides F, G and H were quantified using four assays F, G, H and J (Figure 2-19). Fragments F and G differed by a single terminal nucleotide; there was some cross-reactivity between these assays, most pronounced when oligo F was detected with assay G with a Cq difference of 6.3 from oligo G. Whilst this demonstrates a 76-fold more abundant signal from the correct oligonucleotide, other fragments showed no cross-reactivity. Given target F was the most abundant differentially expressed fragment in MLEVs, target G was not pursued further. The other assays all showed at least 3 nucleotide differences from one another.

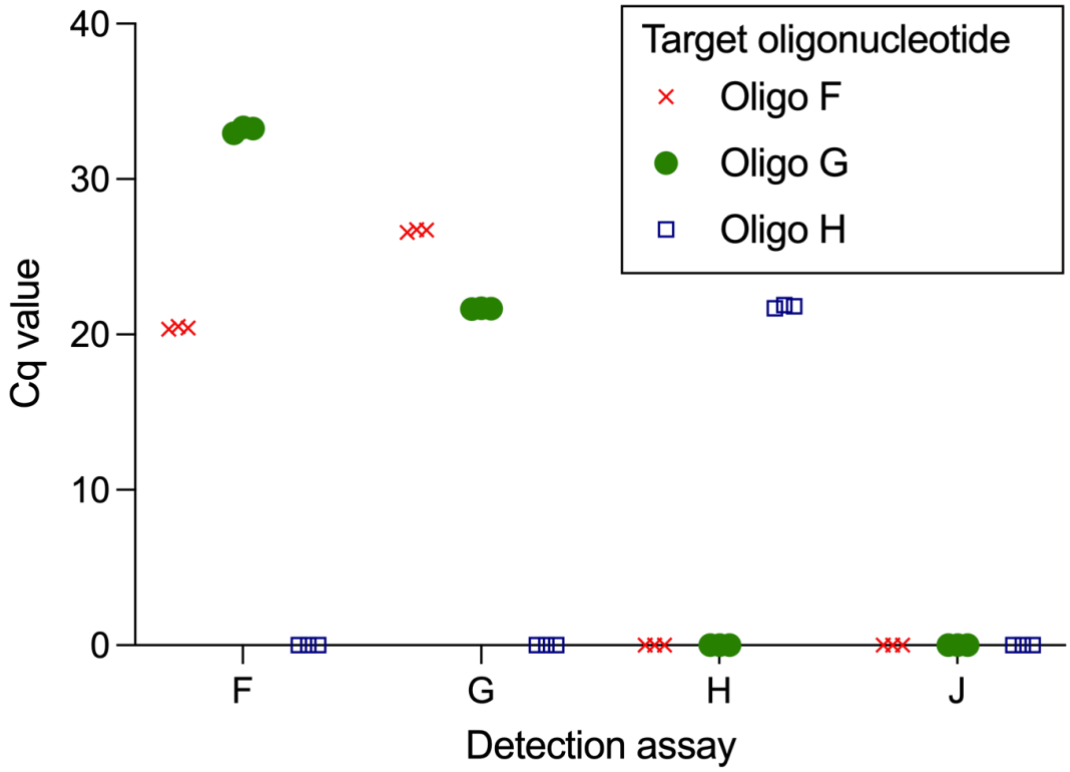


Figure 2-19 – Stem-loop assay specificity determined using synthetic oligonucleotides. Undetermined Cq values representing no oligonucleotide detected are shown as zero, note a lower Cq value represents a greater target abundance. Experiment performed with triplicate repeats.

Two assays were selected to confirm linear dynamic range with RNA dilution. Perfusion STB-EV RNA was diluted 1000-fold and Cq values showed a linear relationship when dilutions were also plotted on a log2 scale (Figure 2-20).

As a consequence of variable access to two PCR instruments during experiments, the two instruments were compared during optimisation (Figure 2-20). Both demonstrated consistent linear dynamic range, but with some absolute differences. Mean Cq differences for assay F ranged between 0.84 and 1.06 and W ranged 0.24 to 0.47. In view of these differences, individual experiments or sample comparisons were conducted on a single instrument.

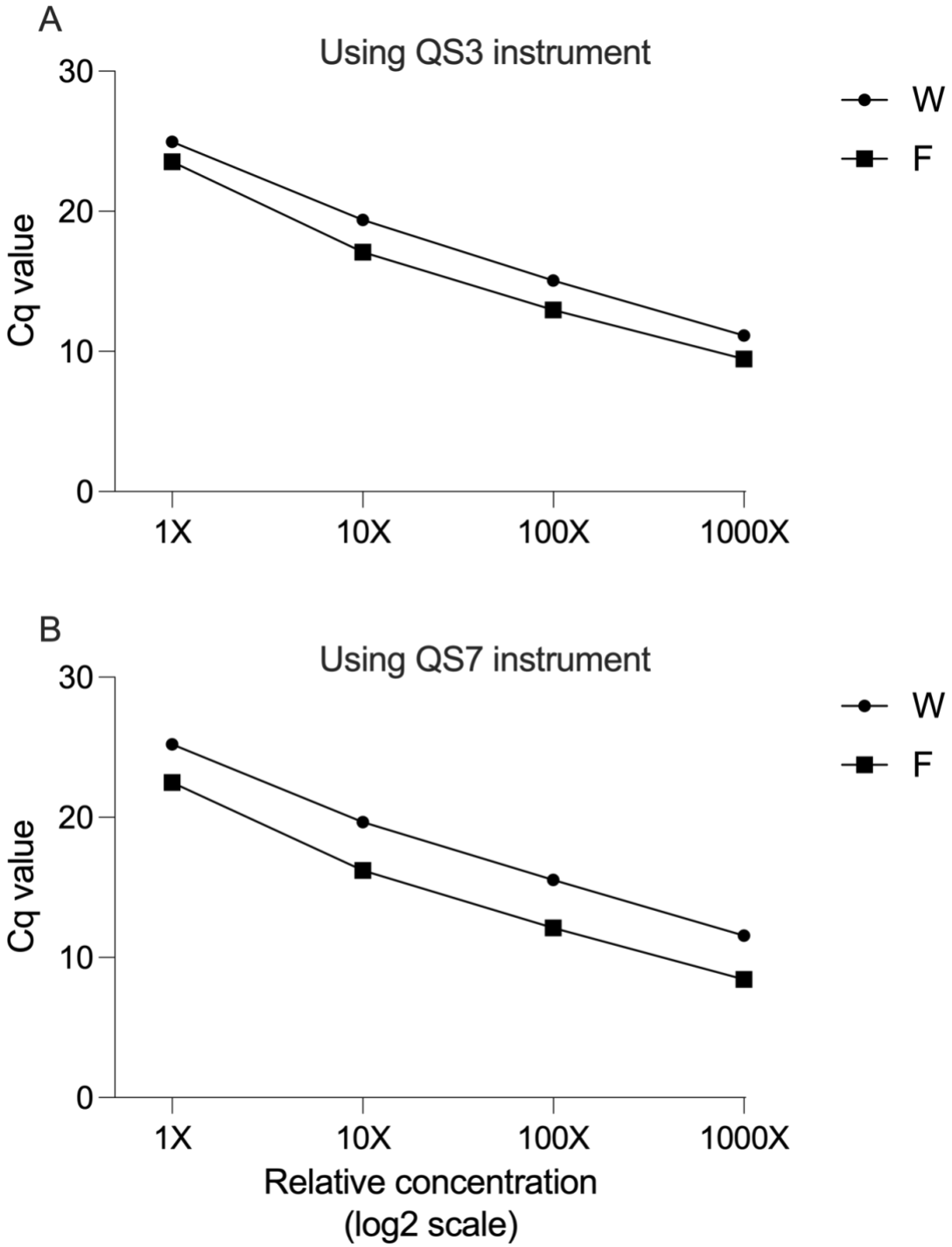


Figure 2-20 – Stem-loop assay linearity with dilution of RNA isolated from perfusion STB-EVs

A. Using QS3 instrument

B. Using QS7 instrument

Note a lower Cq value represents a greater target abundance.

2.3.3.2. Reference gene selection

Normalisation of qPCR data controls for variations in RNA extraction, quantification and loading, reverse transcription and amplification efficiency, allowing target RNA abundance to be compared between different samples. Central to this process is selection of a reference gene (or combination of reference genes) which is stably expressed across different samples and between conditions.

A set of guidelines (MIQE or Minimum Information of Publication of Quantitative real-time PCR Experiments) provides recommendations on qPCR methodology[111]. MIQE advise that reference genes should be empirically validated in the sample type and experimental groups which are being investigated. One recommended approach is to use a purpose-written algorithm called NormFinder[112]. This uses a model to estimate intra- and inter-group expression variation, combining these to create a stability value. The closer the stability value to 0, the more stably expressed the gene.

Three candidate genes (*YWHAZ*, *SDHA* and *TBP*) were identified as candidate reference genes from a prior transcriptomic analysis of STB-EV mRNA (Personal communication, Toluwalase Awoyemi, Vatish Group, Oxford[113]). The expression of these genes was determined in four normal and four preeclampsia STB-EV perfusion samples. The PCR reaction efficiency was determined by linear regression and the raw Cq values transformed to a linear scale by raising the PCR efficiency to the power of the Cq value. The variation and stability values for all three genes were close to zero (Table 2-14). The lowest stability value was for *TBP* alone (0.098), which was superior to the stability value for the best combination of genes (0.120 for *YWHAZ* and *SDHA*, not shown in table). *TBP* was thus selected to normalise qPCR data from perfusion STB-EVs.

Gene name	Stability value	Intragroup variation		Intergroup variation	
		Group 1	Group 2	Group 1	Group 2
YWHAZ	0.187	0.024	0.068	0.099	-0.099
TBP	0.098	0.016	0.011	0.024	-0.024
SDHA	0.190	0.000	0.146	-0.123	0.123

Table 2-14 – Stability values for reference genes in preeclampsia and normal STB-EV samples

2.3.3.3. Differential expression

Figure 2-21A shows the DEUS analysis for the six selected targets, demonstrating differential expression between normal and early-onset preeclampsia MLEVs using RNAseq. Figure 2-21B shows qPCR data for the same six targets from four pairs of the perfusion STB-EV samples, relative to normal pregnancy MLEVs. Four of the targets demonstrated significant differences mirroring the RNAseq data on qPCR despite the small sample size and consequent non-parametric hypothesis test. Target W did not reach significance ($p=0.06$), but the trend reflected the RNAseq data. Target J was downregulated in preeclampsia MLEVs on RNAseq, but showed no significant difference on qPCR. The median value for J in the preeclampsia group was higher than the normal group.

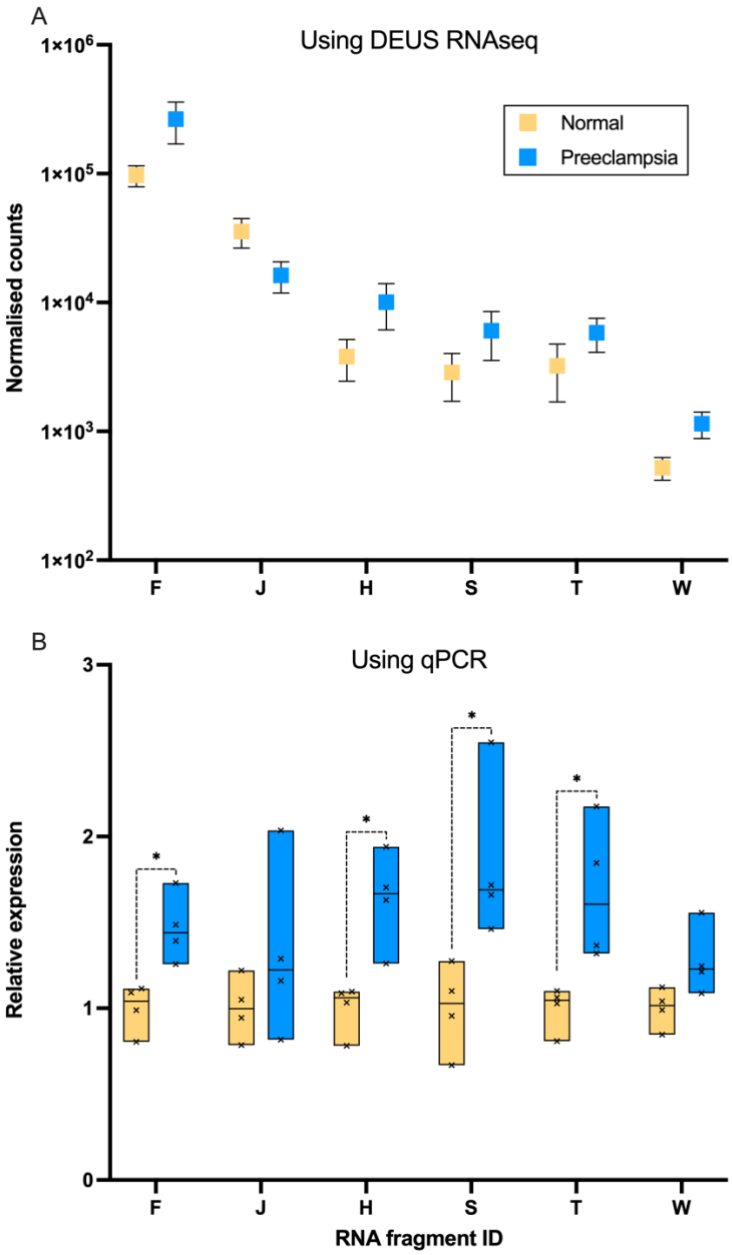


Figure 2-21 – Quantification of target RNA fragments in perfusion STB-EVs Using:

A. DEUS RNAseq

B. qPCR normalised to TBP and relative to normal pregnancy.

*All targets have RNAseq adjusted p-values <0.05; qPCR p-values <0.05 by Mann Whitney test indicated by *. Boxes in A represent mean, error bars represent standard deviation. Boxes in B represent range with a line at the median.*

2.4. Discussion

In the first part of this chapter I compared sRNA molecules contained within MLEVs and SEVs to those within placental biopsies using novel bioinformatic approaches, identifying 5'-tRFs as the predominant sRNA in STB-EVs. This finding is consistent with our prior published analysis of the same dataset, using different methodologies[52]. The presence of tRNA fragments within STB-EVs also aligns with an sRNA analysis of larger explant-derived particles. Wei *et al.* compared explant debris from four preeclampsia and four normotensive placentas, finding miRNA accounted for around 60% of sRNA and tRNA around 20%[46]. The substantial difference in tRNA proportion between this study and my analysis could be explained by a number of methodological differences with the authors' approach. First, they cultured third-trimester explants for 17 hours in air, an oxygen concentration of 160 mmHg. This represents gross hyperoxia by comparison to the term placenta, where intervillous oxygen concentrations are estimated to be around 40 mmHg[114]. tRFs are known to be produced in response to hypoxic stress[66], so it is appropriate that they found a lower tRNA species proportion in sRNA. Second, they appeared to isolate STB-EVs from the first 17 hours of explant culture, when the syncytiotrophoblast is known to be apoptotic[82]. Third, trophoblast debris was isolated by centrifugation at 2000 *g* for 5 minutes, meaning the particles were much larger than classically-described EVs[37]. Finally, they used a sRNA analysis pipeline which does not describe how it handles multi-mapping reads, meaning a proportion of the tRF signal may simply have been disregarded[115]. One publication investigating trophoblast-released sRNA <30 nt, describes tRNA species in placental terminal villi and pregnant plasma sRNA, but does not investigate these further (instead focussing on miRNAs)[116]. Other trophoblast EV miRNA studies used techniques incapable of detecting tRFs such as microarrays and qPCR, or only mapping sequencing data to miRNA databases[49,117,118].

I conclude the DEUS analyses of normal STB-EVs compared to placenta provide sufficient evidence to accept Hypothesis 2.1: specific 5'-tRFs are packaged into STB-EVs

in healthy pregnancies at term. No experimental model to obtain STB-EVs will be without shortcomings. Whilst considered the most physiological model, placental perfusion also works with an organ which would otherwise be apoptotic, perfusing it under hyperoxic conditions. This could be considered the stressor triggering production of tRFs. However, the duration of perfusion is shorter than explants and the system more closely mimics placental physiology, perfusing tissues using existing vasculature rather than macerating tissues and oxygenating them by diffusion across medium in a plate. Whilst many discoveries using perfusion have already been validated in plasma[42,45,86], tRF packaging into STB-EVs also requires *in-vivo* corroboration. This is the goal of Chapter 3.

In the introduction, I highlighted that some 5'-tRFs may have not been detected by the RNA sequencing approach I took. The primers I used would only have bound 5'-phosphate and 3'-hydroxyl RNA fragments. Moreover, RNA modifications may have prevented reverse transcription of some tRFs. If I were designing this study in retrospect, I would compare our sequencing approach to data obtained when RNA were pre-treated to cleave 3'-cP moieties[119]. Whilst this might lead to discovery of further 5'-tRFs, it does not undermine those already discovered, which must have 3'-hydroxyl termini.

The second part of this chapter provides evidence that syncytiotrophoblast MLEV tRF expression changes in preeclampsia, using placental perfusion as a model. I identified over 4000 differentially expressed sRNA fragments in early-onset preeclampsia MLEVs using DEUS. The 12 most abundant fragments accounted for over half of the differentially expressed reads and mapped to four 5'-tRFs. Conversely, the evidence for SEV tRF expression changing in preeclampsia was lacking. DEUS analysis identified only 225 differentially expressed sRNA fragments, with half of the most abundant being too short to represent the 30-35 nt 5'-tRFs identified as the predominant sRNA within SEVs. Our collaborators' analysis did not identify any differentially expressed targets in SEVs.

With the exception of tRAX MLEV analysis, PCA plots consistently showed poor clustering. This implies tRF expression does not explain the majority of differences between diseased and healthy STB-EVs. This finding is consistent with the complexity and heterogeneity of preeclampsia: it is unlikely that tRFs alone would explain whether a woman develops disease; rather the interaction between numerous maternal and fetal factors is likely to explain the variable phenotype and prevalence of the condition[9].

5'-tRFs were normalised to all sRNA during analysis. This cannot take into account the number of vesicles released in each condition, only the abundance of each target per vesicle. Given STB-EV release is convincingly upregulated in early-onset preeclampsia[40,120], this makes the targets upregulated in preeclampsia (e.g. 5'-tRF-Glu-CTC) the more compelling for further investigation. Downregulated targets may still reach target tissues in greater abundance than in normal pregnancy, simply because of increased vesicle release.

This work is entirely novel and direct comparison with the literature is not possible. It is relevant to note extensive evidence from cell culture (including BeWo cells, a syncytiotrophoblast line) demonstrating that cellular stress increases extracellular tRF production (specifically 5'-tRFs of 31-33 nt length)[66]. Together with compelling arguments that syncytiotrophoblast stress is a unifying step in the syndrome of preeclampsia[7], this adds biological plausibility to my findings, but not direct corroboration.

It is also interesting to compare my findings with a study of tRF expression in plasma exosomes from patients with atopic dermatitis and controls[73]. Whilst the disease processes, biofluids and isolation techniques were different, the magnitude of difference in specific 5'-tRF expression between disease and normal was similar to our findings. For example, the two verified differentially expressed 5'-tRFs were approximately 1.5-2 fold less abundant in the dermatitis cohort than the control cohort. This is similar to the

differences between STB-EV 5'-tRF expression in preeclampsia and normal pregnancies (Figure 2-21).

These findings must be considered in the context of their limitations. Cases of preterm preeclampsia could not be gestationally matched to controls (Table 2-7). Early-onset disease was chosen as the most homogenous and severe subtype of preeclampsia, where syncytiotrophoblast stress and differences in STB-EV cargo are most accepted[41]. It was not ethically possible to obtain true gestation-matched controls: pregnancies delivered before 34 weeks of gestation are almost invariably complicated by placental pathology which might confound a comparison with preeclampsia. I aim to overcome this confounding by validating differentially expressed targets in gestation-matched plasma samples (Chapter 4).

This study did not phenotype early-onset preeclampsia, instead considering syncytiotrophoblast stress to be the common feature in all presentations of preeclampsia[7]. The preeclampsia community increasingly recognises that disease heterogeneity might be a barrier to prediction and treatment of preeclampsia[9]. If I had selected a carefully defined subtype of preeclampsia our differential expression analysis might be considered more valuable. However, there remains no consensus within the field as to how subtypes might be defined.

The earlier potential criticism that perfusion itself might drive STB-EV tRF production is countered by the identification of differences between preeclampsia and normal MLEVs. Whilst the vasculature of the placenta is different in preeclampsia, this is unlikely to result in dramatically different oxygen levels reaching the tissues over 3 hours with hyperoxic perfusion medium.

DEUS software provided more complete and useful information than tRAX throughout the analyses and was used for subsequent target selection. DEUS results were corroborated by the independent analysis, which identified many overlapping targets. One highly abundant 5'-tRF downregulated in preeclampsia (5'-tRF-Gly-GCC) was reported by the independent analysis but not DEUS. This is likely due to adjustment of p-values in the DEUS negating this result; p-adjusted was only just significant (0.03) in the independent analysis by our collaborators.

In the third part of the chapter, I sought to corroborate bioinformatic analyses of preeclampsia MLEV sequencing data with qPCR. I successfully optimised qPCR assays to quantify 5'-tRFs in placental perfusion samples, demonstrating assay linearity with RNA dilution. There was some cross-reactivity between assays where the target was only a single terminal nucleotide different, contrary to reported findings in the literature[103]. This led me to select validation targets with more than one single nucleotide difference. I tested stability of reference genes, demonstrating very low inter- and intra-group variation and demonstrating *TBP* alone was the superior reference gene. Ultimately four of the six tested targets validated using qPCR. Interestingly, the downregulated target (J) was non-significantly upregulated using qPCR. It may be that this was simply a false discovery from the sequencing data. Certainly, it adds further support to my earlier conclusion that attention should be focussed on preeclampsia-upregulated targets.

There are two important criticisms of the qPCR validation work. Primarily, the sample size was very small, meaning that investigation of some targets was likely underpowered. Additionally, targets were validated in a selection of the same samples from which they were discovered. Both of these shortcomings were driven by pragmatism: obtaining and successfully perfusing further early-onset preeclampsia placentas would like require a significant investment of time and resources, which I felt were better directed at plasma validation (where gestational age confounding could be overcome).

Overall, the sRNA sequencing analyses and qPCR validation data support acceptance of Hypothesis 2.2: STB-EV tRF expression changes in early-onset preeclampsia, for MLEVs but not for SEVs.

In summary, sRNA sequencing of placental perfusion STB-EVs and placental biopsies has allowed me to demonstrate 1) specific 5'-tRFs are packaged into STB-EVs in healthy pregnancies at term and 2) STB-EV tRF expression changes in early-onset preeclampsia (Figure 2-22). The best way to overcome shortcomings of placental perfusion as a model, and concerns regarding case-control selection, is to attempt to validate these findings in plasma samples using the optimised qPCR assays. This work is presented in Chapter 3 and Chapter 4.

2.5. Summary Figure

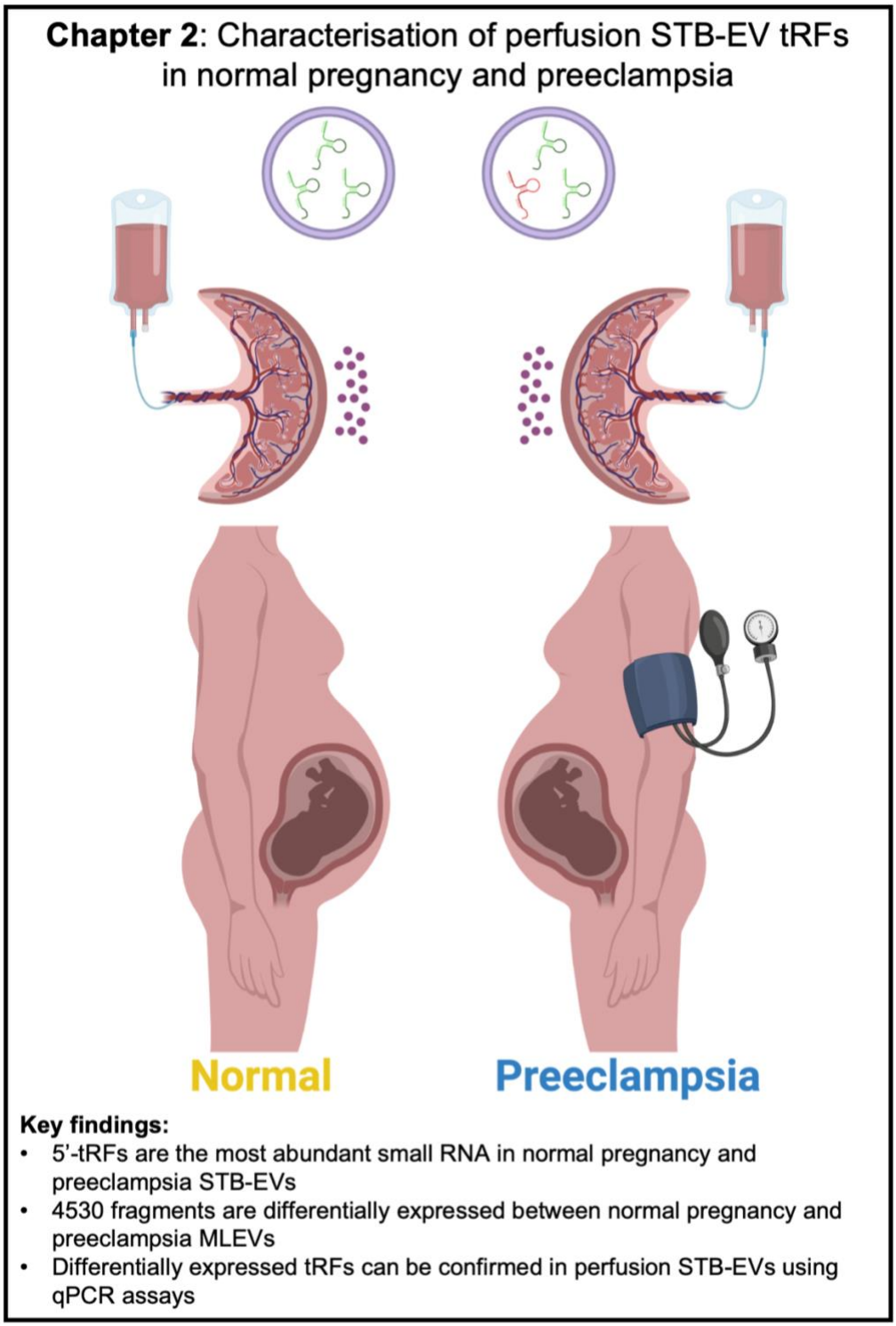


Figure 2-22 – Schematic figure summarising Chapter 2 key experiments and findings.

Created with biorender.com with a publication licence under agreement number ED25OVBN02.

2.6. Appendix 1

Independent analysis by collaborators

Jinyue Bai, Ji Lu and Peiyong Jiang at The Chinese University of Hong Kong conducted an independent analysis of the same dataset. They also found the majority of sRNA fragments in STB-EVs to be 5'-tRFs of 30-35 nt in length (Figure 2-23). They wrote a bespoke bioinformatics pipeline to compare preeclampsia and normal samples, applying the principles of the DEUS approach (mapping after differential expression analysis to avoid data loss – Figure 2-8). They also identified one preeclampsia SEV sample to be a clear outlier and excluded this from their analysis. They identified 983 differentially expressed sRNA fragments in preeclampsia MLEVs compared to controls; 182 mapped to 5'-tRFs using GtRNAdb2.0[62]. No fragments were found to be differentially expressed in preeclampsia SEVs.

The 12 most abundant differentially expressed fragments from their analysis of MLEVs are shown in Table 2-15. Using the sum of preeclampsia MLEV normalised counts as a denominator, these 12 fragments account for 64% of the differentially expressed counts. 5% of these counts were attributed to the 626 least abundant fragments. Thus, a small number of abundant fragments represented the majority of the signal in an otherwise complex dysregulated sRNA profile in preeclampsia MLEVs.

Comparing to human sRNA databases, among the 12 most abundant differentially expressed fragments, three were identified as 5'-tRFs and four as piwi-interacting RNA. The remaining five had no directly matched reference sequences in human sRNA databases and are referred to as "unmatched". Review of fragment sequences demonstrated overlap; indeed all 12 showed only one or two nucleotide insertions or deletions differentiating them from known 5'-tRFs (differences highlighted in Table 2-15). Thus, their analysis supports my conclusion that a complex profile of differential

expression in preeclampsia MLEVs was dominated by minor variants of a handful of abundant 5’-tRNA fragments.

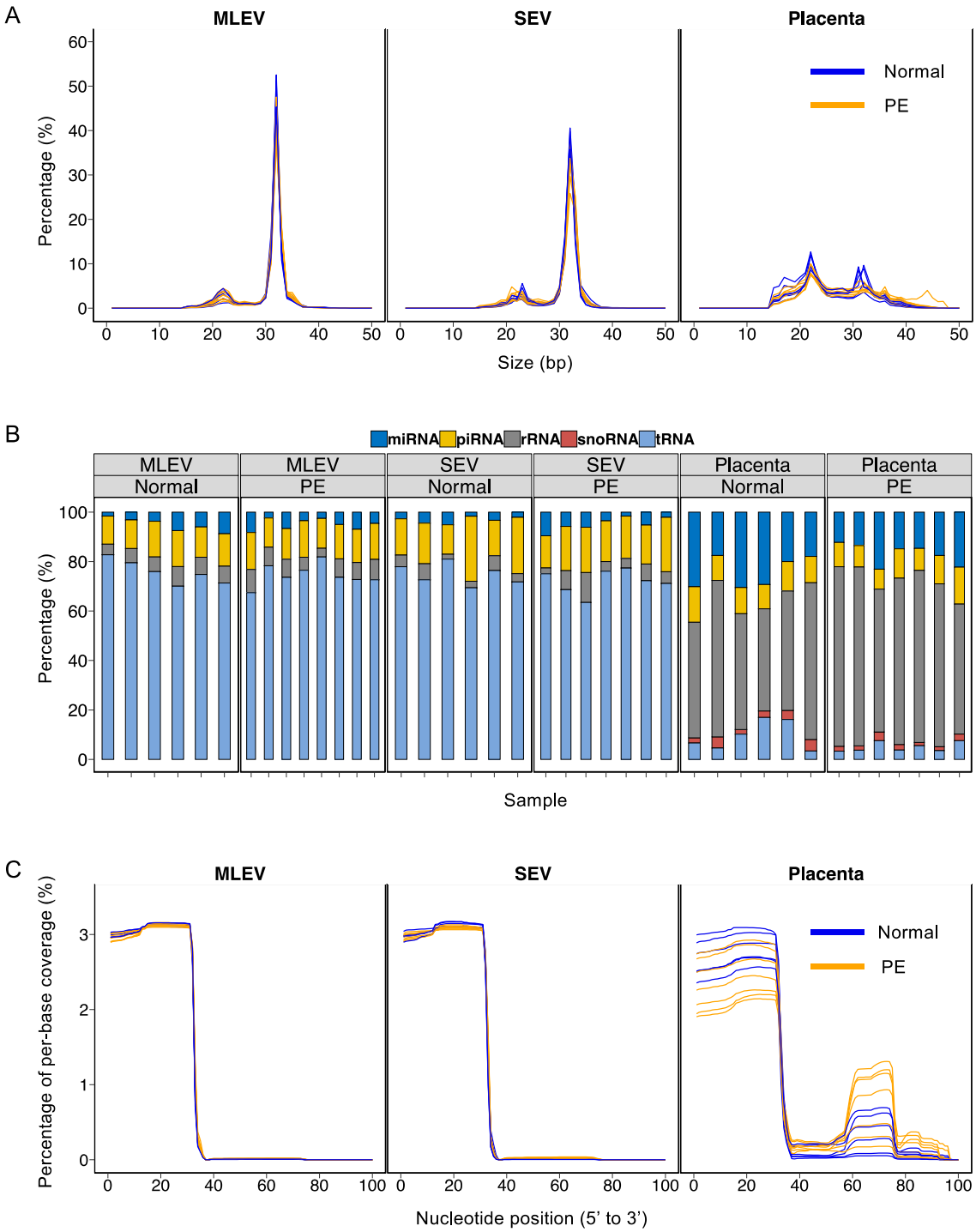


Figure 2-23 – Size distribution, mapping and base coverage of preeclampsia and normal sample sRNA by collaborators.

Rank	Sequence	Length	GtRNAdb mapping	Mapping with ≤2 indels	Log2Fold Change	Adjusted p-value	Mean PE count	Mean N count	% PE DE reads	Cumulative % PE DE reads
1	GCATTGGTGGTTCAGTG GTAGAATTCTCGCCT	32	Gly-GCC	Gly-GCC	0.16	0.0335	273954	305199	24.5	24.5
2	GCATTG_TGGTTCAGTG GTAGAATTCTCGCCT	31	Unmatch	Gly-GCC	0.66	0.0058	102499	161979	9.2	33.6
3	TCCCT_GTGGTCTAGTG GTTAGGATTCGGCGCT	32	Unmatch	Glu-CTC	-1.10	0.0058	91226	42503	8.2	41.8
4	GCATTGGTGGTTCAGTG GTAGAATTCTCGCCC	32	Gly-GCC	Gly-GCC	0.32	0.0150	62934	78646	5.6	47.4
5	TCCCTGGTGGTCTAGTG GTTAGGATTCGGCGCT	33	Glu-CTC	Glu-CTC	-1.50	0.0054	52051	18405	4.7	52.1
6	TCCCTGGTGGTCTAGTG GTTAGGATTCGGCGC_	32	piR-5938	Glu-CTC	-1.29	0.0085	27597	11286	2.5	54.5
7	GCATTGTGGTTCAGTGG TAGAATTCTCGCCC_	31	Unmatch	Gly-GCC	0.80	0.0058	24069	41872	2.2	56.7
8	TCCCTG_TGGTCTAGTG GTTAGGATTCGGCGCC	32	Unmatch	Glu-CTC	-0.88	0.0058	20922	11389	1.9	58.6
9	GCATTGTGGTTCAGTGG TAGAATTCTCGCC__	30	Unmatch	Gly-GCC	0.65	0.0305	20992	32864	1.9	60.4
10	TCCCTGGTGGTCTAGTG GTTAGGATTCGGCG__	31	piR-5938	Glu-CTC	-2.19	0.0085	15003	3282	1.3	61.8
11	GCCCGGCTAGCTCAGT CGGTAGAGCATGAGAC	32	piR-27622	Lys-CTT	0.73	0.0220	12391	20600	1.1	62.9
12	GTTTCCGTAGTGTAGTG GTTATCACGTTCGC__	31	piR-28877	Val-AAC	0.87	0.0128	11802	21618	1.1	63.9

Table 2-15 – Twelve most abundant sRNA fragments differentially expressed (DE) in early-onset preeclampsia compared to normal pregnancy MLEVs, following bespoke analysis by collaborators

Ranked by abundance in preeclampsia MLEVs, annotations coloured by iso-acceptor.

2.7. Appendix 2

Figure 2-3 and Figure 2-11 displaying RNA sequencing data quality control metrics are reproduced in a larger format in this appendix for clarity.

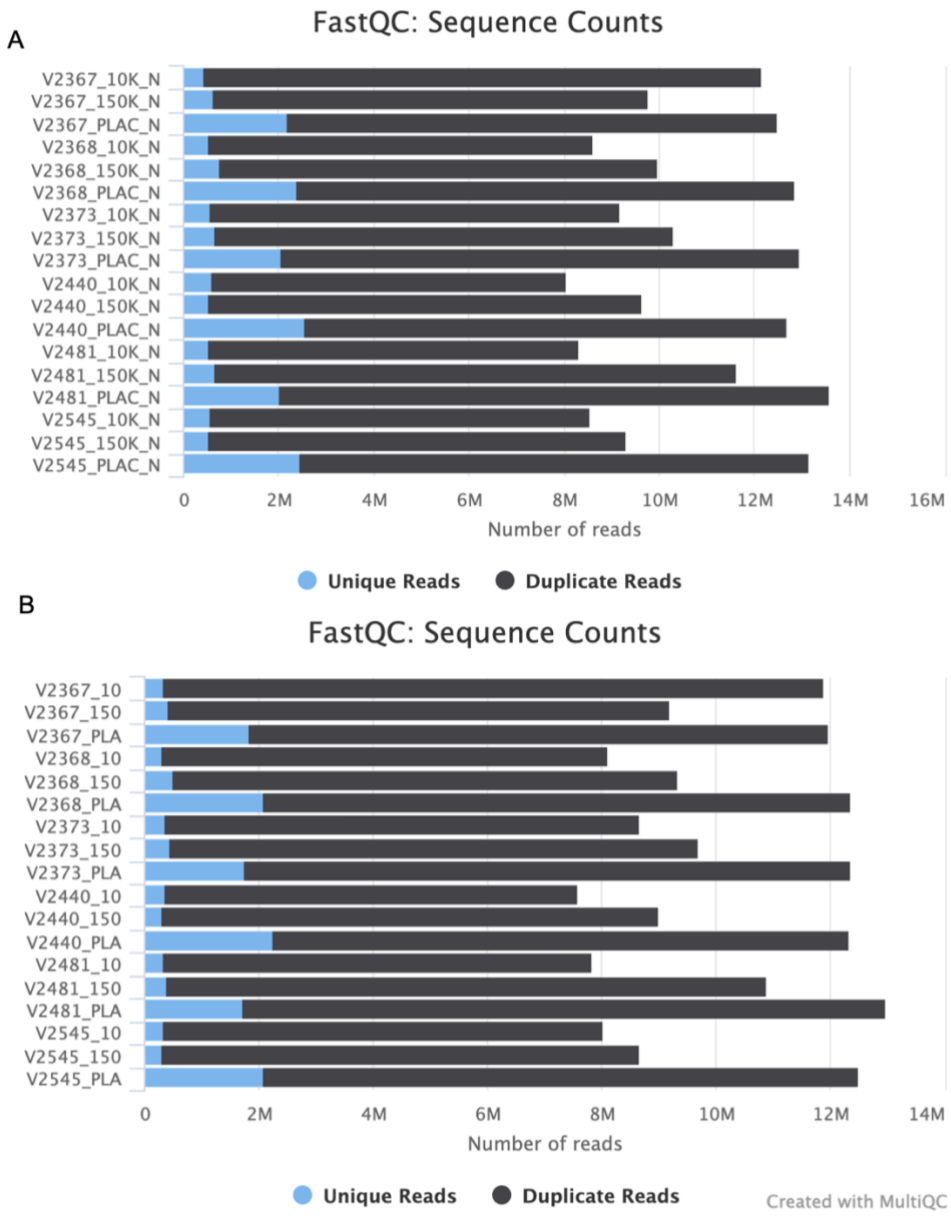


Figure 2-24 – Large format reproduction of quality control data for normal pregnancy samples. Panel labels consistent with Figure 2-3 for ease of reference.

A: sequence counts, raw data

B: sequence counts, after removal of adapters and low-quality reads

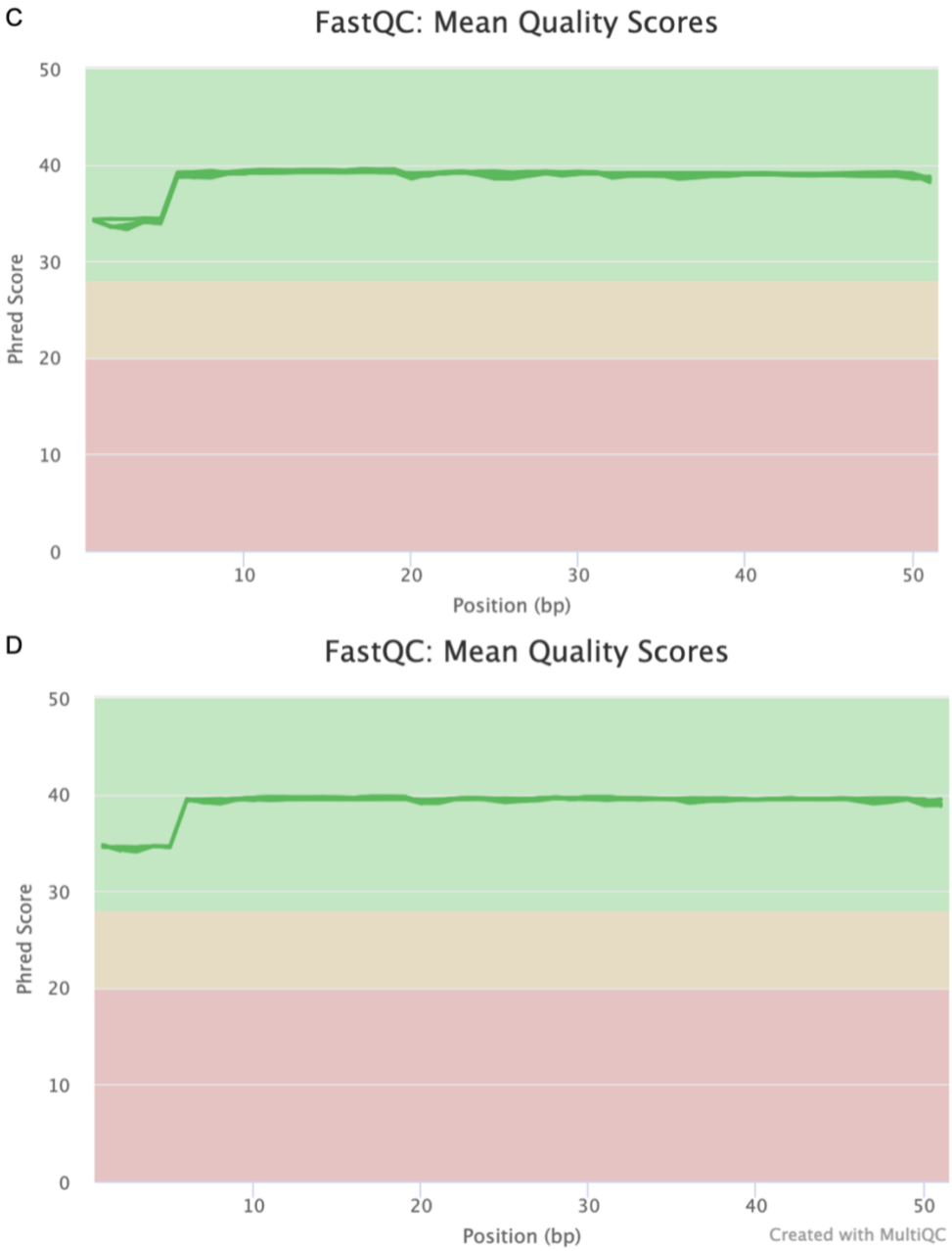


Figure 2-25 – Large format reproduction of quality control data for normal pregnancy samples. Panel labels consistent with Figure 2-3 for ease of reference.

C: mean quality scores, raw data

D: mean quality scores, after removal of adapters and low-quality reads

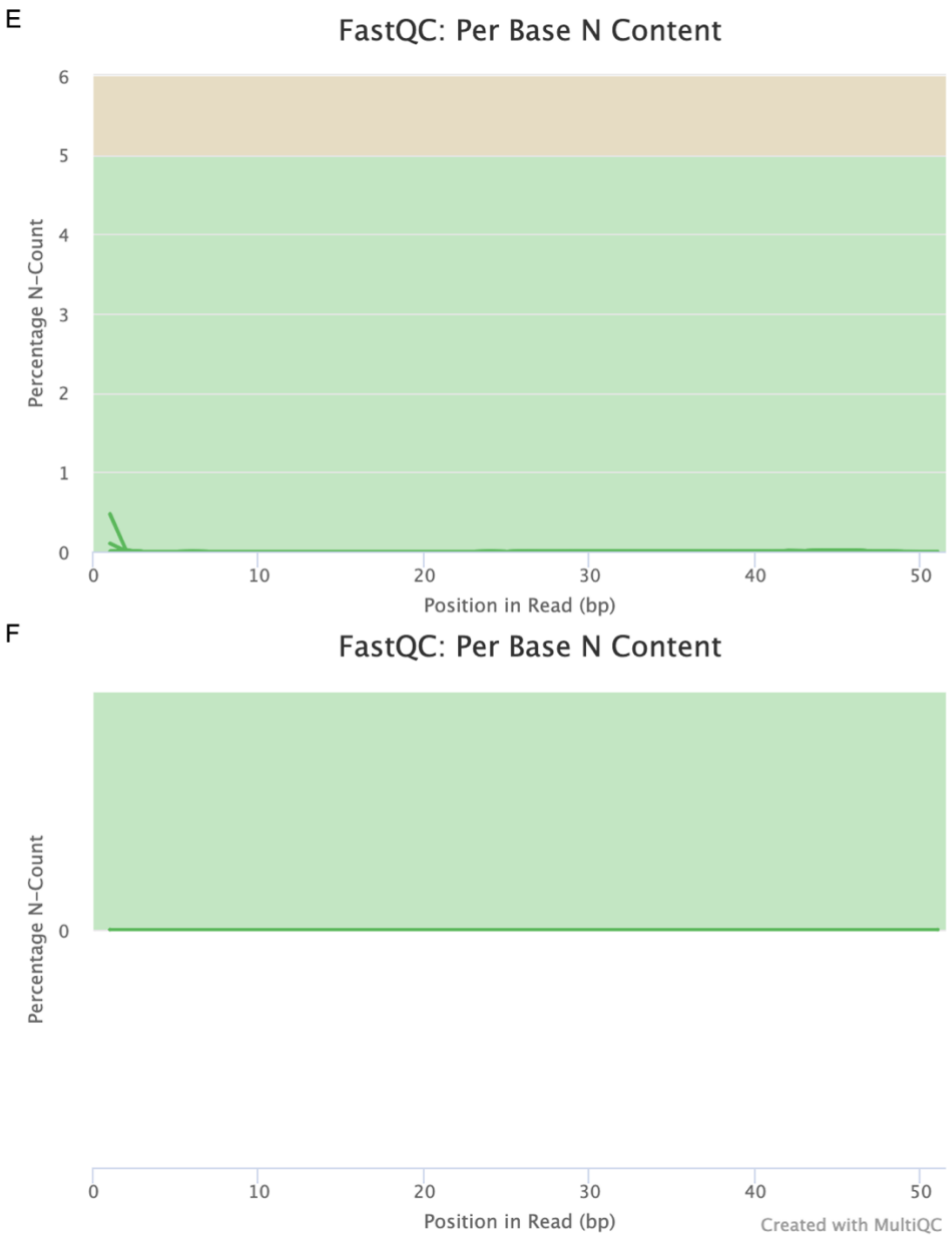


Figure 2-26 – Large format reproduction of quality control data for normal pregnancy samples. Panel labels consistent with Figure 2-3 for ease of reference.

E: per base N content, raw data

F: per base N content, after removal of adapters and low-quality reads

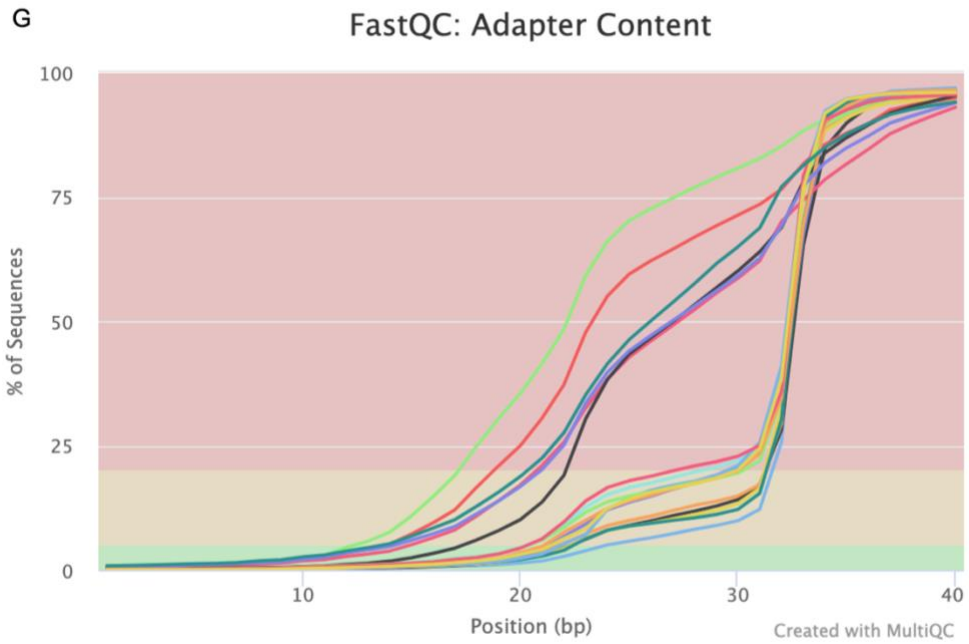


Figure 2-27 – Large format reproduction of quality control data for normal pregnancy samples. Panel label consistent with Figure 2-3 for ease of reference.

G: adapter content, raw data

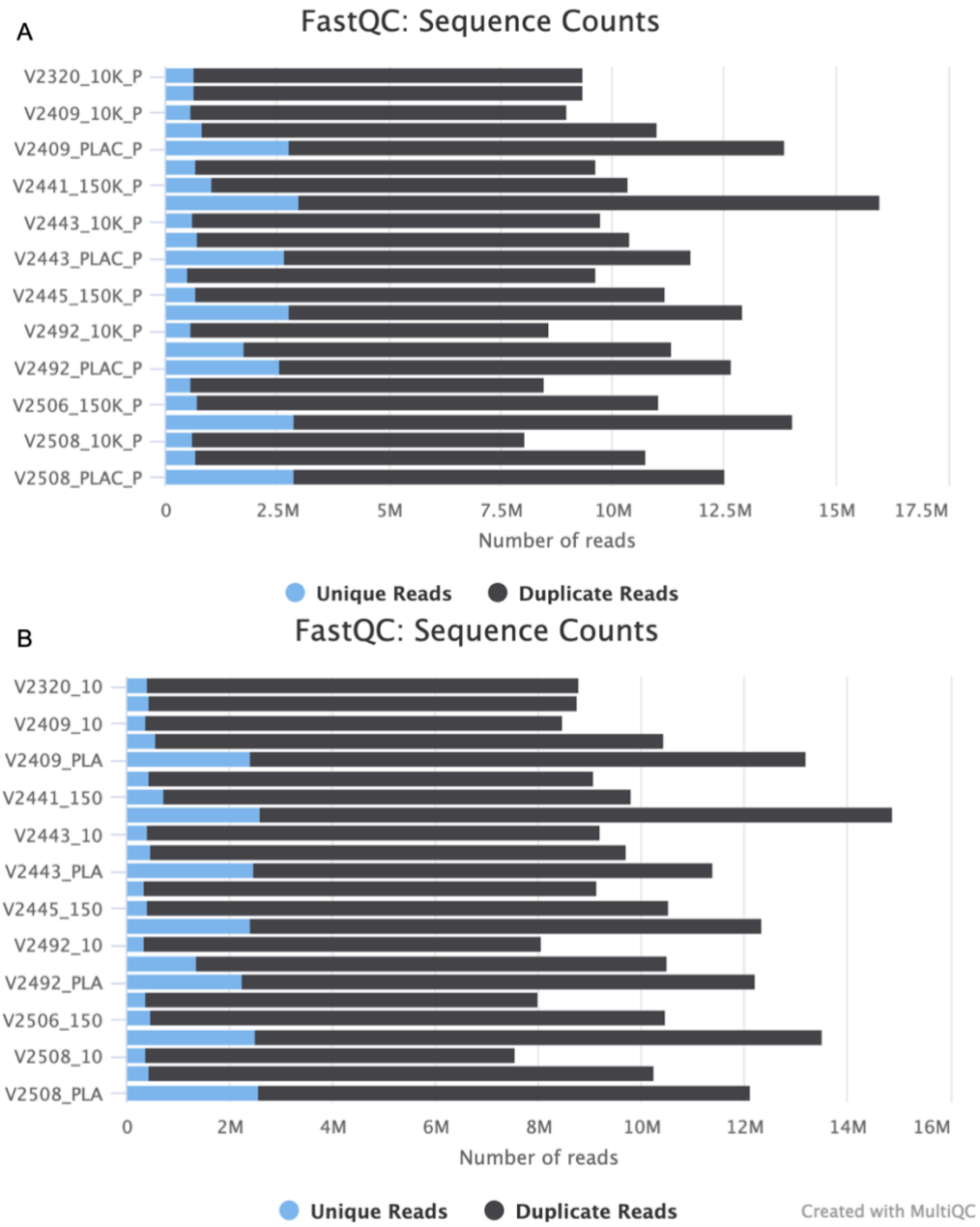


Figure 2-28 – Large format reproduction of quality control data for early-onset preeclampsia pregnancy samples. Panel labels consistent with Figure 2-11 for ease of reference.

A: sequence counts, raw data

B: sequence counts, after removal of adapters and low-quality reads

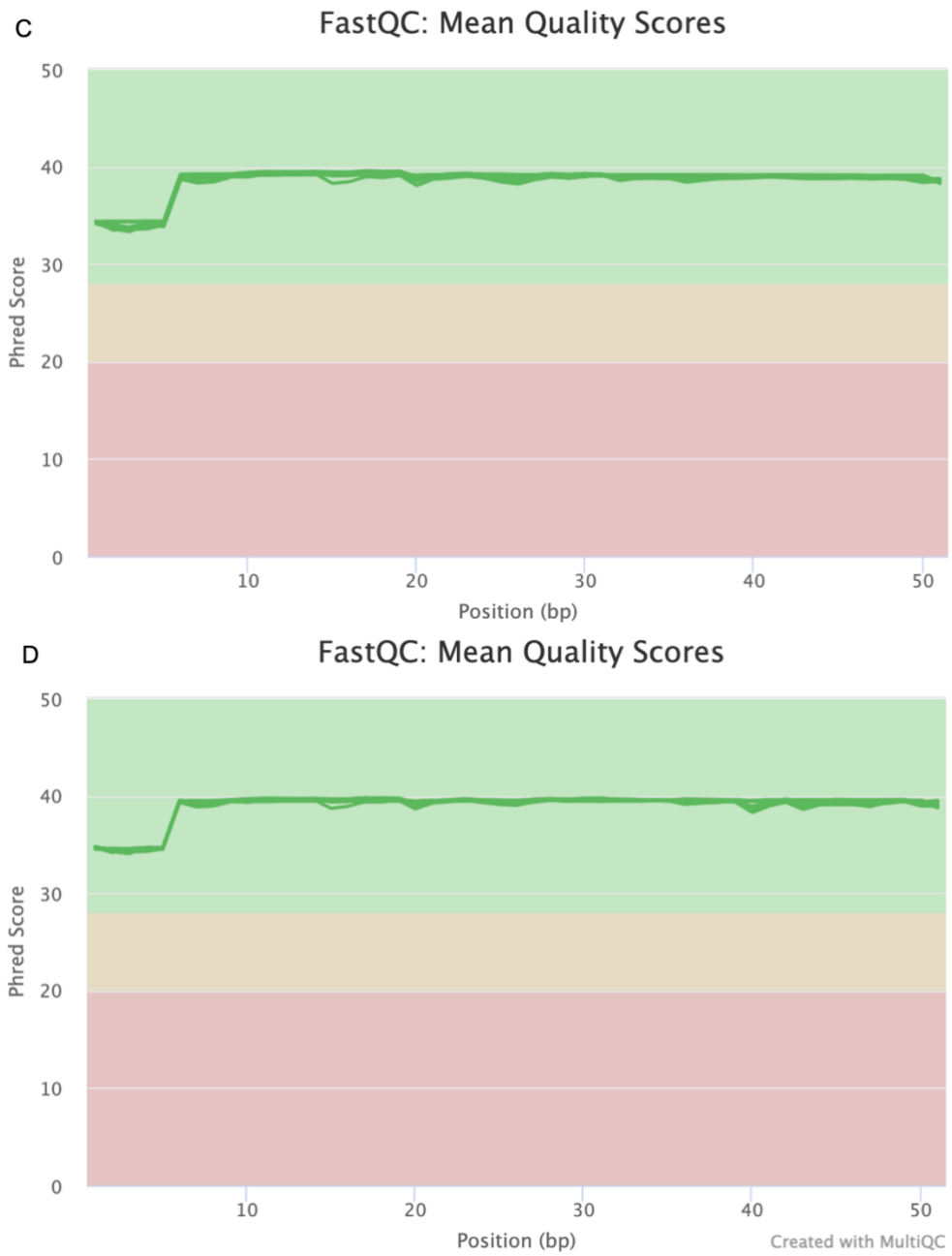


Figure 2-29 – Large format reproduction of quality control data for early-onset preeclampsia pregnancy samples. Panel labels consistent with Figure 2-11 for ease of reference.

C: mean quality scores, raw data

D: mean quality scores, after removal of adapters and low-quality reads

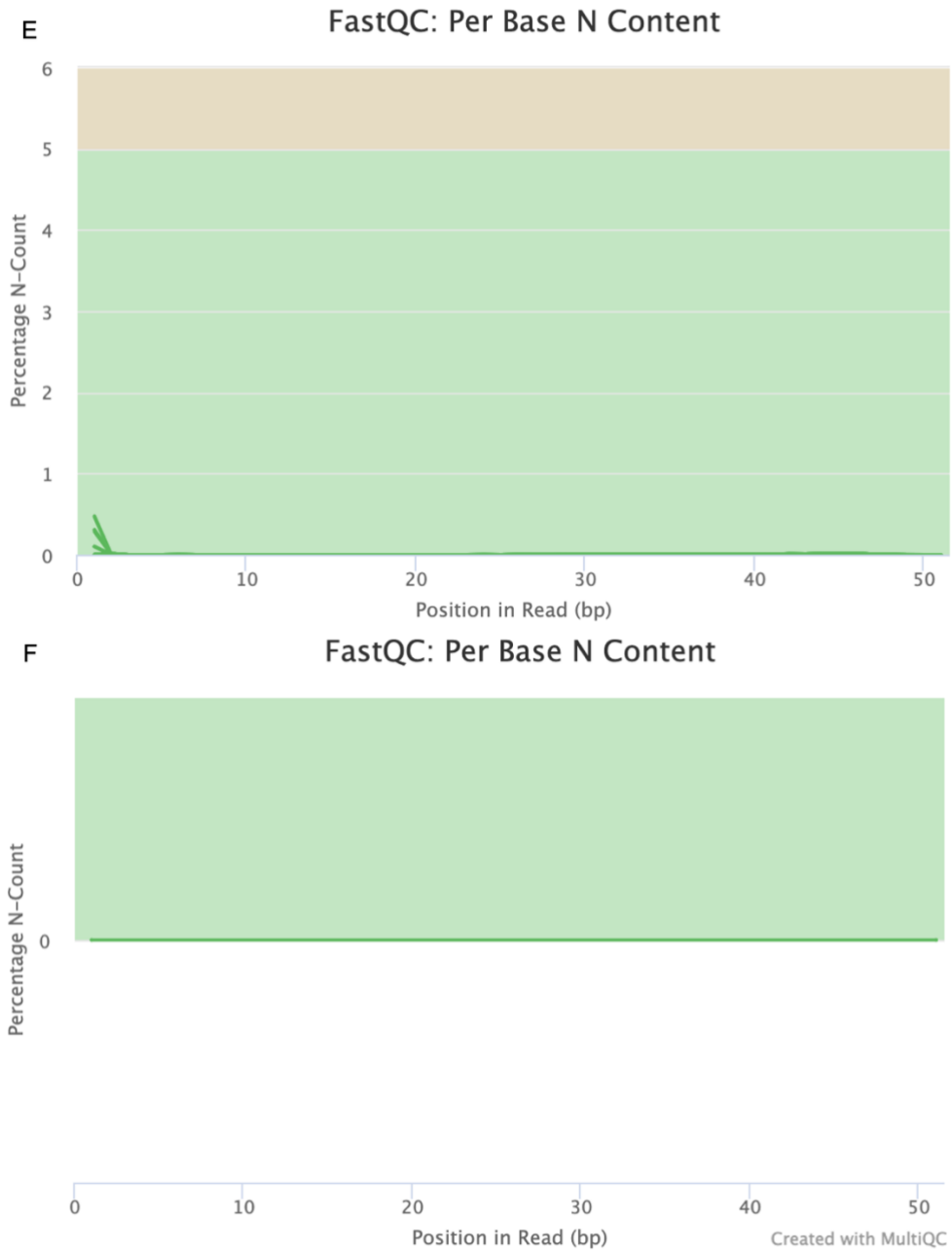


Figure 2-30 – Large format reproduction of quality control data for early-onset preeclampsia pregnancy samples. Panel labels consistent with Figure 2-11 for ease of reference.

E: per base N content, raw data

F: per base N content, after removal of adapters and low-quality reads

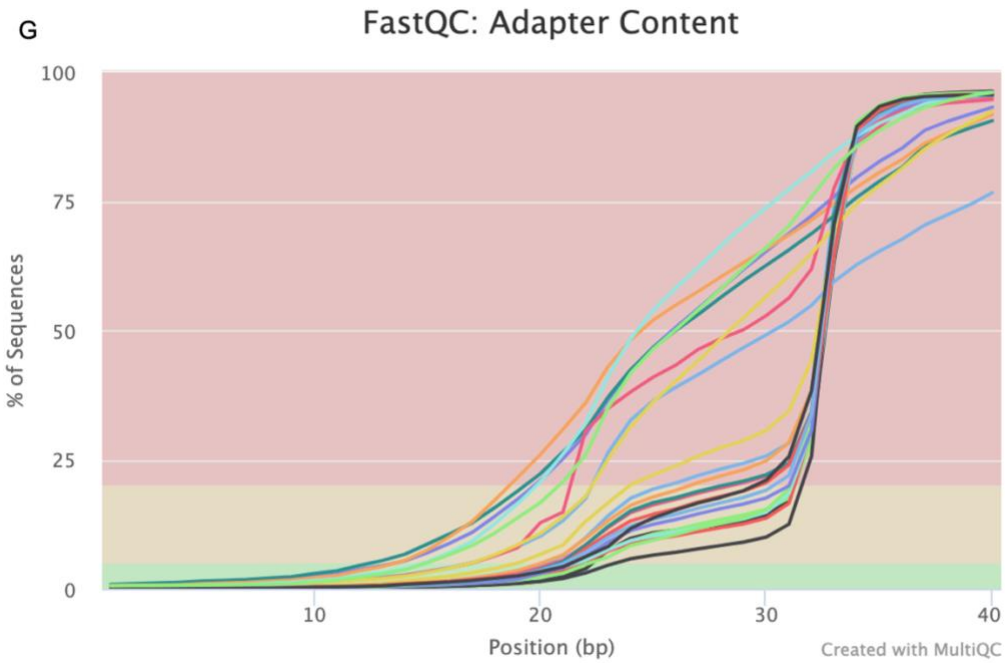


Figure 2-31 – Large format reproduction of quality control data for early-onset preeclampsia pregnancy samples. Panel label consistent with Figure 2-11 for ease of reference.

G: adapter content, raw data

Chapter 3. Investigating syncytiotrophoblast tRNA fragments in the maternal circulation

3.1. Introduction

3.1.1. Rationale for 5'-tRNA fragment validation in the maternal circulation

The discovery of both 5'-tRNA fragment (5'-tRF) release by the placenta in syncytiotrophoblast-derived extracellular vesicles (STB-EVs)[52], and their differential release in preeclampsia (Chapter 2) are based on data derived from *ex-vivo* placental perfusion. Given 5'-tRFs are released in response to cellular stress, it is important to verify that this discovery is not an artefact of the experimental model used[66]. One previously published explant study provides some corroboration, finding that tRNA fragments account for between 12.8% and 17% of the total small RNA (sRNA) population in larger "trophoblast debris"[46]. However, "debris" was isolated by low-speed centrifugation (2000 *g* for 5 minutes), the analysis pipeline was not designed for tRNA analysis and explants should be considered a less physiological model than perfusion (see 2.1.3).

In Chapter 2, 5'-tRF stem-loop qPCR assays were optimised, enabling relatively inexpensive and rapid detection in perfusion STB-EVs with good specificity. Chapter 3 aims to apply these assays to plasma, to determine whether placentally-derived 5'-tRFs can be identified *in-vivo* in the maternal circulation.

3.1.1.1. Hypothesis 3.1

A placental 5'-tRF load can be detected in maternal blood using qPCR assays.

3.1.2. Detecting and isolating EVs from blood

Blood is a complex biofluid. A *Nature Reviews Molecular Cell Biology* article recently reflected that "separating circulating extracellular vesicles from other particulate matter … is bloody difficult"[121]. A 2022 "Blood EV Workshop" organised by the International Society for Extracellular Vesicles (ISEV) in Helsinki brought together experts from across

disciplines working on this problem and highlighted a number of important considerations, which are summarised below.

3.1.2.1. Pre-analytical variables in blood

At least thirty-seven variables have been identified at the pre-analytical stage which can influence EV detection in blood[122]. A common factor across many is the activation of platelets, which generates EVs[123]. At the collection stage, important variables include tourniquet application and duration, needle bore and duration of draw. Untreated blood clots outside the circulation; allowing this to happen (to create serum) results in significant *in vitro* EV release[123]. Different anticoagulants also affect the EV profile and platelet EV release[124]. Sample transportation, centrifugation and storage conditions are all key determinants of EV detection[125].

Studies are ongoing to characterise how many of these variables change EV detection. In the interim, guidelines have been published by ISEV, the International Society of Thrombosis and Haemostasis and the journal *Circulation Research*[37,126,127]. Where evidence is clear, the superior option is recommended. Where data are lacking, they recommend consistency and clear description of methods to allow others to replicate results.

All evidence comparing pre-analytical approaches in the literature is derived from non-pregnant blood. It is not within the scope of this thesis to optimise every variable in pregnancy empircally. For the majority of variables, existing departmental Standard Operating Procedures were used and are described in section 3.2.1. Two key pre-analytical decisions were made and are justified as follows. Citrated plasma was chosen, as recommended by two of the three guidelines because it results in lower levels of platelet and myeloid-derived EV release[124]. Citrate is also well-suited to RNA analysis as it does not interfere with PCR reactions, unlike heparin[128]. A two-step centrifugation

protocol was initially selected to reduce contamination with platelets[129], which might co-isolate with EVs and result in confounding.

3.1.2.2. Contaminating particles in blood

Figure 3-1A illustrates five key categories of small particle which can co-isolate with EVs from blood if size or density separation techniques are used. Lipoproteins and chylomicrons outnumber EVs by several orders of magnitude (Figure 3-1C). Even if EVs are successfully isolated, analysis of the "EV-TRACK" database (where authors can self-record their experimental parameters) identified 1038 unique protocols to isolate EVs from biofluids in 2017[130]. This variety in isolation techniques leads to an equally large spread in estimates of the plasma EV concentration (Figure 3-1B).

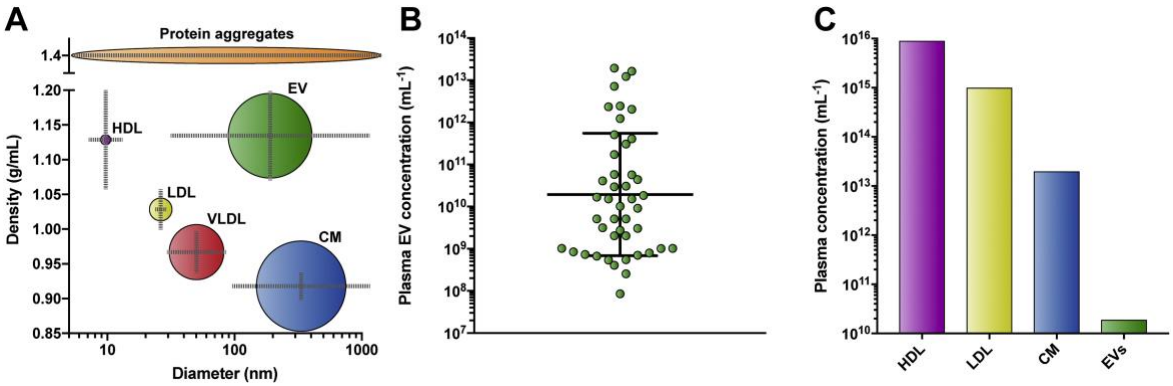


Figure 3-1 – Extracellular vesicles are a minority population amongst small particles in human plasma.

A. Schematic diagram demonstrating the density and size of contaminating particles which can be co-isolated with EVs from plasma.

B. Estimated EV concentration in human plasma using different isolation methods

C. Estimated EV concentration in human plasma compared to similarly sized contaminating particles

Abbreviations: extracellular vesicle, (EV), high density lipoprotein (HDL), low density lipoprotein (LDL), very low density lipoprotein (VLDL), chylomicron (CM).

Reprinted from BBA - Reviews on Cancer, 1871 (1), Johnsen KB, Gudbergsson JM, Andresen TL, Simonsen JB, What is the blood concentration of extracellular vesicles? Implications for the use of extracellular vesicles as blood-borne biomarkers of cancer, © 2019, with permission from Elsevier under licence number 5563150983314.

3.1.2.3. Approaches to enrichment of EVs from blood

EV enrichment protocols can be grouped into six approaches: precipitation (e.g. membrane affinity columns or polyethylene glycol), size exclusion chromatography, differential ultracentrifugation, density gradient centrifugation, asymmetric flow field-flow fractionation (AF4) and immunoprecipitation[131]. Differential ultracentrifugation and density gradient centrifugation risk significant EV loss when resuspending the EV pellet so are less appropriate for quantitative work. The instrument required for AF4 was not available during thesis preparation. In the absence of a ubiquitous EV protein marker, immunoprecipitation only allows EV subgroup isolation. Consequently, two techniques were chosen for initial comparison, both of which were commercially advertised as being optimised for total plasma EV isolation: membrane affinity columns (MAC) and size-exclusion chromatography (SEC).

3.1.3. STB-EVs as a proportion of blood EVs

If the perfect, consistent technique were found to isolate all EVs from the best preparation of plasma, STB-EVs would still represent a small proportion of the total EV load. Figure 3-2 estimates the proportion of non-pregnant plasma EVs derived from different blood cell lineages; solid organ EVs are thought to contribute <1% of the population[132].

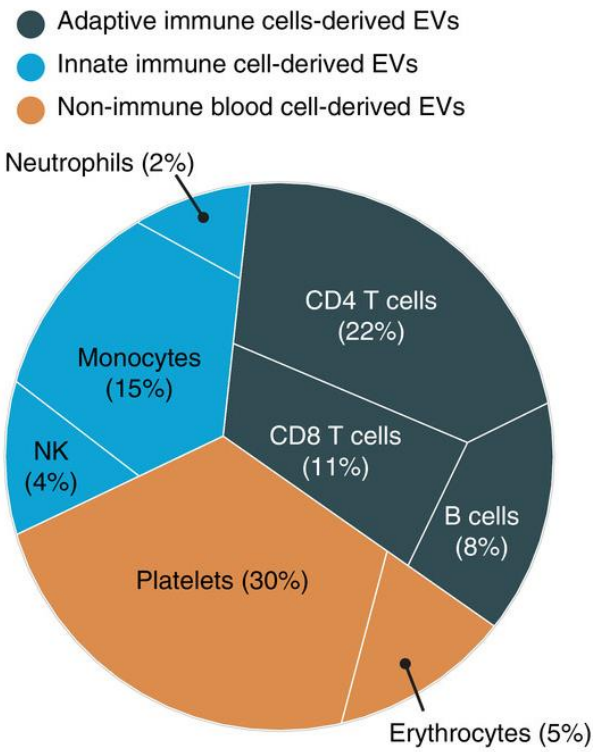


Figure 3-2 – Estimation of plasma EV derivations in non-pregnant donors

Figure reproduced without changes from Auber and Svenningsen[132], under creative commons licence CC BY 4.0, available at https://creativecommons.org/licenses/by/4.0/

Estimations of STB-EV abundance compared to total EV load are variable. Figure 3-3 is from a study which used flow cytometry to analyse EVs in platelet-free pregnant plasma. EVs derived from platelets were identified using CD41 antibody, red cells using CD235a, antibody, leucocytes using HLA class 1 W6/32 antibody, STB-EVs using placental alkaline phosphatase (PLAP) antibody; EVs not captured by any of these markers were labelled as orphan EVs. When expressed as a percentage, STB-EVs account for <1% of the total plasma EV population (Figure 3-3B). Consequently, the second aim of this chapter was to optimise a technique to enrich STB-EVs from maternal blood.

3.1.3.1. Hypothesis 3.2

STB-EVs can be enriched from maternal peripheral blood, allowing 5'-tRF detection using qPCR.

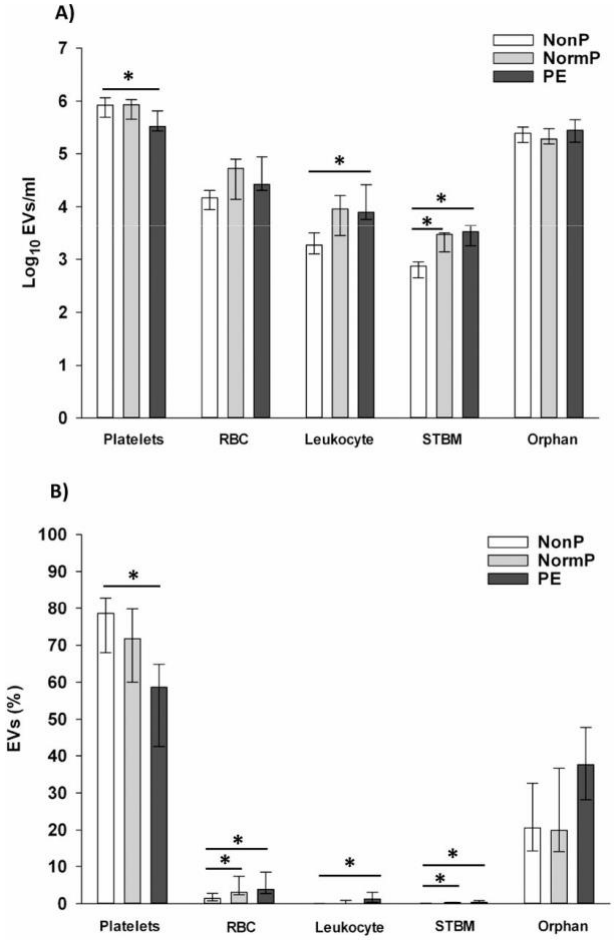


Figure 3-3 – Concentration of EVs in platelet-free plasma from non-pregnant (NonP), normal pregnancies (NormP) and pregnancies with preeclampsia (PE) using flow cytometry analysis.

A. Total EV counts

B. Percentage of EVs

*Bars represent median with the interquartile range. *P<0.05 (n=10 per group)*

Reprinted from Biology of Reproduction, 89 (6), Dragovic RA, Southcombe JH, Tannetta DS, Redman CWG, Sargent IL, Multicolor Flow Cytometry and Nanoparticle Tracking Analysis of Extracellular Vesicles in the Plasma of Normal Pregnant and Pre-eclamptic Women, © 2013, with permission from Elsevier under licence number 5563160415849.

3.1.4. Approaches to enrichment of STB-EVs from blood

STB-EVs can be distinguished from other blood EVs by proteins on their surface. PLAP is most commonly used as a marker of the syncytiotrophoblast. Whilst not unique to the syncytiotrophoblast, it is highly enriched compared to other sources[133].

Two protocols have been published which claim to isolate STB-EVs from blood. One binds biotinylated PLAP antibody to streptavidin-coated magnetic beads which were incubated with unprocessed serum[48]. This technique had never previously been published and no validation data were provided (despite an overall high-impact publication). The approach overlooks the presence of soluble PLAP in the serum, which exceeds vesicle-bound PLAP by orders of magnitude[134]. The RNA isolated and sequenced from PLAP-bound molecules is therefore more likely to represent soluble nucleoprotein complexes than STB-EVs, as the authors claim. Without any validation data (e.g. co-expression of vesicle-markers or placenta-specific RNA) the technique must be considered flawed.

The second published protocol uses PLAP antibody bound to protein A-coated agarose beads, to pull STB-EVs from total plasma EVs (previously pelleted by ultracentrifugation)[135]. The authors do not reference the source of their PLAP antibody and their only validation data use the same antibody to show successful pullout by Western blot. Thus, the reader can only be certain that the method pulls something out of plasma, but without any certainty regarding its specificity or syncytiotrophoblast origin.

Thus, to test Hypothesis 3.2 a novel technique needed to be developed.

3.1.5. Approaches to testing hypotheses

5’-tRFs are abundant in non-pregnant plasma[71]. Detection of a placental 5’-tRF load in maternal blood could be tested by two approaches. EVs isolated from blood by immunoprecipitation using a syncytiotrophoblast-specific marker can be considered

placental; if 5'-tRFs are present within, then Hypothesis 3.1 could be accepted. However, as described above, there is no accepted technique for STB-EV immunoprecipitation from blood. An alternate approach is to use sample selection to test the hypothesis (Figure 3-4). Placental 5'-tRFs should be more abundant in pregnant than non-pregnant plasma, where there is no placenta[40]. Likewise, samples obtained from the uterine vein at caesarean section (directly draining the placenta) should contain more placental signal than those from the peripheral vein, where the placental blood has mixed with blood draining from other organs and passed through the circulation to reach an equilibrium[40]. The sample selection approach was chosen given its simplicity and prior validation for placentally-derived molecules[40,45,136]. It was also deemed appropriate to optimise a protocol to isolate STB-EVs (Hypothesis 3.2) as this would a) provide additional evidence to support Hypothesis 3.1, b) likely improve the accuracy of any biomarker assay for preeclampsia (Chapter 4).

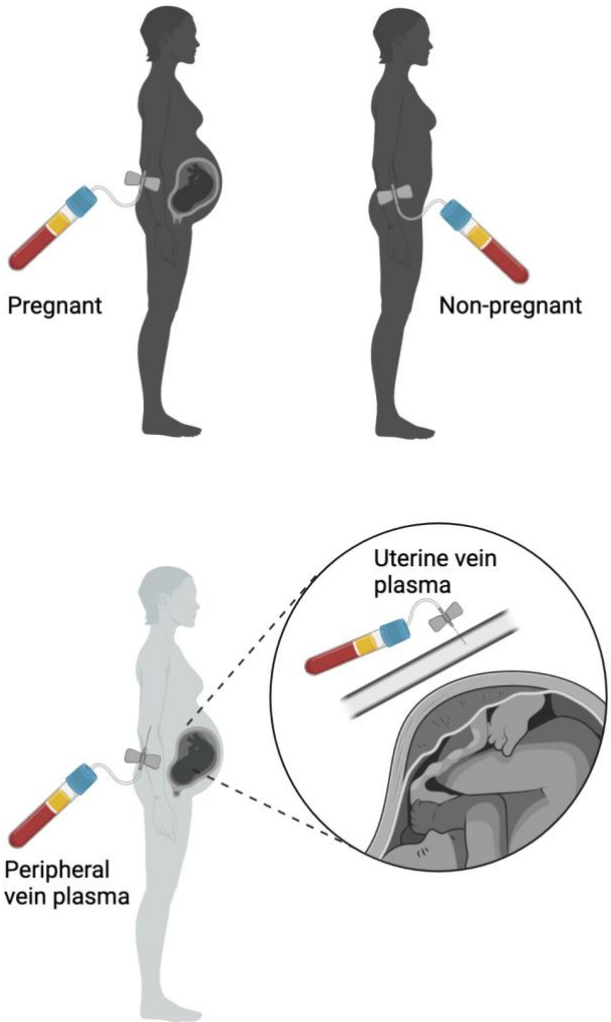


Figure 3-4 – Schematic diagram to illustrate sample types which were selected to test the hypothesis that a placental 5'-tRF load is detectable in maternal plasma. Created with biorender.com with a publication licence under agreement number NU257Q93OV.

3.1.6. Quantification and normalisation in qPCR

Both hypotheses use qPCR to quantify 5'-tRFs. 5'-tRFs can currently be quantified by qPCR or RNA sequencing. The rationale for selecting qPCR was pragmatic: qPCR assays are rapid (allowing protocol optimisation over a feasible timescale), relatively inexpensive and their specificity and linearity have been demonstrated in Chapter 2.

Stem-loop primer 5'-tRF assays (and qPCR more generally) result in the specific accumulation of a fluorophore in proportion to the abundance of an RNA target (see 2.2.4.2 for more detail). qPCR instruments provide quantification cycle (Cq) values, which depend on the concentration of RNA in the starting sample. There are two broad strategies for converting Cq values to linear quantitative data: absolute and relative quantification[137].

In absolute quantification, a set of RNA standards are run alongside samples of interest, allowing interpolation of the exact concentration of target RNA in the samples. There are some shortcomings to using this approach[137]. RNA standard design, optimisation and quantification is not straightforward. Standards are as vulnerable as samples to freeze-thaw changes; consequently, fresh standards are needed for each experiment. Standards necessarily contain the target of interest; qPCR is highly sensitive, rendering these experiments especially vulnerable to cross-contamination. Standards take up significant space on qPCR plates, limiting the number of samples that can be tested in a single experiment. Finally, external calibration curve models require significant validation.

Relative quantification involves comparing RNA concentrations to one or more reference RNA targets which are consistently expressed across different samples. Expression between groups can then be expressed relative to this. Selection of the reference gene is crucial; it must be the same between different patients and conditions of interest. When quantifying targets of interest in pregnant blood samples, there are no studies or data

validating suitable reference genes. Table 3-1 summarises published studies reporting sRNA biomarkers in blood for the prediction or diagnosis of preeclampsia. qPCR studies used one of two reference genes (or none). Five studies used the endogenous *U6* (also known as *RNU6B*), a small non-coding RNA which has been empirically demonstrated to vary too excessively for use as a reference gene in human serum[138]. Another five studies use exogenous *C. Elegans* miRNA, spiked into equal volumes of plasma at the start of the experiment, creating a stably expressed reference.

Population origin	RNA isolation	RNA quantification	Sample size	Reference gene	Reference gene justification	Ref
qPCR studies						
Russia	miRNeasy	Discovery-RNAseq Validation-qPCR	Discovery: 54 (28PE, 26N) Validation: 16 (6PE, 10N)	cel-miR-39	Referenced non-pregnant data[258]	[259]
China	miRVana	qPCR	9 (5sPE, 4N)	cel-miR-39	-	[260]
Czech Republic	mirVana	qPCR	168 (24 mPE, 39sPE, 55N)	cel-miR-39	Lack of accepted standards so spike-in	[156]
Czech Republic	miRVana	qPCR	79 (21PE, 58N)	cel-miR-39	Lack of accepted standards so spike-in	[261]
Bahrain	miRNeasy	qPCR	22 (7mPE, 8sPE, 7N)	cel-miR-39 & *U6*	-	[262]
Egypt	miRNeasy mini	qPCR	200 (100PE, 100N)	*U6*	-	[263]
China	-	qPCR	53 (20 sPE, 33 N)	*U6*	-	[264]
Japan	mirVana	qPCR	40 (20 sPE, 20 N)	*U6*	-	[154]
China	Trizol LS	qPCR	40 (20PE, 20N)	*U6*	-	[265]
UK	miRNeasy	Discovery-RNAseq Validation-qPCR	75 (35PE, 40N)	cDNA conc^{n}	No *a priori* known stable normaliser miRNAs	[266]
China	mirVana	Discovery-RNAseq Validation-qPCR	Discovery: 12 (4 mPE, 4sPE, 4N). Validation: 70 (16 mPE, 22 sPE, 32N)	None	PE relative to N without normalisation, no justification	[267]
RNAseq studies						
China	Trizol	RNAseq	5 (2 mPE, 2 sPE, 1 N)	NA	-	[157]
Chile	miRNeasy mini	RNAseq	47 (15PE, 32N)	NA	-	[47]
Microarray studies						
Turkey	miRVana	Microarray	36 (18sPE, 18N)	cel-miR-39	-	[268]

Table 3-1 – Table summarising studies which investigate blood-borne miRNAs as biomarkers for prediction or diagnosis of preeclampsia.

Once a quantification strategy is chosen, normalisation of data must be considered. Cq values depend not only on the concentration of the RNA target of interest in the sample, but also on the efficacy of RNA isolation, reverse transcription yield, PCR reaction efficiency and machine-specific factors such as laser parameters. qPCR quantification of RNA targets typically involves a large number of handling steps, which can introduce noise. A common approach to normalisation is to spike a unique RNA into all samples at the beginning, and to normalise against this before quantifying. This approach assumes that any variation in RNA isolation, reverse transcription or PCR reactions and pipetting errors will be applied equally to both targets.

It was concluded that the superior approach to normalise and quantify sRNA qPCR data in pregnant plasma would be use of an sRNA spike-in (*C. Elegans* miRNA-39 being the most commonly used). This controls for confounding during RNA isolation and reverse transcription reactions, whilst allowing comparison of the relative quantity of the target RNA in equal volumes of sample. Differences in qPCR reaction efficiency are overcome by using the Pfaffl approach to compute relative expression data with reference to these data (as described in 2.2.4.2).

3.2. Methods

3.2.1. Blood collection and handling

This project was approved by the Central Oxfordshire Research Ethics Committee (07/H0607/74 and 07/H0606/148). Participants provided informed, written consent. Healthy pregnant participants and healthy non-pregnant female volunteers of reproductive age donated samples used in this chapter. Uterine vein samples were taken during caesarean section, just prior to uterine incision, using a 21-gauge needle and syringe. Peripheral blood samples were taken from the antecubital fossa using 21-gauge needle and tourniquet into 4.5 ml sodium citrate/SST vacutainer tubes (BD Diagnostics, UK). Tubes were inverted five times after collection, stored at room temperature and processed within 30 minutes of collection. Antenatal (AN) and postnatal (PN) pairs were taken just prior to caesarean section and 12-18 hours later.

Platelet poor plasma (PPP) was obtained by centrifugation of sodium citrate tubes at 1500 *g* for 15 minutes at room temperature. Platelet-free plasma (PFP) was obtained by centrifuging PPP a second time at 13 000 *g* for 2 minutes at room temperature. Serum was obtained by centrifugation of SST tubes at 3000 revolutions per minute for 10 minutes at room temperature. For each sample type, the supernatant from replicate tubes was mixed by inversion, aliquoted and frozen at -80°C. Just prior to use, plasma aliquots were thawed in a water bath at 37°C, mixed by inversion and centrifuged to remove cryoprecipitates (3000 *g* for 5 minutes at 4°C for PPP, 13 000 *g* for 2 minutes for PFP).

3.2.2. Membrane affinity column plasma EV RNA isolation

Plasma EV RNA was isolated using the ExoRNeasy Midi Kit (#77144, Qiagen, Germany) in line with manufacturer's instructions. An equal volume of buffer XBP was mixed with the plasma and the entire sample added to an ExoEasy spin column and centrifuged for 1 minute at 500 *g*. The flow-through was discarded and the column washed with 3.5 ml

buffer XWP at 5000 *g* for 5 minutes. 700 µL QIAzol lysis reagent was added to the membrane and centrifuged at 5000 *g* for 5 minutes. Lysate was transferred to a Phasemaker™ tube (#A33248, ThermoFisher Scientific, UK), 1 µL 5 nM cel-miR-39 spike-in added where noted, then the tube vortexed for 15 seconds and incubated for 5 minutes at room temperature. 90 µL chloroform was added and the mixture was vortexed for 30 seconds then incubated for 3 minutes at room temperature before phases were separated by centrifugation at 12 000 *g* for 15 minutes at 4°C. The aqueous phase was transferred to a new collection tube and two volumes 100% ethanol added and mixed. The mixture was added to RNeasy MinElute spin columns in 700 µL aliquots, centrifuging at >8000 *g* for 15 seconds and discarding the flow-through each time. The columns were washed with 700 µL buffer RWT and 500 µL buffer RPE twice (each time spinning at >8000 *g* for 15 seconds and discarding the flow-through). After a 5 minute full-speed centrifugation in new collection tubes to dry the columns, RNA was eluted in RNAse-free water. RNA was aliquoted and stored immediately at -80°C. For group comparisons, plasma EVs were isolated from equal volumes of plasma and eluted in equal volumes of water.

3.2.3. Size exclusion column plasma EV RNA isolation

Plasma EVs were isolated using qEV original columns (#SP1, Izon Science Europe Ltd., France) following manufacturer's instructions. Columns were flushed with 10 mL filtered phosphate-buffered saline (PBS) then 500 µL plasma was loaded. The column was topped up with PBS and the 1500 µL EV fraction collected in a separate tube. RNA was isolated using Trizol™ LS reagent (#10296010, Invitrogen, USA) with modifications derived from a *Biological Procedures Online* publication[102]. 4500 µL Trizol was added to the samples, which were vortexed for 15 seconds before 2.5 µL bacteriophage MS2 carrier RNA was added to each sample (#10165948001, Roche, Switzerland). After a 5 minute incubation at room temperature, 1200 µL chloroform was added and samples mixed by vortex for 30 seconds. The mixture was incubated for 15 minutes at room

temperature, then centrifuged at 12 000 *g* for 15 minutes at 4°C. The aqueous phase was transferred to a falcon tube and 1 µL glycogen added to each sample (#10901393001, Roche, Switzerland). RNA was precipitated by adding 3 mL isopropanol to each sample, mixing by vortex and incubating for 10 minutes at room temperature. RNA was pelleted at 12 000 *g* for 10 minutes at 4°C and the pellet washed twice in 6 mL 75% ethanol. After residual ethanol wash had been carefully removed the RNA pellet was air dried for 15 minutes at room temperature and then dissolved in RNAse-free water, aliquoted and stored at -80°C.

3.2.4. Stem-loop reverse transcription

Reverse transcription reactions were conducted using Custom TaqMan® Small RNA Assays and TaqMan® MicroRNA Reverse Transcription Kit (#4398987 and #4366596, Applied Biosystems, USA). Assay numbers are in Table 3-2; cel-miR-39 was quantified using assay ID 000200. The protocol used was described previously in section 2.2.4.2. For multi-plex reactions, 3 µL water per reaction in the reverse transcription master mix was substituted with a second 5X RT primer. Reverse transcription reaction conditions were otherwise unchanged.

3.2.5. Quantitative PCR reactions and data analysis

cDNA transcripts were quantified during qPCR reactions using Fast Advanced Master Mix (#4444557, Applied Biosystems, USA) and conditions described previously in section 2.2.4.2. As in Chapter 2, qPCR reaction efficiency was determined using linear regression and relative expression determined using the Pfaffl approach (with or without normalisation to cel-miR-39 spike-in as noted in the relevant results section). qPCR reactions for the multi-plex reverse transcription reactions were single-plex. As in Chapter 2, hypothesis tests were conducted where data appeared to show differences; they are identified in each corresponding figure legend. Where data were not normally distributed on visual inspection, non-parametric tests were used. Where only a unidirectional

difference was expected, one-tailed tests were used. Uterine and peripheral venous blood samples were taken simultaneously from the same woman so were considered paired samples. Statistical analyses and figures were generated using Prism9 (GraphPad, USA).

3.2.6. Particle size and concentration analysis

Nanoparticle Tracking Analysis (NTA) of EVs was conducted on a Particle Metrix PMX 120 Scanning ZetaView® instrument (Particle Metrix GmbH, Germany). Samples were diluted 1:1000 and particles analysed using a shutter speed of 10, camera sensitivity of 80, and 11 camera positions for 2 cycles. Particle size and concentration were calculated automatically by the inbuilt software.

3.2.7. Whole plasma RNA isolation

Whole plasma RNA was isolated using the miRNeasy Serum/Plasma Advanced Kit (#217204, Qiagen, Germany) following manufacturer's instructions. 200 µL thawed plasma was mixed with 60 µL lysis buffer RPL, mixed by vortex and incubated for 3 minutes. 1 µL of 5 nM cel-miR-39 spike-in was added and protein inhibitors precipitated by adding 60 µL buffer RPP. The precipitate was pelleted by centrifugation at 12 000 *g* for 3 minutes and the supernatant mixed with an equal volume of isopropanol. The whole sample was passed through a RNeasy MinElute column, spinning at >8000 *g* and discarding the flow-through. The membrane was washed with 700 µL RWT, then 500 µL RPE and 500 µL 80% ethanol. After a 5 minute full-speed centrifugation in a new collection tube to dry the column, RNA was eluted in RNAse-free water, aliquoted and stored immediately at -80°C.

3.2.8. Plasma STB-EV RNA isolation

3.2.8.1. Approach 1

Two aliquots of 50 µL sheep anti-mouse IgG magnetic beads (Dynabeads™ M-280, #11201D, Invitrogen, USA) were pre-washed three times with wash buffer (2 mM EDTA

and 1% BSA in PBS). 6 µg appropriate antibody (NDOG2, see 3.3.5, or mouse IgG #400153, BioLegend, USA) was incubated with respective bead aliquots overnight with gentle tilting and rotation at 4°C. Plasma EVs were isolated from two 500 µL pooled pregnant plasma aliquots using SEC as described above (3.2.3); RNA was isolated from one SEC sample as previously explained. 10 µL 10X FcR blocker (Miltenyi Biotec, Germany) was added to the remaining SEC sample (1500 µL) and incubated for 10 minutes at 4°C. The EV fraction was then divided in two and equal quantities of respective washed bead-antibody complexes were resuspended in 750 µL EVs. Beads and EVs were incubated overnight with gentle tilting and rotation at 4°C. Beads were separated on a magnet for 2 minutes, washed three times and resuspended in 500 µL PBS. RNA was isolated from bead-bound EVs using Trizol™ LS as described above but with scaled down volumes. Unbound EVs in the initial supernatant were concentrated by ultracentrifugation at 150 000 *g* for 2 hours at 4°C, the pellet resuspended in 500uL PBS and RNA isolated using Trizol™ LS. All pellets were resuspended in 40 µL RNAse-free water and miRNAs 517c and 518b quantified using TaqMan® microRNA Assays (#4398987, assay IDs 001153 and 001156, Applied Biosystems, USA) as described in 3.2.4.

3.2.8.2. Approach 2

Bead preparation was unchanged from Approach 1. Serum EVs were isolated from three 500 µL aliquots from the same donor using exoEasy columns as described in 3.2.2. One aliquot proceeded to RNA isolation as previously explained. For the remaining two aliquots, EVs were eluted from exoEasy columns using 400 µL buffer XE, mixed with 10 µL 10X FcR blocker and incubated for 10 minutes at 4°C. EV aliquots were next mixed with the respective antibody-bead complexes by rotation for 30 minutes at room temperature. Beads were separated and washed, then resuspended in PBS and RNA isolated using QIAzol as previously described. RNA was also isolated from unbound EVs in the initial supernatant using Trizol™ LS without pelleting EVs by ultracentrifugation as

the volume was low. RNA was eluted from all five sample types in 24 µL RNAse free water and RNA expression quantified as described above. This experiment was conducted three times using samples from three different donors.

3.2.8.3. Optimisation of streptavidin magnetic beads

3.2.8.3.1. Antibody biotinylation

NDOG2 antibody (see 3.3.5) was biotinylated using the EZ-Link™ Sulfo-NHS-LC-Biotinylation Kit (#21435, ThermoFisher Scientific, UK). 1.6 mg (1 mL) antibody was exchanged into PBS from sodium-azide buffer by adding to a Zeba Spin Desalting Column, spinning at spinning at 1000 *g* for 2 minutes. The 1mL flow-through was incubated with 21.6 µL 10mM freshly-prepared Sulfo-NHS-LC-Biotin (20X molar excess of biotin) at room temperature for 1 hour to biotinylate the antibody. Excess biotin reagent was removed by passing through a second desalting column.

The biotinylation kit's HABA-avidin assay was used to measure biotin incorporation. 10 mg avidin and 600 µL 10 mM HABA was added to 19.5 mL PBS. Absorbance of 180 µL of this solution at 500 nm was measured using a ClarioStar® microplate reader (BMG Labtech Ltd, Aylesbury, UK). 20 µL biotinylated antibody was added to the solution and the absorbance measured at 1 minute intervals. Biotin incorporation was quantified using calculations based on Beer's Law within the kit's protocol.

To verify NDOG2 biotinylation, a second approach was applied. Six aliquots of 50 µL Dynabeads™ M-270 streptavidin beads (#65305, Invitrogen, USA) were washed three times. 5 µg biotinylated NDOG2 was added to three tubes, 5 µg non-biotinylated NDOG2 to the next three tubes. Beads and antibody were incubated at room temperature for 30 minutes on a rotator. Washed beads and a positive control of antibody without beads were mixed with 4X Laemmli buffer, heated to 70°C for 10 minutes then loaded onto a 4-12% SDS-PAGE 10-well gel (#NP0321BOX, ThermoFisher Scientific, UK) for

electrophoresis. Antibodies were transferred onto a polyvinylidene difluoride membrane (#1620177, Bio-Rad, USA) using a semi-dry system and the membrane stained with Ponceau red solution (#A40000279, ThermoFisher Scientific, UK) to visualise. Bands at 150 kDa, corresponding to NDOG2 antibody were quantified using ImageJ[139]. During this protocol the beads were noticed to clump together; advice was sought from an industry collaborator who reported the best EV separation with beads of a similar size to the EVs[140]. Following their advice further bead work was undertaken using MojoSort Streptavidin Magnetic Nanobeads (160 nm diameter; #480016, BioLegend, USA).

3.2.8.3.2. Plasticware

The four plastic tubes compared in results section 3.3.5.3.2 were: SafeSeal reaction tube 1.5mL (#72.706.200, Sarstedt, Germany), SafeSeal reaction tube 0.5 mL (#72.704, Sarstedt, Germany), PROTEOSAVE™ 1.5 mL Microtube (#MS-4265MZ, Wako Pure Chemicals, Japan), Protein LoBind® 1.5 mL tube (#10708704, Eppendorf, Germany). 10 µL MojoSort beads and 300 ng biotinylated NDOG2 were mixed in 100 µL PBS in each of the tubes for 30 minutes on a rotator. They were washed with PBS twice then incubated with 100 µL 0.3 µM biotin solution (#B4501, Merck, USA) on a rotator for 30 minutes to saturate free streptavidin. Beads were washed twice with PBS again, resuspended in 100 µL PBS and transferred to a 200 µL tube strip for visualisation.

3.2.8.3.3. Confirming antibody biotinylation by PLAP pullout from MLEVs

50 µL MojoSort beads were incubated in 500 µL PBS (control) or 3 µg biotinylated NDOG2 antibody in 500 µL PBS (condition) for 30 minutes on a rotator at room temperature. Beads were washed once then suspended in 500 µL 0.3 µM biotin for a further 30 minutes. Beads were washed once again, then suspended in 500 µL perfusion-derived MLEVs (see Chapter 2) containing 25 µg protein (titrated from prior publication[42]), equivalent to 1.2E9 EVs. After one hour of rotation at room temperature, beads were washed twice in PBS then resuspended in 250 µL PBS and RNA isolated using Trizol™

LS as described above, including a 1 µL 5 nM cel-miR-39 spike-in. tRF-F was quantified in beads as described above.

3.2.8.3.4. Bead clumping

Two further batches of NDOG2 were biotinylated as described above but using a 10X and 2X molar excess of biotin (i.e. 10.8 µL and 2.16 µL Sulfo-NHS-LC-Biotin solution). 600 ng desalted antibody was incubated with 10 µL MojoSort beads for 30 minutes on a rotator at room temperature. Beads were observed during separation, then suspended in 100 µL PBS and diluted 1:500. Nanoparticle Tracking Analysis (NTA) was performed using NanoSight NS500 instrument equipped with a 405 nm laser and NTA software version 2.3 (Malvern Panalytical, UK). The script used for capture was PRIME, DELAY 5, CAPTURE 30, REPEAT 5; camera level was set to 12 with shutter speed 15 ms. Observations were derived from recorded video clips; particle concentrations were determined using the default software settings.

3.2.8.3.5. Isolation of PLAP+ EVs from perfusion STB-EVs

The efficacy of two biotinylation concentrations in PLAP pullout from MLEVs was assessed using the above protocol but with half volumes to minimise reagent usage. The bead concentration after antibody/biotin binding was measured by NTA and equal bead numbers added to 25 µg MLEVs before RNA isolation and tRF-F quantification.

3.2.8.4. Approach 3

For each reaction 100 µL, containing 600 ng 2X biotinylated NDOG2 antibody, was bound to 10 µL MojoSort beads on a rotator for 30 minutes at room temperature. Beads were washed once with PBS, then resuspended in 100 µL 0.3 uM biotin for 30 minutes, then washed again and quantified with NTA. In parallel 10 µL beads were suspended in 100 µL 0.3 µM biotin for 30 minutes as a control, then washed and quantified with NTA. Reactions were consolidated into volumes up to 1 mL for efficiency.

Two plasma aliquots from three different pregnant women and three different non-pregnant women were used. 500 µL was spun at 10 000 *g* for 30 minutes at 4°C in a microcentrifuge to pellet total EVs with the same conditions used in perfusion MLEV isolation. The resulting pellet was resuspended in PBS to a total volume of 500 µL, then spun again. The washed pellets were resuspended in 250 µL PBS with equal numbers of the appropriate beads and rotated at room temperature for 1 hour. Beads were washed four times in PBS, then RNA isolated with cel-miR-39 spike-in as described above. tRF-F, cel-miR-39 and miR518b were quantified and compared.

3.2.8.5. Approach 4

To reduce non-specific binding, the protocol in 3.2.8.4 was modified to pre-incubate some samples with MojoSort beads that had already been incubated with 0.3 uM biotin for 30 minutes on a rotator at room temperature. The residual supernatant was incubated with beads with antibody/control and RNA isolated from beads without further protocol changes.

After comparing pre-incubation to the protocol in 3.2.8.4, this additional step was incorporated into the protocol to create Approach 4, with no further modifications.

3.3. Results

3.3.1. Target selection

Three STB-EV 5'-tRF targets were initially selected for detection in maternal plasma using qPCR assays. They were given identifiers (F, I and J) for ease of reference in this thesis (Table 3-2).

Target I was chosen as the most abundant sRNA upregulated in normal MLEVs compared to normal placenta (Table 2-5) and normal SEVs compared to normal placenta (Table 2-6). From our collaborators' analysis, target I was also the most abundant differentially expressed sRNA fragment in preeclampsia compared to normal MLEVs (Table 2-15). As the most abundant STB-EV 5'-tRF target, it was considered that if target I were not detectable in plasma, then 5'-tRFs are likely to be below the limit of detection in plasma using existing technologies.

Target F was chosen from the DEUS analysis, as the most abundant differentially expressed sRNA fragment in preeclampsia compared to normal MLEVs (Table 2-10). Target F is upregulated in preeclampsia compared to normal MLEVs. Given Chapter 4 aims to evaluate whether differences between STB-EV 5'-tRF expression in preeclampsia and normal pregnancies can also be seen in plasma, it was considered important to initially validate a target which would likely be used subsequently.

Target J was chosen from the DEUS analysis, as the next most abundant differentially expressed 5'-tRF iso-acceptor or iso-decoder in preeclampsia compared to normal MLEVs (Table 2-10). Target J is downregulated in preeclampsia compared to normal MLEVs. The relative abundance of each of the chosen validation targets in the analyses undertaken in Chapter 2 is shown in Table 3-2.

Thesis	DEUS analysis				Collaborator analysis		Assay information		
ID	ID	Normal MLEV vs Placenta	Normal SEV vs Placenta	MLEV PE vs N	ID	MLEV PE vs N	Length	Assay #	Target Sequence
F	seq_12	11	3	1	Glu-CTC-1-1	5	33	CT2W736	TCCCTGGTGGTCTAGT GGTTAGGATTCGGCGCT
I	seq_1	1	1	-	Gly-GCC-2-1	1	32	CT7DPUX	GCATTGGTGGTTCAGT GGTAGAATTCTCGCCT
J	seq_29	26	20	8	CysGCA-4-1	38	31	CT9HJEV	GGGGGTATAGCTCAGT GGTAGAGCATTTGAC

Table 3-2 – Table showing tRNA target sequences selected for investigation in plasma.

Table includes thesis, DEUS and collaborator identifiers (ID), abundance ranks in DEUS and collaborator analyses from Chapter 2 and manufacturer assay number.

3.3.2. Optimising a technique to quantify total plasma EV tRF expression

The first approach used to seek a placental 5'-tRF load in maternal plasma, was to isolate total plasma EV RNA. Two techniques, size-exclusion chromatography (SEC) and membrane-affinity columns (MAC), were initially compared.

3.3.2.1. Comparison of techniques for plasma EV placental small RNA isolation

For both isolation techniques, EVs were isolated from 500 µL whole plasma and RNA was eluted in 40 µL water. PFP plasma samples were used with no spike-in in the first instance.

Four pairs of peripheral venous plasma taken just prior to caesarean section (AN) and one day after delivery (PN) were obtained. Plasma EVs were isolated using both techniques and expression of two placenta-specific miRNAs (miR517c and miR518b) was quantified (Figure 3-5).

This experiment was conducted using a Corbett qPCR instrument which has since been decommissioned. Plate size on this instrument was restrictive, so samples for each technique were quantified on different plates run sequentially. Cq values >40 or undetermined were substituted with Cq 40 for data presentation purposes.

With both techniques, placenta-specific miRNAs were more abundant in the AN samples. This provides external validity to both approaches: after delivery of the placenta a placenta-specific target is reduced. For both miRNA targets and in both sample timepoints, MAC-isolated EVs from the same samples demonstrated lower Cq values (i.e. a greater miRNA abundance). Given PN values included Cq >35 (with some censored where Cq >40), a comparison was made between AN MAC and SEC for each target. MAC EV isolation gave a mean Cq value 2.7 lower than SEC for miRNA 517c and 4.8 lower for miRNA 518b. These differences were not significant when tested by Wilcoxon

test (p=0.13 for both miRNAs): a paired-sample, two-sided, non-parametric test was selected given the small sample size. However, for this optimisation experiment, the differences were considered substantial and consistent enough to conclude that MAC offered superior enrichment of placental EV sRNA from plasma than SEC. MAC was used for subsequent total plasma EV experiments.

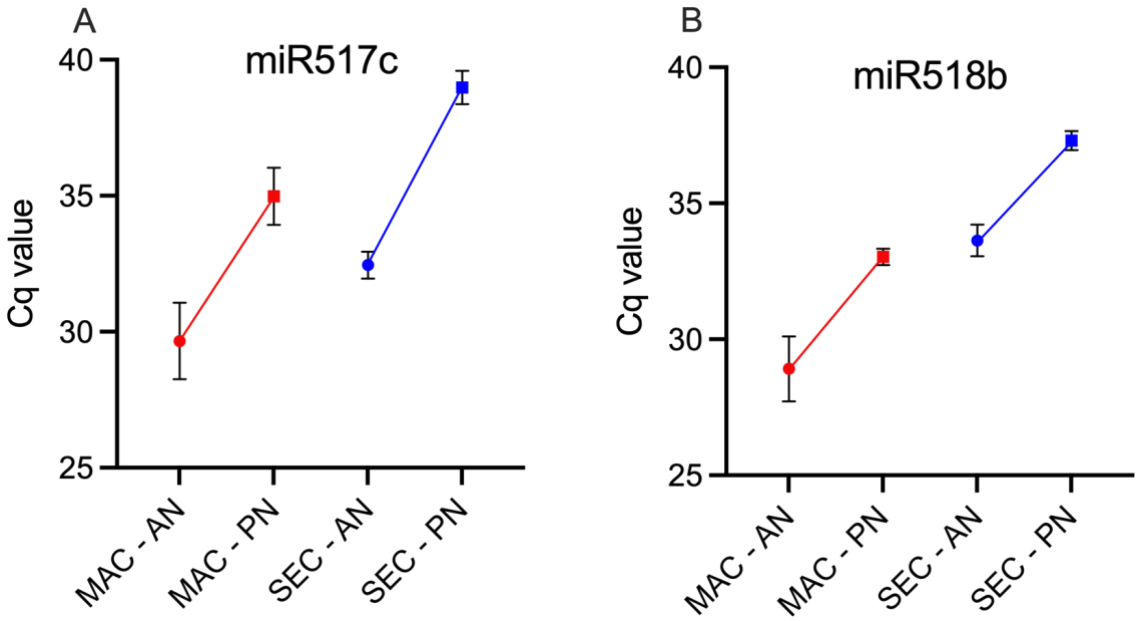


Figure 3-5 – Abundance of two placenta-specific miRNAs in AN and PN total plasma EV isolated using membrane-affinity columns (MAC, red) and size-exclusion chromatography (SEC, blue).

Symbols represent mean with error bars showing standard deviations. Note a lower Cq value represents a greater target abundance.

3.3.2.2. Validation of membrane affinity column isolation particle size

Independent published data demonstrate MAC isolates particles from non-pregnant plasma with the morphology (transmission electron microscopy), size (nanoparticle tracking analysis) and protein expression (Western blot) consistent with EVs[141]. Differences between STB-EV 5'-tRF expression in preeclampsia were most pronounced in MLEVs. Thus, I wished to confirm that perfusion MLEV particle size was consistent with MAC isolation from pregnant plasma.

The size and concentration of particles isolated as MLEVs using ultracentrifugation from placental perfusate was compared to particles isolated from pregnant plasma using MAC (Figure 3-6). Three samples of each type were interrogated. Peak diameter for the three perfusion EV samples was 117-127 nm, compared to 133-152 nm for the three plasma EV samples. The distributions of the two particle sizes showed substantial overlap.

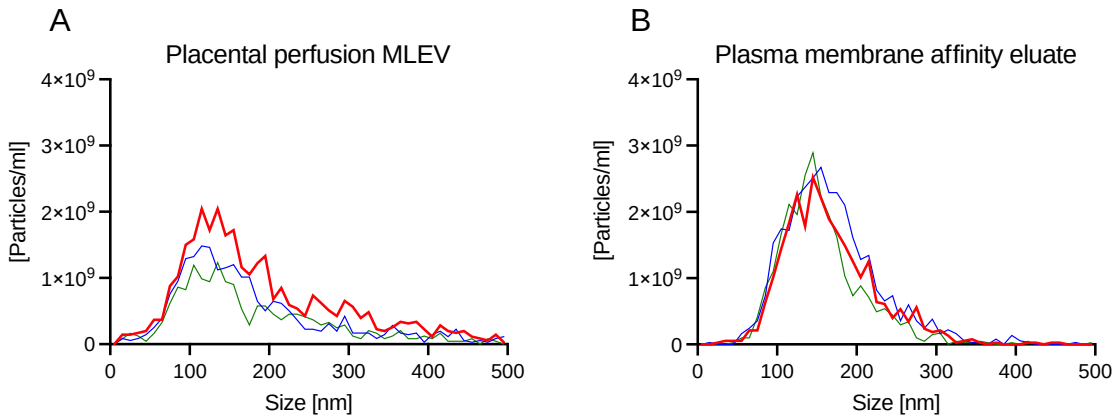


Figure 3-6 – Size and concentration of particles isolated from placental perfusate using ultracentrifugation and from plasma using MAC isolation.

MLEVs isolated during discovery experiments, Chapter 2. Particles characterised using Zetaview NTA. Each line represents a different sample (biological repeats).

3.3.2.3. Evaluation of multiplex reverse transcription assays for tRF detection

Given the likely need to perform a large number of qPCR experiments during this and the subsequent chapter, an early assessment was made of the ability to multiplex 5'-tRF reverse transcription reactions in line with a previous publication[102]. Three plasma EV RNA samples from 3.3.2.1, isolated from different term pregnant donors, underwent singleplex and multiplex reverse transcription reactions for assays F and I. qPCR detection was undertaken in a singleplex manner.

There was a substantial difference in Cq values obtained using singleplex compared to multiplex reverse transcription reactions (Figure 3-7). This difference was most apparent with the assay for tRF-I. The difference was not consistent, meaning a correction could not be applied. It was concluded that multiplex reverse transcription reactions would not be appropriate for further use and only singleplex reactions are used subsequently in this thesis.

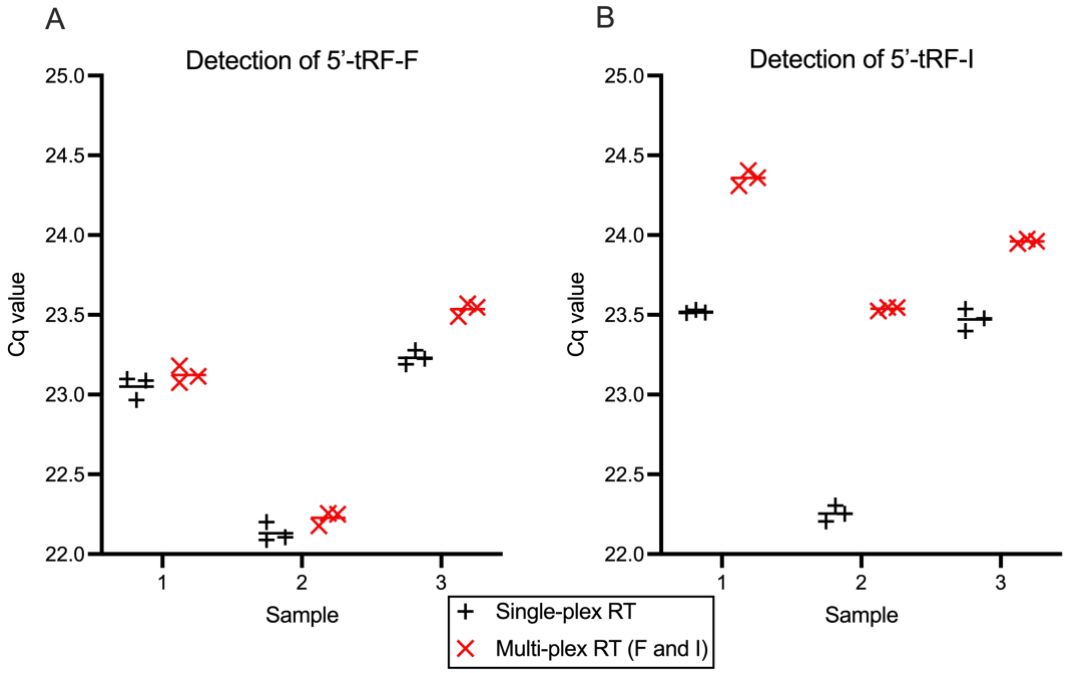


Figure 3-7 – Comparison of target 5'-tRF detection in MAC-isolated pregnant plasma EVs using singleplex or multiplex reverse transcription reactions

Individual data points represent triplicate repeats, lines represent mean values.

3.3.3. Plasma EV tRNA-fragment expression

Concurrent to my assay optimisation, a colleague (Dr Wei Zhang) undertook a series of flow cytometry experiments seeking to quantify placental MLEVs in plasma. Dr Zhang demonstrated that the second centrifugation step from platelet-poor to platelet-free plasma significantly depleted the placental MLEV load[142]. Given the preeclampsia differences from perfusion data were only corroborated in MLEVs, it was decided to use platelet poor plasma for subsequent experiments. Since optimisation was completed, *C. Elegans* miRNA-39 spike-in was used for normalisation in subsequent experiments.

3.3.3.1. Pregnant vs non-pregnant plasma EVs

Expression of targets F, I and J was compared in peripheral plasma EVs from third-trimester normal pregnancies (n=7) and control samples (n=6) from healthy non-pregnant female volunteers of reproductive age (Figure 3-8). Samples were matched by age: range for pregnant women 25-37 years, for non-pregnant controls 23-38 years. Median gestational age for pregnant samples was 32.1 weeks. 900 µL plasma was loaded onto the MAC and RNA eluted in 30 µL water. RNA was diluted 1:20 for targets F and I, but used neat for target J (given its lower abundance). Expression was normalised to a spiked-in control *C. Elegans* miRNA and presented relative to the mean expression in the non-pregnant group. One pregnant sample failed to give a result for tRF-J analysis. Median abundance was 2.3 fold higher in pregnant samples for tRF-F, 1.8 fold higher for tRF-I and 2.3 fold higher for tRF-J ($p<0.004$ for all three). These data suggest a pregnancy-specific load of these target tRFs in peripheral plasma, offering support to Hypothesis 3.1.

Presenting normalised relative abundance is the most intuitive format when comparing two groups, but hides that all three fragments are highly abundant in non-pregnant plasma. This can be quantified by presenting raw mean Cq values, which were 23.7 for F, 23.8 for I and 32.0 for J. These data demonstrate that targets F, I and J are abundant in

non-placental EVs, which may confound subsequent comparisons of expression between preeclampsia and normal (Chapter 4 and Appendix 3).

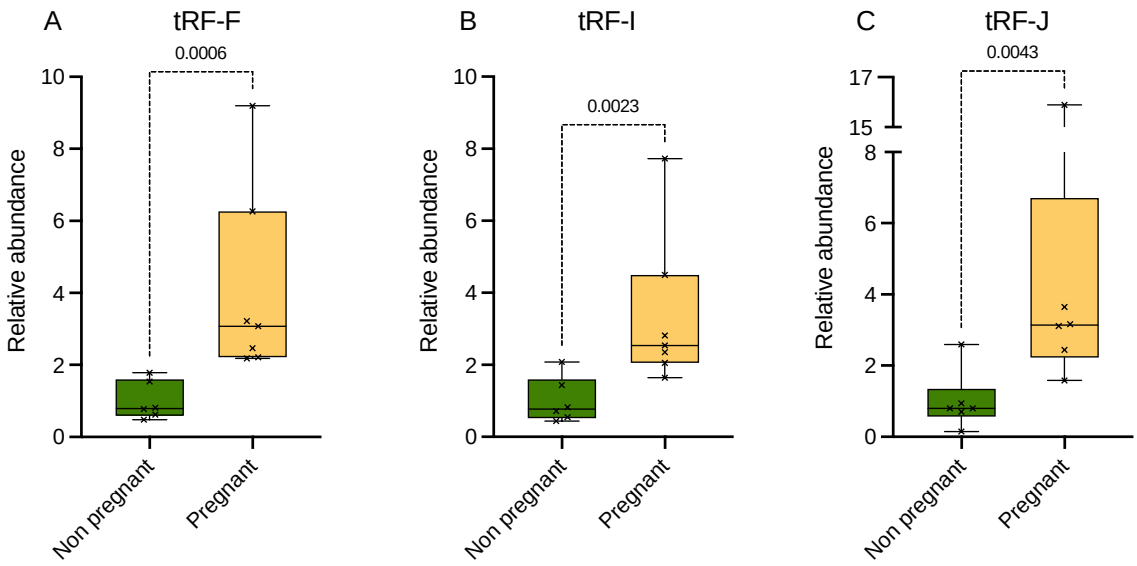


Figure 3-8 – Expression of tRF-F, tRF-I and tRF-J in pregnant and non-pregnant venous plasma EVs, relative to the mean non-pregnant expression.

Boxes represent median and interquartile range, whiskers represent maximum and minimum. Hypothesis tests represent one-sided Mann-Whitney tests given skewed unpaired data where a unidirectional change was anticipated.

3.3.3.2. Uterine vs peripheral venous plasma EVs

Expression of targets F, I and J was compared in plasma EVs from term uterine vein samples, taken just before delivery at caesarean section, and peripheral vein samples from the same woman taken at the same time (n=7 pairs, Figure 3-9). One pair of samples appeared to be outliers; this was confirmed by Grubbs' test for all three targets and the sample pair was removed.

Median abundance was 1.31, 1.38 and 2.76 fold higher in the uterine than the peripheral vein samples for tRFs F, I and J respectively ($p<0.05$ for all three). These data demonstrate a placenta-derived load of target tRF in peripheral plasma, leading me to accept Hypothesis 3.1: a placental 5'-tRF load can be detected in maternal blood using qPCR assays.

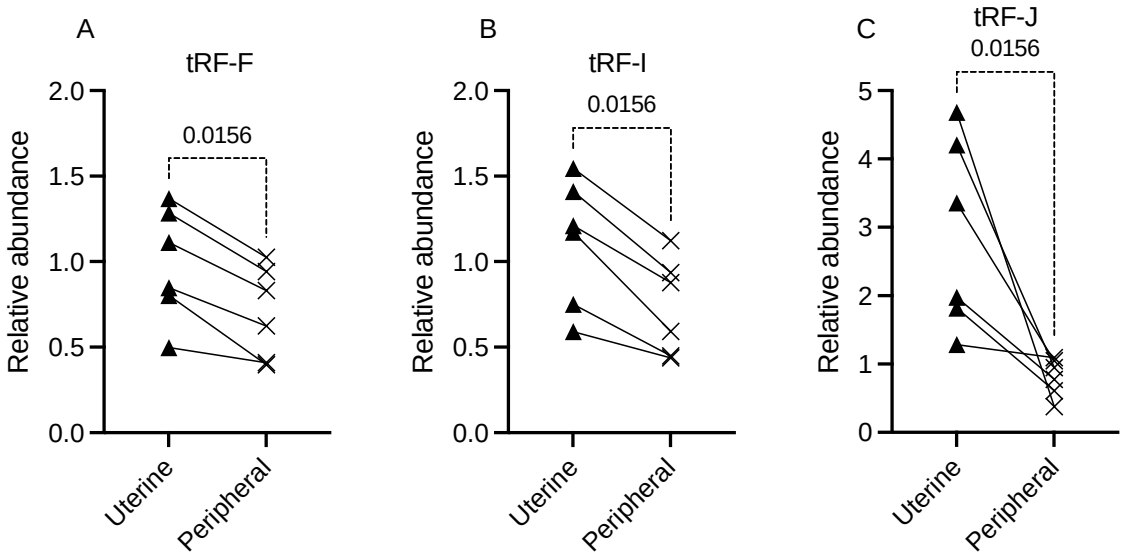


Figure 3-9 – Expression of tRF-F, tRF-I and tRF-J in paired samples of uterine and peripheral venous plasma EVs, relative to the mean peripheral venous abundance. Hypothesis tests represent one-sided Wilcoxon tests chosen for paired data with a small sample size where a unidirectional change was anticipated.

3.3.4. Whole plasma tRF expression

Despite the success of MAC EV isolation from plasma, the process is lengthy with 14 pipetting steps between aliquoting plasma and eluting RNA. This could introduce significant error, which may become important when smaller magnitude differences between preeclampsia and normal are investigated (Chapter 4). It also relies on a proprietary isolation technique. It is well established that different vesicle isolation techniques change the phenotype of isolated particles[143]. I therefore investigated whether a placental 5'-tRF load could be detected using whole plasma isolation.

For the subsequent experiments, RNA was isolated from 200 µL whole plasma. *C. Elegans* miRNA-39 spike-in was used for normalisation. RNA was eluted in 18 µL water and loaded neat into reverse transcription reactions for J given its lower plasma abundance (see 3.3.3.1) and diluted 1:20 for F and I. Serial RNA dilution had identified no PCR inhibitors from sample preparation which might necessitate further dilution (Figure 2-20).

3.3.4.1. Pregnant vs non-pregnant whole plasma

Expression of targets F, I and J was compared in whole plasma samples from term normal pregnancies (n=6) and control samples (n=6) from healthy non-pregnant female volunteers of reproductive age (Figure 3-10). Samples were matched by age: range for pregnant women 29-42 years, for non-pregnant controls 21-38 years. Median gestational age for pregnant samples was 39.8 weeks. Expression was normalised to spiked-in *C. Elegans* miRNA and presented relative to the mean expression in the non-pregnant group. There was one clear outlier in the pregnant group for both F and I, which was confirmed by Grubbs' test for both targets and removed. This was the same sample also found to be outlying previously in experiment 3.3.3.2, where it was also excluded.

There were no apparent differences in expression of targets F and I between the two groups; a pragmatic decision was made not to add further samples. Target J was undetectable in all samples, with Cq >35. This could reflect the low abundance of target J, or the presence of non-placental sources of targets F and I which were confounding the result.

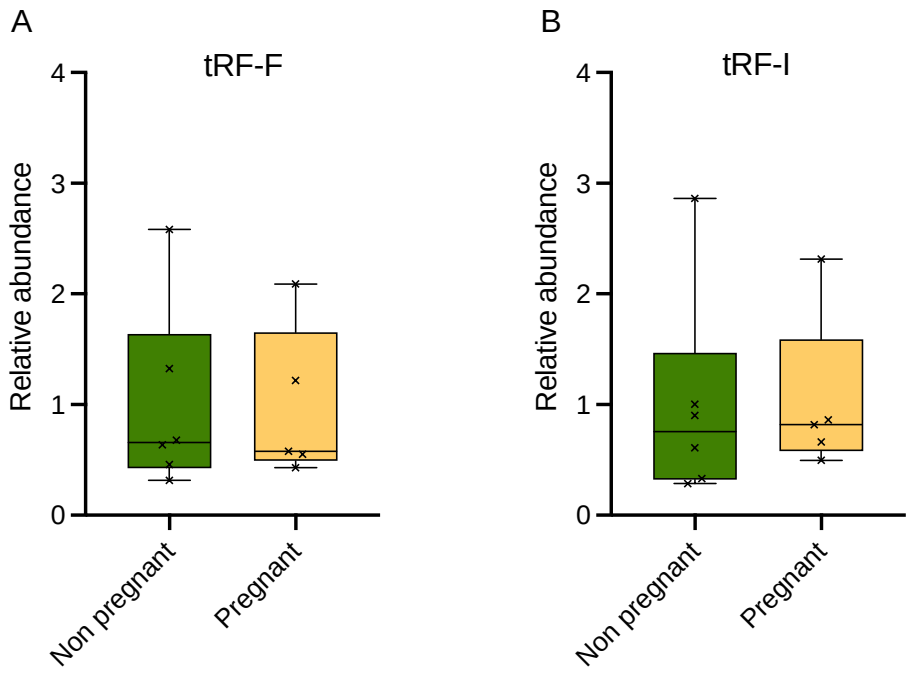


Figure 3-10 – Expression of tRF-F and tRF-I in pregnant and non-pregnant whole venous plasma, relative to the mean non-pregnant abundance.

Boxes represent median and interquartile range, whiskers represent maximum and minimum.

3.3.4.2. Uterine vs peripheral venous whole plasma

Next, expression of targets F, I and J was compared in plasma samples taken from the uterine vein just before delivery at caesarean section and the peripheral vein of the same woman taken at the same time (n=6 pairs, Figure 3-11). Peripheral venous samples were the same as those used as pregnant samples in the experiment described in 3.3.4.1. Consequently, the same outlier was identified and its matching pair removed from further analysis. There were no apparent differences in expression of target F and I between the two groups. Again, a pragmatic decision was made not to seek further samples. Target J was again undetectable, even in uterine venous samples, with Cq >35.

In summary, it was not possible to demonstrate a placental 5'-tRF load in maternal plasma using whole plasma RNA isolation.

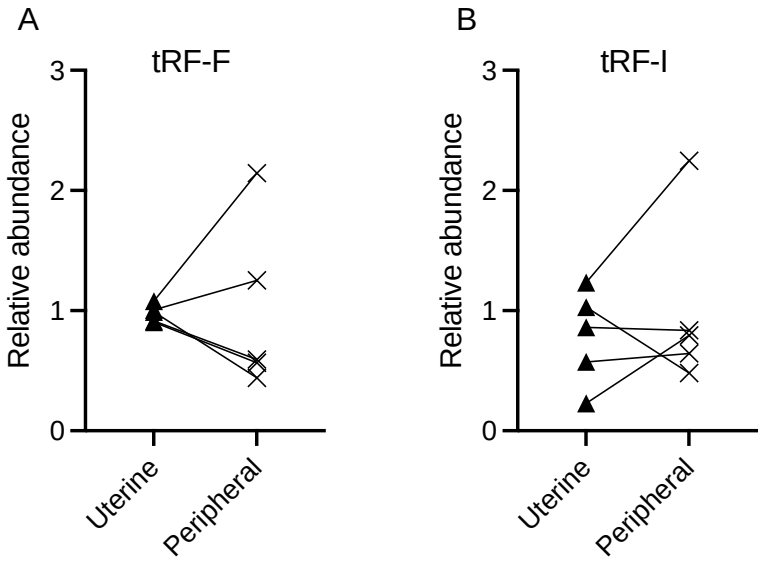


Figure 3-11 – Expression of tRF-F and tRF-I in paired samples of uterine and peripheral whole venous plasma, relative to the mean peripheral venous expression.

3.3.5. Plasma STB-EV isolation approaches

Substantial non-placental EV sources of target tRFs were identified in 3.3.3.1. The second part of this chapter aims to enrich STB-EVs from maternal blood, to allow 5'-tRF detection (Hypothesis 3.2) and comparison of preeclampsia and normal expression (Chapter 4). To do this, I chose to build on a magnetic-bead immunoprecipitation protocol used with placental perfusate in a paper I previously co-authored[42]. Placental alkaline phosphatase (PLAP) was selected as a protein marker which is highly enriched in syncytiotrophoblast[133].

I used an extensively validated in-house PLAP antibody, NDOG2[144]. The immunohistological reactivity of this monoclonal mouse antibody has been tested against fourteen different tissues[145]. Reactivity was found in placenta, cervix, lung, fallopian tube and thymus. Transcriptomic data from the human protein atlas (not dependent on antibody specificity) demonstrate PLAP shows the same distribution[133]. Together these data suggest NDOG2 is a highly specific PLAP antibody.

3.3.5.1. Approach 1: using IgG-coated magnetic beads with SEC

For the first isolation attempt, 500 µL plasma was loaded into SEC to isolate EVs (and separate soluble PLAP from EV-bound PLAP). SEC were used as this experiment was conducted prior to a comparison between SEC and MAC (Figure 3-5). Total EV RNA was isolated from the SEC EV fraction (Figure 3-12A). The EV fraction from a second 500 µL plasma aliquot was split in half. PLAP+ EVs were pulled out from one half by adding NDOG2 coupled to 2.8 µm magnetic beads using sheep anti-mouse IgG (Figure 3-12B). Anti-mouse IgG1 beads were added to the other half as a control. Residual EVs for each pullout were pelleted by ultracentrifugation. RNA was isolated from all five samples: EV fraction, PLAP+ EVs, PLAP- EVs, mouse IgG+ EVs and IgG- EVs. This initial experiment was conducted without repeats, but using plasma pooled from three participants.

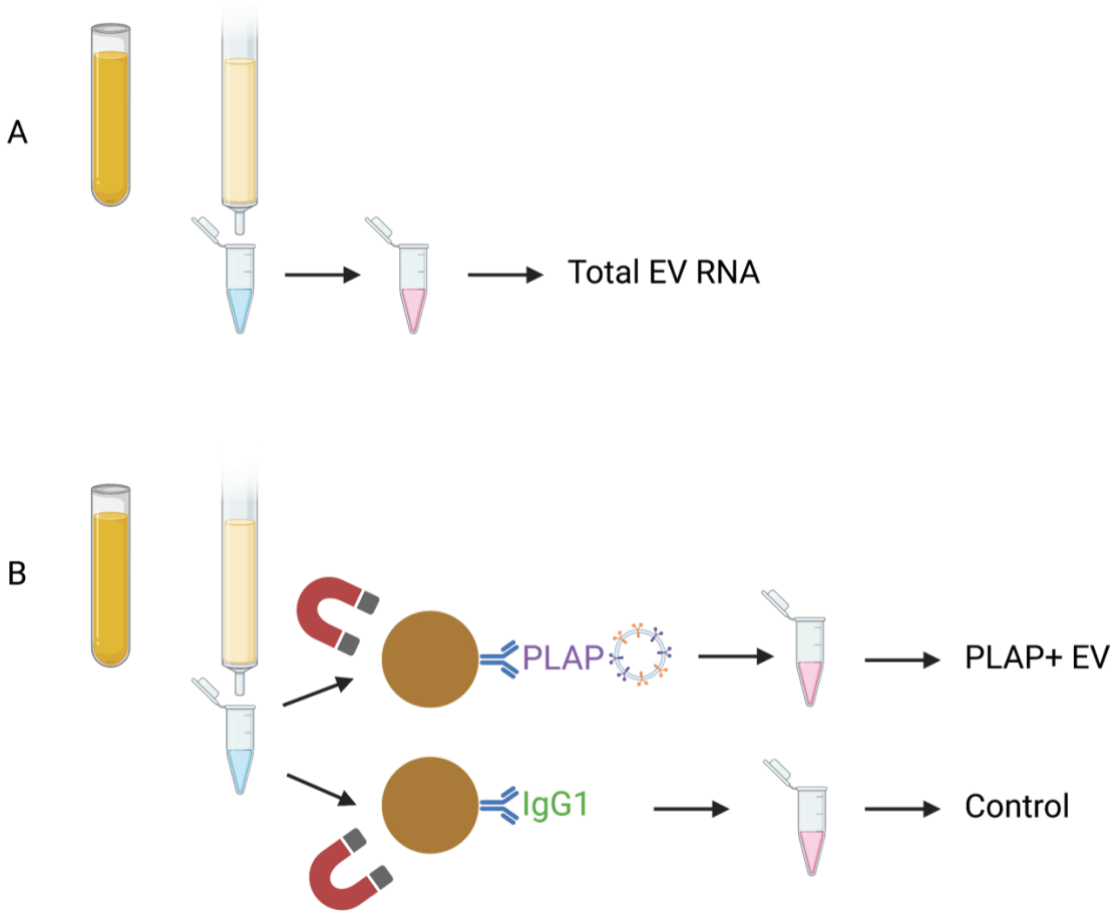


Figure 3-12 – Approach 1 optimised plasma STB-EV isolation protocol.

Created with biorender.com with a publication licence under agreement number HT25OVG64Q.

Two placental miRNAs were quantified in the five samples (Figure 3-13). Both miRNAs showed around three-fold more expression in the PLAP bead than the PLAP supernatant, suggesting some success in STB-EV enrichment. Neither miRNA was detected in the mouse IgG1 beads, demonstrating PLAP specificity. Of concern, the total signal for the four samples derived from a single 500 µL plasma aliquot exceeded the RNA isolated from the total EVs from this aliquot. Given the use of a plasma pool, this cannot be easily explained and suggests further protocol optimisation is required.

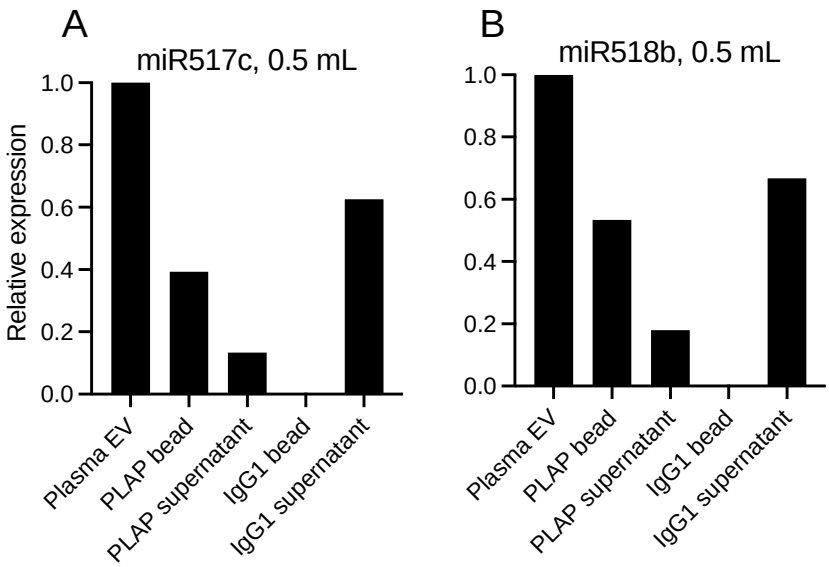


Figure 3-13 – Expression of placenta-specific miRNAs in plasma EVs isolated by SEC, with and without PLAP/IgG1 immunoprecipitation (Approach 1).

Expression shown relative to plasma EV RNA.

3.3.5.2. Approach 2: using IgG-coated magnetic beads with MAC

For the second isolation attempt, two important protocol changes were made. Firstly serum was substituted for plasma, in light of a major publication claiming successful placenta-associated EV miRNA enrichment using PLAP immunoprecipitation from serum[48]. Secondly, MAC were substituted for SEC given the demonstration of their superiority at STB-EV isolation from plasma (Figure 3-5). An initial experiment was conducted to confirm non-inferiority of serum for detecting placentally-derived EVs. The gradient between uterine and peripheral vein plasma EV expression of miR518b was compared between serum and plasma samples (Figure 3-14). Both sample types demonstrated greater miR518b abundance in uterine than peripheral vein EVs (n=3 pairs). There was no significant difference between miR518b abundance between plasma and serum. Of note, this experiment would not be affected by platelet EV contamination as miR518b is a placenta-specific target.

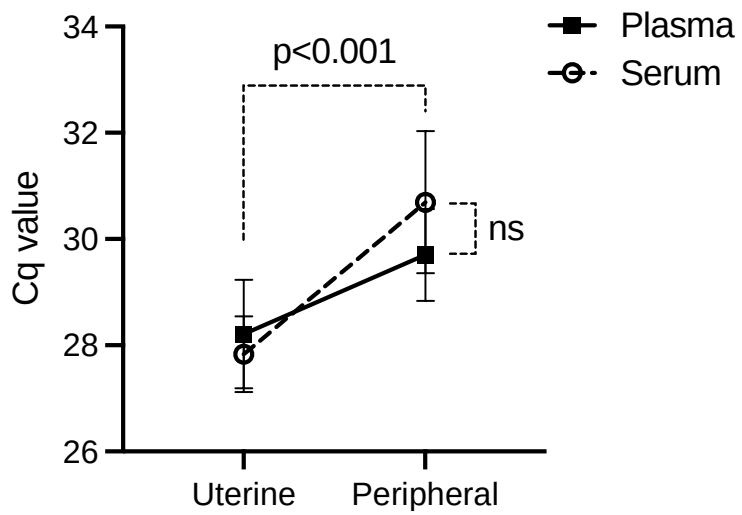


Figure 3-14 – Expression of miR518b in paired samples of uterine and peripheral venous plasma EVs and serum EVs, relative to the mean peripheral venous expression.

Comparisons between groups and sample types by 2-way ANOVA. Note a lower Cq value represents a greater target abundance in that sample type.

The isolation protocol was similar to the first attempt with the following exceptions in addition to serum and MAC isolation. Firstly, EVs were initially isolated from three 500 µL fractions, meaning the total plasma EV load was added to the PLAP beads and the same EV load to the IgG1 beads, rather than being divided between them. Secondly, serum was not pooled, but the experiment repeated three times with three different serum donors. Thirdly, the PLAP supernatant was small volume, so unbound EVs did not need to be concentrated by ultracentrifugation. Finally, only miR518b was quantified given the strong concordance between this and miR517c in prior experiments.

There was no enrichment of miR518b in the PLAP-bead immunoprecipitation (Figure 3-15). Moreover, the same problem of over-detection in the fractions after immunoprecipitation was seen: expression in both PLAP supernatant and IgG1 supernatant was greater than the expression in serum EVs from which they were derived.

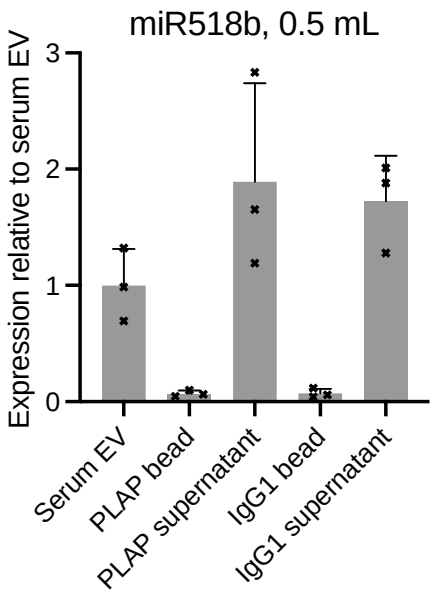


Figure 3-15 – Expression of placenta-specific miRNAs in serum EVs isolated by ExoEasy, with and without PLAP/IgG1 immunoprecipitation (Approach 2).

3.3.5.3. Optimisation of streptavidin magnetic beads

Given the low success in STB-EV isolation from plasma and serum in the prior experiments, I sought advice from an industry partner working on a similar problem. They reported three important observations from their work[140]. Firstly, that beads of a similar size to the vesicles sought offered the most efficient pull down; they recommended 160 nm beads. Secondly, that streptavidin-coated magnetic beads coupled with biotinylated antibodies offered superior efficacy to IgG coupling. Thirdly, that unoccupied streptavidin sites could be saturated with free biotin to minimise non-specific binding. I adopted these recommendations and optimised the protocol for a third time.

3.3.5.3.1. Antibody biotinylation

The NDOG2 antibody was biotinylated using sulfo-NHS-LC-biotin. The manufacturer recommended the HABA-avidin assay was initially used to measure biotin incorporation. Biotinylated NDOG2 was added to a mixture of HABA and avidin; biotin displacement of the HABA-avidin interaction changes the absorbance at 500 nm proportionate to the biotin concentration. I observed fluctuating absorbance over 8 minutes, correlating with ratios of biotin incorporation varying from 2.2 molecules per IgG to <0 molecules per IgG (Table 3-3). Thus, I could not confirm successful NDOG2 biotinylation.

Mins	Absorbance	Moles biotin/ mole antibody
Standard	0.617	-
1	0.577	2.2
2	0.596	1.2
3	0.608	0.50
4	0.613	0.22
5	0.617	0
6	0.621	-0.22
7	0.628	-0.61
8	0.635	-0.99

Table 3-3 – Table showing absorbance at 500 nm of HABA/avidin solution (standard), compared to biotinylated antibody every minute for 8 minutes after reaction started.

In a second experiment, I ran a Western blot comparing beads pre-incubated for 30 minutes with biotinylated antibody (bP) to beads pre-incubated with non-biotinylated antibody (nP). The membrane was stained with Ponceau red and the band at 150 kDa, corresponding to the antibody, was quantified. This appeared to show more bead-bound NDOG2 in the biotinylated antibody lanes, but was also not compelling (Figure 3-16).

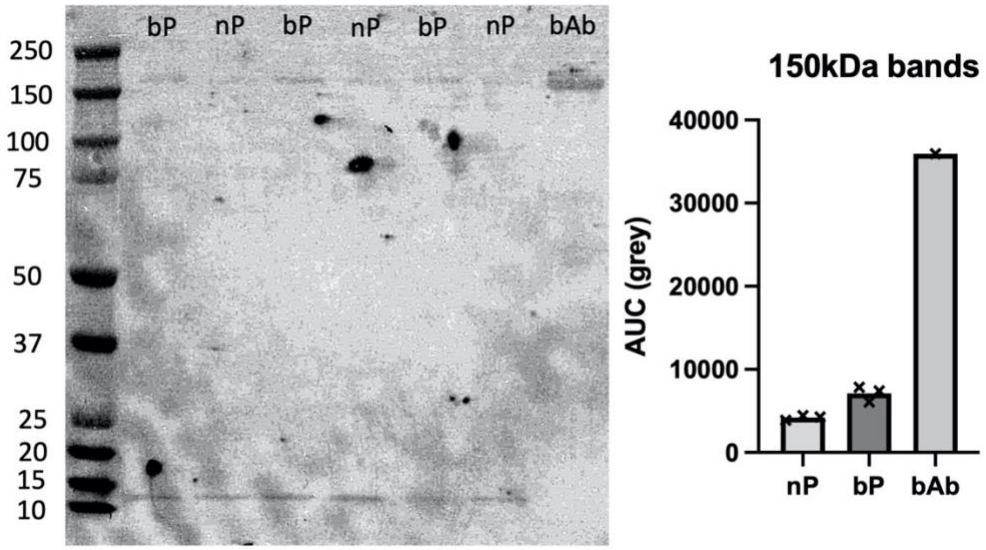


Figure 3-16 – Western blot showing recovery of 5 ug biotinylated PLAP antibody (bP) using 50 uL streptavidin coated beads (n=3) compared to non-biotinylated antibody (nP).

Antibody without bead recovery in lane 8 as positive control (bAb). Stained with Ponceau red. Band intensity quantified using ImageJ.

In a third attempt to evaluate NDOG2 biotinylation, I intended to quantify the NDOG2 protein bound to magnetic beads using the NanoOrange® Protein Quantitation Kit (ThermoFisher Scientific, UK). NanoOrange® dye fluoresces with excitation at 470 nm and emission at 570 nm. Control wells containing beads with PBS and no antibody generated fluorescence at these wavelengths, suggesting that native beads fluoresce at the same wavelength as the NanoOrange® dye and rendering the assay futile.

Macroscopic observations during this experiment suggested that beads were adhering to plastic tubes after biotinylated antibody was added. This problem needed to be overcome before further optimisation work could continue.

3.3.5.3.2. Plasticware

I hypothesised that bead adherence to the plasticware might be a consequence of antibody adsorption, given it only occurred after addition of the biotinylated antibody. I therefore compared beads added to four tubes made from different polymers designed to minimise protein binding. Beads were washed with PBS, incubated with biotinylated NDOG2 antibody then free biotin with washes between. Beads were transferred to a new tube and the polymer with maximal bead recovery (i.e. minimal loss to the tube during washing steps) was sought. Macroscopic inspection suggested that the tube labelled 4 (Eppendorf's Protein LoBind) was superior to the others (Figure 3-17). This was selected for downstream work.



Figure 3-17 – Bead recovery after handling equal quantities in four different tube types (4 to 7), compared to control unhandled beads (8).

3.3.5.3.3. Confirming antibody biotinylation by PLAP pullout from MLEVs

I elected to see if biotinylated NDOG2 bound to magnetic beads could pull STB-EVs from placental perfusion MLEVs as indirect confirmation of antibody biotinylation. Beads were added to biotinylated NDOG2, then saturated with free biotin. Perfusion MLEVs were added and expression of target F in the bead pull-down was quantified (Figure 3-18). Empty beads saturated with free biotin were used as a negative control; perfusion MLEVs as a positive control. tRF-F expression was 15-fold greater in the beads with biotinylated NDOG2 than the empty (biotin-saturated) beads, confirming successful biotinylation and binding of the antibody.

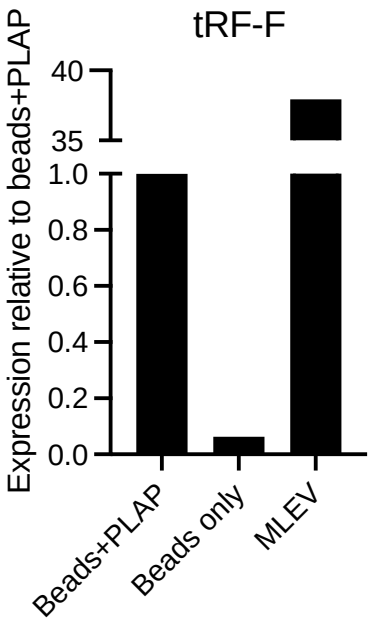


Figure 3-18 – Expression of tRF-F in PLAP bead-bound MLEVs, empty bead-bound MLEVs and unprocessed MLEVs.

Data normalised to cel-miR-39 and shown relative to PLAP bead-bound MLEVs.

3.3.5.3.4. Bead clumping

A further macroscopic observation was made during the preceding experiment that beads clumped and demonstrated poorer separation in a magnetic field after biotinylated NDOG2 was added. I hypothesised that this might be due to over-biotinylation of the antibody, meaning multiple beads could bind to multiple antibody molecules and cross-link, creating macroparticles. To test this hypothesis, I biotinylated the antibody with three different concentrations of sulfo-NHS-LC-biotin calculated to be 20, 10 and 2 fold molar excess of biotin per mole of NDOG2. When added to beads, it was macroscopically visible that NDOG2 with 2X biotin resulted in less clumping and better bead separation after 5 minutes in a magnetic field than 10X or 20X (Figure 3-19).

To confirm that this problem was created by bead clumping, beads were visualised using nanoparticle tracking analysis (NTA). Videos generated from laser scatter demonstrated exclusively small particles when beads alone were analysed (Figure 3-20A). The addition of 20X biotinylated NDOG2 resulted in only occasional large particles and no small particles (Figure 3-20B).

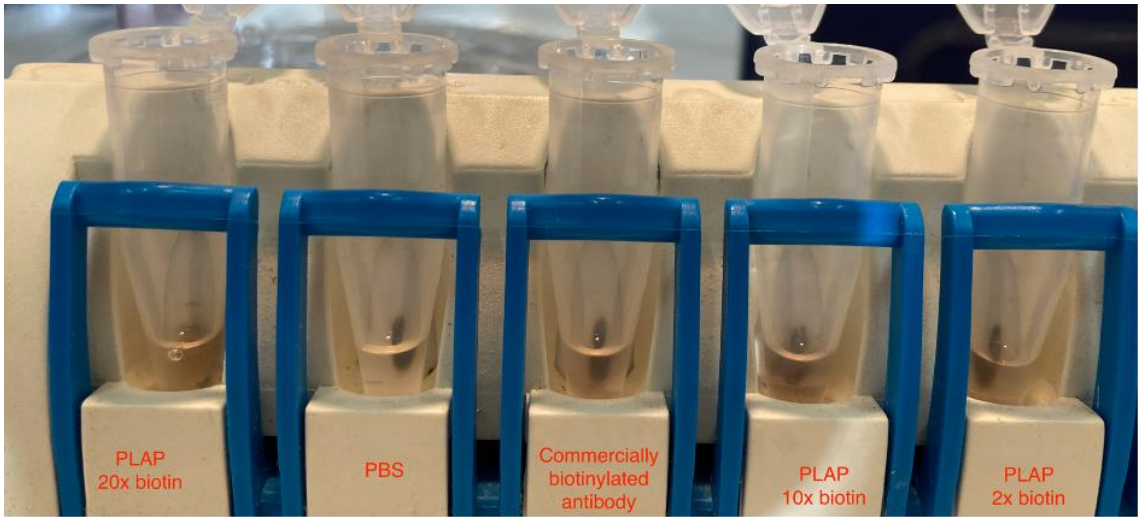


Figure 3-19 – Comparing different NDOG2 (PLAP antibody) biotinylation concentrations to beads with PBS and a commercially biotinylated antibody.

Samples had been in a magnetic field for 5 minutes prior to the image being taken.

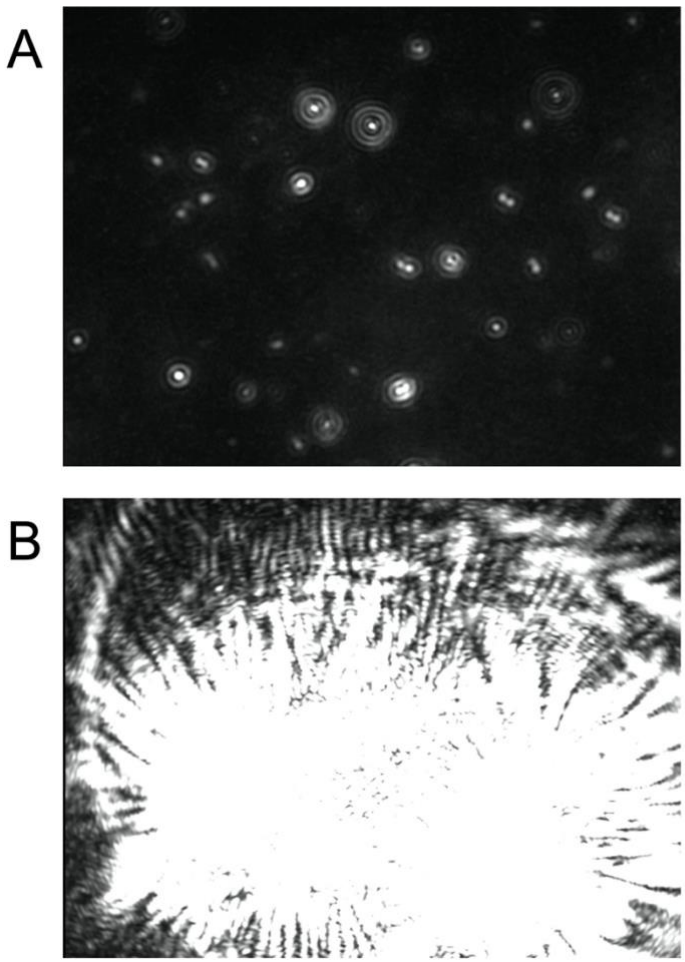


Figure 3-20 – Representative images from NTA of untreated beads (A) and macroscopically clumped beads (B) after addition of 20X biotinylated NDOG2 antibody

NTA software analysis failed to count the large particles, giving no concentration for 20X beads and sequentially increasing bead concentrations for 10X, 2X and beads alone (Table 3-4). This correlated with observations from videos. A small degree of clumping was seen with a commercially biotinylated antibody. It was concluded that the lowest biotinylation ratio 2X resulted in the least bead clumping.

Sample	Observations	Conc particles/ml
Beads only	No large particles	3.96E8
20X PLAP	No particles on NTA	-
10X PLAP	Minimal large particles	3.15E8
2X PLAP	Minimal large particles	3.59E8
Commercially biotinylated antibody	Minimal large particles	3.14E8

Table 3-4 – Table showing observations and software-generated particle concentrations following NTA analysis of different bead samples.

3.3.5.3.5. Isolation of PLAP+ EVs from perfusion STB-EVs

Efficacy of STB-EV isolation from perfusion MLEVs with 2X and 10X biotinylated NDOG2 was investigated next. Target F expression was quantified in MLEVs with and without NDOG2 10X, 2X and empty bead pull-downs (Figure 3-21). NDOG2 (PLAP) 2X offered the most efficacious pulldown and was selected for further work.

Parallel to these experiments, three commercially biotinylated mouse IgG1 control antibodies were tested. All caused significant macroscopic clumping, which could not be optimised as the antibodies were already biotinylated on purchase. It was decided to proceed with optimisation using empty (biotin-saturated) beads as a negative control.

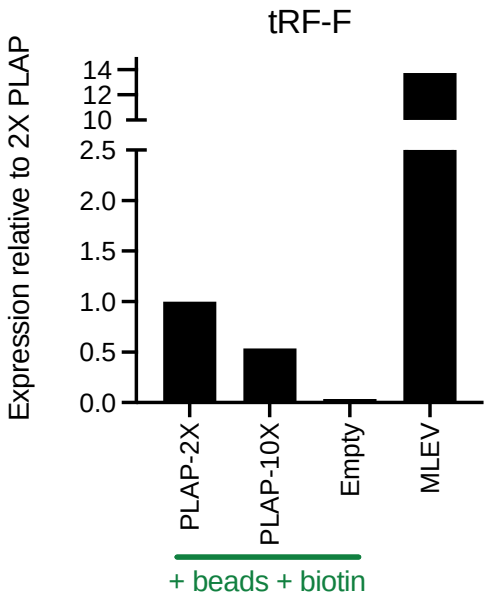


Figure 3-21 – Expression of tRF-F in perfusion MLEVs isolated using NDOG2 antibody with different biotinylation levels, relative to 2X biotinylation.

3.3.5.4. Approach 3: using streptavidin magnetic beads with ultracentrifugation

After successful optimisation of NDOG2 biotinylation and plasticware, a third attempt was made to use magnetic beads to isolate STB-EVs from maternal blood (Figure 3-22). STB-EVs were separated from free PLAP by centrifugation at 10 000 *g* to mimic exactly the conditions that enabled MLEVs to be separated from placental perfusate. The pellet was washed once in PBS and pelleted again, to reduce the free PLAP concentration further. 2X biotinylated NDOG2 antibody was bound to 160 nm streptavidin-coated magnetic beads, which were then saturated with free biotin. Beads were added to the plasma pellet and incubated for 30 minutes. Beads were washed four times in PBS and RNA was isolated.

This protocol was applied to target samples and positive and negative controls, each with three biological repeats. The optimisation target (PLAP-beads with pregnant plasma) was used as a reference condition and other samples expressed relative to it. Non-pregnant plasma with spiked-in perfusion MLEVs was interrogated with PLAP-beads as a positive control. Two negative controls were selected: pregnant plasma with empty beads and non-pregnant plasma with PLAP-beads. Two RNA targets were quantified. miR518b was selected as an STB-EV-specific miRNA. tRF-F was chosen as an abundant but not STB-EV-specific target.

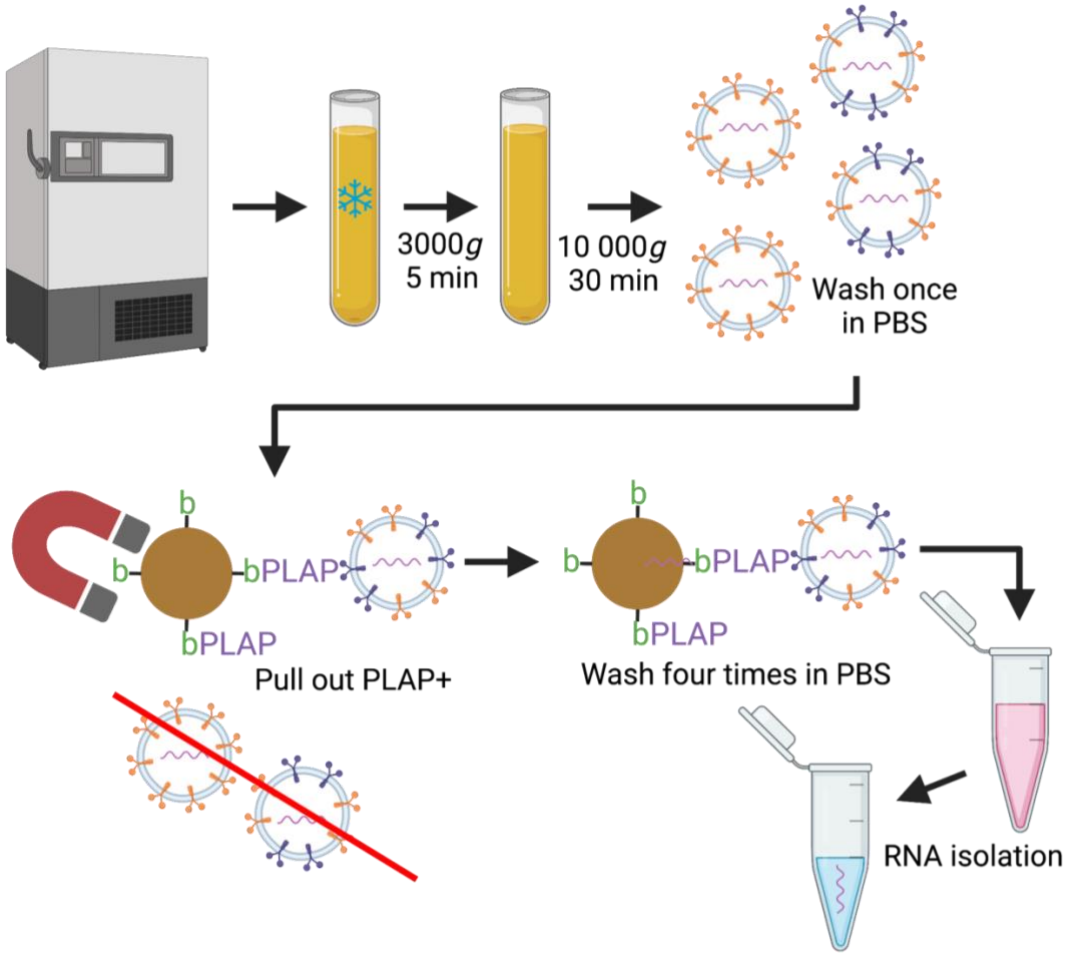


Figure 3-22 – Approach 3 optimised plasma STB-EV isolation protocol.

Created with biorender.com with a publication licence under agreement number HX25OVEW9B.

miR518b and target F were detectable in maternal plasma using PLAP-beads with mean Cq values of 30.4 and 21.1, respectively. Both targets were at least one order of magnitude more abundant in non-pregnant plasma spiked with perfusion MLEVs, demonstrating the beads were not saturated in maternal plasma. miR518b was undetectable in non-pregnant plasma, consistent with it being a pregnancy-specific marker. There was very low expression of miR518b in pregnant plasma with empty (biotin-saturated) beads, suggesting some non-specific binding of STB-EVs to beads.

Target F is not pregnancy-specific. It was detectable in non-pregnant plasma with PLAP beads at around one fifth of the level in pregnant plasma with PLAP-beads, suggesting non-specific binding of plasma EVs (not STB-EVs) to PLAP-beads. Target F was even more abundant in pregnant plasma with empty (biotin-saturated) beads, suggesting this non-specific binding was a property of the beads/streptavidin/biotin, rather than the NDOG2 antibody.

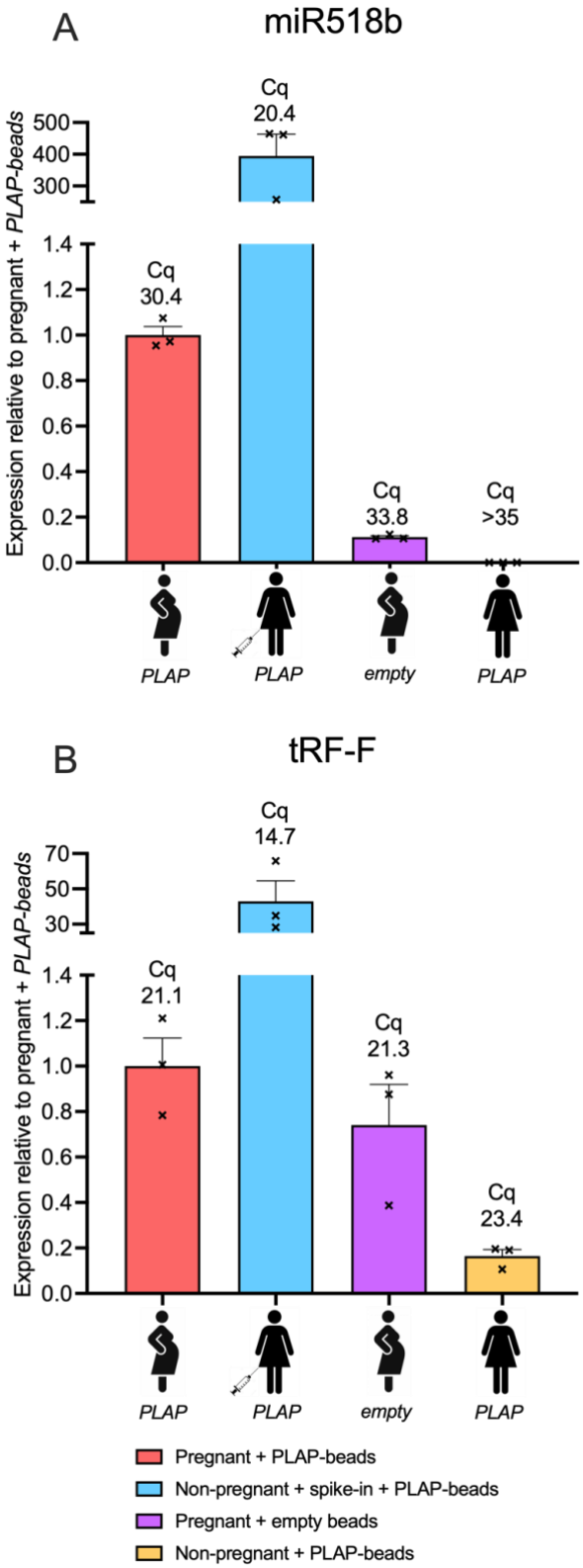


Figure 3-23 – Expression of miR518b and tRF-F in PLAP-EV RNA isolated from pregnant plasma alongside positive and negative controls (Approach 3).

Note a lower Cq value represents a greater target abundance.

To reduce this non-specific bead binding, I considered changing the bead washing. However, beads were already washed four times with PBS and there was an unavoidable bead loss to the tube with each wash: it was felt further washes would introduce error too great to enable quantification. As an alternative strategy, I explored pre-depleting the non-specific binding by pre-incubating plasma EVs with empty (biotin-saturated) beads.

3.3.5.5. Approach 4: pre-depletion of non-specific binding with biotin-saturated beads

In Figure 3-24, target F was quantified in EVs from non-pregnant plasma bound to PLAP beads; this was considered the reference condition. The same plasma sample was mixed with empty (biotin-saturated) beads for 30 minutes before the PLAP-beads were added. This reduced target F expression by 72%. When pre-incubation was applied to pregnant plasma with empty beads (the other negative control), target F expression was reduced by 86%. Thus, it was considered that pre-depletion of non-specific binding would improve the protocol.

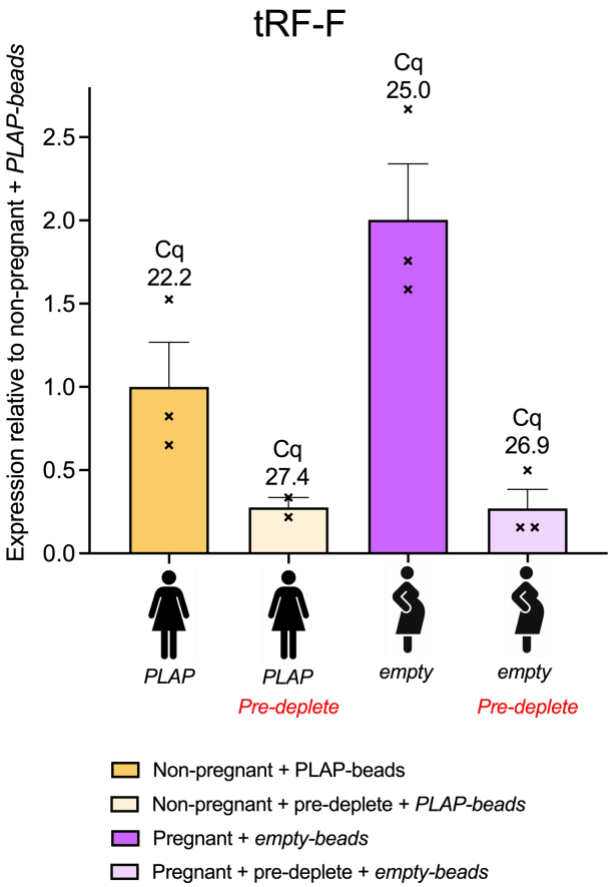


Figure 3-24 – Expression of tRF-F in RNA isolated from pregnant plasma with empty beads and non-pregnant plasma with PLAP-beads, to see whether pre-depletion with empty beads reduces the background signal.

Note a lower Cq value represents a greater target abundance.

The final optimised protocol to remove STB-EVs from pregnant plasma is shown in Figure 3-25. This incorporates all of the improvements demonstrated by prior experiments: streptavidin beads instead of IgG, plasma instead of serum, low-binding plasticware, 2X NDOG2 biotinylation and pre-depletion of non-specific binding with empty (biotin-saturated) beads.

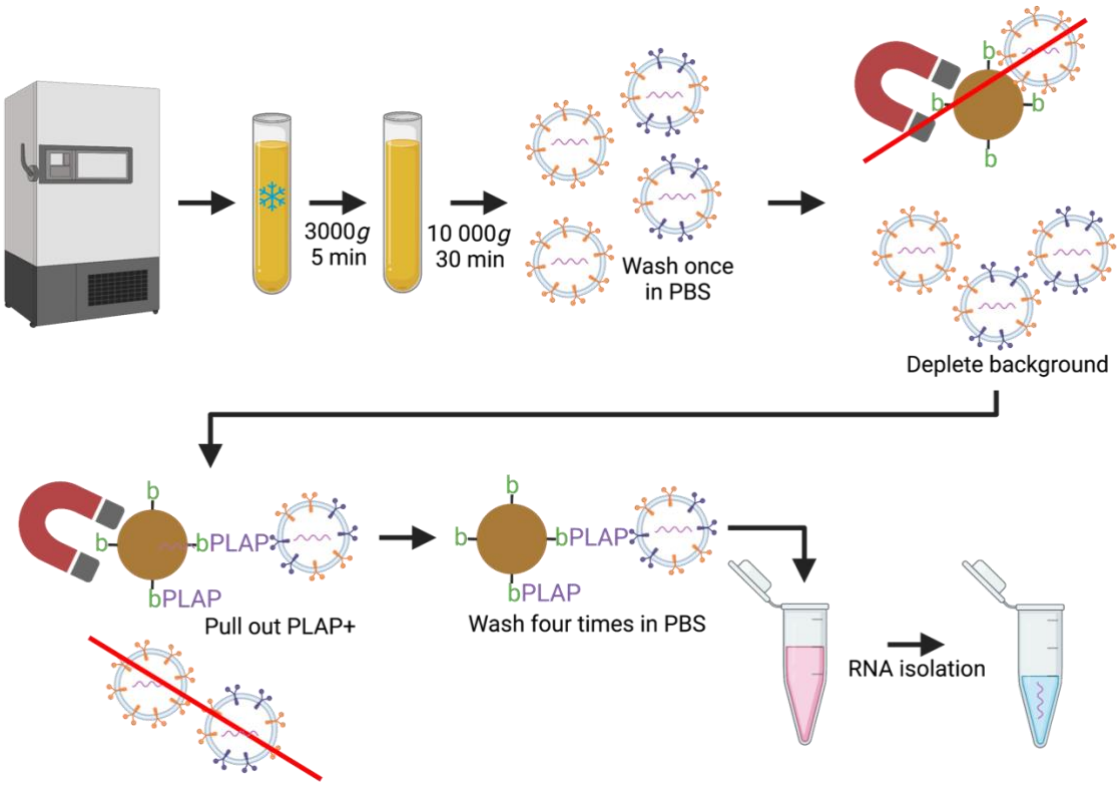


Figure 3-25 – Approach 4 optimised plasma STB-EV isolation protocol.

Created with biorender.com with a publication licence under agreement number BO25OVFD7D.

The application of this protocol to the same positive and negative controls as previously is shown in Figure 3-26. miR518b expression showed less absolute abundance in pregnant plasma, but remained within the limit of detection (Cq 34.3). miR518b was over 2000-fold more abundant in the positive control with perfusion MLEV spike-in, confirming beads and antibody were not saturated. There was no detectable expression in pregnant plasma with empty beads or non-pregnant plasma with PLAP beads. This represented the best protocol tested when a pregnancy-specific marker was assayed.

Target F data were also improved. PLAP-beads from pregnant plasma gave a target F Cq value of 25.8: well within the limit of detection. The positive control was 733-fold more abundant. The negative controls were less abundant, but not negative. Empty (biotin-saturated) beads gave 60% of the signal of PLAP-beads in pregnant plasma. PLAP-beads gave 44% of the signal in non-pregnant plasma. Together these data imply approximately half of the tRF-F signal is STB-EV specific with PLAP-bead pullout. This represents a substantial enrichment: <1% total plasma EV signal was estimated to derive from STB-EVs in a prior publication (Figure 3-3). Further optimisation of the protocol was not considered appropriate given its complexity. One purpose of developing the protocol was to apply it to quantify differences between preeclampsia and normal pregnant plasma; complicating the isolation further would likely increase the error beyond acceptable levels.

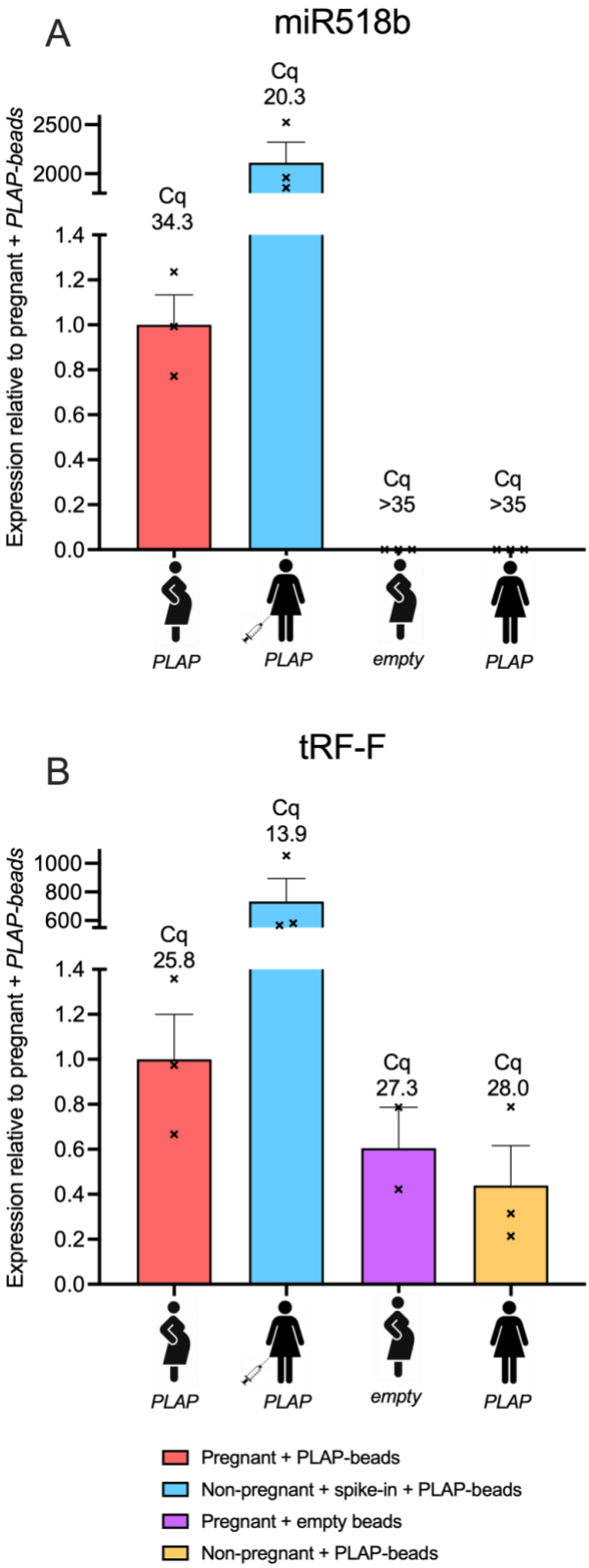


Figure 3-26 –Expression of miR518b and tRF-F in PLAP-EV RNA isolated from pregnant plasma alongside positive and negative controls (Approach 4).

Note a lower Cq value represents a greater target abundance.

3.4. Discussion

This chapter first aimed to determine whether a placental 5'-tRF load was detectable in maternal blood. I originally discovered placental 5'-tRFs in particles isolated from placental perfusate with centrifugation at 10 000 *g* and also at 150 000 *g*[52]. NTA, electron microscopy and Western blotting all suggested these particles were mostly EVs derived from the syncytiotrophoblast. Other small particles may be co-isolated from placental perfusate, including lipoproteins, chylomicrons, apoptotic bodies and protein macrocomplexes. These particles may also contain 5'-tRFs, and may confound the discovery.

Plasma is a complex biofluid in which contaminating small particles are known to outnumber EVs[78]. The distribution of 5'-tRFs throughout plasma compartments is unknown. An early publication from mouse serum proposed that 5'-tRFs were only present in 100-300 kDa nucleoprotein complexes[146]. Subsequent human plasma studies demonstrate 5'-tRFs are present in EV-like particles isolated using a variety of techniques including polyethylene glycol-based precipitation and ultracentrifugation (Table 1-5). Nevertheless, it is likely that nucleoprotein complexes also carry 5'-tRFs in human plasma. Thus, the outcome of experiments investigating the chapter's first aim may depend heavily on the blood compartment investigated.

Given 5'-tRFs in perfusate were attributed to STB-EVs, I first sought the placental 5'-tRF load in plasma by isolating total plasma EVs. My initial comparison of SEC and MAC demonstrated lower Cq values for placenta-specific miRNA targets with MAC (3.3.2.1). This finding is consistent with the literature. One published comparison of SEC and MAC for non-pregnant plasma EV isolation noted higher sRNA recovery from MAC[141]. A second study of non-pregnant serum EV miRNAs also compared SEC and MAC, reporting MAC offered a greater library size, more mapped miRNAs and a greater enrichment of tRNA species[72]. A third study compared 10 plasma extracellular sRNA

isolation techniques, concluding MAC was most efficacious to obtain both tRNA and miRNA (where it offered superior complexity, expression and reproducibility metrics)[71]. The authors of the first two studies also provided data to suggest the higher RNA recovery with MAC is compromised by co-isolation of non-EV particles including proteins and lipoproteins. I performed particle size analysis, which confirmed a similar size profile between plasma MAC particles and placental perfusate MLEV particles (3.3.2.2). These data suggest MAC should incorporate the MLEVs isolated from perfusion (in which the preeclampsia 5'-tRF discoveries were made in Chapter 2). However, by selecting placenta-specific miRNA targets I did not assess the purity of MAC plasma EVs in my expression data. This may be an important shortcoming, given contaminant particles may also contain 5'-tRFs. To my knowledge, no comparison of pregnant plasma EV isolation techniques has been published.

The idea of multi-plexing reverse transcription reactions originated from a methods publication, not the manufacturer's instructions[102]. No data were available to support this proposal, which is why they were empirically evaluated in this chapter (3.3.2.3). The difference in absolute quantification of targets with singleplex and multiplex reverse transcription reactions must be a consequence of a change to the reaction efficacy. This could be due to competitive binding to reverse transcriptase; data from 2.3.3.1 suggest poor stem-loop assay specificity is unlikely to be responsible.

Application of MAC to pregnant and non-pregnant plasma EVs convincingly demonstrated a pregnancy-specific load of target tRFs (3.3.3.1). The increased tRF abundance in uterine venous EVs compared to paired peripheral samples suggests this is in fact a placentally-derived 5'-tRF load (3.3.3.2). These data are consistent with similar experiments investigating other known placentally-derived molecules including PLAP, sFlt-1 and PlGF, as well as STB-EV-bound molecules such as neprilysin and eNOS[40,42,45,136,147]. It is not possible to conclude with certainty that this placental load

contains STB-EVs, as distinct from other EV-like particles originating from the pregnant uterus. However, the data convincingly support acceptance of Hypothesis 3.1: a placental 5'-tRF load can be detected in maternal blood using qPCR assays.

The high abundance of target tRFs in non-pregnant plasma EVs (3.3.3.1) is an important observation. Again, the plasma compartment which contains these contaminating tRFs is uncertain. However, the numerous emerging publications reporting plasma EV tRFs as biomarkers for other diseases support the conclusion that target tRFs are not placenta-specific (pertinent references summarised in Table 1-5).

The lack of a pregnancy-specific or placenta-specific 5'-tRF load in whole plasma (3.3.4) suggests that 5'-tRFs are also present in plasma outside EV-like particles. A discrepancy between 5'-tRF expression in whole plasma and plasma EVs was also seen in a large study of breast cancer tRF biomarkers[75]. Here, the authors investigated six whole plasma disease-downregulated 5'-tRFs in plasma exosomes isolated using Exo-Quick™ (System Biosciences, USA). Only two of the six 5'-tRFs were significantly downregulated in plasma exosomes as well as whole plasma, with the direction of difference reversed in some cases. This inconsistency between plasma compartment tRF expression (in both my data and the breast cancer study) has important implications for subsequent work. In plasma 5'-tRF detection there is a trade-off between isolating the compartment which contains the relevant signal and introducing excessive noise through lengthy or inconsistent processing steps. The whole plasma data suggest that evaluation of 5'-tRFs as biomarkers (in Chapter 4) is likely to be more successful with pre-enrichment of plasma EVs, and indeed STB-EVs. It is therefore important to develop a technique to isolate STB-EVs from other plasma EVs. Additionally, the abundance of tRFs outside EV-like particles (and in non-placental EVs) suggests that the packaging of STB-EV 5'-tRFs to specific target cells is likely to be crucial to any proposed functionality (investigated in Chapter 5).

Numerous studies claim to investigate placental EVs in the maternal circulation. Almost all isolate total EVs from plasma and quantify with a placental marker[40,148]. Only two techniques have been published which claim to allow interrogation of the contents of placental EVs isolated from the maternal circulation. Lai *et al.* used PLAP antibody, cross-linked to protein A-coated agarose beads, to isolate PLAP+ EVs from total plasma EVs isolated using ultracentrifugation[135]. They use the same (un-specified) antibody for isolation and validation and fail to demonstrate the specificity, sensitivity or ability of the assay to quantitate reliably. The technique has been applied alongside mass spectroscopy to profile placental EVs in preterm birth, but again without any data to support its efficacy[149]. Srinivasan *et al.* biotinylated PLAP antibody, binding it to streptavidin-coated magnetic beads which were incubated with unprocessed serum[48]. They overlooked soluble PLAP, which exceeds EV-bound PLAP by two orders of magnitude, and would likely outcompete STB-EVs when binding their beads[134]. The authors similarly provided no validation data to demonstrate their technique had successfully isolated placental EVs.

The first approach taken to enrich STB-EVs from maternal plasma in this chapter (3.3.5.1) built on a parallel immunoprecipitation technique previously optimised in our laboratory in placental perfusate specimens[42]. Validation data for IgG-magnetic bead isolation of PLAP+ EVs demonstrated successful enrichment, without complete pull-out of placental EV signal from plasma. A second approach, which used serum in place of plasma, (3.3.5.2) failed entirely, without clear cause. A third approach, using streptavidin-magnetic beads with biotinylated PLAP antibody, required significant optimisation to overcome problems in the laboratory (3.3.5.4). A final optimised technique that built on this approach showed successful isolation of a placenta-specific signal without antibody/bead saturation, suggesting it would be promising for quantification (3.3.5.5). The placenta-specific tRF-F signal was enriched to around half of the total signal, a substantial increase from the <1% contribution to plasma EVs made by STB-EVs without enrichment (Figure

3-3). Comparison of this final protocol to the literature is not possible in the absence of validatory data for the two other published protocols. Despite limitations, I considered that a reduction of non-placental confounding to around half of the plasma EV signal might prove sufficient for biomarker evaluation in Chapter 4. Certainly, these data were considered sufficient evidence to accept Hypothesis 3.2 (STB-EVs can be enriched from maternal peripheral blood, allowing 5'-tRF detection using qPCR), albeit with substantial residual signal from other particles.

3.5. Summary Figure

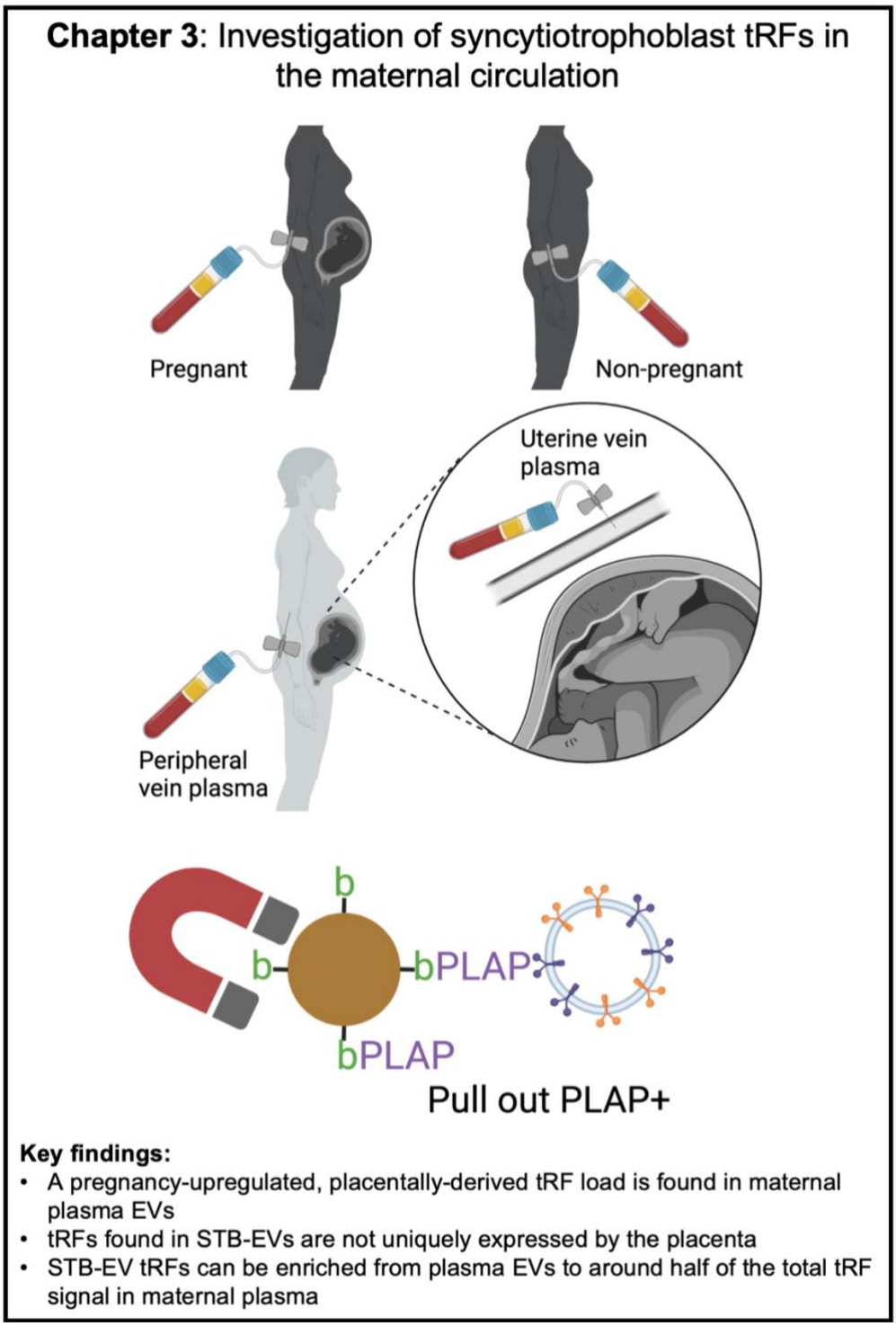


Figure 3-27 – Schematic figure summarising Chapter 3 key experiments and findings.

Created with biorender.com with a publication licence under agreement number ZM25OVC7BE.

Chapter 4. tRNA fragments as blood biomarkers in preeclampsia

4.1. Introduction

Differential expression of tRNA fragments (tRFs) in STB-EVs obtained by placental perfusion from women with early-onset preeclampsia, compared to gestation-matched controls was discovered in Chapter 2. qPCR assays were optimised to enable tRF detection. These assays were applied to maternal plasma in Chapter 3. A placental 5'-tRF load was found, corroborating that STB-EV tRFs are released into the maternal circulation. A technique was developed to enrich STB-EVs from maternal plasma. This chapter aims to validate the disease-related differences identified in Chapter 2 in maternal plasma, using techniques optimised in Chapter 3.

4.1.1. Hypothesis 4.1

Expression of STB-EV tRNA fragments in blood represents a biomarker for preeclampsia.

4.1.2. Rationale to investigate biomarkers for preeclampsia

Preeclampsia is a complex multi-system disease with variable aetiologies, risk factors and clinical features[19]. Globally, it is the second leading cause of maternal mortality, accounting for 14% maternal deaths[3]. Obstetric care can reduce morbidity and mortality from preeclampsia at three key stages:

1. *Prevention* with low-dose aspirin therapy given to women at increased risk of preeclampsia from 12 weeks of gestation[11].
2. *Early diagnosis* allows appropriate targeting of supportive care for preeclampsia, including monitoring of maternal organ function and fetal wellbeing, alongside anti-hypertensive medication[10].
3. *Prognostication* facilitates optimal timing of delivery (the only definitive treatment for preeclampsia) to balance risk of preterm and preeclampsia-related morbidity.

Better preeclampsia biomarkers could improve prevention, diagnosis and prognostication in clinical practice, in turn reducing preeclampsia-associated morbidity and mortality.

Aspirin prophylaxis is currently targeted through risk factors identified from maternal demographics and medical history[10]. This offers a detection rate for preterm preeclampsia around 45%, with a fixed screen-positive rate of 10%[17]. When this screening method is used to direct aspirin prophylaxis, it offers an 18% reduction in proteinuric preeclampsia[11]. This detection rate can be improved to around 75% with the addition of several clinical, ultrasound and blood measurements[150]. Targeting aspirin with the improved prediction model can reduce preeclampsia prevalence by approximately 60%, demonstrating the added value of improved predictive biomarkers[151]. However, these complex prediction algorithms have not been adopted into routine clinical practice due to the cost and inconvenience of measuring multiple parameters as well as the complexity of their application. There is a need for novel blood-based biomarkers of preeclampsia to offer simple, inexpensive and accurate targeting of aspirin prophylaxis.

Diagnosis of preeclampsia has transformed in the last 7 years following the introduction of soluble fms-like tyrosine kinase-1 (sFlt-1) and placental growth factor (PlGF) assays[14]. The angiogenic ratio (sFlt-1/PlGF) offers a negative predictive value of 100% in clinical trials, allowing safe rule-out of the disease[15]. However, the positive predictive value of a ratio >38 is just 41%, leading to over-diagnosis and risking over-intervention[15]. This has led to an increase in the positive diagnostic threshold to a ratio of 85 or 110, leaving a "grey area" of women whose ratio is neither diagnostic nor reassuring[13]. New biomarkers might offer improved diagnostic accuracy. This would optimise targeting of supportive therapy, protecting valuable resources and avoiding unnecessary intervention.

Prediction of preeclampsia complications is challenging. Models such as fullPIERS incorporate a variety of clinical and laboratory measurements to guide this process, but decisions still often rely heavily on clinical accumen[5]. Improved biomarkers for disease progression could be used to optimise timing of delivery, thereby minimising maternal and perinatal morbidity.

tRFs are abundant in normal pregnancy STB-EVs[52]. They are differentially expressed in EVs in a number of disease states outside pregnancy, where they are considered to have strong biomarker potential (summarised in Table 1-5). Better biomarkers have the potential to improve clinical care significantly in preeclampsia. The rationale to investigate STB-EV tRFs as blood-based biomarkers is thus strong. Additionally, if successful, this work could also be considered proof-of-principle for investigation of blood tRFs as biomarkers in other pregnancy-related diseases.

4.1.3. RNA biomarkers in preeclampsia

Three high-profile studies have recently investigated blood-based RNA biomarkers in preeclampsia[48,152,153]. Data are promising but modest, with area under the curve values in validation cohorts for prediction of preeclampsia at 12 weeks of gestation of 0.82 and 0.71 for mRNA transcripts, and 0.70 for miRNA markers. These data are all derived from whole plasma discovery experiments, with EV RNA originating from blood cells, endothelial cells and a full spectrum of other solid organs (Figure 3-3). However, preeclampsia is a placental disease[7]. My approach has identified promising syncytiotrophoblast tRF targets using placental perfusion, eliminating potential confounding from non-placental RNA in maternal blood. STB-EV tRFs may represent a class of RNA biomarker more dependent on placental dysfunction, so better reflecting disease.

4.1.4. Placental perfusion as a preeclampsia biomarker-discovery system

Our group has previously identified two preeclampsia-dysregulated proteins using placental perfusion-derived STB-EVs. Both were subsequently found to be dysregulated in preeclampsia plasma. Endothelial nitric oxide synthase (eNOS) was downregulated in preeclampsia perfusion STB-EVs, as well as in PLAP and eNOS double-positive EVs in maternal plasma[45]. Neprilysin is more abundant in preeclampsia perfusion STB-EVs and also in preeclampsia plasma[42]. No RNA preeclampsia biomarkers discovered by placental

perfusion have yet been validated in plasma, but these protein studies provide a strong rationale to pursue this line of investigation.

4.2. Methods

4.2.1. Ethical approval, sample acquisition and disease definition.

This project was approved by the Central Oxfordshire Research Ethics Committee (07/H0607/74 and 07/H0606/148). Participants provided informed written consent. Peripheral blood samples were taken from the antecubital fossa using 21-gauge needle and tourniquet into 4.5 ml sodium citrate vacutainer tubes (BD Diagnostics, UK). Tubes were inverted 5 times after collection, stored at room temperature and processed within 30 minutes of collection.

Platelet poor plasma (PPP) was obtained by centrifugation of sodium citrate tubes at 1500 *g* for 15 minutes at room temperature. Platelet-free plasma (PFP) was obtained by centrifuging PPP a second time at 13000 *g* for 2 minutes at room temperature. At each stage, the supernatant from replicate tubes was mixed by inversion, aliquoted and frozen at -80°C. Just prior to use, plasma aliquots were thawed in a water bath at 37°C, mixed by inversion and centrifuged to remove cryoprecipitates (5000 *g* for 5 minutes at 4°C for PPP, 13 000 *g* for 2 minutes for PFP).

Preeclampsia was diagnosed by International Society for the Study of Hypertension in Pregnancy (ISSHP) criteria, requiring new-onset hypertension after 20 weeks of gestation accompanied by proteinuria and/or maternal organ dysfunction and/or utero-placental dysfunction[1]. Thresholds for diagnosis are summarised in Table 1-2. Early-onset disease was defined as preeclampsia diagnosed ≤34 weeks of gestation. Multiple pregnancies were excluded. Normal pregnancy was defined as no episodes of hypertension which would meet ISSHP criteria, with no proteinuria or other features suspicious for preeclampsia. Cases and controls were identified from the antenatal wards at the John Radcliffe Hospital, Oxford, UK. Controls were matched so that the date of sample was

within 2 weeks gestational age of its corresponding case. Clinical data were anonymously recorded directly from patient records by Fenella Roseman, research midwife.

4.2.2. General experimental principles

Samples were processed as alternating disease and control specimens throughout experimental protocols to avoid batch effects. Equal volumes of case and control plasma were used at the start of each experiment. RNA was eluted in equal volumes of water within each experiment. Reverse transcription, qPCR reactions and data analysis were performed as described in 2.2.4.2. No template controls were run on every plate and the plate disregarded unless at least two wells for each assay were negative. Samples were run in triplicate except where specified below. Outlying qPCR triplicates were excluded if the standard deviation between Cq values was >0.15 and one result was clearly outlying. Cq values ≥35 were disregarded as below the limit of detection of the instrument. All samples to be compared were assayed on the same qPCR plate. qPCR plates were analysed on a 96-well Quantstudio 3 instrument (Applied Biosystems, USA) for the first and second attempts and a 384-well Quantstudio 5 instrument (Applied Biosystems, USA) for the third, fourth and fifth attempts. Where relative abundance is presented, qPCR reaction efficiency was determined using linear regression, normalisation was undertaken relative to cel-miR-39 and relative expression determined using the Pfaffl approach, as described in 2.2.4.2.

4.2.3. First attempt

Total EVs were isolated using membrane affinity columns (MAC) from 500 µL platelet-free plasma as described in 3.2.2. RNA was eluted in 35 µL RNAse free water.

4.2.4. Second attempt

Total EVs were isolated using MAC from 900 µL PFP; RNA was eluted in 31 µL RNAse free water. Uterine and peripheral venous samples were obtained as described in 3.2.1.

4.2.5. Third attempt

Total EVs were isolated using MAC from 500 µL PPP. cel-miR-39 spike-in was added just after EV elution with Qiazol® lysis reagent (from ExoRNeasy Midi Kit #77144, Qiagen, Germany). RNA was eluted in 30 µL RNAse free water.

4.2.6. Fourth attempt

Whole plasma RNA was isolated as described in 3.2.7. cel-miR-39 spike-in was added just after plasma lysis with buffer RPL (from miRNeasy Serum/Plasma Advanced Kit #217204, Qiagen, Germany). qPCR reactions were conducted in duplicate given the space constraints of a 384-well plate and the number of targets being assayed. It was consequently not possible to review or remove outlying technical qPCR replicates.

4.2.7. Fifth attempt

The final modified protocol for plasma STB-EV isolation is described in 3.2.8.5. cel-miR-39 spike-in was added just after STB-EV lysis with Trizol™ LS reagent (#10296010, Invitrogen, USA) to account for any differences in RNA isolation or reverse transcription reaction, but not to correct for any differences in vesicle counts per µL plasma.

4.2.8. Statistical methods

Hypothesis tests were performed where data appeared to show differences; they are identified in each corresponding figure legend. Where data were not normally distributed on visual inspection, non-parametric tests were used. Uterine and peripheral venous samples were considered paired as they were taken simultaneously from the same

participant. All other tests of continuous variables were unpaired two-tailed tests. Statistical analyses and figures were generated using Prism9 (GraphPad, USA).

4.3. Results

4.3.1. miRNA validation in plasma

I first sought to assess the feasibility of using preeclampsia-dysregulated small RNA (sRNA) discovered in the perfusion analyses in Chapter 2 as blood biomarkers of disease. There is a sizeable body of literature investigating expression of miRNA in blood from women with preeclampsia compared to normotensive pregnancies. I aimed to select miRNA targets identified by the perfusion analyses in Chapter 2 and use published data to determine whether they are differentially expressed in preeclampsia blood samples.

Our collaborators' analysis of perfusion data (Appendix 1), annotated miRNAs as well as tRFs. Of 983 differentially expressed fragments in preeclampsia perfusion STB-EVs, 177 mapped to miRNAs. Target miRNAs were selected by abundance in STB-EVs (median expression >1000 reads per million [RPM] in either group), and low anticipated abundance in blood cells likely to contribute contaminating EVs (mean expression <0.5 RPM in analysis of erythrocytes, platelets and monocytes; see collaborators' analysis in Appendix 3). This approach identified six fragments mapping to four miRNAs, with perfusion MLEV expression data shown in Table 4-1.

Published studies, which have investigated expression of these targets in blood in women with preeclampsia, are summarised in Table 4-2.

Name	Length	Sequence	Median N RPM	Median PE RPM	p-value	Median PE as MoM
520a-3p	22	AAAGTGCTTCCCTTTGGACTGT	2,487	5,585	0.0131	2.25
1323-5p	21	TCAAAACTGAGGGGCATTTTC	3,957	5,588	0.0250	1.41
512-1-3p	22	AAGTGCTGTCATAGCTGAGGTC	2,268	3,496	0.0352	1.54
519d-3p	21	CAAAGTGCCTCCCTTTAGAGT	1,667	1,118	0.0250	0.67
520a-3p	22	AAAGTGCTTCCCTTTGGACTGC	661	1,225	0.0250	1.85
520a-3p	21	AAAGTGCTTCCCTTTGGACTG	543	1,153	0.0131	2.12

Table 4-1 – miRNAs differentially expressed in preeclampsia STB-EVs compared to normal pregnancies.

Data derived from analysis in Appendix 1. MoM (multiple of median), N (normal pregnancy), PE (preeclampsia), RPM (reads per million).

miRNAs studied	Population	Sample type	Gestational age at sampling	Severe PE analysed separately	PE sample size	N sample size	Technique	Ref
520a-5p 1323 519d	Single centre, Japan	EDTA plasma	After diagnosis (27-34 weeks)	Yes	20	20	RT-qPCR (TaqMan MicroRNA assays)	[154]
520a 512-3p	Two centres, Mexico	Serum	Before diagnosis (12/16/20 weeks)	Yes	14	18 (but 13 samples pooled)	RT-qPCR (Taqman MicroRNA Array Card)	[155]
520a 519d	Not specified	EDTA plasma	After diagnosis	No	63	55	RT-qPCR (TaqMan MicroRNA assays)	[156]
519d	Single centre, China	Not specified	After delivery	Yes	4	1	RNA sequencing	[157]
520a	Not specified	Serum	Before diagnosis (12-14 weeks)	Yes	24 (pooled as one)	24 (pooled as one)	RT-qPCR (Taqman Low Density Array)	[158]

Table 4-2 – Summary of published studies quantifying expression of miRNA targets from Table 4-1 in blood. EDTA (ethylenediaminetetraacetic acid), PE (preeclampsia).

Quantitative miRNA expression data could not be extracted from the third study. The fourth study was considered too small to provide meaningful data. Data from the remaining three studies are presented in Figure 4-1, alongside sequencing data from the perfusion STB-EV analysis in Appendix 1. All data are presented as relative differences between preeclampsia and normal pregnancies for ease of comparison; only significantly dysregulated targets are shown. miR520a was upregulated between two and four-fold in preeclampsia in both the perfusion dataset and the two published blood studies (one using plasma taken at preeclampsia diagnosis, the other using serum taken at 12-14 weeks of gestation). miR1323 and miR512 were much more abundantly upregulated in preeclampsia plasma and serum respectively than in preeclampsia perfusion STB-EVs. miR519 was downregulated in preeclampsia perfusion STB-EVs but upregulated in preeclampsia plasma. This may be a result of the well-documented increase in STB-EV release in preeclampsia, discussed in more detail in 4.3.2.3[40].

Overall, miRNA blood expression data from these publications support the validity of the study design, experimental model and sequencing data analyses from the perfusion studies presented in Chapter 2. These data, together with prior publications demonstrating differential plasma expression of proteins discovered using perfusion (summarised in 4.1.4), provide a strong rationale to explore the plasma biomarker potential of preeclampsia-dysregulated tRFs identified in perfusion STB-EVs.

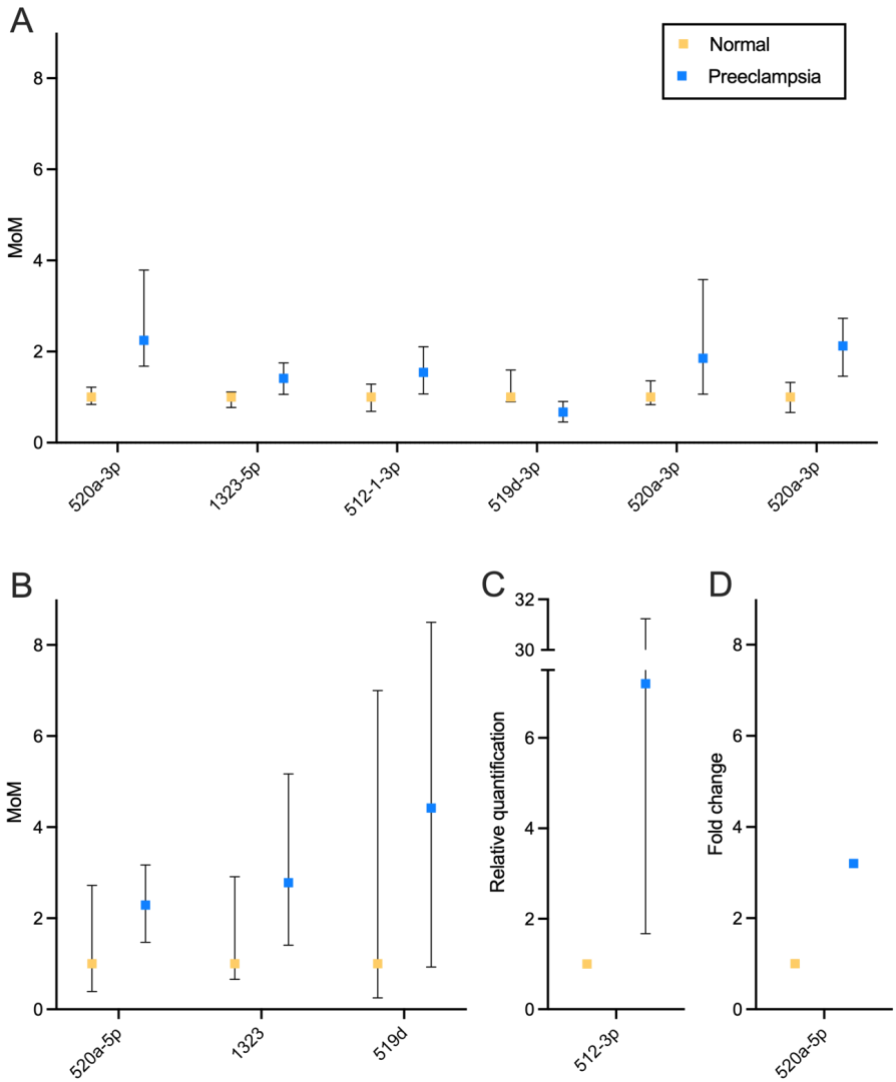


Figure 4-1 – Relative expression of six RNA fragments mapping to four target miRNAs in preeclampsia and normal pregnancies from different samples and studies.

A: Perfusion data from analysis described in Appendix 1, displayed as multiples of median (MoM) by group with error bars showing maximum and minimum values.

B: Plasma data at the time of preeclampsia diagnosis, derived from Miura et al.[154]*, displayed as MoM by group with error bars showing maximum and minimum values.*

C: Serum data at 20 weeks of gestation, derived from Martinez-Fierro et al.[155]*, displayed as relative quantification with error bars showing maximum and minimum values.*

D: Serum data at 12-14 weeks of gestation, derived from Ura et al.[158]*, displayed as fold change; no information regarding spread of data were available.*

4.3.2. tRNA validation in plasma: target optimisation

4.3.2.1. First attempt: target selection using relative abundance in perfusion STB-EVs

Three STB-EV 5'-tRF targets were selected for plasma biomarker evaluation in preeclampsia. Target selection followed the same rationale described in Chapter 3. Namely, the most abundant differentially expressed fragments were chosen to ensure that targets were above the limit of detection in plasma. Targets were assigned identifiers (F, I and J) for ease of reference in this thesis (Table 3-2).

Target F was selected from the DEUS analysis, as the most abundant differentially expressed sRNA fragment in preeclampsia compared to normal MLEVs (Table 2-10). Target F was preeclampsia-upregulated. Target J was the next most abundant differentially expressed 5'-tRF iso-acceptor or iso-decoder in preeclampsia in the DEUS analysis (Table 2-10). Target J was preeclampsia-downregulated. Target I was selected from our collaborators' analysis (Appendix 1), where it was the most abundant differentially expressed sRNA fragment in preeclampsia compared to normal MLEVs (Table 2-15). Target I was preeclampsia-downregulated.

All three targets have previously been assayed in maternal plasma using qPCR in Chapter 3. A pregnancy-specific, placentally-derived load of all three was discovered amongst maternal plasma EVs isolated using MAC (Figure 3-8 and Figure 3-9). Relative abundance of the three targets in the various perfusion STB-EV analyses undertaken in Chapter 2 is summarised in Table 3-2.

Investigation of target F, I and J expression in preeclampsia and normal plasma EVs was undertaken chronologically before optimisation described in 3.3.3; total EVs were thus isolated from platelet-free plasma.

	Normal (n=6)	Preeclampsia (n=5)
Median maternal age (IQR) – years	30 (26-34)	27 (27-34)
Median pre-pregnancy BMI (IQR)	26 (21-28)	29 (22-30)
First pregnancy – no. (%)	3 (50)	3 (60)
Diabetes – no. (%)	0 (0)	0 (0)
Essential hypertension – no. (%)	0 (0)	1 (20)
Current smoker – no. (%)	1 (17)	1 (20)
Male fetus – no. (%)	4 (67)	3 (75)
Gestational age at sample (IQR) – weeks	33.1 (31.9-34.1)	33.1 (29.1-33.6)
Median birthweight (IQR) – g	2950 (2440-4165)	1658 (1330-2248)
Median gestational age at delivery (IQR) – weeks	38.7 (36.6-39.7)	33.4 (32.1-35)
Median highest recorded SBP (IQR) – mmHg	129 (125-140)	174 (160-178)
Median highest recorded DBP (IQR) – mmHg	78 (73-83)	106 (100-114)

Table 4-3 – Demographic data for women donating blood; first attempt. Continuous variables are described using median and interquartile range (IQR). Categorical variables are described using number (no.) and percentage (%). Other abbreviations used: body mass index (BMI), systolic blood pressure (SBP) and diastolic blood pressure (DBP).

Samples from five women with early-onset preeclampsia and six women with normal pregnancies were compared. Demographics are shown in Table 4-3; important differences between groups (highlighted in grey) were considered consequences of preeclampsia, rather than confounders.

When quantified in plasma EVs isolated by MAC, there were no apparent differences in expression of F, I or J between preeclampsia and normal samples (Figure 4-2B). This contrasts with the expression of these three targets in perfusion MLEVs, where they were all shown to be differentially expressed (Figure 4-2A).

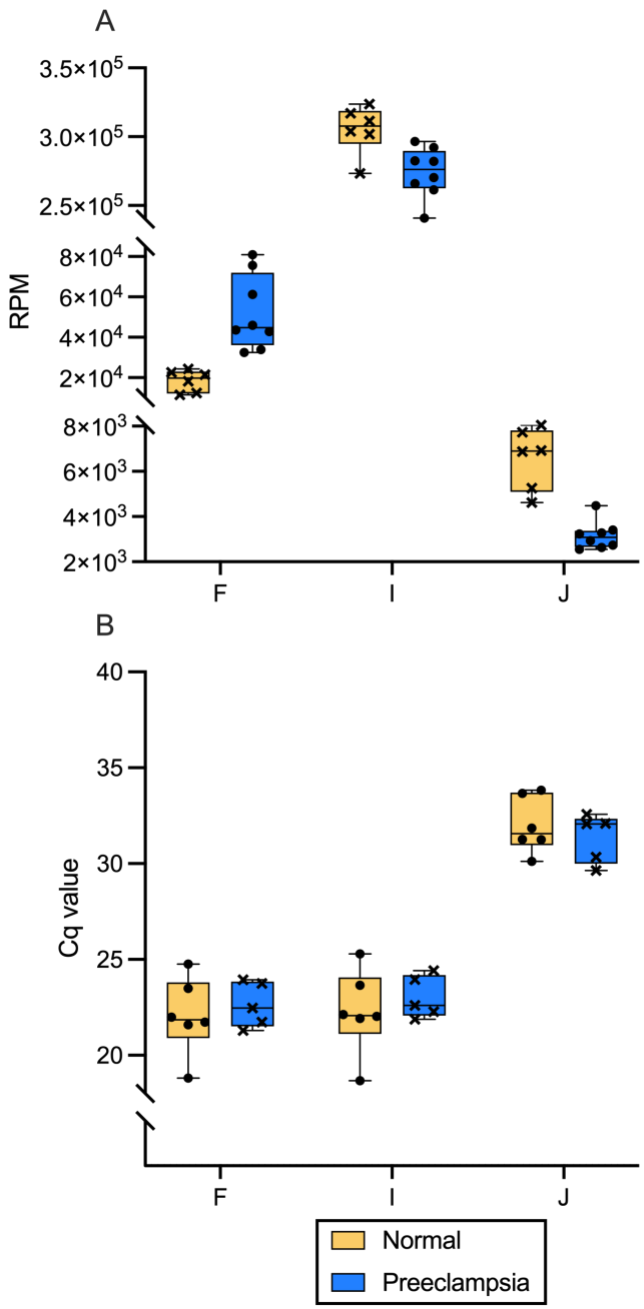


Figure 4-2 – Expression of targets F, I and J in EVs from women with early-onset preeclampsia and normal pregnancies (First attempt).

A. Data from perfusion STB-EVs, compared to term controls, derived using RNA sequencing, displayed in reads per million (RPM)

B. Data from plasma EVs isolated from 500 µL PFP, compared to gestation-matched controls, derived using qPCR and presented as raw Cq values as no spike-in RNA was used preventing normalisation. Note a lower Cq value represents a greater target abundance in that condition.

4.3.2.2. Second attempt: target selection using blood cell data

Two hypotheses to explain the disparity between plasma and perfusion sequencing data were initially considered. Firstly, plasma sample size was small (n=11), with potential confounding from a case of preeclampsia superimposed on essential hypertension. To overcome this concern, a control sRNA, known to be differentially expressed in preeclampsia STB-EVs could be added. Secondly, targets F, I and J were abundant in non-pregnant plasma EVs (3.3.3.1) demonstrating that these targets are not unique to the placenta. Non-placental EV tRFs may therefore be confounding the placental preeclampsia/normal differences in plasma. The most abundant source of non-placental EVs are blood-related cells (Figure 3-2). To guide a new selection of plasma biomarker targets, expression of the 983 perfusion-derived preeclampsia-dysregulated targets was determined in blood cells from publicly available datasets (work by collaborators, Appendix 3).

The following selection process was used:

1. 130 of 983 (13%) preeclampsia-dysregulated fragments had a median expression in either preeclampsia or normal STB-EVs ≥850 RPM. This threshold was determined by extrapolating the correlation between abundance in perfusion STB-EVs and plasma qPCR data from the first attempt, seeking targets above the limit of detection in plasma (i.e. with Cq <35).
2. 36 of 130 (28%) fragments showed very low abundance in blood cells (RPM ≤0.5).
3. 28 of 36 (78%) fragments remained after exclusion of mapped miRNA or rRNA targets.

The 28 fragments are shown in Table 4-4. There was significant overlap between sequences. Similar fragments were matched to avoid picking targets differing by one or two nucleotides, as investigation of assay specificity in 2.3.3.1 demonstrated a small amount of cross-reactivity when targets differed by only a single terminal nucleotide

(Figure 2-19). Five structurally different tRFs were selected and given identifiers P, M, J, L and Q (Table 4-5; J represents the same target as used previously in Table 3-2 and 4.3.2.1). miR519d-3p was selected as a control sRNA from within the 36 targets identified in step 2 above and given the identifier N. N represented the most differentially expressed preeclampsia-dysregulated miRNA in plasma data, which was also identified in the perfusion sequencing analysis (Figure 4-1).

Sequence	Length	Thesis ID	Mapped location	Relation
GCATCGTGGTTCAGTGGTAGAATTCTCGCCT	31	-	Unmatch	2nt from I
GCATGGTGGTTCAGTGGTAGAATTCTCGCCT	31	-	Unmatch	1nt from I
GCATGTGGTTCAGTGGTAGAATTCTCGCCC	30	-	Unmatch	3nt from I
GCATTGGTGGTTCAGTGGTAGAATTCCCGCCT	32	-	tRF-Gly-GCC-2-1	1nt from I
GCATTGGTGGTTCAGTGGTAGAATTCTCGACT	32	-	tRF-Gly-GCC-2-1	1nt from I
GCATTGGTGGTTCAGTGGTAGAATTCTCGCTT	32	-	tRF-Gly-GCC-2-1	1nt from I
GCATTGTGGTTCAGTGGTAGAATTCTCGCTT	31	-	Unmatch	2nt from I
GCCCGGATAGCTCAGTCGGTAGAGCAT	27	P	piR-27622	-
GCCCGGCTAGCTCAGTCGGTAGAGCATGAGACC	33	M	tRF-Lys-CTT-3-1	-
GCCCGGCTAGCTCAGTCGGTAGAGCATGAGAT	32	-	piR-27622	2nt from M
GCGCCGCTGGTGTAGTGGTATCATGCAAGATT	32	-	tRF-Gly-CCC-2-1	-
GCGTTGTGGTTCAGTGGTAGAATTCTCGCCT	31	-	Unmatch	-
GCTTCTGTAGTGTAGTGGTTATCACGTTCGCCTC	34	-	tRF-Val-CAC-2-1	-
GGGGATGTAGCTCAGTGGTAGAGCCGCGCT	30	-	Unmatch	-
GGGGGTATAGCTCAGGGGTAGAGCATTTGAC	31	-	tRF-Cys-GCA-8-1	1nt from J
GGGGGTATAGCTCAGGGGTAGAGCATTTGACC	32	-	tRF-Cys-GCA-13-1	2nt from J
GGGGGTATAGCTCAGTGGTAGAGCATTTGAC	31	J	tRF-Cys-GCA-4-1	-
GGGGGTGTAGCTCAGTGGTAGAGCATTTGACC	32	-	tRF-Cys-GCA-6-1	2nt from J
GGGGGTGTAGCTCAGTGGTAGAGCATTTGACT	32	-	tRF-Cys-GCA-6-1	2nt from J
GGGGGTGTAGCTCAGTGGTAGAGCGCGTGCTTG	33	L	tRF-Ala-CGC-4-1	-
GGTAGCGTGGCCGAGCGGTCTAAGGCTGGATT	32	-	Unmatch	-
GGTGGTTCAGTGGTAGAATTCTCGCC	26	-	piR-25783	-
GTTTCCGTAGTGTAGTGGTCATCACGTTCGC	31	-	piR-28877	1nt from Q
GTTTCCGTAGTGTAGTGGTTATCACGTTCACC	32	-	piR-28877	2nt from Q
GTTTCCGTAGTGTAGTGGTTATCACGTTCGA	31	-	piR-28877	1nt from Q
GTTTCCGTAGTGTAGTGGTTATCACGTTCGT	31	Q	piR-28877	-
TCCATGTGGTCTAGTGGTTAGGATTCGGCGCT	32	-	Unmatch	-
TCCCTGGTGGTCTAGTGGCTAGGATTCGGCGC	32		piR-5938	2nt from F

Table 4-4 – 28 fragments identified by second target selection attempt including nucleotide sequence, length in nucleotides (nt), assigned identifier in this thesis, mapped location and relation to previously investigated targets F, I and J or targets subsequently selected in this attempt (P, M, J, L, Q).

Thesis ID	Sequence	Length	GtRNAdb mapping	Median PE count	Median N count	Log2fold change	p-adj	Max monocyte	Max erythrocyte	Max platelet
P	GCCCGGATAGCTCAGTC GGTAGAGCAT	27	piR-27622	401	1166	1.55	0.009	0	0	0
M	GCCCGGCTAGCTCAGTC GGTAGAGCATGAGACC	33	tRF-Lys-CTT-3-1	921	1235	0.47	0.034	0.1	0	0
J	GGGGGTATAGCTCAGT GGTAGAGCATTTGAC	31	tRF-Cys-GCA-4-1	3085	6901	1.06	0.005	0.1	0	0
L	GGGGGTGTAGCTCAGT GGTAGAGCGCGTGCTTG	33	tRF-Ala-CGC-4-1	850	402	-0.90	0.023	0.2	0	0
Q	GTTTCCGTAGTGTAGTG GTTATCACGTTCGT	31	piR-28877	3483	6996	0.98	0.022	0.3	0	0
N	CAAAGTGCCTCCCCTTTAG AGT	21	miR-519d-3p	1118	1667	0.72	0.025	0	0	0

Table 4-5 – Expression of targets selected for second attempt biomarker evaluation in normal and preeclampsia perfusion STB-EVs as well as blood cell datasets.

The six targets were quantified in five pairs of uterine and peripheral venous blood samples from term normal pregnancies, to confirm that the selection process had correctly identified molecules with a placenta-derived load in the maternal circulation. These experiments were undertaken before optimisation described in 3.3.3; total EVs were thus isolated from platelet-free plasma.

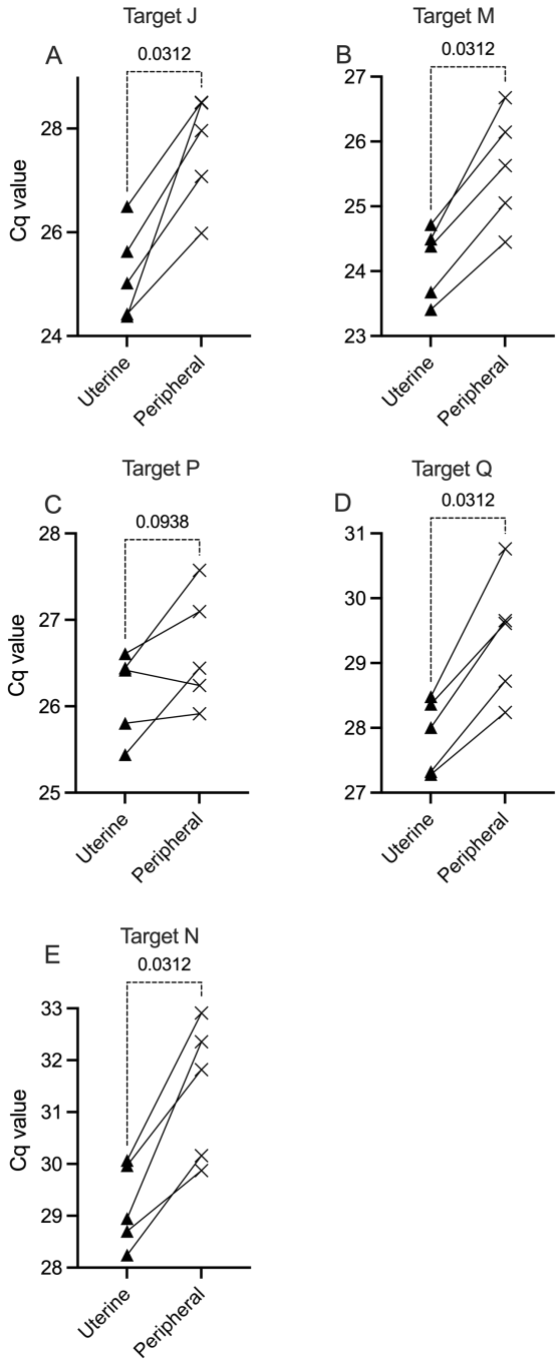


Figure 4-3 – Expression of targets J, M, P, Q and N in paired uterine and peripheral venous plasma from healthy term pregnancies (Second attempt).

Data derived from 900 µL PFP and presented as raw Cq values as no spike-in RNA was used preventing normalisation. Hypothesis tests represent one-sided Wilcoxon tests given paired data with a small sample size where a unidirectional change was anticipated. Note a lower Cq value represents a greater target abundance in that condition.

Targets J, M, Q and control miRNA N were all more abundant in uterine than peripheral venous plasma EVs ($p<0.05$ for all), confirming a circulating placentally-derived load. Target P did not reach significance, and target L was below the limit of detection (Cq >35) in 6 out of 10 plasma samples; these were not pursued further.

The four remaining targets were quantified in peripheral venous plasma from eight women with early-onset preeclampsia and nine matched controls. Demographics are shown in Table 4-6; no confounders were identified.

When quantified in plasma EVs isolated by MAC, control miRNA N was more abundant in preeclampsia than normal plasma EVs ($p=0.01$), consistent with published data (Figure 4-1B). This suggests there was no sampling error and sample size was sufficient. There were no apparent differences in expression of J, Q or M between preeclampsia and normal samples (Figure 4-4B). This contrasts with the expression of these three targets in perfusion MLEVs, where they were all shown to be differentially expressed (Figure 4-4A).

	Normal (n=9)	Preeclampsia (n=8)
Median maternal age (IQR) – years	32 (32-34)	31 (29-34)
Median pre-pregnancy BMI (IQR)	22 (21-25)	23 (22-27)
First pregnancy – no. (%)	5 (56)	5 (63)
Diabetes – no. (%)	0 (0)	0 (0)
Essential hypertension – no. (%)	0 (0)	0 (0)
Current smoker – no. (%)	1 (11)	1 (13)
Male fetus – no. (%)	4 (44)	2 (29)
Gestational age at sample (IQR) – weeks	32.4 (31.3-34.3)	33.2 (31.8-33.6)
Median birthweight (IQR) – g	3160 (2560-3470)	1725 (1495-2558)
Median gestational age at delivery (IQR) – weeks	39.3 (37.9-40.6)	33.7 (32.9-35.7)
Median highest recorded SBP (IQR) – mmHg	127 (124-129)	172 (168-180)
Median highest recorded DBP (IQR) – mmHg	84 (70-87)	109 (105-113)

Table 4-6 – Demographic data for women donating blood; second attempt.

Continuous variables are described using median and interquartile range (IQR).

Categorical variables are described using number (no.) and percentage (%).

Other abbreviations used: body mass index (BMI), systolic blood pressure (SBP) and diastolic blood pressure (DBP).

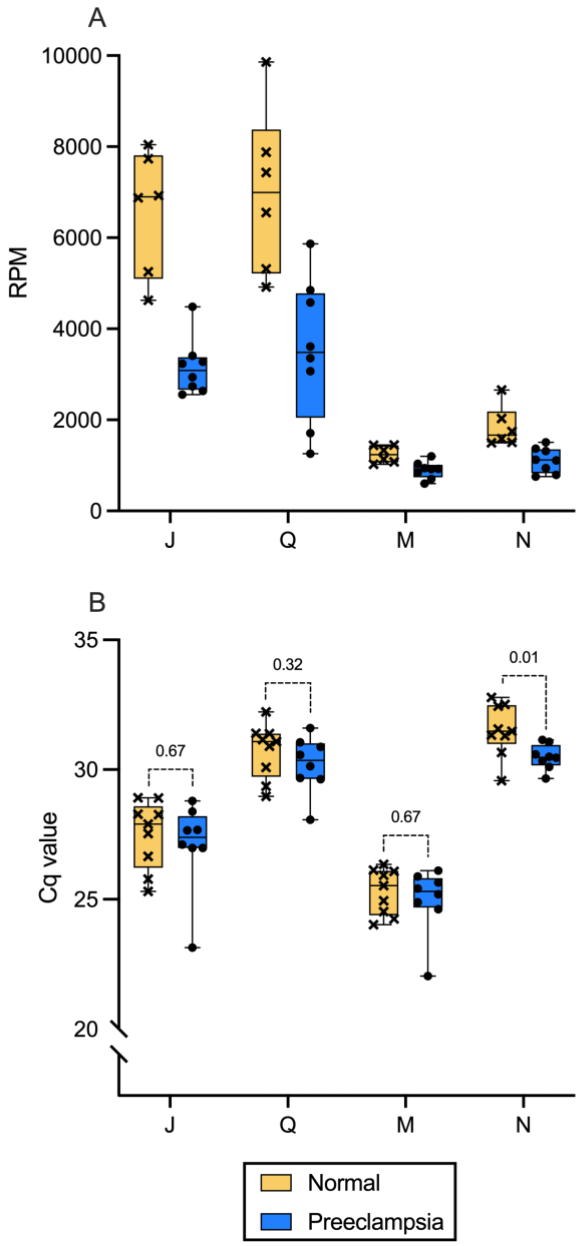


Figure 4-4 – Expression of targets J, Q, M and control miRNA N in EVs from women with early-onset preeclampsia and normal pregnancies (Second attempt).

A. Data from perfusion STB-EVs, compared to term controls, derived using RNA sequencing, displayed in reads per million (RPM)

B. Data from plasma EVs isolated from 900 µL PFP, compared to gestation-matched controls, derived using qPCR and presented as raw Cq values as no spike-in RNA was used preventing normalisation. Hypothesis tests are unpaired, two-sided Mann Whitney test given some evidence of skew. Note a lower Cq value represents a greater target abundance in that condition.

4.3.2.3. Third attempt: target selection using preeclampsia-upregulated targets

Perfusion experiments cannot detect if different quantities of STB-EVs are released into the maternal circulation in a condition, only differences between the vesicle phenotypes released in that condition. It is well established from plasma data that STB-EV release is upregulated in early-onset preeclampsia[40,120]. My perfusion RNAseq analyses suggested all three targets assayed in Figure 4-4 were less abundant in preeclampsia than normal STB-EVs. Perfusion data can be considered as RNA abundance "per vesicle" in each condition: RNA isolated from EVs in perfusate was sequenced and counts normalised using the models within DESeq2. DESeq2 takes raw read data and normalises each sample to account for read depth and RNA composition[159,160]. Thus, downregulation of a target per vesicle in preeclampsia (identified from perfusion data) might be reversed in plasma as a consequence of increased vesicle release, as seen with miR-519d (Figure 4-1). This hypothesis could explain why abundance of targets J, M, and Q in total plasma EVs was not different between normal and preeclampsia samples (Figure 4-4B).

To circumvent this potential shortcoming, new targets were sought with increased expression in preeclampsia STB-EVs as well as the prior criteria of high abundance in perfusion STB-EVs and low abundance in blood cells. Initially, the 28 fragments identified in the second attempt (Table 4-4) were filtered for preeclampsia-upregulated targets: this left four fragments. One was L, below the limit of detection in plasma in experiments in 4.3.2.2. Two differed from F by two nucleotides, so were considered unsuitable for assessment by qPCR as target F may cross-react with their assays, as demonstrated in 2.3.3.1. This left only one new target, which was assigned identifier D.

In order to find further new targets for biomarker evaluation, the abundance in blood cell threshold was lifted from RPM ≤0.5. Instead, expression in blood cells was considered relative to expression in STB-EVs, seeking targets where the highest median expression in either preeclampsia or normal STB-EVs was at least 200-fold greater than the highest

median expression in blood cells (using data from Appendix 3). Thus, the following selection process was used:

1. 130 of 983 (13%) fragments had a median expression in either preeclampsia or normal pregnancy STB-EVs ≥850 RPM
2. 60 of 130 (46%) fragments were more abundant in preeclampsia than normal pregnancy STB-EVs
3. 34 of 60 (57%) fragments were ≥200-fold more abundant in STB-EVs than in blood cells
4. 27 of 36 (75%) fragments remained after exclusion of mapped miRNA or rRNA targets.

The 27 fragments are shown in Table 4-7. F and L had already been investigated; 21 showed homology with F, two showed homology with I. Four targets were selected for further investigation, alongside miR-519d (N) as a control (Table 4-8). F was investigated again as so many fragments were closely aligned to it and the initial investigation in 4.3.2.1 was compromised by small sample size with no control RNA. W and S were selected as relations of the previously investigated F and I, which should be distinguishable by qPCR assay. D was chosen as an unrelated tRF target, also identified in the second attempt search for further targets.

One methodological change to the plasma EV isolation process was also made. As described in 3.3.3, flow cytometry data from a colleague suggested that the second centrifugation step to produce platelet-free plasma may also deplete STB-MLEVs[142]. Consequently platelet-poor plasma was used instead.

Sequence	Length	Thesis ID	Mapped location	Relation
TCCTGTGGTCTAGTGGTTAGGATTCGGCGCT	31	-	Unmatch	2nt from F
TCCCTGTGGTCTAGTGGTTAGGATTCGGCGT	31	-	Unmatch	2nt from F
TCCCTGTGGTCTAGTGGTTAGGATTCGGCGCTC	33	-	Unmatch	2nt from F
TCCCTGTGGTCTAGTGGTTAGGATTCGGCGCT	32	-	Unmatch	1nt from F
TCCCTGTGGTCTAGTGGTTAGGATTCGGCGCC	32	-	Unmatch	2nt from F
TCCCTGTGGTCTAGTGGTTAGGATTCGGCGCA	32	-	Unmatch	2nt from F
TCCCTGTGGTCTAGTGGTTAGGATTCGGCGC	31	-	Unmatch	2nt from F
TCCCTGTGGTCTAGTGGCTAGGATTCGGCGCT	32	-	Unmatch	2nt from F
TCCCTGGTGGTCTAGTGTTAGGATTCGGCGCT	32	-	Unmatch	1nt from F
TCCCTGGTGGTCTAGTGGTTAGGATTCGGCGT	32	-	piR -5938	1nt from F
TCCCTGGTGGTCTAGTGGTTAGGATTCGGCGCT	33	F	tRF-Glu-CTC-1-1	-
TCCCTGGTGGTCTAGTGGTTAGGATTCGGCGCC	33	-	tRF-Glu-CTC-1-1	1nt from F
TCCCTGGTGGTCTAGTGGTTAGGATTCGGCGC	32	-	piR -5938	1nt from F
TCCCTGGTGGTCTAGTGGTTAGGATTCGGCGA	32	-	piR -5938	2nt from F
TCCCTGGTGGTCTAGTGGCTAGGATTCGGCGCT	33	-	tRF-Glu-TTC-4-1	1nt from F
TCCCTGGTGGTCTAGTGGCTAGGATTCGGCGC	32	-	piR-5938	2nt from F
TCCCTGGTCTAGTGGTTAGGATTCGGCGCT	30	-	Unmatch	3nt from F
TCCCTGGTCTAGTGGTTAGGATTCGGCGCC	30	-	Unmatch	4nt from F
TCCCCTGTGGTCTAGTGGTTAGGATTCGGCGCT	33	-	tRF-Glu-CTC-1-1	2nt from F
TCCCCTGTGGTCTAGTGGTTAGGATTCGGCGCC	33	-	Unmatch	3nt from F
TCCATGTGGTCTAGTGGTTAGGATTCGGCGCT	32	-	Unmatch	2nt from F
GGGGGTGTAGCTCAGTGGTAGAGCGCGTGCTTG	33	L	tRF-Ala-CGC-4-1	-
GCTTCTGTAGTGTAGTGGTTATCACGTTCGCCTC	34	D	tRF-Val-CAC-2-1	-
GCCGTGATCGTATAGTGGTTAGTACTCTGCGTTG	34	-	tRF-His-GTG-1-1	-
GCATTTGTGGTTCAGTGGTAGAATTCTCGCCTG	33	S	tRF-Gly-GCC-2-1	2nt from I
GCATTGGTGGTTCAGTGGTAGAATTCTCGCCTT	33	-	tRF-Gly-GCC-2-1	1nt from I
CCCCTGTGGTCTAGTGGTTAGGATTCGGCGCC	32	W	Unmatch	3nt from F

Table 4-7 – 27 fragments identified by third target selection attempt including nucleotide sequence, length in nucleotides (nt), assigned identifier in this thesis, mapped location and relation to previously investigated targets F and I.

Thesis ID	Sequence	Length	GtRNAdb mapping	Median PE count	Median N count	Log2fold change	p-adj	Max monocyte	Max erythrocyte	Max platelet
F	TCCCTGGTGGTCTAGTGGTTAGGATTCGGCGCT	33	tRF-Glu-CTC-1-1	44786	19826	-1.50	0.005	205	43	10
S	GCATTTGTGGTTCAGTGGTAGAATTCTCGCCTG	33	tRF-Gly-GCC-2-1	1233	608	-1.12	0.023	6	0.8	2
W	CCCCTGTGGTCTAGTGGTTAGGATTCGGCGCC	32	Unmatch	981	526	-0.87	0.006	0.9	0	0
D	GCTTCTGTAGTGTAGTGGTTATCACGTTCGCCTC	34	tRF-Val-CAC-2-1	1489	1011	-0.60	0.02	0.2	0.1	0.1
N	CAAAGTGCCTCCCTTTAGAGT	21	miR-519d-3p	1118	1667	0.72	0.025	0	0	0

Table 4-8 – Expression of targets selected for third attempt biomarker evaluation in normal pregnancy and preeclampsia perfusion STB-EVs as well as blood cell datasets.

The five selected targets were quantified in peripheral venous plasma from nine women with early-onset preeclampsia and eight matched controls. Demographics are shown in Table 4-9; no confounders were identified.

Targets F, S, W and D were all more abundant per vesicle in preeclampsia, from perfusion data (Figure 4-5A). In contrast, all targets were downregulated in preeclampsia EVs (Figure 4-5B). It was not considered ethically or financially judicious to increase the sample size: there was no evidence of differences reflecting the perfusion data in target tRF molecules, despite the optimisations made during target selection.

	Normal (n=8)	Preeclampsia (n=9)
Median maternal age (IQR) – years	32 (31-33)	33 (30-35)
Median pre-pregnancy BMI (IQR)	28 (22-36)	23 (23-28)
First pregnancy – no. (%)	3 (38)	3 (33)
Diabetes – no. (%)	0 (0)	0 (0)
Essential hypertension – no. (%)	0 (0)	0 (0)
Current smoker – no. (%)	1 (13)	0 (0)
Male fetus – no. (%)	2 (25)	2 (22)
Gestational age at sample (IQR) – weeks	28.4 (26.5-30.8)	31.8 (28.7-33.3)
Median birthweight (IQR) – g	2930 (2819-3739)	1725 (1410-1885)
Median gestational age at delivery (IQR) – weeks	39 (37.9-39.4)	32.4 (29.7-33.7)
Median highest recorded SBP (IQR) – mmHg	117 (112-120)	178 (166-182)
Median highest recorded DBP (IQR) – mmHg	74 (70-84)	102 (100-112)

Table 4-9 – Demographic data for women donating blood; third attempt.

Continuous variables are described using median and interquartile range (IQR).

Categorical variables are described using number (no.) and percentage (%).

Other abbreviations used: body mass index (BMI), systolic blood pressure (SBP) and diastolic blood pressure (DBP).

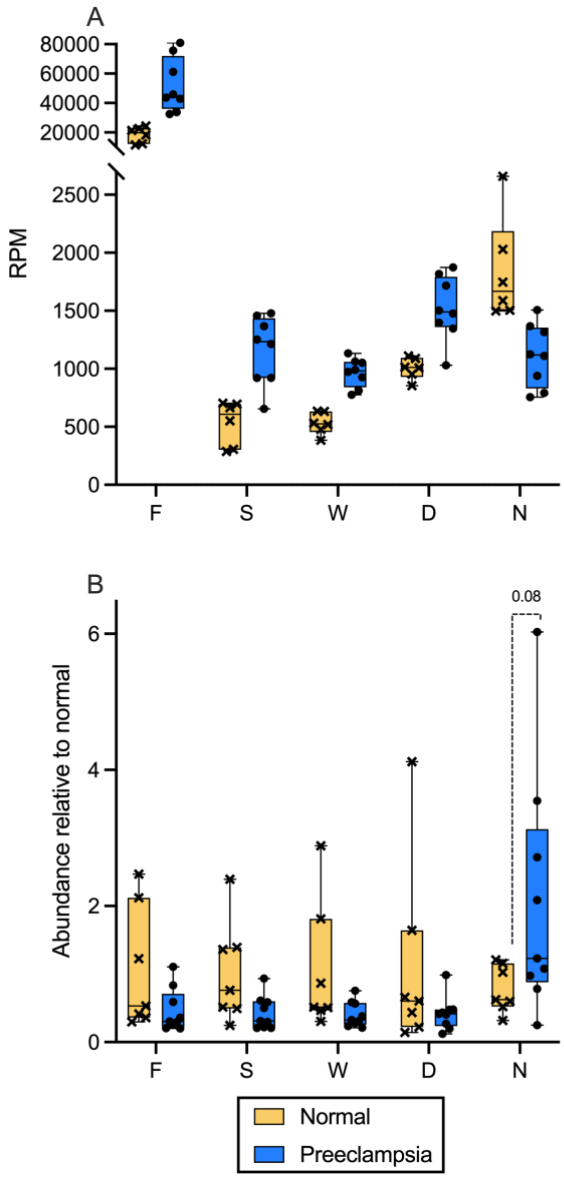


Figure 4-5 – Expression of targets F, S, W, D and control miRNA N in EVs from women with early-onset preeclampsia and normal pregnancies (Third attempt).

A. Data from perfusion STB-EVs, compared to term controls, derived using RNA sequencing, displayed in reads per million (RPM)

B. Data from plasma EVs isolated from 500 µL PPP, compared to gestation-matched controls, derived using qPCR and presented as abundance relative to normal pregnancies. One outlier was identified from control miRNA data, confirmed by Grubbs' test, and removed. Data normalised to spike-in RNA. Hypothesis test is unpaired, one-sided Mann Whitney test given some evidence of skew but a difference only anticipated in one direction from prior work.

4.3.3. tRNA validation in plasma: plasma preparation optimisation

4.3.3.1. Fourth attempt: whole plasma

One hypothesis for the failure to corroborate preeclampsia-dysregulated targets from perfusion in plasma is that MAC columns (for plasma EV isolation) are a source of error. There are 14 pipetting steps from plasma aliquoting to RNA elution, each of which can introduce noise. Columns are proprietary and there are minimal independent data evaluating their linearity in EV isolation[141]. Whilst this has allowed pregnant/non-pregnant and uterine/peripheral venous differences to be elucidated (Chapter 3), it may be that the smaller magnitude differences between preeclampsia and normal perfusion STB-EVs are overcome by noise with MAC isolation. As a consequence, target expression was investigated in 200 µL whole platelet-poor plasma from 10 women with normal pregnancies and 12 women with early-onset preeclampsia. Demographics are shown in Table 4-10; no confounding factors were identified.

It was decided to use a smaller panel of the targets selected in 4.3.2.3: F, S and W. J was added back as a preeclampsia-downregulated but highly placentally-enriched target in case a ratio of two tRFs offered better prediction than a single tRF.

Target J was below the limit of detection in eight out of 20 samples, reducing the sample size to 12 (seven normal and five preeclampsia) for J. Targets F, S and W were all less abundant in preeclampsia samples than normal (non-significant); target J was more abundant in preeclampsia samples (non-significant). The direction of difference is reversed from those seen in perfusion data (Figure 4-4A, Figure 4-5A).

	Normal (n=11)	Preeclampsia (n=8)
Median maternal age (IQR) – years	32 (30-34)	32 (29.5-35.3)
Median pre-pregnancy BMI (IQR)	27 (22.3-31.5)	24.8 (22.8-29)
First pregnancy – no. (%)	5 (45)	3 (38)
Diabetes – no. (%)	0 (0)	0 (0)
Essential hypertension – no. (%)	0 (0)	0 (0)
Current smoker – no. (%)	1 (9)	0 (0)
Male fetus – no. (%)	2 (22)	2 (25)
Gestational age at sample (IQR) – weeks	29.4 (26.4-32.2)	31.6 (28.7-33.2)
Median birthweight (IQR) – g	2910 (2773-2941)	1708 (1370-1879)
Median gestational age at delivery (IQR) – weeks	38 (26.9-39.2)	32.1 (29.5-33.6)
Median highest recorded SBP (IQR) – mmHg	117 (113-120)	181 (172-190)
Median highest recorded DBP (IQR) – mmHg	70.5 (70-74)	110 (101-112)

Table 4-10 – Demographic data for women donating blood; fourth attempt

Continuous variables are described using median and interquartile range (IQR).

Categorical variables are described using number (no.) and percentage (%).

Data excluding preeclampsia outlier identified in Figure 4-6A.

Other abbreviations used: body mass index (BMI), systolic blood pressure (SBP) and diastolic blood pressure (DBP).

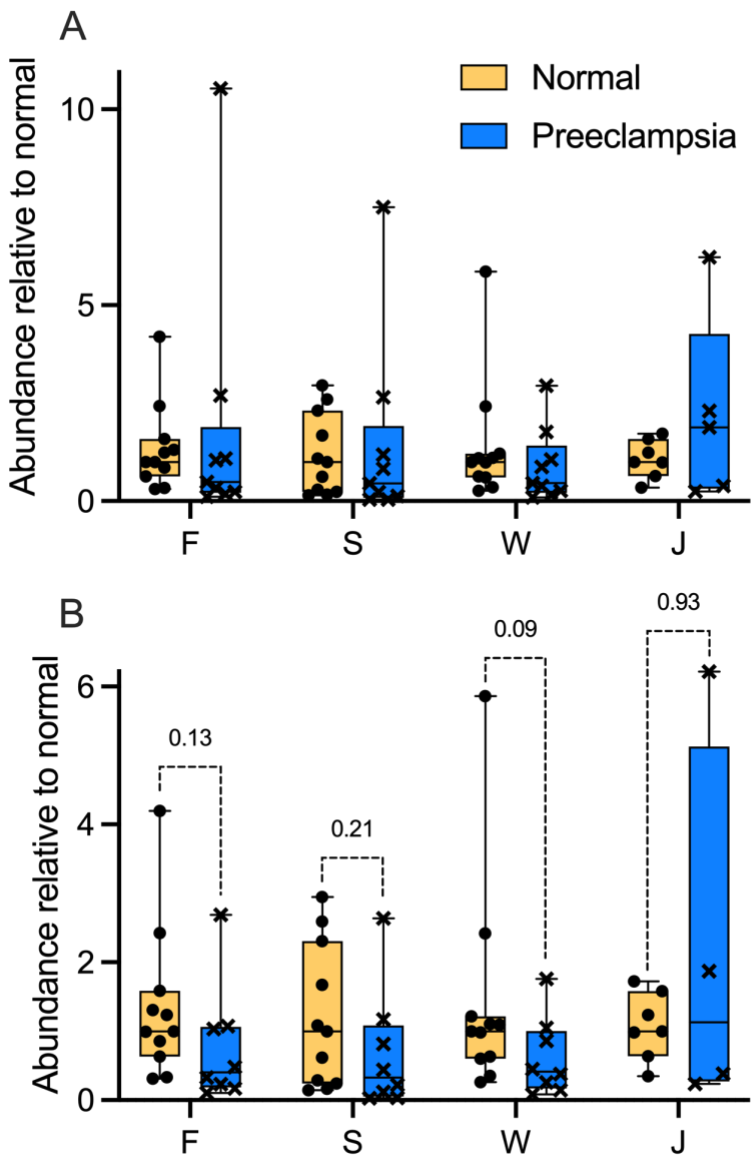


Figure 4-6 – Expression of targets F, S, W and J in whole plasma from women with early-onset preeclampsia and gestation-matched controls (Fourth attempt).

Data derived from 200 µL PPP, normalised to cel-miR-39 spike-in and displayed relative to median abundance in normal group.

A: Raw data

B: After removal of one preeclampsia outlier result (confirmed by Grubbs' test for targets F and S, removed from all targets). Hypothesis test was unpaired, two-sided Mann Whitney test given skewed data.

No target delineated disease from normal in isolation. Given the direction of change in disease was different for J compared with the other fragments, ratios of each target's Cq value against J were compared to see if this enabled delineation of groups (Figure 4-7). The sample size was 12, in line with the lower detection rate of J. All three targets in ratio with J demonstrated differential expression between disease and normal ($p<0.05$).

To better assess the diagnostic power of a tRF assay using whole plasma (potentially as part of a logistic regression model), a validation cohort of further samples was analysed. A further 26 samples were assayed (12 preeclampsia, 14 normal). Target J expression was below the limit of detection in all 26 samples. The discriminatory power of tRFs between preeclampsia and normal was entirely dependent on Target J (Figure 4-7). Whole plasma tRFs as biomarkers for preeclampsia were consequently not pursued further.

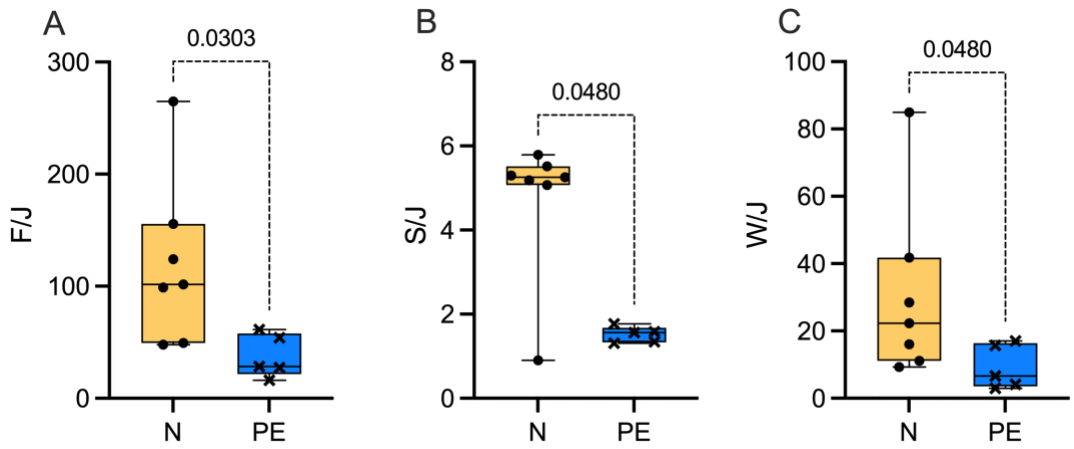


Figure 4-7 – Expression of targets F, S and W relative to J in whole plasma from women with early-onset preeclampsia and gestation-matched controls (Fourth attempt). Data derived from 200 µL PPP. Hypothesis test was unpaired, two-sided Mann Whitney test given skewed data.

4.3.3.2. Fifth attempt: STB-EV pre-enrichment

Data from Chapter 3 demonstrate 5'-tRFs are present: a) in plasma EVs which are not syncytiotrophoblast-derived (3.3.3.1), b) in plasma, but outside EVs (3.3.4.1). Differences between preeclampsia and normal pregnancy 5'-tRFs were discovered in perfusion-derived STB-EVs (Chapter 2). A technique was therefore optimised to enrich STB-EVs from total plasma EVs, achieving around 50% enrichment compared to <1% abundance in unprocessed plasma (3.3.5.5 and Figure 3-3). This technique was applied to 500 µL PPP from 10 women with normal pregnancies and 12 women with early-onset preeclampsia. The same targets from 4.3.3.1 were used, with the exception of J. Demographics are shown in Table 4-11; no confounding factors were identified.

Target F was more abundant in preeclampsia STB-EV-enriched plasma than normal pregnancy (median 0.54 fold higher in preeclampsia). This difference was not significant ($p=0.31$), but the direction of change matched perfusion data (Figure 4-5A). There were no discernible differences in expression of Targets S and W between preeclampsia and normal STB-EV-enriched plasma.

	Normal (n=10)	**Preeclampsia (n=12)**
Median maternal age (IQR) – years	30 (28.3-33)	31 (25-35)
Median pre-pregnancy BMI (IQR)	23.5 (21.5-27)	24 (22-28.3)
First pregnancy – no. (%)	7 (70)	11 (92)
Diabetes – no. (%)	0 (0)	0 (0)
Essential hypertension – no. (%)	0 (0)	0 (0)
Current smoker – no. (%)	1 (10)	0 (0)
Male fetus – no. (%)	8 (80)	7 (58)
Median gestational age at sample (IQR) – weeks	33.3 (31.8-34)	31.3 (29.3-32.3)
Median birthweight (IQR) – g	3356 (3165-3669)	1553 (1288-1725)
Median gestational age at delivery (IQR) – weeks	39.9 (39.3-41.1)	31.5 (30.4-33.6)
Median highest recorded SBP (IQR) – mmHg	120 (119-129)	180 (178-180)
Median highest recorded DBP (IQR) – mmHg	72 (68.5-74.5)	110 (105-110)

Table 4-11 – Demographic data for women donating blood; fifth attempt.

Continuous variables are described using median and interquartile range (IQR).

Categorical variables are described using number (no.) and percentage (%).

Other abbreviations used: body mass index (BMI), systolic blood pressure (SBP) and diastolic blood pressure (DBP).

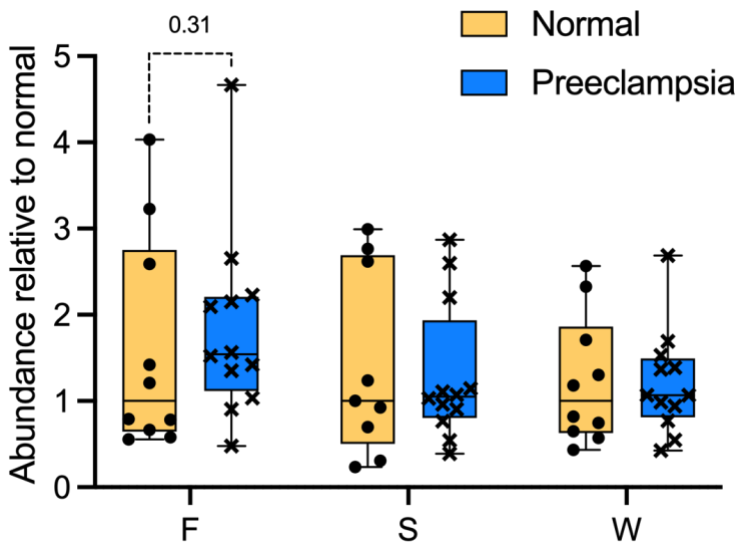


Figure 4-8 – Expression of targets F, S and W in STB-EV enriched from peripheral plasma from women with early-onset preeclampsia and gestation-matched controls (Fifth attempt)

Data derived from 500 µL PPP, normalised to cel-miR-39 spike-in and displayed relative to median abundance in normal group. Hypothesis test was unpaired, two-sided Mann Whitney test given skewed data.

4.4. Discussion

This chapter aimed to determine whether expression of tRFs in blood represents a biomarker for preeclampsia. Differences identified in perfusion STB-EVs were assayed in gestation-matched plasma samples across five experiments. tRF target selection was iteratively optimised to overcome potential confounding factors such as differential STB-EV release and non-placental vesicular tRFs. Preeclampsia tRF expression was assessed across three plasma compartments: whole plasma, plasma EVs and plasma STB-EVs. This approach sought to overcome potential methodological confounders such as sample-handling errors, extravesicular tRFs and non-placental vesicular tRFs. No experiment identified significant differences in expression of a tRF between preeclampsia and normal plasma. These data are contrary to the discoveries from perfusion experiments in Chapter 2.

If true, this result has two important implications. Firstly, tRFs in blood are not a biomarker for preeclampsia; Hypothesis 4.1 is rejected. Secondly, this throws into question functional implications of tRF dysregulation in preeclampsia pathophysiology. STB-EVs are hypothesised to play a role in feto-maternal signalling: their cargo are thought to be carried to target cells, where they change cellular function[41]. If STB-EV tRF concentrations are no different in the maternal circulation, then any difference in target cell function must be a consequence of differential STB-EV targeting in preeclampsia. STB-EV targeting has been demonstrated in the literature. One published study showed that STB-EV expression of apolipoprotein-E results in specific STB-EV uptake by hepatocytes expressing the LDL receptor[161]. However, no study has investigated STB-EV targeting in preeclampsia compared to normal pregnancy. It thus remains important to establish whether the perfusion data for STB-EV tRFs in Chapter 2 or the data in this plasma chapter represent the true *in-vivo* biology.

It is not possible to compare the plasma findings of this chapter to published data on blood tRF expression in preeclampsia, as these experiments are original. Similar studies of preeclampsia-dysregulated proteins (4.1.4) and miRNAs (Figure 4-1) found perfusion STB-EV differences could be replicated in plasma. Whilst protein differences retained the same direction of change in disease between perfusion and plasma, some miRNA targets were reversed. In parallel disciplines, blood EV tRFs represent valuable biomarkers of disease (relevant literature summarised in Table 1-5). Moreover, tRFs discovered in experimental models have been subsequently shown to be dysregulated in *ex-vivo* samples. For example, one study identified a specific tRF upregulated in breast cancer cell lines with greater metastatic capacity; expression of this tRF in breast cancer tissues was then shown to correlate inversely with patient survival[109]. Another study identified tRFs dysregulated in colon cancer tissue, compared to normal colon; these tRFs were also elevated in plasma exosomes from colon cancer patients compared to healthy controls[162]. This kind of study is subject to significant publication bias: tRFs which do not validate as blood biomarkers are unlikely to achieve publication. Nevertheless, review of the literature suggests that the rejection of Hypothesis 4.1 is less likely to be a consequence of a) placental perfusion representing a poor model for blood EV expression in preeclampsia, b) blood EV tRFs not representing a suitable biomarker for disease more generally (due, for example, to instability or technical problems with detection), or c) tRF biology being sufficiently inconsistent that targets discovered in experimental models have never been validated in blood.

Despite the optimisations described, several reasons remain which may explain why the differences identified in Chapter 2 were not corroborated in plasma; these are summarised in Figure 4-9.

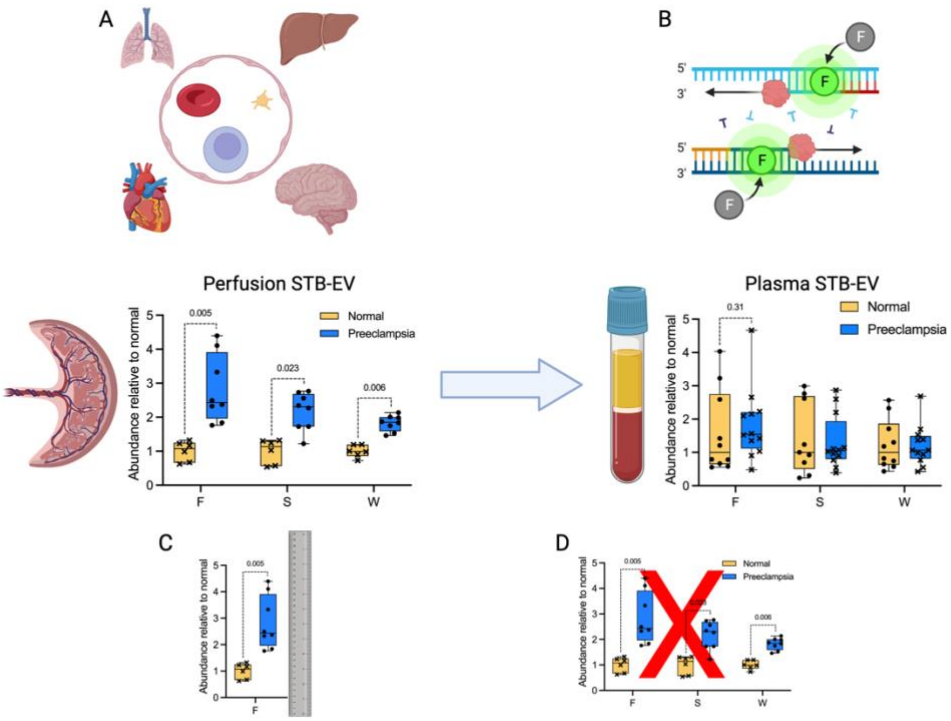


Figure 4-9 – Schematic diagram illustrating hypotheses which may explain why differences in STB-EV tRF expression between preeclampsia and normal pregnancies, identified using placental perfusion, may not reflect plasma tRF expression.

A: Confounding from plasma EV tRFs not arising from the syncytiotrophoblast;

B: qPCR cross-activation by near homologues of target tRFs;

C: Differences in perfusion data not of sufficient magnitude to be identifiable in plasma;

D: The original perfusion data are confounded.

Created with biorender.com with a publication licence under agreement number XK25QQ0KN7.

Perhaps the most likely explanation for failed plasma validation of potential tRF preeclampsia biomarkers, is confounding from tRF expression in plasma EVs not originating from the syncytiotrophoblast. It is well-established that STB-EVs constitute a very small proportion (<1%) of total plasma EVs[163]. Figure 3-26B suggests around half of the target F signal from plasma STB-EVs (isolated using antibody-bound beads) is placentally-derived. Thus 50% of the signal is non-placental in origin. Comparison of whole plasma (Figure 4-6B), total plasma EV (Figure 4-5B) and plasma STB-EV (Figure 4-8B) expression of the same three tRFs shows a pattern which more closely resembles perfusion STB-EV data (Figure 4-5A) as circulating STB-EVs are sequentially more enriched. Extensive work in Chapter 3 led to the conclusion that existing techniques would not allow enrichment of STB-EVs from plasma beyond 50%. Thus, technical limitations in plasma STB-EV isolation may account for lack of tRF differences in preeclampsia plasma.

An alternate hypothesis is that differences identified in perfusion data were not of sufficient magnitude to be detectable in plasma. Of the eight tRF targets assayed in plasma, the greatest magnitude differences between preeclampsia and normal pregnancies in perfusion data were 2.3-fold upregulated (F) and 2.9-fold downregulated (P). True plasma tRF concentrations might be different in preeclampsia, but simply not detectable as the noise created during plasma quantification may confound the small magnitude differences. To counter this hypothesis, similar magnitude differences in plasma exosomal tRF expression were seen in a sample of 40 patients, comparing those with breast cancer to healthy controls[75]. However, these targets were both discovered and validated in plasma.

The plasma data could be invalid because the qPCR assays used are being cross-activated by near-homologues of the tRFs which are differently expressed. Figure 2-19 demonstrates some signal detected by qPCR assays when an oligonucleotide with a

single terminal nucleotide difference is tested. However, the signal from the near-homologue is 76-fold less abundant, suggesting that any cross-activation would probably be minimal and unlikely to affect the 2.3-fold difference between tRF-F expression seen in Figure 4-2A.

The unsuccessful plasma validation may be a result of the original discovery experiments being confounded. The perfused placentas from preeclampsia and normal pregnancies were of different gestational ages (this was ethically unavoidable as described in 2.4). This might account for the tRF differences seen in perfusion data, which then disappeared when assayed in gestationally-matched plasma samples. Alternatively, the small preeclampsia sample size used (n=8) for such a heterogeneous condition may mean sampling error accounts for the differences originally discovered in the perfusion dataset. It could be that the broad population chosen represents different disease processes with different pathophysiologies, and consequently different STB-EV tRF release. This might mean the sample selected is simply confounded by different (but specific) STB-EV tRF release in preeclampsia subtypes, which were incorrectly grouped together. Whilst these criticisms are pertinent, the identification of established miRNA biomarkers in the perfusion analysis (Figure 4-1) would counter these hypotheses.

In conclusion, it is possible to reject the hypothesis that tRNA fragments represent blood biomarkers for preeclampsia using current technology. It is less clear whether differential STB-EV tRF expression identified from placental perfusion is invalid as a result of the plasma data presented in this chapter. Technical barriers regarding the purity of STB-EV isolation suggest that a conclusion cannot be drawn at this time. Thus, it seems appropriate to investigate whether preeclampsia-dysregulated tRFs from perfusion data have any functional effects in putative target cells. This is the aim of Chapter 5.

4.5. Summary Figure

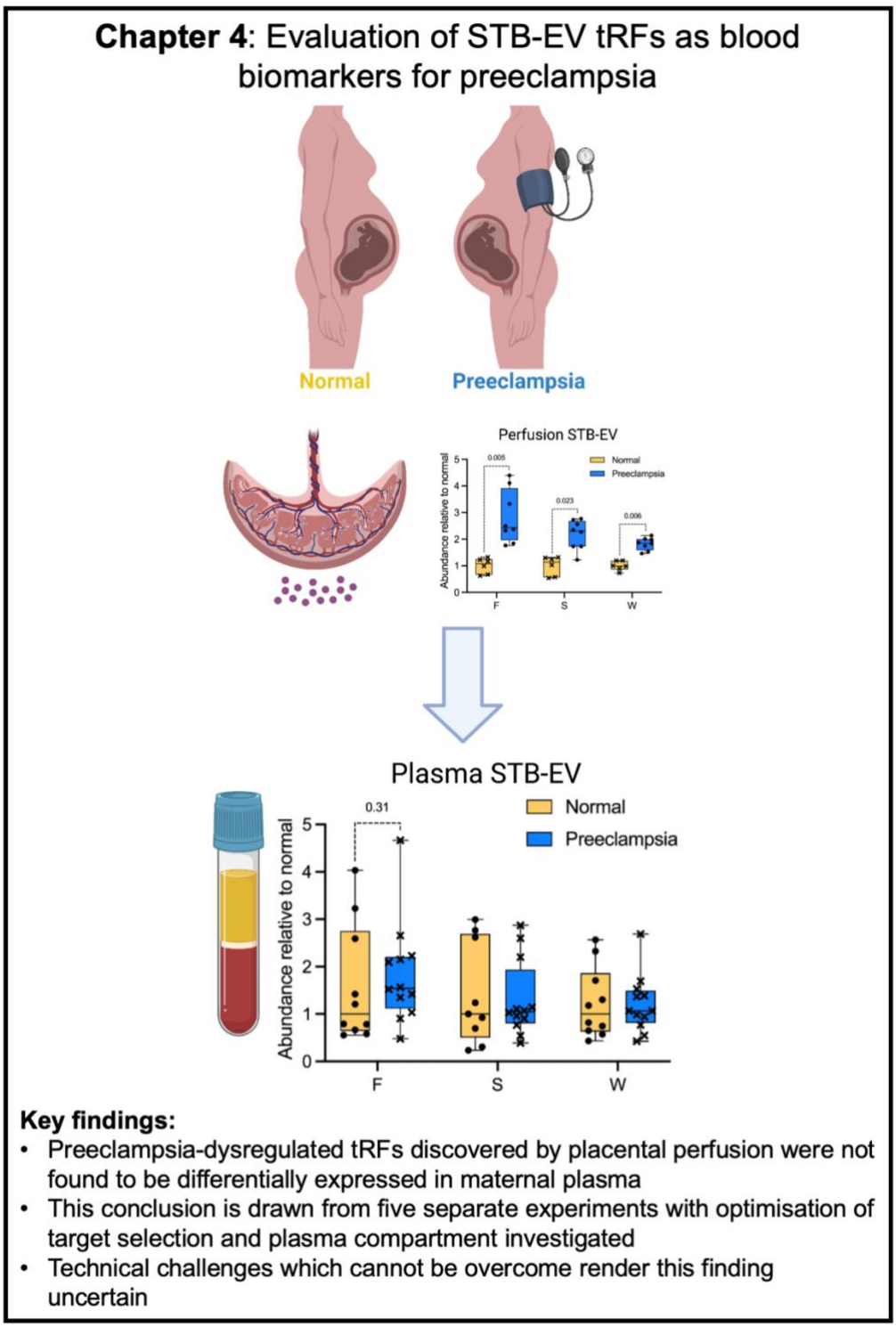


Figure 4-10 – Schematic figure summarising Chapter 4 key experiments and findings.

Created with biorender.com with a publication licence under agreement number QP25PAIYFL.

4.6. Appendix 3

Analysis of expression of MLEV targets in blood cells by collaborators

I found tRFs to be abundant in non-pregnant plasma EVs (3.3.3.1). Blood cell EVs constitute the greatest proportion of plasma EVs (Figure 3-2). Erythrocyte and T cell EVs are known to contain tRFs[77,164]; platelet and monocyte EVs are yet to be investigated. I proposed that blood cell EVs might contribute confounding tRF signal, accounting for disease-specific differences being seen in perfusion samples but not plasma. A solution to this problem would be to select preeclampsia-dysregulated tRF targets which are enriched in STB-EVs, but not blood cell EVs.

Our collaborators (Jinyue Bai, Ji Lu and Peiyong Jiang) at The Chinese University of Hong Kong interrogated publicly available blood cell small RNA sequencing datasets (Table 4-12). They quantified expression of the 983 differentially expressed fragments from their analysis in Appendix 1 in blood cells. This enabled me to select targets for plasma interrogation which were of low abundance in blood cells (and so likely low abundance in blood cell EVs), but high abundance in STB-EVs. These data were used to select miRNA targets for literature plasma validation in 4.3.1, and tRF targets evaluated in plasma in the second and third attempts (4.3.2.2 and 4.3.2.3). Data from this analysis are displayed in Table 4-5 and Table 4-8, where they were used to guide target selection.

Sample	SRA ID
Monocyte_1	SRR6453428
Monocyte_2	SRR6453427
Monocyte_3	SRR6453426
Monocyte_4	SRR6453386
Monocyte_5	SRR6453387
Monocyte_6	SRR6453388
Erythrocyte_1	SRR1664893
Erythrocyte_2	SRR1664894
Erythrocyte_3	SRR1664895
Erythrocyte_4	SRR1664896
Erythrocyte_5	SRR1664897
Platelet_1	SRR10282877, SRR10282878
Platelet_2	SRR10282879, SRR10282880

Table 4-12 – Sequence read archive identifiers for blood cell datasets

Chapter 5. Functional activity of syncytiotrophoblast tRNA-fragments in endothelial cells, macrophages and monocytes

5.1. Introduction

Preeclampsia is a complex multi-system disorder with a variable maternal phenotype[4]. The two-stage model (see 1.1.5) describes how syncytiotrophoblast stress in the asymptomatic first phase of preeclampsia results in release of blood-borne factors into the maternal circulation, triggering the second clinical phase. Recent diagnostic criteria describe this clinical phase as new-onset hypertension after 20 weeks of gestation, associated with one or more other features including renal insufficiency, liver impairment, pulmonary oedema, neurological complications, haematological complications and uteroplacental dysfunction[1,10,19]. These broad clinical features can be unified by two common underlying mechanisms: systemic endothelial dysregulation and sterile inflammation[19]. STB-EVs have been proposed as circulating feto-maternal signals in preeclampsia[41]. This chapter seeks to elucidate whether STB-EV tRFs play a role in endothelial dysregulation and sterile inflammation.

5.1.1. Endothelial dysfunction in preeclampsia

Roberts and colleagues' seminal paper in 1989 first advanced the argument that preeclampsia is an endothelial disorder[24]. They supported this hypothesis with wide-ranging evidence. Hypertension could be explained by disrupted endothelial regulation of vascular tone. *Ex-vivo* vessel studies had shown that rabbit carotid artery perfused with preeclampsia serum increased sensitivity to vasoconstrictors; investigators hypothesised that this smooth muscle effect is mediated by the endothelium[165]. Oedema and hypoalbuminaemia could represent a failure of the endothelial barrier. Clotting dysfunction might be a consequence of endothelial activation of the clotting cascade. The most consistent histological feature of preeclampsia, glomerular endotheliosis, describes glomerular endothelial cell engorgement with intracellular inclusions[166]. A number of endothelial cell factors had been shown to be dysregulated in the circulation of women with preeclampsia, including fibronectin, factor VIII antigen and prostacyclin[167–169]. Finally,

preeclampsia serum has been shown to injure human umbilical vein endothelial cells (HUVEC) in culture[170].

Since then, the body of evidence supporting endothelial cell injury in preeclampsia has grown further. A number of authors have shown that molecules expressed or released by endothelial cells are dysregulated in the plasma or serum of women with preeclampsia. This includes upregulated fibronectin[167,171–173], von Willebrand factor[173], endothelin[174], thrombomodulin[175,176], tumour necrosis factor α (TNFα)[177] and downregulated prostacyclin[169,178] and nitrite[179] levels. Four *ex-vivo* studies used wire myography to compare blood vessel constriction and dilatation in preeclampsia. Two of these manuscripts compared vessels taken from women with preeclampsia to normotensive women, finding a loss of endothelium-dependent relaxation in arteries from women with preeclampsia[180,181]. This effect was abrogated by denuding the endothelium, demonstrating a key function of the endothelium in regulating systemic vascular resistance. Two other studies added plasma or serum from women with preeclampsia to blood vessels from other donors, reporting a similar loss of endothelium-dependent vessel relaxation in the presence of preeclampsia blood[165,182]. *In-vitro* studies have allowed investigators to determine cell-specific changes in response to blood from women with preeclampsia. Studies have shown morphological changes in HUVEC treated with preeclampsia serum including cytotoxicity[170,183], suppressed cellular growth[184] and acquisition of cellular lipids[185]. Others have reported functional changes to HUVEC treated with preeclampsia serum, including increased release of mitogens[186], prostacyclin[185] and cellular fibronectin[187], as well as cadherin-5 accumulation[188]. Together these findings suggest specific and widespread changes to endothelial cells in response to blood-borne factors in preeclampsia.

5.1.1.1. STB-EVs as mediators of endothelial dysfunction in preeclampsia

There is substantial evidence that STB-EVs contribute to endothelial dysfunction in preeclampsia. Smarason and colleagues first treated HUVEC with mechanically-prepared STB-EVs, showing dramatically suppressed proliferation, viability and disruption of cell growth as a monolayer[79]. Elegant work since has investigated the effects of more physiologically-prepared STB-EVs (from explants and placental perfusion)[85]. These preparations had a significant but less severe effect on HUVEC proliferation, without causing detachment or apoptosis. The authors concluded impairment of endothelial cell function (rather than integrity) is more consistent with the clinical phenotype of preeclampsia. Functional changes in endothelial cells have also been reported in response to STB-EVs. Villalobos-Labra and colleagues report STB-EVs increased HUVEC nuclear factor k-light-chain-enhancer (NF-κB) activation and reduced nitric oxide levels[189]. EVs sourced from preeclamptic plasma have also been investigated. Human aortic endothelial cells were treated with preeclampsia and normal plasma total EVs isolated by ExoQuick columns[190]. Preeclampsia plasma EVs impaired endothelial cell migration and endothelial nitric oxide synthase (eNOS) protein expression. Whilst these findings cannot be attributed to STB-EVs alone, it is reasonable to infer that they make a contribution. A wire myography study perfused arteries with STB-EVs, demonstrating impaired relaxation to acetylcholine when compared to red cell EVs[191], suggesting STB-EVs may promote hypertension through endothelial dysfunction.

Work to elucidate the mechanism by which STB-EVs disrupt the endothelium is ongoing. A microarray study in HUVEC treated with STB-EVs found only 28 out of 10 000 genes changed 2-fold or more[192]. This finding implicates non-transcriptional signal transduction. Protein studies found that whilst integrins a5, aV and DPPIV play a role, they do not completely account for the antiproliferative effects of STB-EVs[193,194]. Other work suggests lipids within STB-EVs might play a role in their toxicity to endothelial cells[85]. Only one study has investigated STB-EV RNA as an endothelial effector[49]. Human coronary artery

endothelial cells were shown to internalise STB-EVs and placenta-specific miRNAs were transferred into the cells. This caused downregulation of specific miRNA target genes including *FLT1*. In Chapter 2, I discovered that miRNAs constitute <10% small RNA (sRNA) within STB-EVs and tRNA species >80%. I identified differential expression of >4000 STB-EV tRNA fragments (tRFs) in preeclampsia. I therefore hypothesise that tRFs may contribute to endothelial disruption in response to STB-EVs.

5.1.1.2. tRFs as mediators of endothelial dysfunction

One paper investigating ischaemic injury has studied the effect of tRFs on HUVEC[108]. The authors reported that two specific tRFs inhibited HUVEC proliferation, migration and tube formation. One of the tRFs studied (named "Oligo-Gly") had the identical sequence to the most abundant tRF discovered in STB-EVs (see Table 2-5 and Table 2-6). These functional effects exactly mirror the effect of STB-EVs on HUVEC proliferation[79,85] and of plasma preeclampsia EVs on HUVEC migration[190].

5.1.1.3. Hypothesis 5.1

Dysregulated tRFs in preeclampsia STB-EVs act on HUVEC to inhibit proliferation, induce activation and impair nitric oxide synthesis.

5.1.2. Sterile inflammation in preeclampsia

In 1999, Redman *et al.* built on the endothelial model of preeclampsia[23]. They proposed that endothelial activation represents a single component of a global inflammatory response that is characteristic of preeclampsia. They noted that normal pregnancy is a pro-inflammatory state and that preeclampsia represents an excessive inflammatory response. A variety of evidence supports this hypothesis, which persists (alongside endothelial activation) in models of preeclampsia pathophysiology published in 2022[4,19].

Studies of circulating leucocytes in preeclampsia have shown neutrophil activation and increased basal intracellular reactive oxygen species across neutrophils, monocytes and lymphocytes when compared to normal pregnancy[195,196]. Another study demonstrated enhanced peripheral blood mononuclear cell (PBMC) migration and phagocytic response in preeclampsia[197]. Studies of T-cells demonstrate more inflammatory T-cells (identified by intracellular IL-17 and IFNγ) and fewer T-regulatory cells in the maternal circulation in preeclampsia[198,199]. Circulating levels of a variety of pro-inflammatory cytokines (including TNFα[200], IL-6[201], IL-1B[202], IL-12[203]) and TNF receptors are more abundant in preeclampsia plasma. Conversely, anti-inflammatory cytokines such as IL-10 and IL-4 are reduced in preeclampsia placenta and plasma[204,205]. The complement system is activated in normal pregnancy, and further in preeclampsia[206]. Immune activation is not confined to the intravascular compartment: a study of adipose tissue-resident macrophages demonstrated greater activation in preeclampsia[207].

5.1.2.1. STB-EVs as mediators of sterile inflammation in preeclampsia

As with endothelial cells, a body of evidence is accumulating to implicate STB-EVs as drivers of immune activation in preeclampsia. PBMCs from non-pregnant women produced pro-inflammatory cytokines when co-cultured with STB-EVs[120]. This result has been replicated, alongside imaging flow cytometry studies demonstrating internalisation of STB-EVs by monocytes and B cells[83]. One further study compared PBMC response to preeclampsia and normal pregnancy STB-EVs, finding an enhanced pro-inflammatory response to lipopolysaccharide with preeclampsia vesicles[208]. Parallel work in macrophages has also demonstrated phagocytosis of STB-EVs, resulting in release of pro-inflammatory cytokines[209,210]. The mechanism by which STB-EVs activate immune cells has not been well investigated. One study attempted to correlate STB-EV lipidomics with the macrophage transcriptome, using these conclusions to suggest lipid changes may mediate STB-EV functions[210]. In the absence of interventional experiments, it is not possible to verify this correlation is causative. I found no studies have yet investigated

specific proteins or RNA as STB-EV immune cell effectors. Given tRFs represent the majority of STB-EV sRNA, I hypothesise that tRFs may contribute to monocyte and macrophage activation in response to STB-EVs.

5.1.2.2. tRFs as mediators of inflammation

Work in mycobacterial infection demonstrates that treatment of macrophages with EV-bound tRFs triggers macrophage activation to a pro-inflammatory phentoype[76]. This effect was specific to certain tRFs. A series of elegant experiments suggest that activation of endosomal Toll-like receptor 7 might account for the signal transduction. Another study found that a different tRF released in exosomes by colorectal cancer cells modulates M2 macrophage polarisation[162]. RNA pull-down assays, Western blot, RNA immunoprecipitation and RNA immunofluorescence all suggested these effects were mediated by binding to the proteins galectin 1 and macrophage migration inhibitory factor. Both studies used THP-1 cells (leukaemic monocyte cell line) differentiated with phorbol 12-myristate 13-acetate (PMA) as model macrophages. Given STB-EVs trigger macrophage M1 (pro-inflammatory) polarisation[210] and blocking EV tRFs modulates macrophage M2 (anti-inflammatory) polarisation[74], I speculated that it may be the tRFs within STB-EVs that mediate their effects on macrophages. No studies were identified which have investigated the effect of tRFs on monocytes.

5.1.2.3. Hypothesis 5.2

Macrophages and monocytes are activated by EV-bound tRFs identified within preeclampsia STB-EVs.

5.1.3. Summary

Figure 5-1 summarises known actions of STB-EVs on endothelial and immune cells which could directly account for the spectrum of clinical features associated with preeclampsia.

In testing hypotheses 5.1 and 5.2, this chapter aims to determine whether these preeclampsia STB-EV actions are mediated by the tRFs within them.

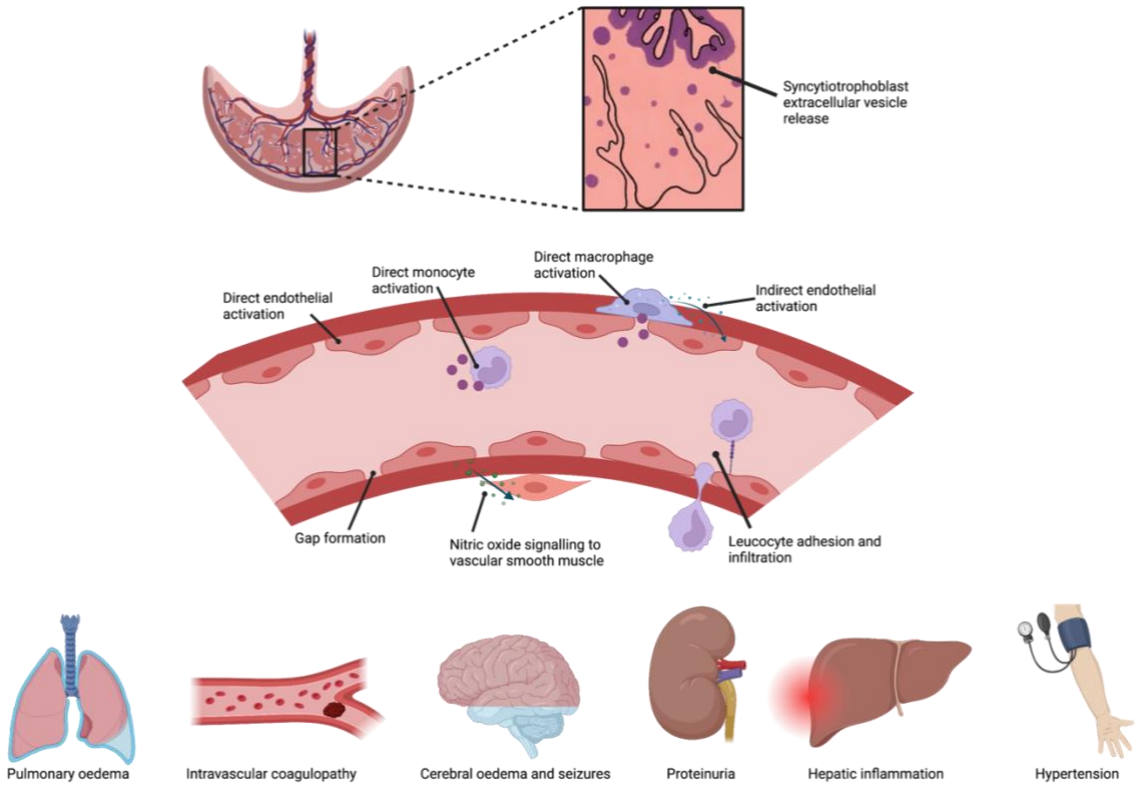


Figure 5-1 – Schematic figure showing known functions of STB-EVs relating to endothelial activation and sterile inflammation in the context of preeclampsia. Created with biorender.com with a publication licence under agreement number KY25PEWUWF.

5.2. Methods

5.2.1. Cell culture

Pooled human umbilical vein endothelial cells (HUVEC) from multiple donors were purchased (Promocell®, Germany) under catalogue number C-12208. These primary cells were phenotyped by the manufacturer using flow cytometry, demonstrating positivity to CD31 and Dil-Ac-LDL uptake. They were also confirmed free of microbiological contaminants including mycoplasma. Cells were thawed on arrival and grown in phenol red-free Endothelial Cell Growth Medium 2 (C-22216 and C-39216, Promocell, Germany) on Nunclon™ delta surface treated cell culture plastic (ThermoFisher, UK). Cells were frozen at passage 2 or 3 for subsequent experimental work and never used beyond passage 4.

THP-1 cells are an immortalised monocyte cell line derived from the blood of an acute leukaemia patient and sold by ATCC® (Manassas, USA). Cells in suspension were grown in RPMI-1640 medium supplemented with 10% Fetal Calf Serum. Cells were grown with 6.2 ng/mL (= 10 nM) phorbol 12-myristate-13-acetate (PMA, #AB147465, Abcam, UK) on Nunclon™ treated cell culture plastic for 24 hours to differentiate into adherent macrophages. All experiments were conducted in cells which had been subcultured 18 times or fewer i.e., passage 18 (P18) or lower.

5.2.2. tRF target and negative control selection and transfection

Two target tRFs were selected to investigate as STB-EV effectors (previously defined in Table 3-2 and given identifiers tRF-I and tRF-F for ease of reference in this thesis). tRF-I was chosen as the most abundant sRNA upregulated in normal medium-large STB-EVs compared to normal placenta (Table 2-5, identifier in Table 3-2) and normal small STB-EVs compared to normal placenta (Table 2-6, identifier in Table 3-2). tRF-F was chosen from the DEUS analysis, as the most abundant differentially expressed sRNA fragment in preeclampsia compared to normal medium-large STB-EVs (Table 2-10, identifier in Table

3-2). tRF-F is upregulated in preeclampsia compared to normal medium-large STB-EVs. A placentally-derived load of both targets had been found in the maternal circulation in 3.3.3.2.

tRF oligonucleotides were purchased from IDT (San Diego, USA) with a 5'-monophosphate modification and a standard 3'-hydroxyl group. These terminal moieties are consistent with tRFs that our RNA sequencing approach would have detected (see 2.4).

Scrambled RNA controls were used as negative controls to ensure that effects seen with tRF targets were not a consequence of other components of the RNA treatment, Scramble 1 RNA control was designed by removing the 5'-P modification and using an online tool which changed the order of nucleotides in tRF-I, but demonstrated the weakest match with any human RNA[211]. Scramble 2 used the same base tRF-I (without 5'-P) and replaced U nucleotides with A, in line with the approach used by Pawar *et al*[76]. Scramble controls were validated against known sequences using NCBI's Basic Local Alignment Tool; no alignments were identified[212]. A third control, ssRNA40-M, an inactive mutant of an HIV-derived sRNA from the Pawar study was also assessed[76]. Control sequences are shown in Table 5-1.

ID	Mapped tRNA	Length	Sequence
tRF-I	Gly-GCC-2-1	32	5'P-GCAUUGGUGGUUCAGUGGUAGAAUUCUCGCCU-3'
tRF-F	Glu-CTC-1-1	33	5'P-UCCCUGGUGGUCUAGUGGUUAGGAUUCGGCGCU-3'
Scr1	-	32	5'-AUUGCACACAAGUGUCUCGGUGUGGUGUUCGU-3'
Scr2	-	32	5'-GCAAAGGAGGAACAGAGGAAGAAAACACGCCA-3'
ssRNA40-M	-	20	5'-GCCCGACAGAAGAGAGACAC-3'

Table 5-1 – Oligonucleotide sequences used in this chapter

Cell	Assay	Control	Final conc^{n}	Source/*catalogue #*	Ref
HUVEC	Various qPCR	TNFα	10 ng/mL	R&D Systems/*210-TA/CF*	[213]
THP-1	NF-κB migration, various qPCR	LPS	10 ng/mL	Merck/*L3129*	[214]

Table 5-2 – Information regarding positive controls

Lyophilised oligonucleotides were resuspended in an appropriate volume of Hepes-buffered PBS to create a stock solution of 100 µM, which was aliquoted and further diluted. Oligofectamine transfection was carried out following manufacturer's instructions (Invitrogen, USA), using either Opti-MEM® medium (Gibco, USA) or endothelial cell growth medium as described in corresponding figure legends. 24 hours after seeding 96-well plates at 1000 cells per well, 100 µL oligofectamine-RNA solution was added. The final RNA concentration applied to cells was 50 nM, consistent with the dose necessary to see effect in the tRF publication from Li *et al*[108]*.* Four hours after treatment, 50 µL 3X serum medium was added to the cells.

9.2 µM RNA was packaged into lipid vesicles using N-[1-(2,3-Dioleoyloxy)propyl]-N,N,N-trimethylammonium methylsulfate (DOTAP), following manufacturer's instructions (Roche, Switzerland). The final RNA concentration applied to cells was 214 nM, consistent with the dose necessary to see an effect in the tRF publication by Pawar *et al.*[76].

5.2.3. STB-EV treatment and positive controls

STB-EVs derived by placental perfusion (see 2.2.2) from three normal placentas were pooled with equal protein concentrations. 24 µg STB-EVs suspended in appropriate growth medium were added to each well for treatment, in line with prior published dose-response experiments[85].

Positive controls, sources and relevant references are shown in Table 5-2.

5.2.4. Cell proliferation assay

HUVEC passage 4 or lower were seeded to 96-well plates, seeding one plate for each day. All plates underwent medium change every 48 hours. Proliferation was quantified using the CyQUANT assay, following manufacturer's protocol (Invitrogen, USA). To end the experiment, the relevant plate was removed from the incubator (at the same time

each day), medium was discarded and the plate frozen at -80°C. A dilutional series was created by pelleting a known quantity of trypsinised HUVEC and resuspending in dye solution, before performing a serial dilution in dye solution and transferring to 96-well plates. Plates were read by thawing to room temperature, adding dye solution, incubating for 2 minutes protected from light and measuring fluorescence using a ClarioStar® microplate reader (BMG Labtech Ltd, UK) with filters appropriate for 480 nm excitation and 520 nm emission.

5.2.5. NF-κB migration

Cells were grown on ibiTreat™ coated 8-well high walled µ-slide chambered coverslips (#80806, Ibidi, Germany). After treatment, cells were washed twice with warm PBS. They were fixed in 4% paraformaldehyde for 10 minutes, then blocked in blocking buffer (1% BSA/0.3% TritonX-100 in PBS) for 30 minutes. Cells were incubated in NF-κB mouse monoclonal antibody (#6956, Cell Signaling Technology, Netherlands) diluted 1 in 500 in blocking buffer for 1 hour. After washing in washing buffer (1% TritonX-100 in PBS) three times, cells were incubated in AF-488 anti-mouse IgG antibody (#A21202, Invitrogen, USA) for 1 hour. After three further washes in washing buffer, chambers were removed and coverslips mounted using Fluoroshield™ mounting medium with 4',6-diamidino-2-pheylindole (DAPI, #ab104139, Abcam, UK). Slides were imaged using a Leica SP8 confocal microscope (Leica, Germany).

An ImageJ macro was written to quantify co-localisation of NF-κB and DAPI staining by Pearson correlation coefficient[139]. A Gaussian blur was applied to NF-κB-stained images before thresholding using the default algorithm. Holes were filled, areas overlapping the edge of the field excluded and resulting areas of NF-κB staining (approximately corresponding to cell outlines) were selected as regions of interest. A Pearson co-localisation analysis was performed for DAPI and NF-κB in each region of interest, generating one correlation coefficient for each single cell or group of adjoining cells.

5.2.6. Co-culturing HUVEC with macrophage supernatants

To study indirect HUVEC activation via tRF macrophage treatment, HUVEC were treated with 50% macrophage cell culture supernatant mixed with 50% 2X endothelial growth cell medium. The latter was prepared by taking a small aliquot of phenol red-free Endothelial Cell Basal Medium 2 (C-22216) and supplementing it with 2X SupplementMix (C-39216) instead of the usual 1X. The rationale was that human primary endothelial cells require a specific mix of growth factors for optimal growth; without 2X supplementation, the medium would be deficient in key factors which may confound the experimental result.

5.2.7. RNA expression

After washing once with warm PBS, cellular RNA was isolated using the RNeasy™ Plus Mini Kit according to manufacturer's instructions (Qiagen, Germany). Cells were lysed and homogenised in buffer RLT plus. Genomic DNA was removed by spin column and RNA precipitated onto RNeasy spin columns with 70% ethanol. After washing, RNA was eluted in 30 µL RNAse-free water. RNA quantity and quality was assessed using Nanodrop™ (ThermoFisher, UK) and equal quantities were loaded into reverse transcription reactions using the High Capacity cDNA Reverse Transcription Kit (Applied Biosystems, CA, USA). Samples were incubated in a QIAamplifier 96 thermal cycler (Qiagen, Germany) at 25°C for 10 minutes, 37°C for 2 hours then 85°C for 5 minutes. Target mRNA expression was quantified on a QuantStudio™ 6 instrument using the following TaqMan™ Assays (Applied Biosystems, USA): Hs02758991_g1, Hs00164932_m1, Hs01003372_m1, Hs01574665_m1, Hs00174128_m1, Hs01555410_m1, Hs01011518_m1 and standard thermal cycling conditions. Quantification cycles (Cq) were determined automatically by instrument-associated software using standard settings. Relative expression was determined by following the Pfaffl approach, using *GAPDH* as a reference gene[106].

For quantification of IL-12β in macrophages, pre-amplification was required. Taqman® PreAmp Master Mix (#4391128, Applied Biosystems, USA) was used following manufacturer's instructions with 10 preamplification cycles.

5.2.8. Data presentation

Statistical analyses were performed and figures produced using Prism9 (GraphPad, USA). In larger sample size experiments with continuous data, where normality could be confirmed by data visualisation, two-tailed t-tests were used. For experiments of n=4 or fewer, two-tailed Mann-Whitney tests were used given normality could not reasonably be assessed. CyQUANT® data were analysed using linear regression and comparison made between groups by following the ANCOVA methodology. Hypothesis tests used for each comparison shown are described in figure legends.

5.3. Results

5.3.1. Endothelial cell responses to STB-EV tRNA fragments

5.3.1.1. Proliferation

A number of studies demonstrate that STB-EVs impair HUVEC proliferation[79,85]; one study shows specific tRFs have the same effect[108]. I hypothesised tRFs found within STB-EVs contribute to their effect on HUVEC proliferation.

I chose the CyQUANT® assay (Invitrogen, USA) to quantify proliferation. This assay uses a dye which fluoresces when bound to cellular nucleic acid. Adherent cells are frozen (for lysis), the dye is added and the fluorescence of each well correlates with the number of cells within that well. I first determined the linear detection range of the assay by creating a dilutional series using HUVEC (Figure 5-2A). There was a strong positive correlation between cell counts and fluorescence; the r^2 statistic was 0.9635 demonstrating low variance. The assay maintained linearity to the lowest dilution tested (2500 cells per well).

The optimal seeding density to quantify HUVEC proliferation in 96-well plates was tested. Cells were seeded on day 0 and proliferation quantified on days 1 to 5. Proliferation rate appeared to be reduced in the plate seeded at 10 000 cells per well compared to lower seeding densities (Figure 5-2B). This difference was more apparent when a linear regression model was applied (slope 2904 for 10 000 cells per well, compared to 9558 for 5000 and 9941 for 1000; Figure 5-2C). Microscopy suggested qualitatively this might be due to overcrowding. Thus, subsequent plates were seeded at 5000 cells per well. The spread of data was noted to be large on some plates (Figure 5-2B), so the number of replicates per treatment was increased from three to five.

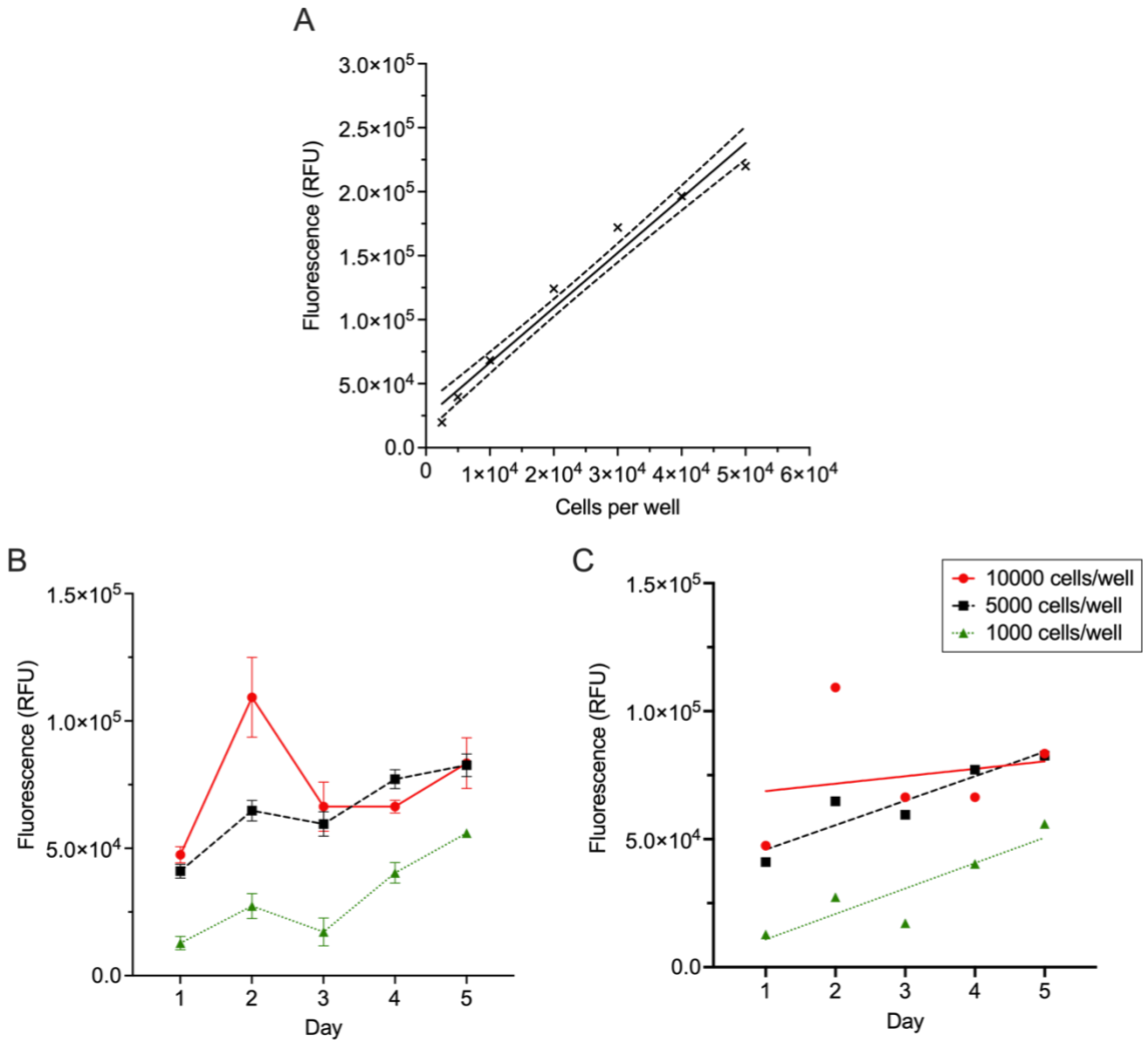


Figure 5-2 – Optimisation of CyQUANT® proliferation assay in HUVEC

A. Fluorescence reading for dilutions of a known quantity of HUVEC (counted manually using haemocytometer). Crosses represent means, solid line represents linear regression, hashed lines represent 95% confidence interval [CI]).

B, C. Fluorescence readings to quantify HUVEC proliferation with three different seeding densities. Mean and standard error [SEM] (B); mean and linear regression (C).

With the CyQUANT® assay optimised for HUVEC, I aimed to determine the effect of tRFs identified within STB-EVs on HUVEC proliferation. Two target tRFs and a corresponding scramble control, Scr1 were used (see 5.2.2). I used oligofectamine™ reagent (Invitrogen, UK) for transfection (selected to replicate the HUVEC tRF transfection experiments conducted by Li *et al.*[108]) and treated cells with oligofectamine only as an additional negative control. A positive control of pooled medium-large STB-EVs obtained by placental perfusion from three normal pregnancies was used (see 0).

The experiment was first conducted in endothelial cell growth medium (Figure 5-3A). The CyQUANT® assay requires an entire 96-well plate to be frozen and read simultaneously, meaning data for each day derive from different plates, which may account for the substantial variation seen between different days. To enable easier visualisation of any differences between the treatments, linear regression analyses were applied (Figure 5-3B). Day 5 data were excluded from these analyses because mean fluorescence was lower than on days 3 and 4, which suggested HUVEC overcrowding as seen with higher cell densities during optimisation (Figure 5-2B). STB-EVs significantly impaired proliferation (slope 16428 RFU/day [CI 12655 to 20201] for medium and 8262 RFU/day [CI 5078-11446] for STB-EVs, p=0.001). There was no discernible effect of tRF-I, tRF-F or Scr1 when compared to medium alone. The experiment was repeated using opti-MEM® reduced-serum medium (Gibco, USA) and supplementing with fetal calf serum 4 hours after treatment, exactly following the oligofectamine manufacturer's protocol (Figure 5-3C, D). There was no evidence that any of the tRFs changed HUVEC proliferation with opti-MEM.

I considered four reasons my results did not replicate the findings of Li *et al.* despite one of the targets (tRF-I) and all other conditions being the same[108]. First, proliferation in the Li study was most impaired 5 days after treatment; my data from day 5 suggested overcrowding of HUVEC globally impaired growth. The seeding density of the next

experiment (Figure 5-3E,F) was thus reduced to 1000 cells/well to enable day 5 data to be included. Secondly the oligonucleotide treatments may have bound to the CyQUANT® dye, creating spurious signal. Thus, cells were washed with PBS before freezing in Figure 5-3E,F. Thirdly, another study had compared tRF transfection with lipofectamine and DOTAP (N-[1-(2,3-Dioleoyloxy)propyl]-N,N,N- trimethylammonium methylsulfate), only seeing a change in cellular function with the latter[76]. The authors attributed this difference to lipofectamine lipid complexes allowing tRFs to cross into the cytoplasm, where DOTAP forms lipid vesicles which would be endocytosed to the endosomal compartment. Thus, tRFs were transfected with DOTAP in the next experiment. Finally, I hypothesised that Li *et al.*'s scramble control may have been a stimulator of HUVEC proliferation, accounting for the differences they reported between scramble and tRF-I. I contacted the corresponding author to discuss their scramble sequence, as it was notated to be an unusual DNA-RNA hybrid with both uracil and thymidine moieties, but received no response.

Applying these modifications to this third HUVEC proliferation experiment did not reduce variation (Figure 5-3E). After linear regression analysis (Figure 5-3F), STB-EVs still appeared to non-significantly reduce proliferation (slope 3345 RFU/day [CI 1188 to 5502] for medium and 1640 RFU/day [CI -856-4136] for STB-EVs, p=0.29), but no other treatments had an effect. I considered switching to a different proliferation assay to reduce inter-plate variation, but given the data consistently showed impaired proliferation with a positive control I felt there was sufficient evidence to reject the first part of Hypothesis 5.1, that tRFs within STB-EVs inhibit HUVEC proliferation.

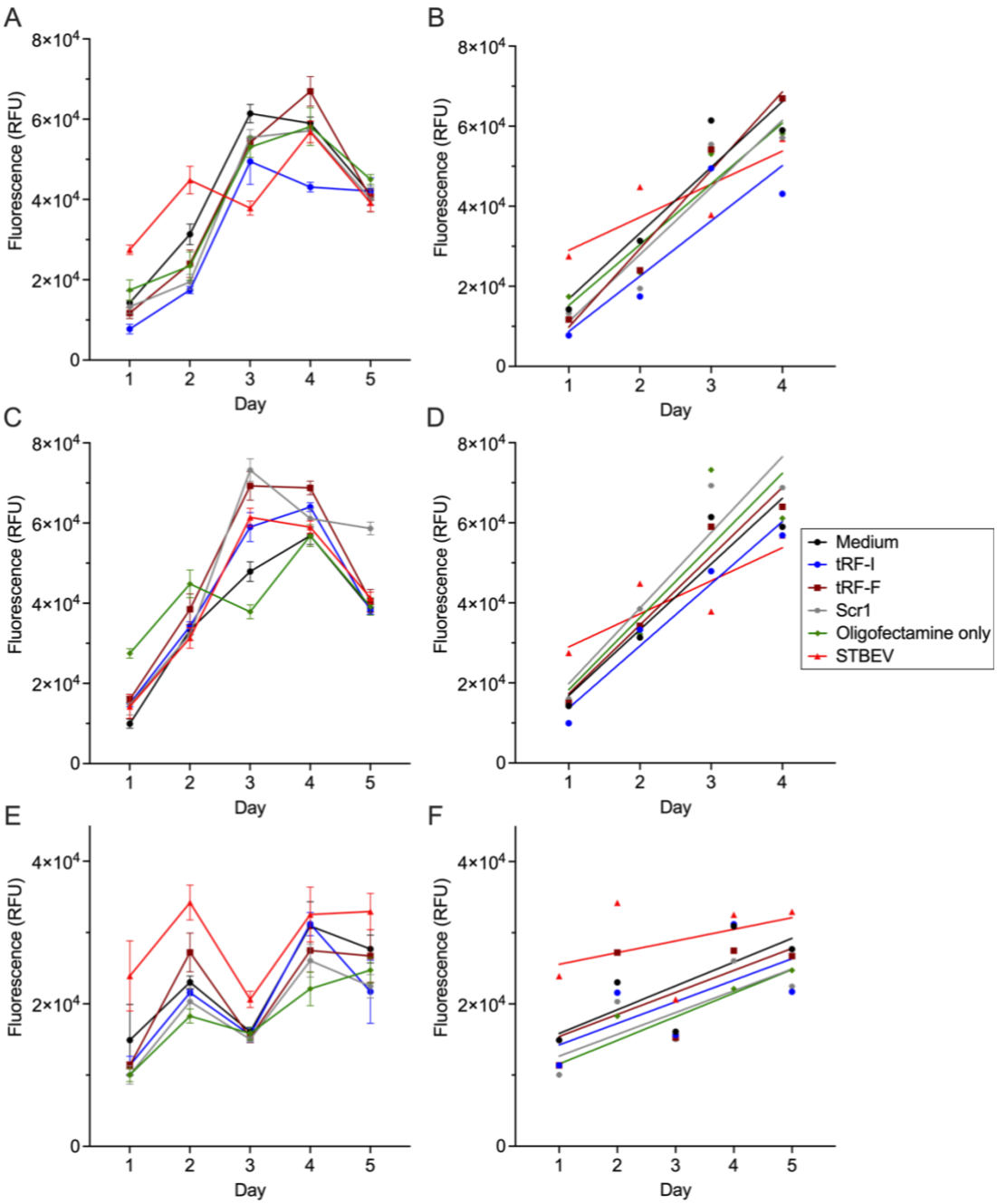


Figure 5-3 – HUVEC proliferation quantified by CyQUANT® assay

A, B. Oligofectamine transfection reagent and endothelial cell growth medium

(A, mean and SEM; B, mean and linear regression)

C, D. Oligofectamine transfection reagent and opti-MEM reduced-serum medium

(C, mean and SEM; D, mean and linear regression)

E, F. DOTAP liposomal transfection reagent and endothelial cell growth medium

(E, mean and SEM; F, mean and linear regression)

5.3.1.2. NF-κB migration

Recent work has shown STB-EVs trigger migration of NF-κB to the nucleus in HUVEC[189]. NF-κB is a transcription factor which initiates inflammation and reduces endothelial nitric oxide synthase (eNOS) expression, so nuclear migration might be an early event contributing to endothelial dysfunction and hypertension in preeclampsia. I hypothesised that tRFs contribute to NF-κB migration in HUVEC treated with STB-EVs.

Simultaneous to HUVEC experiments I optimised an assay to quantify NF-κB nuclear translocation in macrophages (presented subsequently, see 5.2.5 and 5.3.2.1). One of these experiments demonstrated Scr2 to be a superior scramble control to Scr1 (presented subsequently, see Figure 5-5D), so Scr2 was used as a control for the remaining HUVEC work.

HUVEC were treated with oligonucleotides using DOTAP and STB-EVs as a positive control. NF-κB nuclear translocation was quantified 20 hours later, in line with treatment times showing a positive response in macrophages (see 5.3.2.1). STB-EVs caused a significant increase in correlation coefficient between NF-κB and nuclear stain DAPI, compared to untreated cells (mean difference 0.14, $p<0.0001$, Figure 5-4A). No significant differences were seen when HUVEC were treated with any of the tRNA fragments using DOTAP.

5.3.1.3. Expression of adhesion molecules and endothelial nitric oxide synthase

Cell adhesion molecules such as Vascular Cell Adhesion Molecule 1 (VCAM-1) and Intercellular adhesion molecule 1 (ICAM-1) are well-recognised markers of endothelial activation[215]. In the healthy endothelium, eNOS constitutively produces nitric oxide (NO), which is a vasodilator[215]. Preeclampsia STB-EVs have been shown to reduce eNOS protein expression, which may contribute to maternal hypertension[189]. I hypothesised that

EV-bound tRFs might activate the endothelium, increasing VCAM-1 and ICAM-1 expression, whilst reducing eNOS expression.

To test this hypothesis, HUVEC were seeded onto 24 well plates 24 hours prior to treatment with tRF-I, tRF-F, Scr2 using DOTAP and TNFα as a positive control. After 6 hours treatment (duration recommended after discussion with endothelial cell biologist Dr Naveed Akbar, Oxford University[216]), HUVEC RNA was isolated and VCAM-1, ICAM-1 and eNOS mRNA expression was quantified using RT-qPCR. Cells treated with TNFα showed a significant and marked upregulation of adhesion molecules and downregulation of eNOS compared to untreated cells ($p=0.03$ for all three). No tRF or scramble had a discernible effect on any of these targets (Figure 5-4B-D).

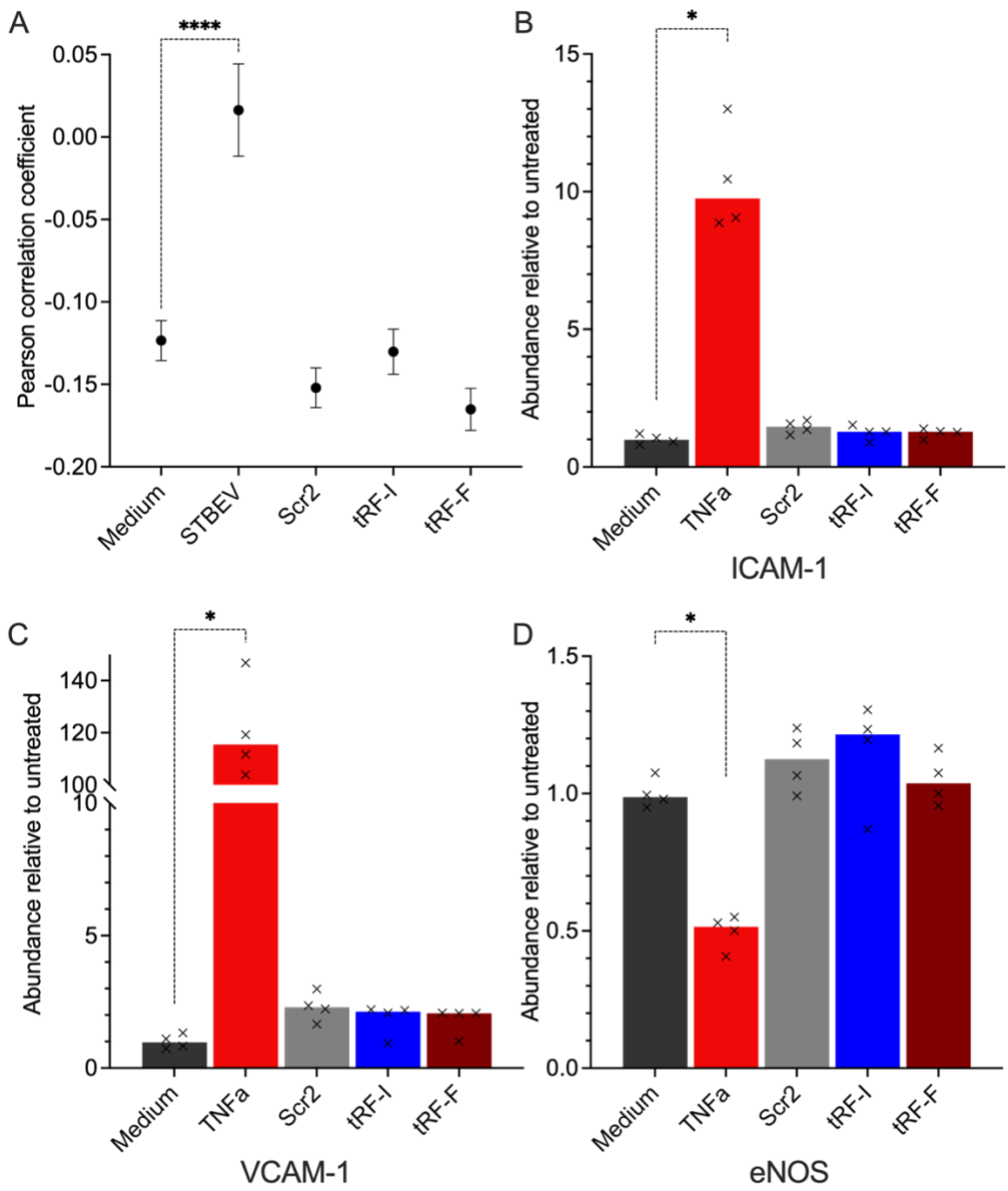


Figure 5-4 – HUVEC functions following treatment with EV tRFs packaged with DOTAP

A. Co-localisation of NF-κB and nuclear stains in HUVEC following treatment with Scr2, tRF-I, tRF-F and perfusion STB-EVs.

*Data for each condition derived from >84 individual cells across three experiments (mean and SEM; comparisons using unpaired t-test; **** denotes p<0.0001).*

*B, C, D. Expression of ICAM-1 (B), VCAM-1 (C) and eNOS (D) in HUVEC treated with Scr2, tRF-F and tRF-I using DOTAP and TNFα (positive control), relative to untreated. (quantified by RT-qPCR, n=4 per condition, bars represent median. Comparisons using Mann-Whitney tests, * denotes p<0.05).*

5.3.2. Macrophage responses to STB tRNA fragments

Macrophage activation by STB-EVs has been described in relation to preeclampsia[210]. Some tRFs have been noted to activate macrophages when contained within EVs[76]. I hypothesised tRFs contribute to macrophage activation by STB-EVs. I used differentiated THP-1 cells as a macrophage model.

5.3.2.1. NF-κB migration

NF-κB nuclear translocation is a common initiating step in the expression of pro-inflammatory cytokines in macrophages[217]. I optimised an assay to quantify NF-κB nuclear translocation, for use as a screening test to determine whether STB-EV tRFs activate macrophages.

Two seeding densities for THP-1 cells (100 000 and 50 000 cells per ml, replicated from Pondman *et al.*[217]) were compared qualitatively. The higher density was superior for imaging, offering maximal cells per field of view, with minimal cell overlap. Two phorbol 12-myristate-13-acetate (PMA) concentrations to differentiate THP-1 cells into macrophages were also compared (100 nM from Pondman *et al.*[217] and 10 nM from Pawar *et al.*[76]). 10 nM PMA resulted in equal cell adherence to 100 nM (qualitative observation), so was selected for subsequent work to minimise any cellular pre-activation.

THP-1 cells were seeded directly onto chambered coverslips with PMA for 24 hours (duration replicated from Pondman *et al.*[217]). Cells were then treated for 16 hours with tRF-I, tRF-F, Scr1 and DOTAP, with lipopolysaccharide (LPS) and perfusion STB-EVs as positive controls (timecourse replicated from Pawar *et al.*[76]). Coverslips were stained with NF-κB primary antibody, AFP-488 secondary antibody and the nuclear stain DAPI (Figure 5-5A). Co-localisation of the stains was quantified using a bespoke ImageJ analysis (Figure 5-5B). There was a small but significant difference in Pearson correlation coefficient between cells treated with DOTAP only and DOTAP with tRF-I (mean

difference 0.10, p=0.015), but not DOTAP with tRF-F (mean difference 0.04, p=0.26). Because tRF-F showed no effect on NF-κB migration in optimisation experiments, only tRF-I was pursued for further macrophage NF-κB experiments. However, I went on to assess tRF-F activity on other parameters associated with preeclampsia pathogenesis (see 5.3.2.2).

The experiment was also conducted with IFNγ 10 ng/mL pre-treatment in case the effect size was greater, after discussion with immunologist Dr Uday Kishore (Brunel University, UK)[218]. All conditions showed greater correlation between NF-κB and nuclear stains, confirming generalised pre-activation of the cells (Figure 5-5C). There was no increase in the effect size between conditions, so IFNγ pre-treatment was not pursued further.

The scramble RNA Scr1 resulted in greater NF-κB nuclear migration compared to DOTAP (mean difference 0.14 in Figure 5-5B, p=0.008) than either of the target tRFs, suggesting it may be functional. In light of this, two alternative control RNAs were tested: Scr2 (designed using the Pawar *et al.* approach, see 5.2.2) and an inactive mutant of an HIV-derived sRNA used as a negative control in the Pawar *et al.* study (ssRNA40-M)[76]. Scr2 resulted in the least NF-κB nuclear migration, comparable to untreated cells (mean difference -0.009, p=0.84, Figure 5-5D), and was selected for subsequent experimental work.

The action of tRF-I treatment on NF-κB migration was compared to Scr2 across four experiments alongside positive and negative controls (Figure 5-5E,F). tRF-I caused a significant increase in NF-κB migration (mean difference 0.09, p<0.0001), suggesting this STB-EV tRF caused macrophage activation.

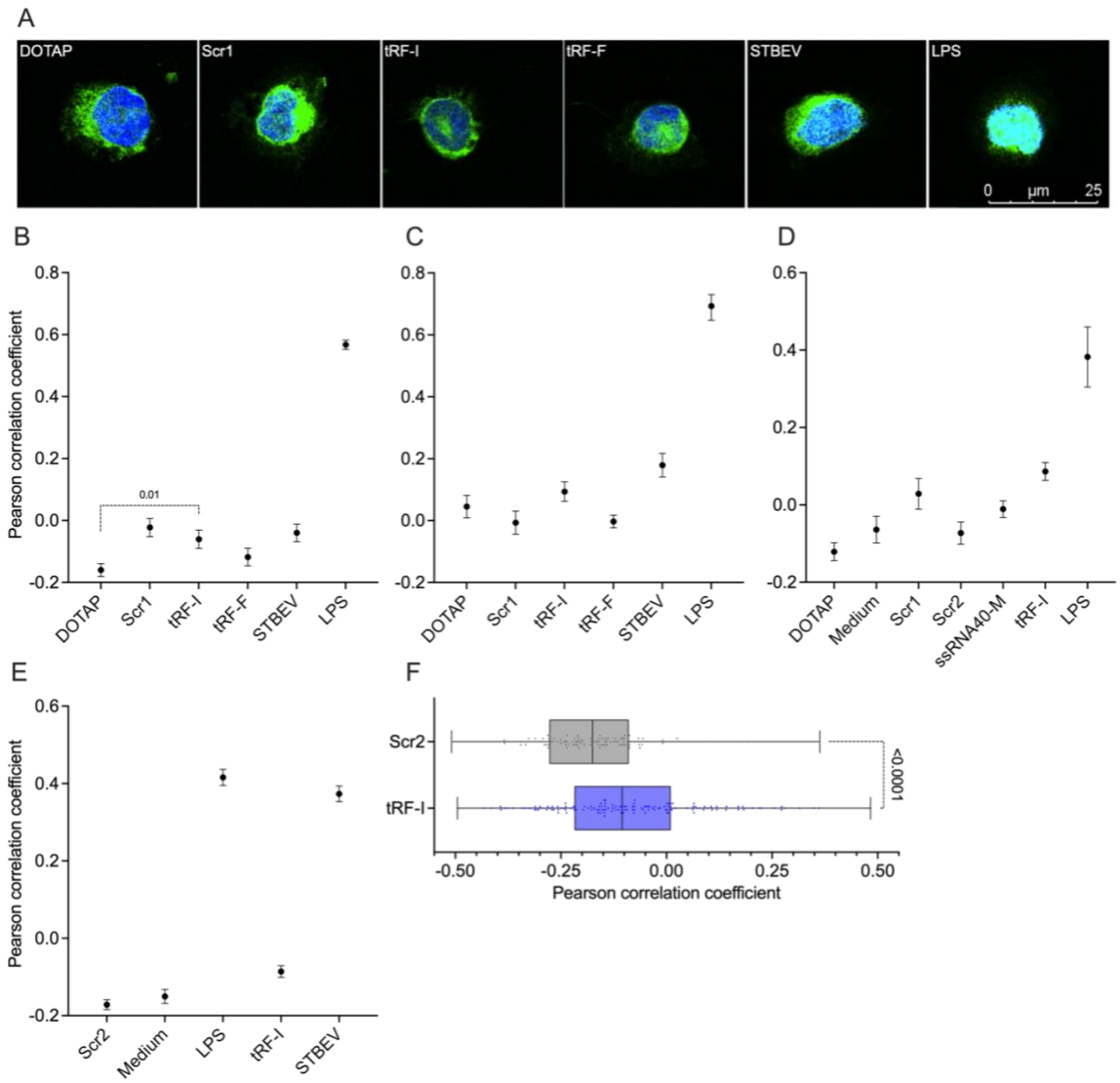


Figure 5-5 – NF-κB migration in macrophages

Macrophages treated with oligonucleotides using DOTAP, perfusion STB-EVs and LPS as positive control and stained for NF-κB and nucleus

A. Representative confocal microscopy images

B, C. Co-localisation of NF-κB and DAPI without (B) and with (C) IFNγ pre-treatment

D. Co-localisation of NF-κB and DAPI comparing different scramble controls (no IFNγ)

E, F. Co-localisation of NF-κB and DAPI using data from four experiments with >100 cells per condition (no IFNγ)

Dots/error bars represent mean/SEM; box plots represent median/IQR with whiskers showing minimum and maximum values. Comparisons using unpaired t-tests.

5.3.2.2. Expression of cytokines

Given tRF-I packaged in EVs caused nuclear NF-κB migration in macrophages, I hypothesised STB-EV tRF treatment would change macrophage cytokine expression. tRF-F did not cause NF-κB migration in macrophages (Figure 5-5B). However, tRF-F (and not tRF-I) is upregulated in preeclampsia STB-EVs (5.2.2). Consequently, tRF-F was considered an important biologically plausible target to assess when testing Hypothesis 5.2 and was included again in subsequent experiments.

I first compared different durations of macrophage treatment to determine the optimal experiment duration. THP-1 cells were seeded into 24 well plates at 5E5 cells per well (in line with experiments published by Awoyemi *et al*.[209]) and differentiated into macrophages using low-dose PMA. After 24 hours, cells were treated with tRF-I, tRF-F and Scr2 using DOTAP, perfusion STB-EVs and LPS positive control. The experiment was ended by isolating cellular RNA and using RT-qPCR to quantify TNFα expression at 6 hours (Figure 5-6A) and 12 hours (Figure 5-6B) as recommended by immunologist Dr Uday Kishore (Brunel University, UK)[218]. TNFα expression was upregulated at both timepoints with both tRF-F treatment (median increase 2.2-fold at 6 hours and 4.8-fold at 12 hours, p=0.03 for both) and tRF-I treatment (median increase 3.6-fold at 6 hours and 6.6-fold at 12 hours, p=0.03 for both). The greatest effect size was seen after 12 hours, which was selected for evaluation of subsequent cytokines. Cells treated with both tRF-F and tRF-I showed a significant increase in the pro-inflammatory cytokines IL-1β (median for tRF-F 1.5-fold compared to Scr2, p=0.03) and IL-12β (median for tRF-F 18.3-fold compared to Scr2, p=0.03), but not the anti-inflammatory cytokine IL-10 (Figure 5-6C-E).

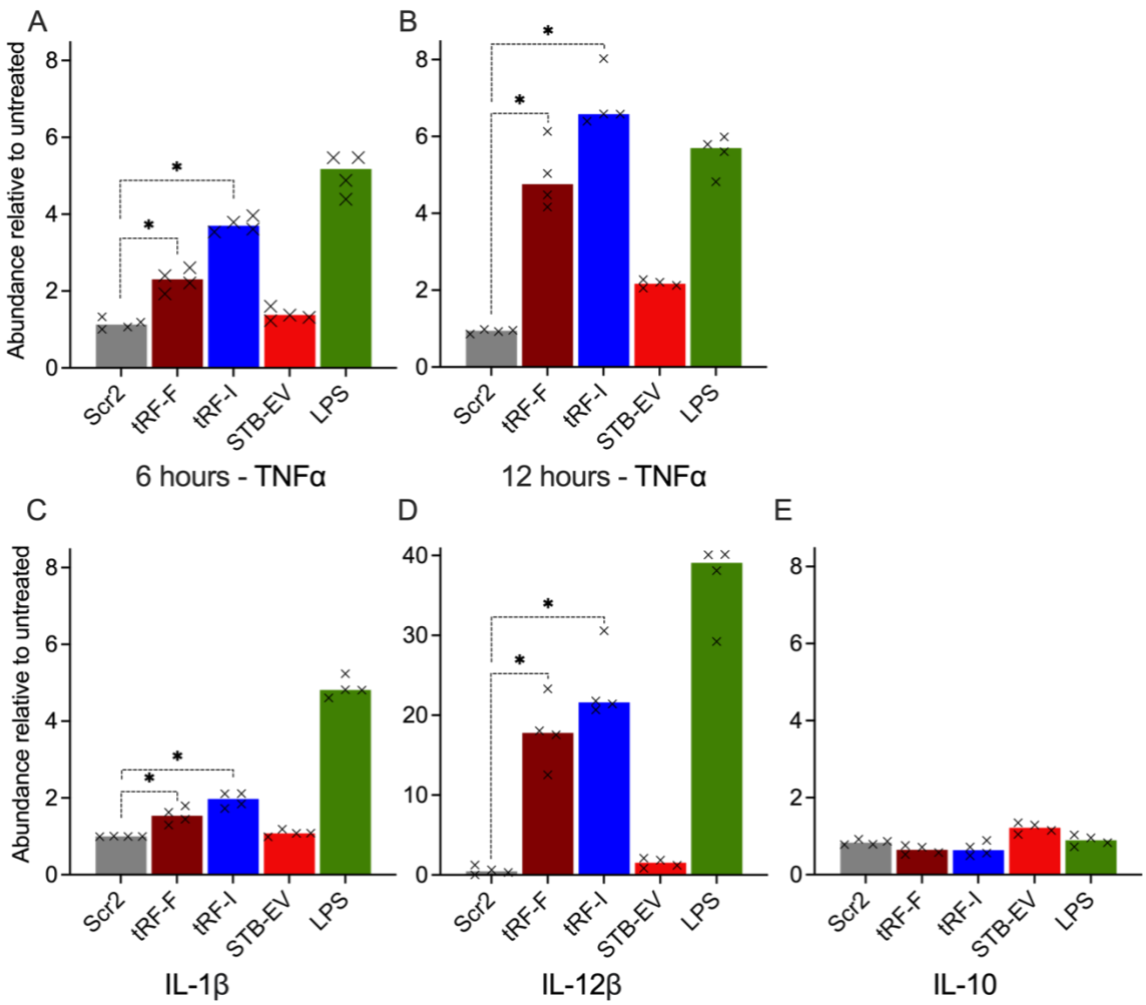


*Figure 5-6 – Cytokine mRNA expression in differentiated THP-1 cells (macrophages) Expression of TNFα in macrophages after treatment with tRF-F, tRF-I or Scr2 using DOTAP, perfusion STB-EVs and LPS positive control for 6 hours (A) and 12 hours (B). Expression of IL-1β (C), IL-12β (D), IL-10 (E) under same conditions as (B). Quantified by RT-qPCR, n=4 per condition, bars represent median. Comparisons using Mann-Whitney tests, * denotes p<0.05.*

5.3.3. Monocyte responses to STB tRNA fragments

In light of the significant macrophage activation seen with both tRF-F and tRF-I packaged in EVs, I investigated monocyte activation to the same stimuli.

Undifferentiated THP-1 cells were used as a model. Cells were seeded into 24 well plates in the same manner as macrophages (see 5.3.2.2), but without PMA. After 12 hours of treatment with tRF-F, tRF-I and Scr2 using DOTAP or LPS positive control, cellular RNA was isolated and cytokine expression quantified using RT-qPCR. Neither tRF caused notable increase in pro-inflammatory or anti-inflammatory cytokine expression in monocytes (Figure 5-7). A good response to LPS positive controls demonstrates experimental validity.

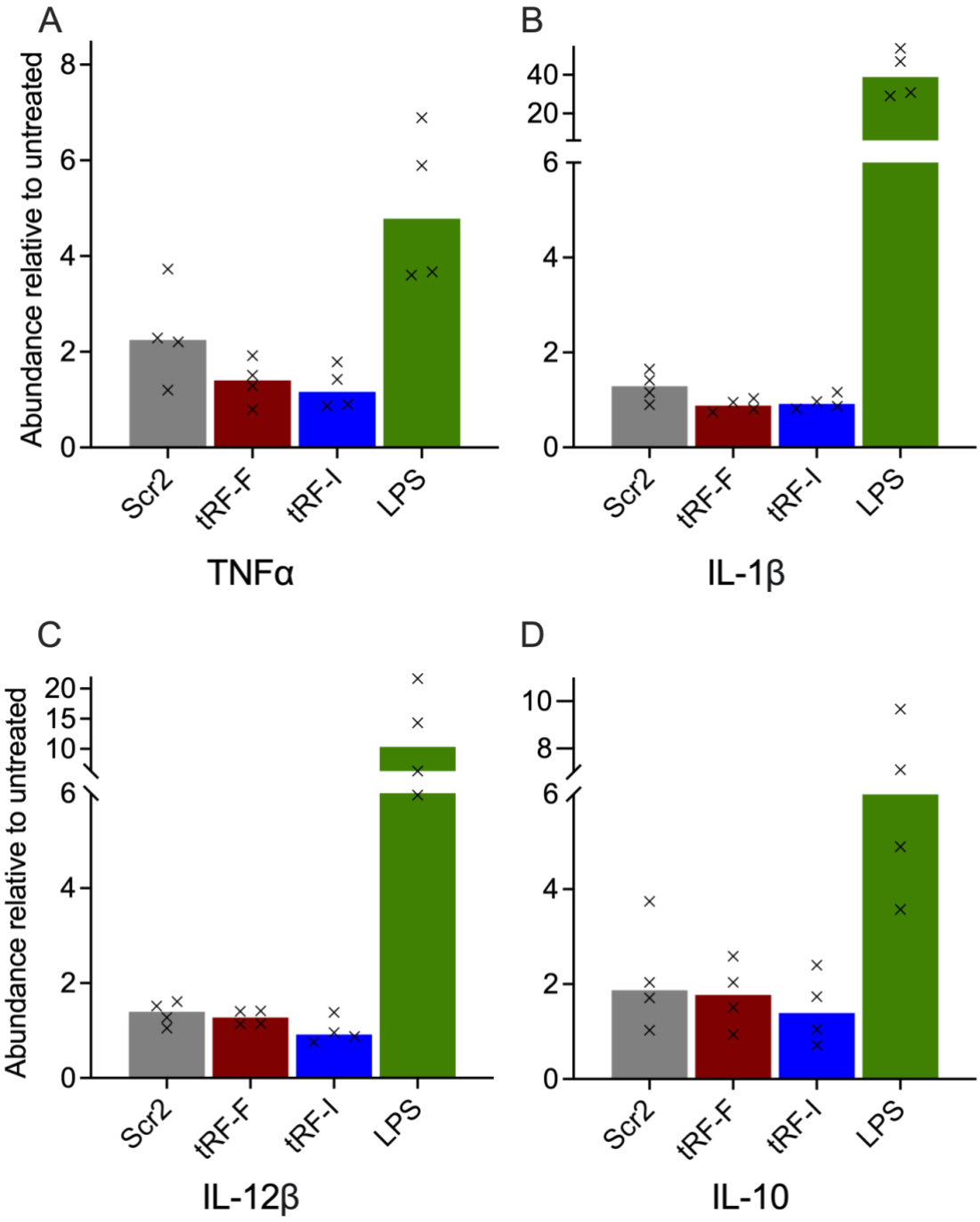


Figure 5-7 – Cytokine mRNA expression in undifferentiated THP-1 cells (monocytes) Expression of cytokines, TNFα (A), IL-1β (B), IL-12β (C), IL-10 (D), in monocytes treated with tRF-F, tRF-I and Scr2 using DOTAP or LPS positive control for 12 hours. Quantified by RT-qPCR, n=4 per condition, bars represent median.

5.3.4. Endothelial cell response to macrophage activation by STB tRNA fragments

Vascular macrophages are known to modulate adjacent endothelial cell actions[219,220]. I saw potent STB-EV tRF macrophage activation (Figure 5-6) and no direct effect of STB-EV tRFs on HUVEC (Figure 5-3 and Figure 5-4). I hypothesised that STB-EV tRFs might indirectly activate endothelial cells via macrophage cytokine release.

To test this hypothesis, macrophages were cultured in tRF-F, tRF-I and Scr2 (as described in 5.3.2.2) for 24 hours (duration recommended after discussion with immunologist Dr Uday Kishore regarding peak cytokine release[218]). HUVEC were then co-cultured with 50% macrophage supernatant and 50% 2X endothelial cell medium, seeking to mimic the vascular tissue microenvironment in preeclampsia. After 6 hours, HUVEC RNA was isolated and expression of cell adhesion molecules (VCAM-1 and ICAM-1) alongside eNOS was quantified using RT-qPCR. In response to supernatants from macrophages treated with tRF-F, HUVEC ICAM-1 expression was median 18.2-fold higher than from macrophages treated with Scr2 ($p<0.03$, Figure 5-8A). A similar response was seen with VCAM-1 expression (median 25.6-fold greater with tRF-F than Scr2, $p<0.03$, Figure 5-8B). Conversely eNOS expression was downregulated by median 30% in HUVEC treated with supernatants from macrophages treated with tRF-F compared to Scr2 ($p<0.03$, Figure 5-8C). Similar changes were seen with tRF-I treatment (all assays, $p<0.03$, Figure 5-8A-C).

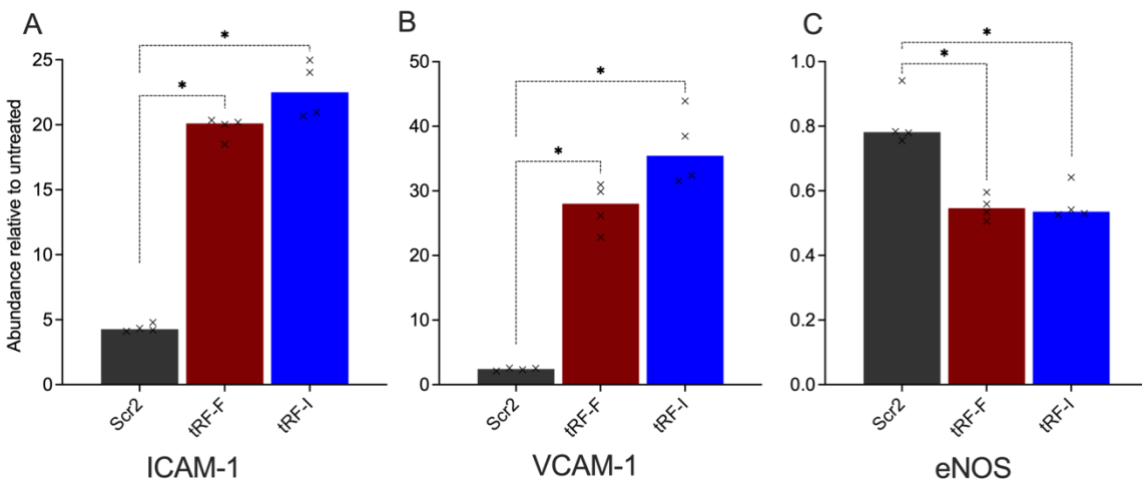


Figure 5-8 – Macrophage activation by STB-EV tRFs can induce endothelial cell activation

*Expression of ICAM-1 (A), VCAM-1 (B) and eNOS (C) in HUVEC co-cultured with supernatants from macrophages pre-treated with Scr2, tRF-F and tRF-I using DOTAP, relative to untreated cells. Quantified by RT-qPCR, n=4 per condition, bars represent median. Comparisons using Mann-Whitney tests, * denotes p<0.05.*

5.4. Discussion

tRFs are known to regulate cellular function through a variety of mechanisms which can interrupt transcription, translation and epigenetic regulation (summarised in Table 1-4). EV-bound tRFs have recently been reported as signalling molecules in colorectal cancer, macrophages and T-cells[76,77,162]. This chapter aimed to investigate whether STB-EV tRFs contribute to endothelial dysfunction and sterile inflammation in preeclampsia.

EV-bound tRFs (identified from STB-EVs) were shown to have no discernible direct effect on endothelial cell proliferation, NF-κB migration, adhesion molecule expression or eNOS expression. In contrast, the same tRFs potently activated macrophages, but not monocytes, causing expression of pro-inflammatory cytokines. EV-bound tRF activation of macrophages was shown to indirectly activate endothelial cells, demonstrated by co-culture of HUVEC with macrophage supernatants. These findings are summarised in Figure 5-9.

These data support rejection of Hypothesis 5.1: dysregulated tRFs in preeclampsia STB-EVs act on HUVEC to inhibit proliferation, induce activation and impair nitric oxide synthesis. My data would support an alternate hypothesis that STB-EV tRFs activate HUVEC indirectly (through macrophages) inducing adhesion molecule expression and impairing nitric oxide synthesis.

I also propose to reject Hypothesis 5.2: macrophages and monocytes are activated by EV-bound tRFs identified within preeclampsia STB-EVs. My data would support a modified hypothesis that macrophages, but not monocytes, are activated by STB-EV tRFs.

When comparing my data with those in the literature, I was able to replicate previously reported actions of STB-EVs on both endothelial cells[79,85,189] and macrophages[209,210],

suggesting my assays and models were appropriate. Positive controls performed as anticipated in every investigatory experiment in this chapter, supporting suitable experimental timescales and conduct.

I was unable to reproduce the effects of tRFs on HUVEC reported by Li *et al*, despite using the same reagents, one tRF with an identical sequence and a purportedly more accurate assay to quantitate proliferation[108]. Key hypotheses to explain this disparity were discussed and the protocol iteratively optimised in 5.3.1.1. One outstanding concern relates to the published scramble control, which contained both thymidine and uracil moieties suggesting a DNA-RNA hybrid; attempts to communicate with the authors about this were unsuccessful. This unusual negative control molecule may have promoted HUVEC proliferation, accounting for the published differences. A recently published paper also investigated the actions of tRFs on HUVEC, identifying target molecules from atherosclerotic arterial biopsies[221]. In this study the authors tested a tRF labelled as Gly-GCC, the same iso-acceptor as both tRF-I and the tRF investigated by Li *et al.* However, they did not publish the sequence of Gly-GCC, preventing replication of their experiments or direct comparison with other studies. They used a CCK8 assay to assess proliferation (the same as Li *et al.*) and found increased HUVEC proliferation compared to a scramble control; the opposite from Li *et al.* Whilst this experiment is less open to independent interrogation than Li *et al.*, the conflicting outcomes from two similar experiments lend important context (and credibility) to my finding of no direct STB-EV tRF effect on HUVEC proliferation, NF-κB migration or adhesion molecule/eNOS expression.

My findings in macrophages are consistent with those of Pawar *et al.*, who reported pro-inflammatory cytokine upregulation in cells treated with specific tRFs[76]. A study by Lu *et al.,* found knock-down of a specific tRF promoted M2 macrophage polarisation (these cells release anti-inflammatory cytokines such as IL-10), which is also consistent with my results[162]. It is important to note that both of these studies investigated specific tRFs which

were not identified as targets in STB-EVs from Chapter 2. It is internally consistent that I found upregulation of pro-inflammatory cytokines and downregulation of the anti-inflammatory cytokine IL-10. The specificity of tRF actions in macrophages but not monocytes or endothelial cells might be a consequence of enhanced phagocytosis in macrophages causing more tRFs to reach endosomal Toll-like receptors. It is consistent that tRF-I caused both nuclear NF-κB migration and increased pro-inflammatory cytokine expression. It is unexpected that tRF-F would not cause nuclear NF-κB migration, despite causing increased pro-inflammatory cytokine expression; further work is required to understand the mechanism by which tRF-F changes cytokine expression.

The indirect activation of endothelial cells by tRF-activated macrophage supernatants is consistent with a study of monocytes activated by cell-free fetal DNA (cffDNA)[222]. Here, the authors found that monocytes released pro-inflammatory cytokines in response to cffDNA, and that co-culture of HUVEC with cffDNA-activated monocyte media resulted in increased expression of E-selectin and ICAM-1.

The experimental models I used to test my hypotheses have limitations. HUVEC were used to model maternal endothelium, but are derived from fetal vasculature. THP-1 cells are a leukaemia cell line and may have a different phenotype from the maternal vascular macrophages they were used to model. However, both HUVEC and THP-1 are widely used as models for maternal endothelium and vascular macrophages in the literature[189,209]. It is possible that the experiments showing no effect were conducted at the wrong timepoints; although I obtained expert advice and ran successful positive controls, future work could include a time-course optimisation.

In conclusion, STB-EVs are complex particles, decorated with surface proteins and filled with proteins, tRFs, mRNAs, miRNAs, piRNAs and lipids[41]. My finding, that tRFs account for some (but not all) of the known effects of STB-EVs in relation to preeclampsia, is

highly biologically plausible. It is consistent with other mechanistic studies showing different proteins and RNA also play a role in STB-EV actions. My data implicate tRFs as signalling molecules, which contribute to the pathophysiology of preeclampsia by triggering sterile inflammation and indirect endothelial activation via STB-EVs, but do not account for all of the known effects of STB-EVs on these target cells.

5.5. Summary Figure

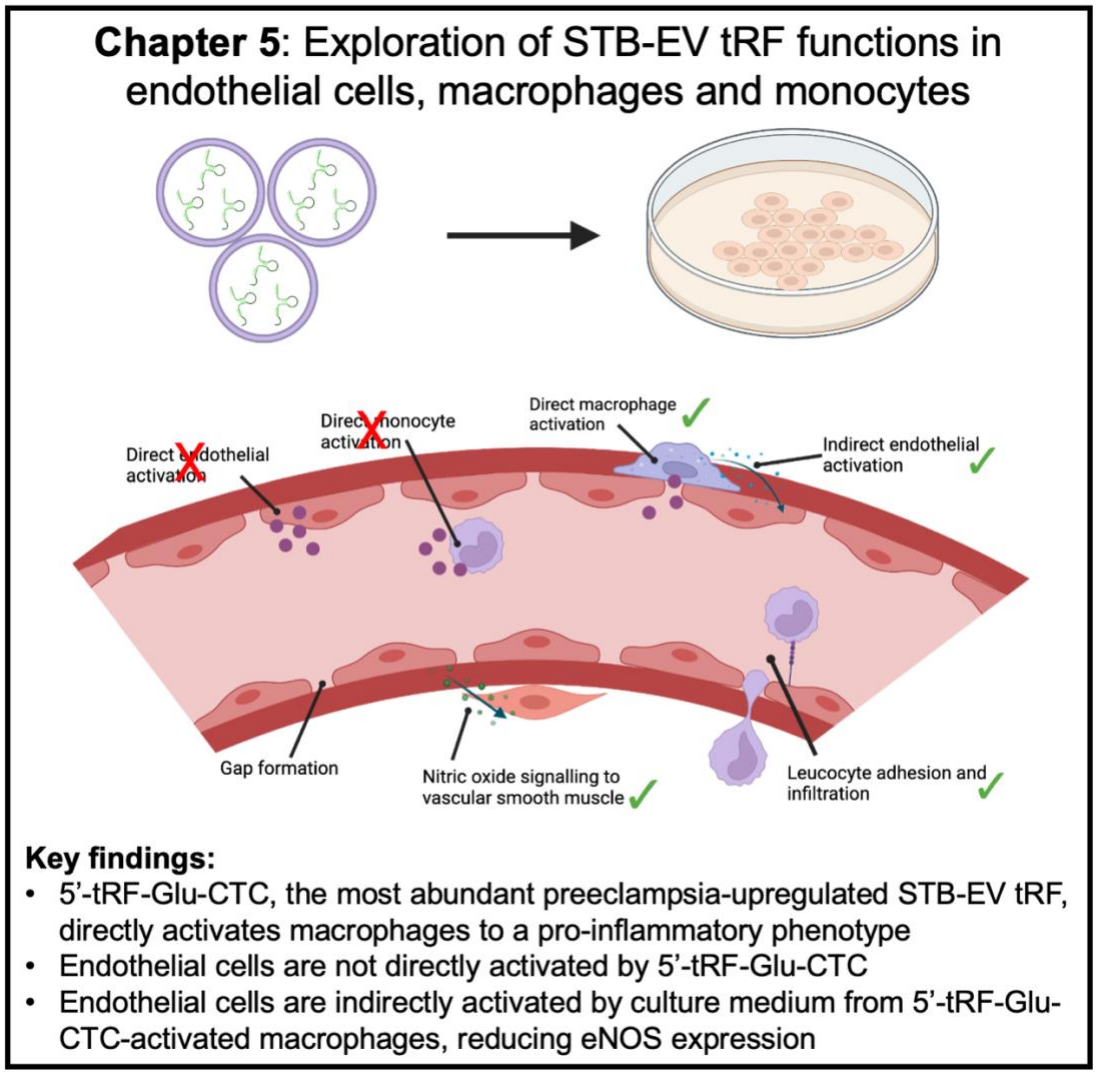


Figure 5-9 – Schematic figure summarising Chapter 5 key experiments and findings. Known functions of STB-EVs relating to endothelial activation and sterile inflammation are shown. Green ticks denote processes to which data suggest tRFs contribute; red crosses denote processes to which data suggest tRFs do not contribute.
Created with biorender.com with a publication licence under agreement number GR25PFDCLQ.

Chapter 6. General discussion

6.1. Context

This thesis represents the first comprehensive investigation of tRNA fragments (tRFs) in relation to preeclampsia. Just prior to commencing my DPhil, we had discovered 5'-tRFs accounted for the majority of small RNA (sRNA) in syncytiotrophoblast-derived extracellular vesicles (STB-EVs) in normal pregnancy[52]. 5'-tRFs are active signalling molecules, generated in response to stress[66,223]. I hypothesised that syncytiotrophoblast stress, a common feature in different phenotypes of preeclampsia[7], may cause differential expression of tRFs in STB-EVs. If exported into the maternal circulation, STB-EV tRFs could represent valuable biomarkers of preeclampsia. As signalling molecules, STB-EV tRFs might play a role in preeclampsia pathophysiology.

These hypotheses can be summarised in four overarching aims, answered by the four thesis data chapters:

1. Characterise tRFs in perfusion-derived STB-EVs in normal pregnancy and early-onset preeclampsia
2. Investigate syncytiotrophoblast tRFs in the maternal circulation
3. Evaluate tRFs as blood biomarkers in preeclampsia
4. Explore functional activity of STB-EV tRFs in endothelial cells, macrophages and monocytes

6.2. Summary of results

The main findings of my thesis are summarised in Figure 6-1.

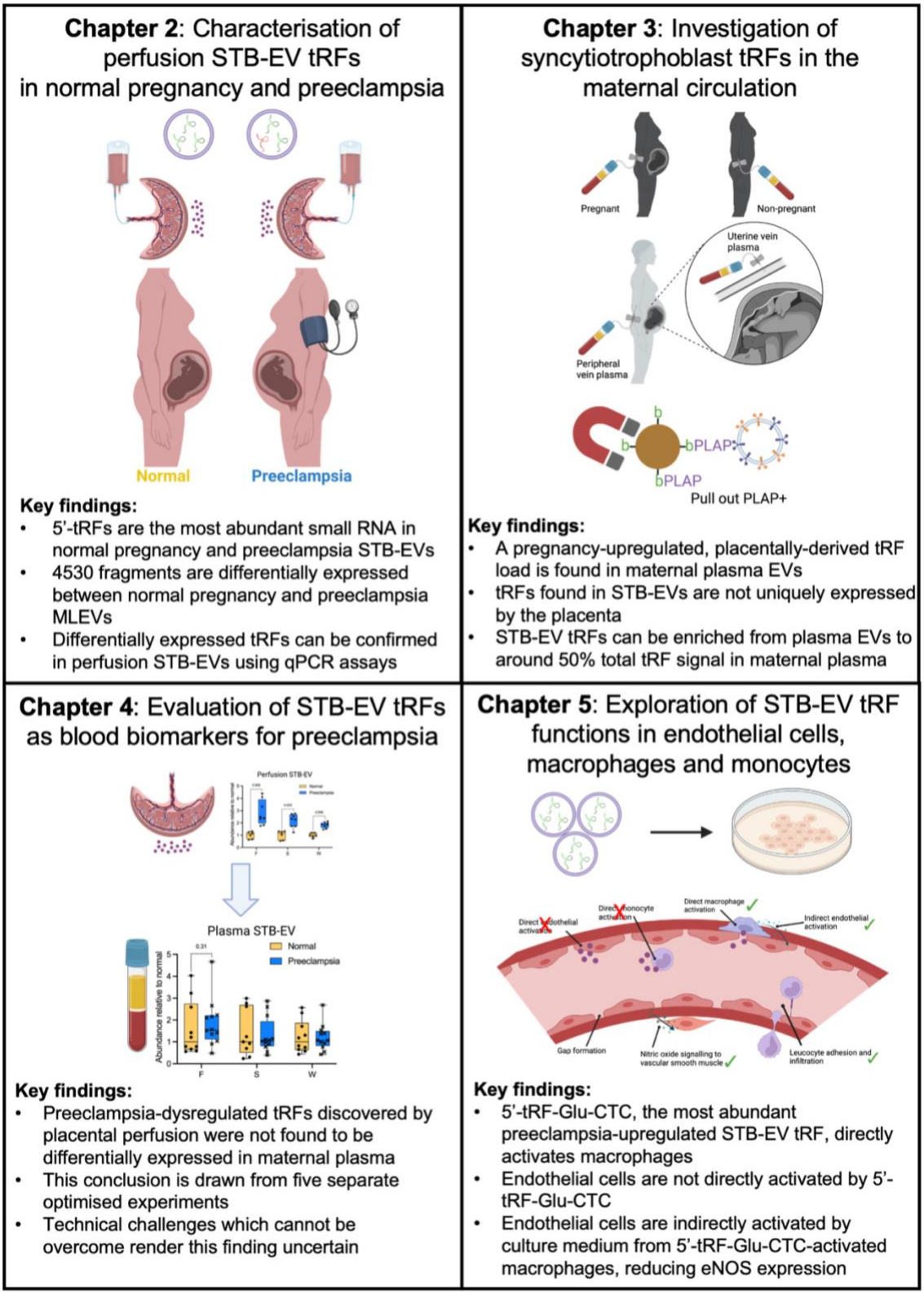


Figure 6-1 – Schematic figure summarising key results from this thesis.

Images created with biorender.com, with publication licences under agreement numbers ED25OVBN02, ZM25OVC7BE, QP25PAIYFL, GR25PFDCLQ.

Initially, I used placental perfusion to characterise sRNA expression in normal pregnancy and early-onset preeclampsia STB-EVs (Chapter 2). Using a placental model for discovery work allowed me to isolate the placental signal from other sources of sRNA in blood. Placental perfusion is considered the most physiological model to prepare STB-EVs (2.1.3). RNA sequencing analyses demonstrated the majority of sRNA in normal and preeclampsia STB-EVs were 30-34 nt in length and mapped to 5'-tRFs. Two approaches were taken to differential expression analysis. The DEUS approach retained unmapped fragments throughout the analysis, overcoming bioinformatic problems presented by sRNA. Comparisons of STB-EVs and placental tissue (from which they originate) identified over 50 000 differentially expressed fragments in both medium-large extracellular vesicles (MLEVs) and small extracellular vesicles (SEVs). Almost half of the differentially expressed reads were accounted for by the 12 most abundant fragments. A complex tRF fingerprint in normal pregnancy STB-EVs is dominated by a few highly abundant fragments.

Comparison of STB-EVs between preeclampsia and normal pregnancies identified 4530 differentially expressed fragments in MLEVs and 225 in SEVs. An independent analysis by our collaborators corroborated these findings; attention was focussed on MLEVs. qPCR assays using stem-loop reverse transcription primers were optimised for tRF detection. Four out of six differentially expressed targets investigated with qPCR in perfusion STB-EVs were validated.

Next, I quantified three abundant STB-EV tRFs in plasma extracellular vesicles (EVs) (Chapter 3). I discovered these tRFs were more abundant in normal pregnant than non-pregnant plasma EVs. I also found them to be more abundant in uterine than peripheral venous plasma EVs in normal pregnancy. Together these findings suggest a circulating placentally-derived tRF load. Notably these tRFs were also present in non-pregnant plasma EVs, demonstrating they are not uniquely expressed by the placenta. Moreover,

data suggested tRFs were also found outside EVs in plasma. In light of this, I iteratively optimised a technique to enrich STB-EVs from plasma. Ultimately, I achieved approximately 50% STB-EV enrichment (from a baseline of <1%), concluding that further optimisation would be unlikely to yield significant gain.

Having demonstrated that STB-EV tRFs were detectable in the maternal circulation, I investigated their potential as blood biomarkers for preeclampsia (Chapter 4). I found miRNAs which were dysregulated in preeclampsia STB-EVs from perfusion (Chapter 2) were reported to be differentially expressed in preeclampsia plasma/serum in prior publications. I investigated preeclampsia dysregulation of eight tRFs in plasma EVs, sequentially selecting novel targets to overcome potential shortcomings in the experimental approach. I also changed the experimental approach, both confining investigation to STB-EVs enriched from plasma as well as simplifying RNA isolation to look at whole plasma. A miRNA target from the same perfusion analysis was verified in these experiments as being differentially expressed between normal and diseased samples. However, across five experiments, no differences were seen in tRF expression between preeclampsia and normal plasma samples. This conclusion may be undermined by technical problems which cannot be overcome at present.

Finally, I investigated the functional activity of preeclampsia-dysregulated STB-EV tRFs (Chapter 5). EV-bound tRFs had no apparent effect on endothelial cell proliferation, NF-κB migration, adhesion molecules or eNOS expression. In contrast, EV-bound tRFs directly activated macrophages (but not monocytes), causing expression of pro-inflammatory cytokines. EV-bound tRF activation of macrophages resulted in indirect activation of endothelial cells, with increased expression of cell adhesion molecules and reduced expression of nitric oxide synthase. These actions, in response to a preeclampsia-upregulated tRF (identified in Chapter 2), are consistent with known actions

of preeclampsia STB-EVs as well as our existing understanding of preeclampsia pathophysiology.

6.3. Synthesis of results

When considered together, I propose the findings of this thesis contribute two original concepts to the field. Additionally, the findings collectively create one significant inconsistency. These three concepts are discussed below.

6.3.1. STB-EV tRFs as placental endocrine signals

5'-tRFs are emerging as important regulatory signals across disciplines. In breast cancer, intracellular expression of a cysteine 5'-tRF is upregulated in cell lines with greater metastatic capacity[109]. Upregulation of this 5'-tRF was shown to be necessary for metastatic lung colonisation. In immunology, T-cell activation triggers release of specific 5'-tRFs in EVs, proposed to act in a negative feedback loop as autocrine inhibitors of T-cell activation[77]. Mycobacterial infection of human macrophages triggers expression of various 5'-tRFs[76]. These 5'-tRFs are packaged into EVs, where they act in an autocrine and paracrine manner to activate Toll-like receptor 7.

Pregnancy provides a unique opportunity to investigate 5'-tRFs at a whole-organ level. The placenta is expelled during parturition and can be studied intact *ex-vivo*. Additionally, the vascular access afforded by caesarean section means findings from placental perfusion can be validated *in-vivo* by comparing expression in uterine and peripheral venous blood.

Using these approaches, I have demonstrated:

1. Differential expression of STB-EV tRFs in preeclampsia
2. A pregnancy-specific, placentally-derived load of EV-bound 5'-tRFs in the maternal circulation

3. The most abundant preeclampsia-upregulated 5’-tRF triggers inflammation in potentially distant macrophages and indirectly activates endothelial cells.

Together these findings suggest STB-EV 5’-tRFs are placental endocrine signals in preeclampsia, linking syncytiotrophoblast stress with maternal symptoms in preeclampsia (Figure 6-2). This novel 5’-tRF function, distant from the site of production, has implications for other disciplines studying their biology.

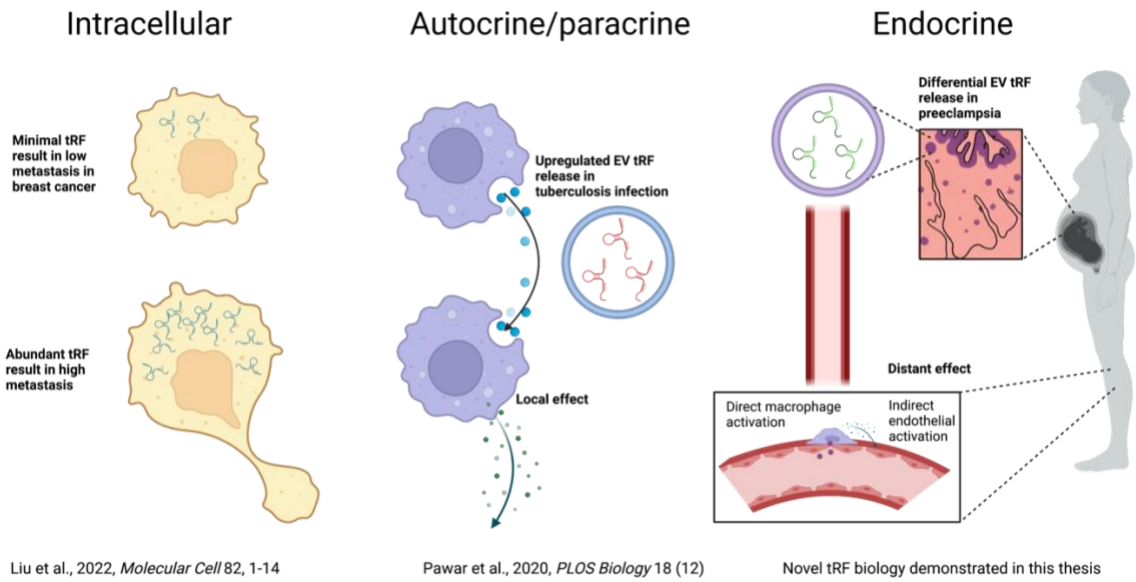


Figure 6-2 – Schematic figure highlighting the novelty of tRFs as endocrine signals. Created with biorender.com with a publication licence under agreement number QN25PP8OER.

6.3.2. STB-EV tRFs as molecular mediators of preeclampsia

Preeclampsia is a complex placental syndrome with many causes and a variable phenotype[4]. Clinical features include hypertension, proteinuria, hepatic inflammation, pulmonary oedema, cerebral oedema and intravascular coagulopathy. These features can be unified at a cellular level by maternal sterile inflammation and consequent endothelial dysfunction with gap formation resulting in vascular leakage and impaired nitric oxide signalling[23,24]. A point of convergence in preeclampsia pathophysiology is stress in the syncytiotrophoblast[19]. The link between syncytiotrophoblast stress and maternal symptoms, likely through blood-borne factors, is incompletely characterised[7]. Soluble fms-like tyrosine kinase-1 (sFlt-1) and placental growth factor (PlGF) are important syncytiotrophoblast stress signals which contribute to the preeclamptic syndrome[215]. Excess sFlt-1 sensitises endothelial cells to pro-inflammatory cytokines[224]. Altered STB-EV release, also a contributor to the pathophysiology of preeclampsia, remains underexplored[41].

In cell culture experiments, STB-EVs have been found to trigger cellular changes which correlate with preeclampsia pathophysiology. STB-EVs activate macrophages to a pro-inflammatory phenotype[209,210]. STB-EVs impair endothelial cell proliferation, increase NF-κB activation, reduce eNOS expression and nitric oxide levels[79,85,189,190]. STB-EVs are complex microparticles containing a variety of proteins, RNA, DNA and lipids. The specific molecules which mediate the effects of STB-EVs relevant to preeclampsia are not known.

In this thesis I have discovered:

1. Differential expression of specific tRFs within STB-EVs in preeclampsia
2. These specific dysregulated tRFs were found in STB-EVs in the maternal circulation, where they have been shown to be placentally-derived
3. When packaged in EVs, 5'-tRF-Glu-CTC (the most abundant preeclampsia-upregulated tRF), triggered pro-inflammatory changes in macrophages, indirectly activating endothelial cells, consistent with the pathophysiology of preeclampsia.

Considered as one, these findings point to 5'-tRFs as a new class of molecule which may mediate actions of STB-EVs in preeclampsia, adding to our understanding of the disease mechanisms (Figure 6-3). This novel contribution opens further avenues of investigation: the actions of other tRFs and sRNA within STB-EVs warrant investigation. The spectrum of STB-EV tRFs may work in concert to dysregulate distant maternal organs in preeclampsia.

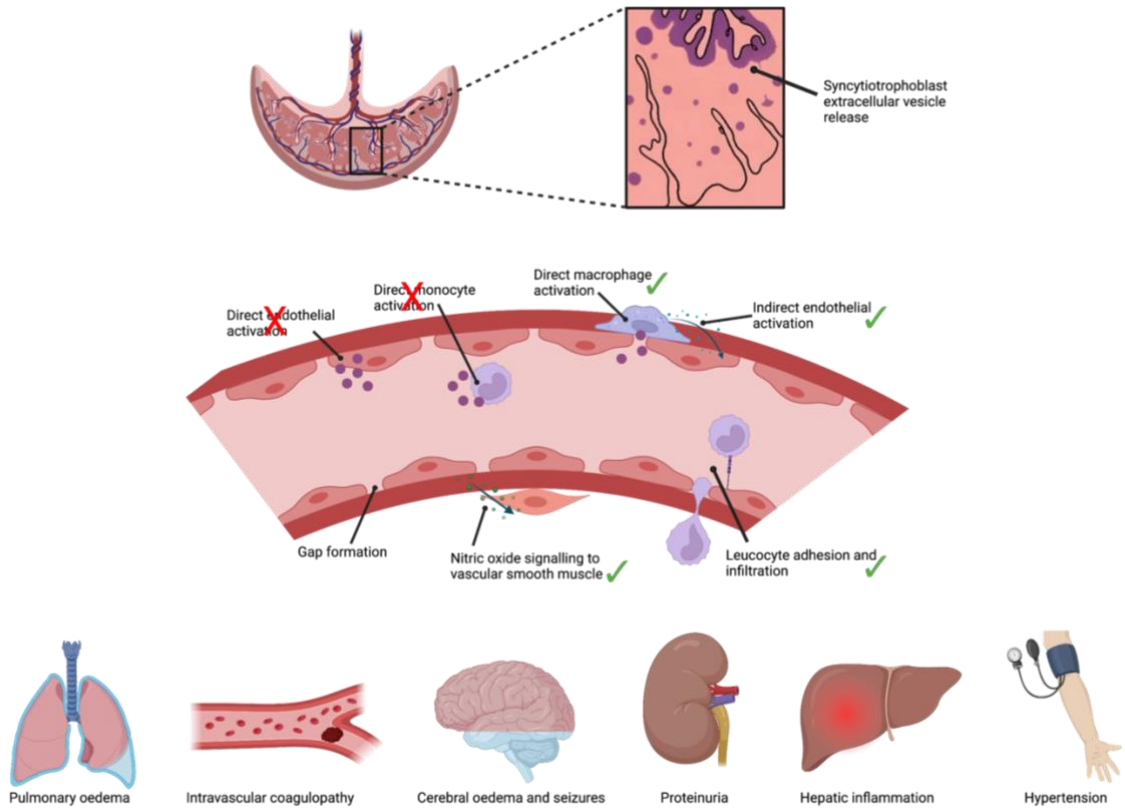


Figure 6-3 – Schematic figure highlighting the novelty of tRFs as molecular mediators of preeclampsia pathophysiology.

Known functions of STB-EVs are labelled in the schematic blood vessel. Green ticks denote actions attributable to STB-EV tRFs; red crosses denote actions not attributable to STB-EV tRFs. Created with biorender.com with a publication licence under agreement number SX25PP941E.

6.3.3. Preeclampsia STB-EV tRF dysregulation in plasma

Preeclampsia plasma tRF expression represents an important inconsistency in the data generated in this thesis. 4530 sRNA fragments, mostly tRFs, were found to be differentially expressed in preeclampsia perfusion STB-EVs. These findings from RNA sequencing were corroborated in perfusion STB-EVs by qPCR. The most abundant differentially expressed STB-EV tRFs were present in the maternal circulation and some of this signal was placentally-derived. A preeclampsia-upregulated tRF activates macrophages and may indirectly alter endothelial function and eNOS expression. Yet STB-EV tRFs were not found to be differentially expressed in maternal plasma.

Some possible confounding factors to account for this disparity can be excluded: sample selection bias thanks to control miRNA data, failure of EV isolation techniques to adequately quantitate thanks to differences seen in Chapter 3, differential STB-EV release in preeclampsia thanks to selection of upregulated targets. Other potential factors cannot be entirely overcome: expression of the same tRFs in plasma but outside EVs; expression of the same tRFs in non-placental plasma EVs; random error introduced during RNA isolation and quantification; small magnitude initial differences between preeclampsia and normal pregnancy. Data from Chapters 2, 3 and 5 are all internally consistent. Their inconsistency with findings in Chapter 4 cannot be answered with the existing data. Differential expression of tRFs in plasma STB-EVs is still plausible. Technical limitations mean a conclusive experiment is not obvious.

In spite of this concern, I remain convinced that tRFs play an important role in pregnancy and preeclampsia for the following reasons:

1. Strong tRF enrichment in STB-EVs compared to the tissue of origin demonstrates significant energy is expended by the syncytiotrophoblast to package and export them. This process would likely not be evolutionarily conserved if it did not offer some advantage to the individual or species.

2. Only the 5'-tRF is found within STB-EVs. The specificity of this packaging strongly suggests that it is likely to have a role beyond disposal of whole tRNAs.
3. Preeclampsia-dysregulated STB-EV tRFs have functional effects which match disease progression in preeclampsia. This coincidence is unlikely if they do not play a role in preeclampsia pathophysiology.
4. tRFs have a wide variety of known functions, some of which are wholly dependent on their precise structure. Whilst this makes their importance challenging to unpick experimentally, the degree of complexity contained within an STB-EV tRF signal matches the heterogeneity seen in preeclampsia, making tRFs biologically plausible contributors to preeclampsia mechanism.

6.4. Findings in context

The findings of each chapter are considered in the context of the literature in the discussion section of the corresponding chapter. In this section I will consider how the syntheses of results compare to the established literature.

The discovery that EV-bound tRFs can act as placental endocrine signals, distant from the site of synthesis, has not been reported before. A study in colorectal cancer has found that two EV-bound tRFs produced by cancer tissues are upregulated in plasma exosomes from patients with the disease[162]. The authors demonstrated a mechanism of action for these tRFs which was local to the site of release. The implication is that EV-bound tRFs act in a paracrine manner, but also spill into the circulation. A manuscript investigating breast cancer tRFs as plasma biomarkers also identified differential expression of two EV-bound tRFs in plasma exosomes[75]. This study predicted target genes for these tRFs, but did not investigate whether they had functional actions or consider their site of action. Other studies already described in 6.3.1 have demonstrated autocrine, paracrine and intracellular actions of tRFs[76,77,109]. Evidence which could support endocrine STB-EV miRNA signalling in preeclampsia has been published previously[49]. However, in this study

the authors did not isolate the action of specific miRNAs from the other components of STB-EVs. Moreover, there were no data presented to demonstrate differences in plasma STB-EV expression of these miRNAs in preeclampsia, which would be necessary to demonstrate circulatory transfer of miRNAs from site of release to site of action.

This thesis provides the first evidence that STB-EV tRFs act as molecular mediators of preeclampsia. It has been established in other fields that EV-bound tRFs contribute to disease pathophysiology (summarised in 1.2.4.2). Specifically, EV-bound tRFs alter macrophage function in tuberculosis infection and colorectal cancer[76,162]. T-cell activation is inhibited by EV-bound tRFs[77]. In the field of preeclampsia, as described above, there is evidence that STB-EV miRNAs alter endothelial cell gene expression[49]. Thus, it is highly biologically plausible that STB-EV tRFs contribute to preeclampsia pathophysiology; however, evidence to support this theory is entirely novel. The specificity of tRF actions demonstrated in Chapter 5 (directly activating macrophages but not endothelial cells) is consistent with both the complexity of the signal contained with STB-EVs[41], as well as the clinical heterogeneity of preeclampsia[9].

As discussed in 4.4, it is difficult to contextualise the conflict between perfusion and plasma STB-EV tRF expression data in preeclampsia. Studies in parallel disciplines where data from models do not correlate with plasma expression are unlikely to be published. One previously discussed colorectal cancer study where mechanistic experiments are corroborated by plasma data has been published[162].

6.5. Thesis limitations and future work

With the benefit of knowing the results within this thesis, it is possible to appreciate a number of limitations that could have been avoided by alternative approaches from the outset.

The decision to undertake the tRF discovery experiments using placental perfusion as a model is both a strength and a weakness. A major advantage is that the tRFs uncovered are incontrovertibly placental in origin. However, the experimental system remains a model with greater cellular stresses than are seen *in-vivo*. It was not possible to gestationally match the early-onset preeclampsia and normal placentas, creating an important confounder between groups. Differential vesicle release in preeclampsia could not be accounted for.

The small sample sizes throughout this thesis, paired with a broad case definition in preeclampsia, are important shortcomings. Preeclampsia is a variable syndrome with multiple aetiologies and phenotypes, all of which likely have different underlying pathophysiology[7]. The field as a whole has failed to classify and subdivide preeclampsia in a manner which may cast light on the mechanistic differences within the disease[9]. My assumption in designing this study was that I might avoid disease heterogeneity compromising our findings, because I was studying STB-EVs; syncytiotrophoblast stress is thought to unify cases of preeclampsia[19]. The discovered miRNA targets, validated both in the literature and in plasma experiments offer a suggestion this weakness did not overwhelm the study design. Nevertheless, if the biology underlying preeclampsia were better understood, I might have been able to select a disease subtype to study which could have resulted in more uniform tRF expression and successful plasma validation.

RNA sequencing was initially conducted with the intention of investigating miRNAs in preeclampsia; tRFs were an unexpected finding. Consequently, sequencing techniques were not adapted to account for the post-transcriptional modifications carried by many tRFs. cP-RNA sequencing involves pre-treatment of 3'-cyclic phosphate moieties to remove the cyclic phosphate and enable detection of these tRFs by standard RNA sequencing[119]. If this study were planned again, I would perform both standard and cP-RNA sequencing to more completely characterise tRFs.

In planning this project, I did not anticipate that specific preeclampsia-dysregulated tRFs would be so widely expressed by different tissues. The field is an emerging one; publications are increasing exponentially, and so are the reports of tRF dysregulation across diseases and species. In retrospect, it may have been better to fully phenotype which tRFs are placentally enriched *in-vivo* by sequencing paired uterine and peripheral venous plasma samples. This would have allowed differentially expressed preeclampsia targets to be filtered so that the most placentally-enriched could be investigated in plasma. This strategy may have avoided the inconclusive results seen in Chapter 4.

Criticism could be levelled at the decision to proceed and investigate tRFs as biomarkers despite: a) the small absolute differences between preeclampsia and healthy pregnancies in the perfusion data, b) clear evidence that targets were abundant in non-placental EVs and in extravesicular RNA from plasma. Acknowledging the interest in tRFs as novel targets, the miRNAs uncovered by perfusion had greater biomarker potential: many were placentally unique and differences between preeclampsia and normal were greater. However, the miRNA targets found were not original; tRFs have never been explored in preeclampsia plasma before.

Studies modelling tRF function relevant to preeclampsia were necessarily simplistic; a common problem in molecular biology. STB-EVs are complex particles containing a variety of RNA, DNA, proteins and lipids. It was decided that the effect of one tRF was best studied in isolation, to avoid misattributing the effects of other molecules within STB-EVs. It may be that specific tRFs act in concert with other tRFs, or even other molecules, to have effects which I have not yet appreciated. Unpicking this biology is extraordinarily complex.

Future work could proceed in a number of different directions:

- A gestational profile of STB-EV tRF release might shed light on whether the preeclampsia perfusion differences are truly confounded by gestational age.
- A more comprehensive phenotype of the effect of 5'-tRF-Glu-CTC on macrophages could be achieved through multi-omic studies of treated cells.
- Functional effects of the majority of preeclampsia-dysregulated tRFs discovered in this thesis are yet to be investigated. A wider screen may identify lower abundance molecules with highly potent actions.
- The effect of preeclampsia-dysregulated tRFs remains uninvestigated in the majority of target tissues in preeclampsia. Studies of tRF effects on renal epithelium, the blood brain barrier, hepatic sinusoids, platelets and the coagulation cascade could demonstrate other important mechanistic roles for tRFs in preeclampsia.
- There is evidence that 5'-tRFs influence DNA methylation[60]. Preeclampsia has long term effects on maternal health, such as increased cardiovascular risk. Molecular mechanisms for this are uncertain and it would be interesting to investigate whether 5'-tRFs modify endothelial cell epigenetics.
- tRFs are generated in response to stress. Studying the regulatory mechanisms by which STB-EV tRFs are produced may identify unifying pathways earlier in disease pathophysiology, opening opportunities for diagnostics and intervention.
- Given the immunomodulatory function of tRFs, it would be interesting to investigate their expression in the invading placenta. The origins of preeclampsia can be easily traced to the success of placentation[225].
- Cellular targeting of circulating STB-EVs may be critical to any functional effects. Proteomic studies seeking proteins known to target specific cell types might allow STB-EVs to be phenotyped by their destination tissue.
- An assessment of differences between uterine vein, peripheral vein and non-pregnant plasma expression of sRNA might identify novel placentally-derived molecules which

play a role in feto-maternal signalling, including tRFs. These data could be compared to preeclampsia plasma samples, so that only placental targets can be investigated. Using *ex-vivo* samples would circumvent the need for experimental models. Combining uterine/peripheral and preeclampsia/normal samples would overcome confounding from non-placental correlates of preeclampsia, which are less likely to be causal and confound some existing publications[152,153].

6.6. Concluding remarks

Cumulatively, this thesis presents a body of work which describes the expression of tRFs in preeclampsia STB-EVs, evaluates their biomarker potential and explores possible functions. There is significant novelty, both in the experimental and analytical approaches taken. Two major original contributions are offered: evidence for tRF endocrine signalling and for STB-EV tRFs as molecular mediators of preeclampsia pathophysiology. This project has opened a new field for investigation: future work will proceed in diverse directions to unpick the role of syncytiotrophoblast tRF signalling in preeclampsia.

References

1. Brown, M. A. *et al.* Hypertensive disorders of pregnancy: ISSHP classification, diagnosis, and management recommendations for international practice. *Hypertension* **72**, 24–43 (2018).
2. Abalos, E., Cuesta, C., Grosso, A. L., Chou, D. & Say, L. Global and regional estimates of preeclampsia and eclampsia: A systematic review. *European Journal of Obstetrics and Gynecology and Reproductive Biology* vol. 170 1–7 (2013).
3. Say, L. *et al.* Global causes of maternal death: a WHO systematic analysis. *Lancet. Glob. Heal.* **2**, e323-33 (2014).
4. Chappell, L. C., Cluver, C. A., Kingdom, J. & Tong, S. Pre-eclampsia. *Lancet* **398**, 341–354 (2021).
5. von Dadelszen, P. *et al.* Prediction of adverse maternal outcomes in pre-eclampsia: development and validation of the fullPIERS model. *Lancet (London, England)* **377**, 219–227 (2011).
6. Aughey, H. *et al.* Iatrogenic and spontaneous preterm birth in England: A population-based cohort study. *BJOG* **130**, 33–41 (2023).
7. Redman, C. W. G., Staff, A. C. & Roberts, J. M. Syncytiotrophoblast stress in preeclampsia: the convergence point for multiple pathways. *American Journal of Obstetrics and Gynecology* vol. 226 S907–S927 (2022).
8. von Dadelszen, P., Magee, L. A. & Roberts, J. M. Subclassification of preeclampsia. *Hypertens. pregnancy* **22**, 143–148 (2003).
9. Roberts, J. M., Rich-Edwards, J. W., McElrath, T. F., Garmire, L. & Myatt, L. Subtypes of Preeclampsia: Recognition and Determining Clinical Usefulness. *Hypertens. (Dallas, Tex. 1979)* **77**, 1430–1441 (2021).
10. National Institute for Health and Care Excellence. Hypertension in pregnancy: diagnosis and management. *[NG133]* https://www.nice.org.uk/guidance/ng133

(2019).

11. Duley, L., Meher, S., Hunter, K. E., Seidler, A. L. & Askie, L. M. Antiplatelet agents for preventing pre-eclampsia and its complications. *Cochrane Database Syst. Rev.* (2019) doi:10.1002/14651858.CD004659.pub3.
12. National Institute for Health and Care Excellence (NICE). *Antenatal care [NG201]*. https://www.nice.org.uk/guidance/ng201 (2021).
13. National Institute for Health and Care Excellence (NICE). *PlGF-based testing to help diagnose suspected pre-eclampsia [DG 49]*. https://www.nice.org.uk/guidance/dg49 (2022).
14. Zeisler, H. *et al.* Predictive Value of the sFlt-1:PlGF Ratio in Women with Suspected Preeclampsia. *N. Engl. J. Med.* **374**, 13–22 (2016).
15. Cerdeira, A. S. *et al.* Randomized Interventional Study on Prediction of Preeclampsia/ Eclampsia in Women With Suspected Preeclampsia INSPIRE. *Hypertension* **74**, (2019).
16. Wu, P. *et al.* Preeclampsia and Future Cardiovascular Health: A Systematic Review and Meta-Analysis. *Circ. Cardiovasc. Qual. Outcomes* **10**, (2017).
17. Wright, D., Syngelaki, A., Akolekar, R., Poon, L. C. & Nicolaides, K. H. Competing risks model in screening for preeclampsia by maternal characteristics and medical history. *Am. J. Obstet. Gynecol.* **213**, 62.e1-62.e10 (2015).
18. Redman, C. W. G. Pre-eclampsia and the placenta. *Placenta* **12**, 301–308 (1991).
19. Magee, L. A., Nicolaides, K. H. & von Dadelszen, P. Preeclampsia. *N. Engl. J. Med.* **386**, 1817–1832 (2022).
20. Burton, G. J. & Fowden, A. L. The placenta: a multifaceted, transient organ. *Philos. Trans. R. Soc. London. Ser. B, Biol. Sci.* **370**, 20140066 (2015).
21. Burton, G. J., Woods, A. W., Jauniaux, E. & Kingdom, J. C. P. Rheological and Physiological Consequences of Conversion of the Maternal Spiral Arteries for Uteroplacental Blood Flow during Human Pregnancy. *Placenta* **30**, 473–482 (2009).

22. Stevens, D. U., Al-Nasiry, S., Bulten, J. & Spaanderman, M. E. A. Decidual vasculopathy in preeclampsia: lesion characteristics relate to disease severity and perinatal outcome. *Placenta* **34**, 805–809 (2013).

23. Redman, C. W. G., Sacks, G. P. & Sargent, I. L. Preeclampsia: An excessive maternal inflammatory response to pregnancy. *Am. J. Obstet. Gynecol.* **180**, 499–506 (1999).

24. Roberts, J. M. *et al.* Preeclampsia: An endothelial cell disorder. *Am. J. Obstet. Gynecol.* **161**, 1200–1204 (1989).

25. Ness, R. B. & Roberts, J. M. Heterogeneous causes constituting the single syndrome of preeclampsia: A hypothesis and its implications. *Am. J. Obstet. Gynecol.* **175**, 1365–1370 (1996).

26. Redman, C. W. G. & Staff, A. C. Preeclampsia, biomarkers, syncytiotrophoblast stress, and placental capacity. *Am. J. Obstet. Gynecol.* **213**, S9.e1, S9-11 (2015).

27. Obiri, D. *et al.* Histopathological lesions and exposure to Plasmodium falciparum infections in the placenta increases the risk of preeclampsia among pregnant women. *Sci. Rep.* **10**, 8280 (2020).

28. Zaki, M., Greenwood, C. & Redman, C. W. G. The spontaneous reversal of pre-eclampsia associated with parvovirus-induced hydrops and the placental theory of pre-eclampsia: a case report. *BJOG* **110**, 1125–1126 (2003).

29. Staff, A. C. The two-stage placental model of preeclampsia: An update. *J. Reprod. Immunol.* **134**–**135**, 1–10 (2019).

30. Maynard, S. E. *et al.* Excess placental soluble fms-like tyrosine kinase 1 (sFlt1) may contribute to endothelial dysfunction, hypertension, and proteinuria in preeclampsia. *J. Clin. Invest.* **111**, 649–58 (2003).

31. He, H. *et al.* Vascular endothelial growth factor signals endothelial cell production of nitric oxide and prostacyclin through flk-1/KDR activation of c-Src. *J. Biol. Chem.* **274**, 25130–25135 (1999).

32. Yang, J. C. *et al.* A randomized trial of bevacizumab, an anti-vascular endothelial

growth factor antibody, for metastatic renal cancer. *N. Engl. J. Med.* **349**, 427–434 (2003).

33. Levine, R. J. *et al.* Circulating Angiogenic Factors and the Risk of Preeclampsia. *N. Engl. J. Med.* **350**, 672–683 (2004).
34. Thadhani, R. *et al.* Removal of soluble fms-like tyrosine kinase-1 by dextran sulfate apheresis in preeclampsia. *J. Am. Soc. Nephrol.* **27**, 903–913 (2016).
35. Winkler, K. *et al.* Treatment of very preterm preeclampsia via heparin-mediated extracorporeal LDL-precipitation (H.E.L.P.) apheresis: The Freiburg preeclampsia H.E.L.P.-Apheresis study. *Pregnancy Hypertens.* **12**, 136–143 (2018).
36. Cerdeira, A. S., Agrawal, S., Staff, A. C., Redman, C. W. & Vatish, M. Angiogenic factors: potential to change clinical practice in pre-eclampsia? *BJOG: An International Journal of Obstetrics and Gynaecology* vol. 125 1389–1395 (2018).
37. Théry, C. *et al.* Minimal information for studies of extracellular vesicles 2018 (MISEV2018): a position statement of the International Society for Extracellular Vesicles and update of the MISEV2014 guidelines. *J. Extracell. Vesicles* **7**, (2018).
38. Smith, N. C., Brush, M. G. & Luckett, S. Preparation of human placental villous surface membrane. *Nature* **252**, 302–3 (1974).
39. Lüscher, B. P. *et al.* Placental glucose transporter (GLUT)-1 is down-regulated in preeclampsia. *Placenta* **55**, 94–99 (2017).
40. Knight, M., Redman, C. W. G., Linton, E. A. & Sargent, I. L. Shedding of syncytiotrophoblast microvilli into the maternal circulation in pre-eclamptic pregnancies. *BJOG An Int. J. Obstet. Gynaecol.* **105**, 632–640 (1998).
41. Cooke, W. R., Jones, G. D., Redman, C. W. G. & Vatish, M. Syncytiotrophoblast Derived Extracellular Vesicles in Relation to Pre-eclampsia. *Matern. Med.* (2021).
42. Gill, M. *et al.* Placental Syncytiotrophoblast-Derived Extracellular Vesicles Carry Active NEP (Neprilysin) and Are Increased in Preeclampsia. *Hypertension* **73**, 1112–1119 (2019).
43. Bayes-Genis, A., Barallat, J. & Richards, A. M. A Test in Context: Neprilysin:

Function, Inhibition, and Biomarker. *J. Am. Coll. Cardiol.* **68**, 639–653 (2016).

44. Gardiner, C. *et al.* Syncytiotrophoblast microvesicles released from pre-eclampsia placentae exhibit increased tissue factor activity. *PLoS One* **6**, (2011).

45. Motta-Mejia, C. *et al.* Placental Vesicles Carry Active Endothelial Nitric Oxide Synthase and Their Activity is Reduced in Preeclampsia. *Hypertension* **70**, 372–381 (2017).

46. Wei, J. *et al.* Placental trophoblast debris mediated feto-maternal signalling via small RNA delivery: Implications for preeclampsia. *Sci. Rep.* **7**, 1–12 (2017).

47. Salomon, C. *et al.* Placental Exosomes as Early Biomarker of Preeclampsia: Potential Role of Exosomal MicroRNAs Across Gestation. *J. Clin. Endocrinol. Metab.* **102**, 3182–3194 (2017).

48. Srinivasan, S. *et al.* Discovery and Verification of Extracellular miRNA Biomarkers for Non-invasive Prediction of Pre-eclampsia in Asymptomatic Women. *Cell Reports Med.* **1**, 100013 (2020).

49. Cronqvist, T. *et al.* Syncytiotrophoblast derived extracellular vesicles transfer functional placental miRNAs to primary human endothelial cells. *Sci. Rep.* **7**, 1–14 (2017).

50. Shen, L. *et al.* Placenta-associated serum exosomal miR-155 derived from patients with preeclampsia inhibits eNOS expression in human umbilical vein endothelial cells. *Int. J. Mol. Med.* **41**, 1731–1739 (2018).

51. Awoyemi, T. Characterisation of protein and RNA expressed in syncytiotrophoblast membrane extracellular vesicles (STB-EVs) in preeclampsia. (University of Oxford, 2022).

52. Cooke, W. R. *et al.* Maternal circulating syncytiotrophoblast-derived extracellular vesicles contain biologically active 5’-tRNA halves. *Biochem. Biophys. Res. Commun.* **518**, 107–113 (2019).

53. Crick, F. Central Dogma of Molecular Biology. *Nature* **227**, 561–563 (1970).

54. Orellana, E. A., Siegal, E. & Gregory, R. I. tRNA dysregulation and disease. *Nat.*

Rev. Genet. **23**, 651–664 (2022).

55. Borek, E. *et al.* High turnover rate of transfer RNA in tumor tissue. *Cancer Res.* **37**, 3362–3366 (1977).

56. Yamasaki, S., Ivanov, P., Hu, G. F. & Anderson, P. Angiogenin cleaves tRNA and promotes stress-induced translational repression. *J. Cell Biol.* **185**, 35–42 (2009).

57. Fu, H. *et al.* Stress induces tRNA cleavage by angiogenin in mammalian cells. *FEBS Lett.* **583**, 437–442 (2009).

58. Di Fazio, A. & Gullerova, M. An old friend with a new face: tRNA-derived small RNAs with big regulatory potential in cancer biology. *Br. J. Cancer* 1–11 (2023).

59. Magee, R. & Rigoutsos, I. On the expanding roles of tRNA fragments in modulating cell behavior. *Nucleic Acids Res.* **48**, 9433–9448 (2020).

60. Zhang, X. *et al.* IL-4 Inhibits the Biogenesis of an Epigenetically Suppressive PIWI-Interacting RNA To Upregulate CD1a Molecules on Monocytes/Dendritic Cells. *J. Immunol.* **196**, 1591–1603 (2016).

61. Yu, X. *et al.* tRNA-derived fragments: Mechanisms underlying their regulation of gene expression and potential applications as therapeutic targets in cancers and virus infections. *Theranostics* vol. 11 461–469 (2020).

62. Chan, P. P. & Lowe, T. M. GtRNAdb 2.0: An expanded database of transfer RNA genes identified in complete and draft genomes. *Nucleic Acids Res.* **44**, D184–D189 (2016).

63. Griffiths-Jones, S., Grocock, R. J., van Dongen, S., Bateman, A. & Enright, A. J. miRBase: microRNA sequences, targets and gene nomenclature. *Nucleic Acids Res.* **34**, D140-4 (2006).

64. Loher, P., Telonis, A. G. & Rigoutsos, I. MINTmap: fast and exhaustive profiling of nuclear and mitochondrial tRNA fragments from short RNA-seq data. *Sci. Rep.* **7**, 41184 (2017).

65. Lyons, S. M., Fay, M. M. & Ivanov, P. The role of RNA modifications in the regulation of tRNA cleavage. *FEBS Letters* vol. 592 2828–2844 (2018).

66. Li, G. *et al.* Distinct Stress-Dependent Signatures of Cellular and Extracellular tRNA-Derived Small RNAs. *Adv. Sci.* **9**, (2022).

67. Liu, D. S. K., Yang, Q. Z. C., Asim, M., Krell, J. & Frampton, A. E. The Clinical Significance of Transfer RNAs Present in Extracellular Vesicles. *Int. J. Mol. Sci.* **23**, (2022).

68. Balatti, V. *et al.* tsRNA signatures in cancer. *Proc. Natl. Acad. Sci. U. S. A.* **114**, 8071–8076 (2017).

69. Xue, M. *et al.* Serum tRNA-derived small RNAs as potential novel diagnostic biomarkers for pancreatic ductal adenocarcinoma. *Am. J. Cancer Res.* **11**, 837–848 (2021).

70. Jia, Y., Tan, W. & Zhou, Y. Transfer RNA-derived small RNAs: potential applications as novel biomarkers for disease diagnosis and prognosis. *Ann. Transl. Med.* **8**, 1092–1092 (2020).

71. Srinivasan, S. *et al.* Small RNA Sequencing across Diverse Biofluids Identifies Optimal Methods for exRNA Isolation. *Cell* **177**, 446-462.e16 (2019).

72. Buschmann, D. *et al.* Evaluation of serum extracellular vesicle isolation methods for profiling miRNAs by next-generation sequencing. *J. Extracell. Vesicles* **7**, (2018).

73. Meng, L. *et al.* Transfer RNA-derived fragment tRF-28-QSZ34KRQ590K in plasma exosomes may be a potential biomarker for atopic dermatitis in pediatric patients. *Exp. Ther. Med.* **21**, 489 (2021).

74. Lu, S. *et al.* A novel tRNA-derived fragment tRF-3022b modulates cell apoptosis and M2 macrophage polarization via binding to cytokines in colorectal cancer. *J. Hematol. Oncol.* **15**, 176 (2022).

75. Wang, J. *et al.* Plasma tRNA Fragments Derived from 5’ Ends as Novel Diagnostic Biomarkers for Early-Stage Breast Cancer. *Mol. Ther. Nucleic Acids* **21**, 954–964 (2020).

76. Pawar, K., Shigematsu, M., Sharbati, S. & Kirino, Y. Infection-induced 5’-half molecules of tRNAHisGUG activate Toll-like receptor 7. *PLoS Biol.* **18**, (2020).

77. Chiou, N.-T., Kageyama, R. & Ansel, K. M. Selective Export into Extracellular Vesicles and Function of tRNA Fragments during T Cell Activation. *Cell Rep.* **25**, 3356-3370.e4 (2018).

78. Johnsen, K. B., Gudbergsson, J. M., Andresen, T. L. & Simonsen, J. B. What is the blood concentration of extracellular vesicles? Implications for the use of extracellular vesicles as blood-borne biomarkers of cancer. *Biochim. Biophys. Acta - Rev. Cancer* **1871**, 109–116 (2019).

79. Smárason, A. K., Sargent, I. L., Starkey, P. M. & Redman, C. W. G. The effect of placental syncytiotrophoblast microvillous membranes from normal and pre-eclamptic women on the growth of endothelial cells in vitro. *BJOG An Int. J. Obstet. Gynaecol.* **100**, 943–949 (1993).

80. Eaton, B. M. & Oakey, M. P. Sequential preparation of highly purified microvillous and basal syncytiotrophoblast membranes in substantial yield from a single term human placenta: inhibition of microvillous alkaline phosphatase activity by EDTA. *Biochim. Biophys. Acta* **1193**, 85–92 (1994).

81. Tong, M. & Chamley, L. W. Isolation and Characterization of Extracellular Vesicles from Ex Vivo Cultured Human Placental Explants. in *Preeclampsia : Methods and Protocols* (eds. Murthi, P. & Vaillancourt, C.) 117–129 (Springer New York, 2018). doi:10.1007/978-1-4939-7498-6_9.

82. Simán, C. M., Sibley, C. P., Jones, C. J., Turner, M. A. & Greenwood, S. L. The functional regeneration of syncytiotrophoblast in cultured explants of term placenta. *Am. J. Physiol. Regul. Integr. Comp. Physiol.* **280**, R1116-22 (2001).

83. Southcombe, J., Tannetta, D., Redman, C. & Sargent, I. The Immunomodulatory Role of Syncytiotrophoblast Microvesicles. *PLoS One* **6**, e20245 (2011).

84. Dragovic, R. A. *et al.* Isolation of syncytiotrophoblast microvesicles and exosomes and their characterisation by multicolour flow cytometry and fluorescence Nanoparticle Tracking Analysis. *Methods* **87**, 64–74 (2015).

85. Gupta, A. K. *et al.* A comparative study of the effect of three different

syncytiotrophoblast micro-particles preparations on endothelial cells. *Placenta* **26**, 59–66 (2005).

86. Kandzija, N. *et al.* Placental extracellular vesicles express active dipeptidyl peptidase IV; levels are increased in gestational diabetes mellitus. *J. Extracell. Vesicles* **8**, (2019).

87. Shapiro, R., Riordan, J. F. & Vallee, B. L. Characteristic ribonucleolytic activity of human angiogenin. *Biochemistry* **25**, 3527–3532 (1986).

88. Shigematsu, M., Kawamura, T. & Kirino, Y. Generation of 2′,3′-Cyclic Phosphate-Containing RNAs as a Hidden Layer of the Transcriptome. *Front. Genet.* **9**, (2018).

89. Holmes, A. D., Howard, J. M., Chan, P. P. & Lowe, T. M. tRNA Analysis of eXpression (tRAX): A tool for integrating analysis of tRNAs, tRNA-derived small RNAs, and tRNA modifications. *bioRxiv* 2022.07.02.498565 (2022) doi:10.1101/2022.07.02.498565.

90. Liao, Y., Smyth, G. K. & Shi, W. featureCounts: an efficient general purpose program for assigning sequence reads to genomic features. *Bioinformatics* **30**, 923–930 (2013).

91. Southcombe, J., Tannetta, D., Redman, C. & Sargent, I. The Immunomodulatory Role of Syncytiotrophoblast Microvesicles. *PLoS One* **6**, e20245 (2011).

92. FASTQ files explained - Illumina Knowledge. https://knowledge.illumina.com/software/general-software/software-general-reference_material-list/000002211.

93. Illumina. Understanding Illumina Quality Scores. (2012).

94. Andrews, S. FastQC: a quality control tool for high throughput sequence data. *2010* https://www.bioinformatics.babraham.ac.uk/projects/fastqc/.

95. Ewels, P., Magnusson, M., Lundin, S. & Käller, M. MultiQC: Summarize analysis results for multiple tools and samples in a single report. *Bioinformatics* **32**, 3047–3048 (2016).

96. Bolger, A. M., Lohse, M. & Usadel, B. Trimmomatic: A flexible trimmer for Illumina

sequence data. *Bioinformatics* **30**, 2114–2120 (2014).

97. Martin, M. Cutadapt removes adapter sequences from high-throughput sequencing reads. *EMBnet.journal* **17**, 10 (2011).

98. Lee, B. T. *et al.* The UCSC Genome Browser database: 2022 update. *Nucleic Acids Res.* **50**, D1115–D1122 (2022).

99. Langmead, B. & Salzberg, S. L. Fast gapped-read alignment with Bowtie 2. *Nat. Methods* **9**, 357–359 (2012).

100. Love, M. I., Huber, W. & Anders, S. Moderated estimation of fold change and dispersion for RNA-seq data with DESeq2. *Genome Biol.* **15**, 550 (2014).

101. Jeske, T. *et al.* DEUS: An R package for accurate small RNA profiling based on differential expression of unique sequences. *Bioinformatics* **35**, 4834–4836 (2019).

102. Roberts, T. C., Coenen-Stass, A. M. L., Betts, C. A. & Wood, M. J. A. Detection and quantification of extracellular microRNAs in murine biofluids. *Biol. Proced. Online* **16**, 5 (2014).

103. Chen, C. *et al.* Real-time quantification of microRNAs by stem-loop RT-PCR. *Nucleic Acids Res.* **33**, e179–e179 (2005).

104. Ruijter, J. M. *et al.* Amplification efficiency: linking baseline and bias in the analysis of quantitative PCR data. *Nucleic Acids Res.* **37**, (2009).

105. Tuomi, J. M., Voorbraak, F., Jones, D. L. & Ruijter, J. M. Bias in the Cq value observed with hydrolysis probe based quantitative PCR can be corrected with the estimated PCR efficiency value. *Methods* **50**, 313–322 (2010).

106. Pfaffl, M. W. A new mathematical model for relative quantification in real-time RT-PCR. *Nucleic Acids Res.* **29**, E45 (2001).

107. Teng, F. & Fussenegger, M. Shedding Light on Extracellular Vesicle Biogenesis and Bioengineering. *Adv. Sci.* **8**, 2003505 (2021).

108. Li, Q. *et al.* TRNA-Derived Small Non-Coding RNAs in Response to Ischemia Inhibit Angiogenesis. *Sci. Rep.* **6**, 1–10 (2016).

109. Liu, X. *et al.* A pro-metastatic tRNA fragment drives Nucleolin oligomerization and

stabilization of its bound metabolic mRNAs. *Mol. Cell* **82**, 2604-2617.e8 (2022).

110. Redshaw, N. *et al.* A comparison of miRNA isolation and RT-qPCR technologies and their effects on quantification accuracy and repeatability. *Biotechniques* **54**, 155–164 (2013).

111. Bustin, S. A. *et al.* The MIQE guidelines: Minimum information for publication of quantitative real-time PCR experiments. *Clin. Chem.* **55**, 611–622 (2009).

112. Andersen, C. L., Jensen, J. L. & Ørntoft, T. F. Normalization of Real-Time Quantitative Reverse Transcription-PCR Data: A Model-Based Variance Estimation Approach to Identify Genes Suited for Normalization, Applied to Bladder and Colon Cancer Data Sets. *Cancer Res.* **64**, 5245–5250 (2004).

113. Awoyemi, T. Personal Communication. (2021).

114. Tuuli, M. G., Longtine, M. S. & Nelson, D. M. Review: Oxygen and trophoblast biology-a source of controversy. *Placenta* **32 Suppl 2**, S109-18 (2011).

115. Quek, C., Jung, C.-H., Bellingham, S. A., Lonie, A. & Hill, A. F. iSRAP - a one-touch research tool for rapid profiling of small RNA-seq data. *J. Extracell. vesicles* **4**, 29454 (2015).

116. Luo, S.-S. *et al.* Human Villous Trophoblasts Express and Secrete Placenta-Specific MicroRNAs into Maternal Circulation via Exosomes1. *Biol. Reprod.* **81**, 717–729 (2009).

117. Donker, R. B. *et al.* The expression profile of C19MC microRNAs in primary human trophoblast cells and exosomes. *Mol. Hum. Reprod.* **18**, 417–424 (2012).

118. Delorme-Axford, E. *et al.* Human placental trophoblasts confer viral resistance to recipient cells. *Proc. Natl. Acad. Sci.* **110**, 12048–12053 (2013).

119. Honda, S., Morichika, K. & Kirino, Y. Selective amplification and sequencing of cyclic phosphate-containing RNAs by the cP-RNA-seq method. *Nat. Protoc.* **11**, 476–489 (2016).

120. Germain, S. J., Sacks, G. P., Soorana, S. R., Sargent, I. L. & Redman, C. W. Systemic inflammatory priming in normal pregnancy and preeclampsia: the role of

circulating syncytiotrophoblast microparticles. *J. Immunol.* **179**, 1390–1390 (2007).

121. Hendrix, A. The nature of blood(y) extracellular vesicles. *Nat. Rev. Mol. Cell Biol.* **22**, 243 (2021).
122. Clayton, A. *et al.* Considerations towards a roadmap for collection, handling and storage of blood extracellular vesicles. *J. Extracell. vesicles* **8**, 1647027 (2019).
123. Suades, R., Padró, T., Vilahur, G. & Badimon, L. Platelet-released extracellular vesicles: the effects of thrombin activation. *Cell. Mol. Life Sci.* **79**, 190 (2022).
124. Wisgrill, L. *et al.* Peripheral blood microvesicles secretion is influenced by storage time, temperature, and anticoagulants. *Cytom. Part A J. Int. Soc. Anal. Cytol.* **89**, 663–672 (2016).
125. Görgens, A. *et al.* Identification of storage conditions stabilizing extracellular vesicles preparations. *J. Extracell. vesicles* **11**, e12238 (2022).
126. Lacroix, R. *et al.* Standardization of pre-analytical variables in plasma microparticle determination: Results of the International Society on Thrombosis and Haemostasis SSC Collaborative workshop. *J. Thromb. Haemost.* **11**, 1190–1193 (2013).
127. Coumans, F. A. W. *et al.* Methodological Guidelines to Study Extracellular Vesicles. *Circ. Res.* **120**, 1632–1648 (2017).
128. Yokota, M., Tatsumi, N., Nathalang, O., Yamada, T. & Tsuda, I. Effects of heparin on polymerase chain reaction for blood white cells. *J. Clin. Lab. Anal.* **13**, 133–140 (1999).
129. Lacroix, R. *et al.* Impact of pre-analytical parameters on the measurement of circulating microparticles: Towards standardization of protocol. *J. Thromb. Haemost.* **10**, 437–446 (2012).
130. Consortium, E.-T. *et al.* EV-TRACK: transparent reporting and centralizing knowledge in extracellular vesicle research. *Nat. Methods 2017 143* (2017).
131. Cocozza, F., Grisard, E., Martin-Jaular, L., Mathieu, M. & Théry, C. SnapShot: Extracellular Vesicles. *Cell* **182**, 262-262.e1 (2020).

132. Auber, M. & Svenningsen, P. An estimate of extracellular vesicle secretion rates of human blood cells. *J. Extracell. Biol.* **1**, (2022).

133. Karlsson, M. *et al.* A single-cell type transcriptomics map of human tissues. *Sci. Adv.* **7**, (2021).

134. Sembaj, A., Carriazo, C. & Moreno Barral, J. Placental alkaline phosphatase of high molecular weight in plasma of pregnant women in the last trimester of gestation. *Rev. Fac. Cien. Med. Univ. Nac. Cordoba.* **57**, 115–119 (2000).

135. Lai, A., Elfeky, O., Rice, G. E. & Salomon, C. Optimized Specific Isolation of Placenta-Derived Exosomes from Maternal Circulation. in *Preeclampsia : Methods and Protocols* (eds. Murthi, P. & Vaillancourt, C.) 131–138 (Springer New York, 2018). doi:10.1007/978-1-4939-7498-6_10.

136. Cerdeira, A. S. *et al.* Circulating soluble fms-like tyrosine kinase-1 is placentally derived in normal pregnancy: First in vivo evidence. *Pregnancy Hypertens.* **16**, 145–147 (2019).

137. Abdel Nour, A. M. & Pfaffl, M. W. *MIQE qPCR & dPCR: How to apply the MIQE Guidelines. 5th Edition*. (bioMCC, 2022).

138. Benz, F. *et al.* U6 is unsuitable for normalization of serum miRNA levels in patients with sepsis or liver fibrosis. *Exp. Mol. Med.* **45**, e42 (2013).

139. Schneider, C. A., Rasband, W. S. & Eliceiri, K. W. NIH Image to ImageJ: 25 years of image analysis. *Nat. Methods 2012 97* **9**, 671–675 (2012).

140. Sairanen, M. Personal Communication. (2022).

141. Stranska, R. *et al.* Comparison of membrane affinity-based method with size-exclusion chromatography for isolation of exosome-like vesicles from human plasma. *J. Transl. Med.* **16**, 1–9 (2018).

142. Zhang, W. Personal Communication. (2021).

143. Tian, Y. *et al.* Quality and efficiency assessment of six extracellular vesicle isolation methods by nano-flow cytometry. *J. Extracell. Vesicles* **9**, 1697028 (2020).

144. Sunderland, C. A., Redman, C. W. & Stirrat, G. M. Monoclonal antibodies to human

syncytiotrophoblast. *Immunology* **43**, 541–546 (1981).

145. Sunderland, C. A., Davies, J. O. & Stirrat, G. M. Immunohistology of normal and ovarian cancer tissue with a monoclonal antibody to placental alkaline phosphatase. *Cancer Res.* **44**, 4496–4502 (1984).
146. Dhahbi, J. M. *et al.* 5' tRNA halves are present as abundant complexes in serum, concentrated in blood cells, and modulated by aging and calorie restriction. *BMC Genomics* **14**, 1–14 (2013).
147. Cerdeira, A. S. *et al.* In vivo evidence of significant placental growth factor release by normal pregnancy placentas. *Sci. Rep.* **10**, 1–5 (2020).
148. Salomon, C. *et al.* A gestational profile of placental exosomes in maternal plasma and their effects on endothelial cell migration. *PLoS One* **9**, (2014).
149. Menon, R. *et al.* Protein Profile Changes in Circulating Placental Extracellular Vesicles in Term and Preterm Births: A Longitudinal Study. *Endocrinology* **161**, (2020).
150. Wright, D., Wright, A. & Nicolaides, K. H. The competing risk approach for prediction of preeclampsia. *Am. J. Obstet. Gynecol.* **223**, 12-23.e7 (2020).
151. Rolnik, D. L. *et al.* Aspirin versus Placebo in Pregnancies at High Risk for Preterm Preeclampsia. *N. Engl. J. Med.* **377**, 613–622 (2017).
152. Rasmussen, M. *et al.* RNA profiles reveal signatures of future health and disease in pregnancy. *Nat. 2022 6017893* **601**, 422–427 (2022).
153. Moufarrej, M. N. *et al.* Early prediction of preeclampsia in pregnancy with cell-free RNA. *Nat. 2022 6027898* **602**, 689–694 (2022).
154. Miura, K. *et al.* Circulating chromosome 19 miRNA cluster microRNAs in pregnant women with severe pre-eclampsia. *J. Obstet. Gynaecol. Res.* **41**, 1526–1532 (2015).
155. Martinez-Fierro, M. L. *et al.* Circulating levels of specific members of chromosome 19 microRNA cluster are associated with preeclampsia development. *Arch. Gynecol. Obstet.* **297**, 365–371 (2018).

156. Hromadnikova, I. *et al.* Circulating C19MC MicroRNAs in preeclampsia, gestational hypertension, and fetal growth restriction. *Mediators Inflamm.* **2013**, (2013).

157. Yang, S., Li, H., Ge, Q., Guo, L. & Chen, F. Deregulated microRNA species in the plasma and placenta of patients with preeclampsia. *Mol. Med. Rep.* **12**, 527–534 (2015).

158. Ura, B. *et al.* Potential role of circulating microRNAs as early markers of preeclampsia. *Taiwan. J. Obstet. Gynecol.* **53**, 232–234 (2014).

159. Love, M. I., Huber, W. & Anders, S. Moderated estimation of fold change and dispersion for RNA-seq data with DESeq2. *Genome Biol.* **15**, 550 (2014).

160. Love, M., Anders, S. & Huber, W. Analyzing RNA-seq data with DESeq2. *Bioconductor.org* http://bioconductor.org/packages/devel/bioc/vignettes/DESeq2/inst/doc/DESeq2.html (2023).

161. Tersigni, C. *et al.* HLA-DR is aberrantly expressed at feto-maternal interface in pre-eclampsia. *J. Reprod. Immunol.* **129**, 48–52 (2018).

162. Lu, S. *et al.* A novel tRNA-derived fragment tRF-3022b modulates cell apoptosis and M2 macrophage polarization via binding to cytokines in colorectal cancer. *J. Hematol. Oncol.* **15**, 176 (2022).

163. Dragovic, R. A., Southcombe, J. H., Tannetta, D. S., Redman, C. W. G. & Sargent, I. L. Multicolor flow cytometry and nanoparticle tracking analysis of extracellular vesicles in the plasma of normal pregnant and pre-eclamptic women. *Biol. Reprod.* **89**, 151 (2013).

164. Babatunde, K. A. *et al.* Malaria infected red blood cells release small regulatory RNAs through extracellular vesicles. *Sci. Rep.* **8**, 884 (2018).

165. Tulenko, T., Schneider, J., Floro, C. & Sicilla, M. The in vitro effect on arterial wall function of serum from patients with pregnancy-induced hypertension. *Am. J. Obstet. Gynecol.* **156**, 817–823 (1987).

166. Spargo, B., P., M. C. & Winemiller, R. Glomerular capillary endotheliosis in toxemia

of pregnancy. *Arch. Pathol.* **68**, 593–599 (1959).

167. Stubbs, T. M., Lazarchick, J. & Horger, E. O. Plasma fibronectin levels in preeclampsia: A possible biochemical marker for vascular endothelial damage. *Am. J. Obstet. Gynecol.* **150**, 885–887 (1984).

168. Thornton, C. A. & Bonnar, J. Factor VIII-related antigen and factor VIII coagulant activity in normal and pre-eclamptic pregnancy. *Br. J. Obstet. Gynaecol.* **84**, 919–923 (1977).

169. Fitzgerald, D. J., Entman, S. S., Mulloy, K. & FitzGerald, G. A. Decreased prostacyclin biosynthesis preceding the clinical manifestation of pregnancy-induced hypertension. *Circulation* **75**, 956–963 (1987).

170. Rodgers, G. M., Taylor, R. N. & Roberts, J. M. Preeclampsia is associated with a serum factor cytotoxic to human endothelial cells. *Am. J. Obstet. Gynecol.* **159**, 908–914 (1988).

171. Lockwood, C. J. & Peters, J. H. Increased plasma levels of ED1+ cellular fibronectin precede the clinical signs of preeclampsia. *Am. J. Obstet. Gynecol.* **162**, 358–362 (1990).

172. Taylor, R. N. *et al.* High plasma cellular fibronectin levels correlate with biochemical and clinical features of preeclampsia but cannot be attributed to hypertension alone. *Am. J. Obstet. Gynecol.* **165**, 895–901 (1991).

173. Deng, L., Bremme, K., Hansson, L. O. & Blombäck, M. Plasma levels of von willebrand factor and fibronectin as markers of persisting endothelial damage in preeclampsia. *Obstet. Gynecol.* **84**, 941–945 (1994).

174. Nova, A., Sibai, B. M., Barton, J. R., Mercer, B. M. & Mitchell, M. D. Maternal plasma level of endothelin is increased in preeclampsia. *Am. J. Obstet. Gynecol.* **165**, 724–727 (1991).

175. Hsu, C. D. *et al.* Elevated circulating thrombomodulin in severe preeclampsia. *Am. J. Obstet. Gynecol.* **169**, 148–149 (1993).

176. Minakami, H., Takahashi, T., Izumi, A. & Tamada, T. Increased levels of plasma

thrombomodulin in preeclampsia. *Gynecol. Obstet. Invest.* **36**, 208–210 (1993).

177. Cackovic, M. *et al.* Fractional excretion of tumor necrosis factor-alpha in women with severe preeclampsia. *Obstet. Gynecol.* **112**, 93–100 (2008).

178. Mills, J. L. *et al.* Prostacyclin and thromboxane changes predating clinical onset of preeclampsia: a multicenter prospective study. *JAMA* **282**, 356–362 (1999).

179. Sandrim, V. C. *et al.* Nitric oxide formation is inversely related to serum levels of antiangiogenic factors soluble fms-like tyrosine kinase-1 and soluble endogline in preeclampsia. *Hypertension* **52**, 402–407 (2008).

180. McCarthy, A. L., Woolfson, R. G., Raju, S. K. & Poston, L. Abnormal endothelial cell function of resistance arteries from women with preeclampsia. *Am. J. Obstet. Gynecol.* **168**, 1323–1330 (1993).

181. Ashworth, J. R., Warren, A. Y., Baker, P. N. & Johnson, I. R. Loss of endothelium-dependent relaxation in myometrial resistance arteries in pre-eclampsia. *BJOG An Int. J. Obstet. Gynaecol.* **104**, 1152–1158 (1997).

182. Myers, J., Mires, G., Macleod, M. & Baker, P. In preeclampsia, the circulating factors capable of altering in vitro endothelial function precede clinical disease. *Hypertension* **45**, 258–263 (2005).

183. Tsukimori, K. *et al.* The possible role of endothelial cells in hypertensive disorders during pregnancy. *Obstet. Gynecol.* **80**, 229–233 (1992).

184. Smárason, A. K., Sargent, I. L. & Redman, C. W. Endothelial cell proliferation is suppressed by plasma but not serum from women with preeclampsia. *Am. J. Obstet. Gynecol.* **174**, 787–793 (1996).

185. Lorentzen, B., Endresen, M. J., Hovig, T., Haug, E. & Henriksen, T. Sera from preeclamptic women increase the content of triglycerides and reduce the release of prostacyclin in cultured endothelial cells. *Thromb. Res.* **63**, 363–372 (1991).

186. Taylor, R. N., Musci, T. J., Rodgers, G. M. & Roberts, J. M. Preeclamptic sera stimulate increased platelet-derived growth factor mRNA and protein expression by cultured human endothelial cells. *Am. J. Reprod. Immunol.* **25**, 105–108 (1991).

187. Taylor, R. N. *et al.* Selective effects of preeclamptic sera on human endothelial cell procoagulant protein expression. *Am. J. Obstet. Gynecol.* **165**, 1705–1710 (1991).

188. Groten, T., Kreienberg, R., Fialka, I., Huber, L. & Wedlich, D. Altered subcellular distribution of cadherin-5 in endothelial cells caused by the serum of pre-eclamptic patients. *Mol. Hum. Reprod.* **6**, 1027–1032 (2000).

189. Villalobos-Labra, R. *et al.* Placenta-derived extracellular vesicles from preeclamptic and healthy pregnancies impair ex vivo vascular endothelial function. *Biosci. Rep.* **42**, 20222185 (2022).

190. Murugesan, S. *et al.* Extracellular Vesicles From Women With Severe Preeclampsia Impair Vascular Endothelial Function. *Anesth. Analg.* (2021) doi:10.1213/ANE.0000000000005812.

191. Cockell, A. P. *et al.* Human placental syncytiotrophoblast microvillous membranes impair maternal vascular endothelial function. *Br. J. Obstet. Gynaecol.* **104**, 235–240 (1997).

192. Hoegh, A. M. *et al.* Effect of syncytiotrophoblast microvillous membrane treatment on gene expression in human umbilical vein endothelial cells. *BJOG* **113**, 1270–1279 (2006).

193. Kertesz, Z. *et al.* Purification and characterization of a complex from placental syncytiotrophoblast microvillous membranes which inhibits the proliferation of human umbilical vein endothelial cells. *Placenta* **20**, 71–79 (1999).

194. Kertesz, Z., Linton, E. A. & Redman, C. W. Adhesion molecules of syncytiotrophoblast microvillous membranes inhibit proliferation of human umbilical vein endothelial cells. *Placenta* **21**, 150–159 (2000).

195. Barden, A. *et al.* Neutrophil CD11B expression and neutrophil activation in pre-eclampsia. *Clin. Sci. (Lond).* **92**, 37–44 (1997).

196. Sacks, G. P., Studena, K., Sargent, I. L. & Redman, C. W. G. Normal pregnancy and preeclampsia both produce inflammatory changes in peripheral blood leukocytes akin to those of sepsis. *Am. J. Obstet. Gynecol.* **179**, 80–86 (1998).

197. Berge, L. N., Østensen, M. & Revhaug, A. Phagocytic cell activity in pre-eclampsia. *Acta Obstet. Gynecol. Scand.* **67**, 499–504 (1988).

198. Santner-Nanan, B. *et al.* Systemic increase in the ratio between Foxp3+ and IL-17-producing CD4+ T cells in healthy pregnancy but not in preeclampsia. *J. Immunol.* **183**, 7023–7030 (2009).

199. Prins, J. R. *et al.* Preeclampsia is associated with lower percentages of regulatory T cells in maternal blood. *Hypertens. pregnancy* **28**, 300–311 (2009).

200. Kupferminc, M. J., Peaceman, A. M., Aderka, D., Wallach, D. & Socol, M. L. Soluble tumor necrosis factor receptors and interleukin-6 levels in patients with severe preeclampsia. *Obstet. Gynecol.* **88**, 420–427 (1996).

201. Vince, G. S., Starkey, P. M., Austgulen, R., Kwiatkowski, D. & Redman, C. W. G. Interleukin-6, tumour necrosis factor and soluble tumour necrosis factor receptors in women with pre-eclampsia. *Br. J. Obstet. Gynaecol.* **102**, 20–25 (1995).

202. Kalinderis, M. *et al.* Elevated serum levels of interleukin-6, interleukin-1β and human chorionic gonadotropin in pre-eclampsia. *Am. J. Reprod. Immunol.* **66**, 468–475 (2011).

203. Daniel, Y. *et al.* Plasma interleukin-12 is elevated in patients with preeclampsia. *Am. J. Reprod. Immunol.* **39**, 376–380 (1998).

204. Arriaga-Pizano, L. *et al.* The predominant Th1 cytokine profile in maternal plasma of preeclamptic women is not reflected in the choriodecidual and fetal compartments. *J. Soc. Gynecol. Investig.* **12**, 335–342 (2005).

205. Hennessy, A., Pilmore, H. L., Simmons, L. A. & Painter, D. M. A deficiency of placental IL-10 in preeclampsia. *J. Immunol.* **163**, 3491–3495 (1999).

206. Derzsy, Z., Prohászka, Z., Rigó, J. J., Füst, G. & Molvarec, A. Activation of the complement system in normal pregnancy and preeclampsia. *Mol. Immunol.* **47**, 1500–1506 (2010).

207. Huda, S. S. *et al.* Visceral adipose tissue activated macrophage content and inflammatory adipokine secretion is higher in pre-eclampsia than in healthy

pregnancys. *Clin. Sci. (Lond).* **131**, 1529 (2017).

208. Holder, B. S., Tower, C. L., Jones, C. J. P., Aplin, J. D. & Abrahams, V. M. Heightened Pro-Inflammatory Effect of Preeclamptic Placental Microvesicles on Peripheral Blood Immune Cells in Humans1. *Biol. Reprod.* **86**, (2012).
209. Awoyemi, T. *et al.* Syncytiotrophoblast Extracellular Vesicles From Late-Onset Preeclampsia Placentae Suppress Pro-Inflammatory Immune Response in THP-1 Macrophages. *Front. Immunol.* **12**, (2021).
210. Liu, X. *et al.* Trophoblast-Derived Extracellular Vesicles Promote Preeclampsia by Regulating Macrophage Polarization. *Hypertension* **79**, 2274–2287 (2022).
211. Sequence Scramble. https://www.genscript.com/tools/create-scrambled-sequence.
212. BLAST: Basic Local Alignment Search Tool. https://blast.ncbi.nlm.nih.gov/Blast.cgi.
213. Majewska, E. *et al.* Role of tyrosine kinase enzymes in TNF-alpha and IL-1 induced expression of ICAM-1 and VCAM-1 on human umbilical vein endothelial cells. *Scand. J. Immunol.* **45**, 385–392 (1997).
214. Hobbs, S., Reynoso, M., Geddis, A. V., Mitrophanov, A. Y. & Matheny, R. W. LPS-stimulated NF-κB p65 dynamic response marks the initiation of TNF expression and transition to IL-10 expression in RAW 264.7 macrophages. *Physiol. Rep.* **6**, (2018).
215. Powe, C. E., Levine, R. J. & Karumanchi, S. A. Preeclampsia, a disease of the maternal endothelium: the role of antiangiogenic factors and implications for later cardiovascular disease. *Circulation* **123**, 2856–2869 (2011).
216. Akbar, N. Personal Communication. (2022).
217. Pondman, K. M. *et al.* Pulmonary surfactant protein SP-D opsonises carbon nanotubes and augments their phagocytosis and subsequent pro-inflammatory immune response. *Nanoscale* **9**, 1097–1109 (2017).
218. Kishore, U. Personal Communication. (2022).
219. Baer, C., Squadrito, M. L., Iruela-Arispe, M. L. & De Palma, M. Reciprocal

interactions between endothelial cells and macrophages in angiogenic vascular niches. *Exp. Cell Res.* **319**, 1626–1634 (2013).

220. Hernandez, G. E. & Iruela-Arispe, M. L. The many flavors of monocyte / macrophage-endothelial cell interactions. *Curr. Opin. Hematol.* **27**, 181 (2020).
221. He, X. *et al.* Expression profiles and potential roles of transfer RNA-derived small RNAs in atherosclerosis. *J. Cell. Mol. Med.* **25**, 7052–7065 (2021).
222. Yeganeh Kazemi, N. *et al.* Maternal Monocytes Respond to Cell-Free Fetal DNA and Initiate Key Processes of Human Parturition. *J. Immunol.* **207**, 2433–2444 (2021).
223. Cristodero, M. & Polacek, N. The multifaceted regulatory potential of tRNA-derived fragments. *Non-coding RNA Investig.* **1**, (2017).
224. Cindrova-Davies, T., Sanders, D. A., Burton, G. J. & Charnock-Jones, D. S. Soluble FLT1 sensitizes endothelial cells to inflammatory cytokines by antagonizing VEGF receptor-mediated signalling. *Cardiovasc. Res.* **89**, 671–679 (2011).
225. Fisher, S. J. Why is placentation abnormal in preeclampsia? *Am. J. Obstet. Gynecol.* **213**, S115-22 (2015).
226. Goswami, D. *et al.* Excess syncytiotrophoblast microparticle shedding is a feature of early-onset pre-eclampsia, but not normotensive intrauterine growth restriction. *Placenta* **27**, 56–61 (2006).
227. Pillay, P., Maharaj, N., Moodley, J. & Mackraj, I. Placental exosomes and pre-eclampsia: Maternal circulating levels in normal pregnancies and, early and late onset pre-eclamptic pregnancies. *Placenta* **46**, 18–25 (2016).
228. Lok, C. A. R. *et al.* Changes in microparticle numbers and cellular origin during pregnancy and preeclampsia. *Hypertens. Pregnancy* **27**, 344–360 (2008).
229. Chen, Y. *et al.* Association of placenta-derived extracellular vesicles with pre-eclampsia and associated hypercoagulability: a clinical observational study. *BJOG* (2020) doi:10.1111/1471-0528.16552.
230. Marques, F. K. *et al.* Circulating microparticles in severe preeclampsia. *Clin. Chim.*

Acta **414**, 253–258 (2012).

231. Verma, S., Pillay, P., Naicker, T., Moodley, J. & Mackraj, I. Placental hypoxia inducible factor -1α & CHOP immuno-histochemical expression relative to maternal circulatory syncytiotrophoblast micro-vesicles in preeclamptic and normotensive pregnancies. *Eur. J. Obstet. Gynecol. Reprod. Biol.* **220**, 18–24 (2018).

232. Pai, D. A. *et al.* RNAs nonspecifically inhibit RNA polymerase II by preventing binding to the DNA template. *RNA* **20**, 644–655 (2014).

233. Maute, R. L. *et al.* TRNA-derived microRNA modulates proliferation and the DNA damage response and is down-regulated in B cell lymphoma. *Proc. Natl. Acad. Sci. U. S. A.* **110**, 1404–1409 (2013).

234. Kumar, P., Anaya, J., Mudunuri, S. B. & Dutta, A. Meta-analysis of tRNA derived RNA fragments reveals that they are evolutionarily conserved and associate with AGO proteins to recognize specific RNA targets. *BMC Biol.* **12**, (2014).

235. Luo, S. *et al.* Drosophila tsRNAs preferentially suppress general translation machinery via antisense pairing and participate in cellular starvation response. *Nucleic Acids Res.* **46**, 5250–5268 (2018).

236. Karaiskos, S., Naqvi, A. S., Swanson, K. E. & Grigoriev, A. Age-driven modulation of tRNA-derived fragments in Drosophila and their potential targets. *Biol. Direct* **10**, 51 (2015).

237. Deng, J. *et al.* Respiratory Syncytial Virus Utilizes a tRNA Fragment to Suppress Antiviral Responses Through a Novel Targeting Mechanism. *Mol. Ther.* **23**, 1622–1629 (2015).

238. Goodarzi, H. *et al.* Endogenous tRNA-derived fragments suppress breast cancer progression via YBX1 displacement. *Cell* **161**, 790–802 (2015).

239. Ivanov, P., Emara, M. M., Villen, J., Gygi, S. P. & Anderson, P. Angiogenin-Induced tRNA Fragments Inhibit Translation Initiation. *Mol. Cell* **43**, 613–623 (2011).

240. Gebetsberger, J., Wyss, L., Mleczko, A. M., Reuther, J. & Polacek, N. A tRNA-derived fragment competes with mRNA for ribosome binding and regulates

translation during stress. *RNA Biol.* **14**, 1364–1373 (2017).

241. Couvillion, M. T., Bounova, G., Purdom, E., Speed, T. P. & Collins, K. A Tetrahymena Piwi Bound to Mature tRNA 3' Fragments Activates the Exonuclease Xrn2 for RNA Processing in the Nucleus. *Mol. Cell* **48**, 509–520 (2012).
242. Kim, H. K. *et al.* A transfer-RNA-derived small RNA regulates ribosome biogenesis. *Nature* **552**, 57–62 (2017).
243. Boskovic, A., Bing, X. Y., Kaymak, E. & Rando, O. J. Control of noncoding RNA production and histone levels by a 5' tRNA fragment. *Genes Dev.* **34**, 118–131 (2020).
244. Chen, Q. *et al.* Sperm tsRNAs contribute to intergenerational inheritance of an acquired metabolic disorder. *Science (80-.).* **351**, 397–400 (2016).
245. Emara, M. M. *et al.* Angiogenin-induced tRNA-derived stress-induced RNAs promote stress-induced stress granule assembly. *J. Biol. Chem.* **285**, 10959–10968 (2010).
246. Lyons, S. M., Achorn, C., Kedersha, N. L., Anderson, P. J. & Ivanov, P. YB-1 regulates tiRNA-induced Stress Granule formation but not translational repression. *Nucleic Acids Res.* **44**, 6949–6960 (2016).
247. Saikia, M. *et al.* Angiogenin-Cleaved tRNA Halves Interact with Cytochrome c, Protecting Cells from Apoptosis during Osmotic Stress. *Mol. Cell. Biol.* **34**, 2450–2463 (2014).
248. Wang, J. *et al.* Plasma tRNA Fragments Derived from 5′ Ends as Novel Diagnostic Biomarkers for Early-Stage Breast Cancer. *Mol. Ther. - Nucleic Acids* **21**, 954–964 (2020).
249. Cho, O., Kim, D.-W. & Cheong, J.-Y. Screening Plasma Exosomal RNAs as Diagnostic Markers for Cervical Cancer: An Analysis of Patients Who Underwent Primary Chemoradiotherapy. *Biomolecules* **11**, (2021).
250. Xi, J., Zeng, Z., Li, X., Zhang, X. & Xu, J. Expression and Diagnostic Value of tRNA-Derived Fragments Secreted by Extracellular Vesicles in Hypopharyngeal

Carcinoma. *Onco. Targets. Ther.* **14**, 4189–4199 (2021).

251. Zhu, L. *et al.* Exosomal tRNA-derived small RNA as a promising biomarker for cancer diagnosis. *Mol. Cancer* **18**, (2019).

252. Kumar, S. R. *et al.* RNA cargos in extracellular vesicles derived from blood serum in pancreas associated conditions. *Sci. Rep.* **10**, 2800 (2020).

253. Khurana, R. *et al.* Identification of urinary exosomal noncoding RNAs as novel biomarkers in chronic kidney disease. *RNA* **23**, 142–152 (2017).

254. Sundar, I. K., Li, D. & Rahman, I. Small RNA-sequence analysis of plasma-derived extracellular vesicle miRNAs in smokers and patients with chronic obstructive pulmonary disease as circulating biomarkers. *J. Extracell. vesicles* **8**, 1684816 (2019).

255. Fang, S., He, T., Jiang, J., Li, Y. & Chen, P. Osteogenic effect of TsRNA-10277-loaded exosome derived from bone mesenchymal stem cells on steroid-induced osteonecrosis of the femoral head. *Drug Des. Devel. Ther.* **14**, 4579–4591 (2020).

256. Zhang, Y. *et al.* Transfer RNA-derived fragments as potential exosome tRNA-derived fragment biomarkers for osteoporosis. *Int. J. Rheum. Dis.* **21**, 1659–1669 (2018).

257. Zhang, Q. *et al.* Circulatory exosomal tRF-Glu-CTC-005 and tRF-Gly-GCC-002 serve as predictive factors of successful microdissection testicular sperm extraction in patients with nonobstructive azoospermia. *Fertil. Steril.* **117**, 512–521 (2022).

258. Vigneron, N. *et al.* Towards a new standardized method for circulating miRNAs profiling in clinical studies: Interest of the exogenous normalization to improve miRNA signature accuracy. *Mol. Oncol.* **10**, 981–992 (2016).

259. Timofeeva, A. V. *et al.* Identification of potential early biomarkers of preeclampsia. *Placenta* **61**, 61–71 (2018).

260. Wu, L. *et al.* Circulating microRNAs are elevated in plasma from severe preeclamptic pregnancies. *Reproduction* **143**, 389–397 (2012).

261. Hromadnikova, I., Kotlabova, K., Ivankova, K. & Krofta, L. First trimester screening of circulating C19MC microRNAs and the evaluation of their potential to predict the onset of preeclampsia and IUGR. *PLoS One* **12**, e0171756 (2017).

262. Jairajpuri, D. S., Malalla, Z. H., Mahmood, N. & Almawi, W. Y. Circulating microRNA expression as predictor of preeclampsia and its severity. *Gene* **627**, 543–548 (2017).

263. Motawi, T. M. k., Sabry, D., Maurice, N. W. & Rizk, S. M. Role of mesenchymal stem cells exosomes derived microRNAs; miR-136, miR-494 and miR-495 in pre-eclampsia diagnosis and evaluation. *Arch. Biochem. Biophys.* **659**, 13–21 (2018).

264. Xu, P. *et al.* Variations of microRNAs in human placentas and plasma from preeclamptic pregnancy. *Hypertension* **63**, 1276–1284 (2014).

265. Gan, L. *et al.* MIR-210 and miR-155 as potential diagnostic markers for pre-eclampsia pregnancies. *Med. (United States)* **96**, (2017).

266. Yoffe, L. *et al.* Early Detection of Preeclampsia Using Circulating Small non-coding RNA. *Sci. Rep.* **8**, 3401 (2018).

267. Li, H., Ge, Q., Guo, L. & Lu, Z. Maternal plasma miRNAs expression in preeclamptic pregnancies. *Biomed Res. Int.* **2013**, (2013).

268. Gunel, T. *et al.* Expression profiling of maternal plasma and placenta microRNAs in preeclamptic pregnancies by microarray technology. *Placenta* **52**, 77–85 (2017).